Synthesis, Properties and Noncovalent Control of Bullvalenes

WILLIAM JAMES MATURI

Durham University
Department of Chemistry

Synthesis, Properties and Noncovalent Control of Bullvalenes

William Maturi

A Thesis Submitted for the Degree of Doctor of Philosophy

March 2024

Dedicated to my loving family

Peter Maturi Luisa Maturi

Tom Maturi Andrew Morton

Table of Contents

Abstract

Bullvalene is a fluxional molecule which may undergo Cope rearrangements to interconvert between up to 1,209,600 isomers. This occurs *via* rapid Cope rearrangements at room temperature due to internal molecular strain. This ability grants access to a dynamic library of structures, from just one isolatable structure.[1]

These unique properties have thus far resulted in bullvalene being used in a variety of applications, as the molecule possesses the ability to adapts its isomer distribution to its environment through noncovalent interactions.[2] Due to historic difficulties in its synthesis, collective understanding of bullvalene is limited, however, recent advances in synthesis has made the compound much more accessible.[3]

This Thesis discusses bullvalene, as it has been understood since its conception, and explores fundamental details of its rearrangements and shape in 3-D space. Exploration into bullvalene synthesis introduces the challenge of making tetrasubstituted bullvalenes (Figure 1a) through previously reported methods[4] and altogether novel syntheses. Also, bullvalene is investigated further in a supramolecular context. Alterations of bullvalene's behaviour due to imposed steric constrains, both intra- and intermolecular (Figures 1b and 1c), are investigated in an attempt to further explore its unique shapeshifting properties.

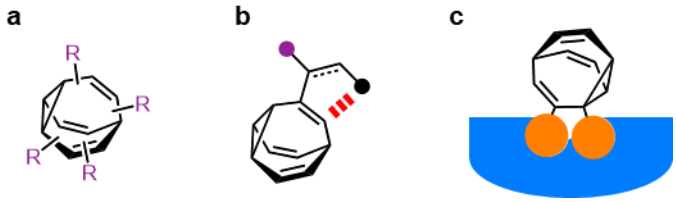

Figure 1: Illustrations of (a) tetrasubstituted bullvalene. (b) Intramolecular interactions on a bullvalene core. (c) bullvalene acting as a supramolecular guest.

---

1. (a) W. von Eggers Doering and W. R. Roth, *Tetrahedron*, 1963, **19**, 715–737. (b) A. N. Bismillah, B. M. Chapin, B. A. Hussein and P. R. McGonigal, *Chem. Sci.*, 2020, **11**, 324–332
2. (a) G. Schröder, *Angew. Chem. Int. Ed. Engl.*, 1979, **18**, 311–312. (b) A. R. Lippert, V. L. Keleshian and J. W. Bode, *Org. Biomol. Chem.*, 2009, **7**, 1529–1532. (c) A. P. Birvé, H. D. Patel, J. R. Price, W. M. Bloch, and T. Fallon, 2021, **61**, e202115468.
3. O. Yahiaoui, L. F. Pašteka, B. Judeel, and T. Fallon, *Angew. Chem. Int. Ed. Engl.*, **57**, 2570–2574.
4. M. Jones, S. D. Reich and L. T. Scott, *J. Am. Chem. Soc.*, 1970, **92**, 3118–3126.

Declaration

The scientific work described in this Thesis was carried out in the Chemistry Department in Durham University between October 2020–December 2022, at the Chemistry Department in the University of York between January 2023–March 2024 and at the Chemistry Department in Tulane University between September 2023–October 2024. Unless otherwise stated, it is the work of the author and has not been submitted in whole or in support of an application for another degree or qualification at this or any other University or institute of learning.

Signed: 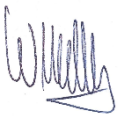

Date: 27th March 2024.

Conferences Attended and Presentations Given

1. European Symposium on Organic Reactivity (ESOR2021) | **Attended Online**

2. Macrocyclic and Supramolecular Chemistry (MASC). Nottingham, UK, 2022 | **Poster Presentation.**

3. RSC Organic Division North East Regional Meeting. Newcastle, UK, 2023 | **Poster Presentation.**

4. Durham Chemistry Annual Postgraduate Symposium. Durham, UK, 2023 | **Oral Presentation.**

5. International Symposium on Macrocyclic and Supramolecular Chemistry (ISMSC). Reykjavik, Iceland, 2023 | **Poster Presentation.**

6. Chem@York Conference. York, UK, 2023 | **Oral Presentation.**

7. Macrocyclic and Supramolecular Chemistry (MASC). Birmingham, UK, 2023 | **Poster Presentation.**

Acknowledgements

"I was a victim of a series of accidents, as are we all."

- Kurt Vonnegut, *The Sirens of Titan*

Firstly, I would like to thank Dr. Paul McGonigal, my supervisor and mentor. You have given me everything I have needed to fulfil my potential and have consistently trusted and supported me in my time with the group to go out and explore the chemistry that I have loved so much. I'd like to thank you for the many things you have taught me, and for encouraging me to hold myself and my work consistently to the high standard that I know I can achieve. It has been a pleasure to work under your guidance in the McGonigal group.

I would like to thank all of the incredible scientists who have helped me in my studies throughout my PhD, whose contributions are outlined at the beginning of each chapter in this thesis. As Carl Sagan said, "science is a collaborative enterprise" and without the invaluable contributions of those around me, much of this work would not be possible. Thank you also to the technical staff at Durham University and the University of York for their continual support and invaluable knowledge throughout my PhD.

Since I was young, I had always dreamed of going to work in North America, I would like to thank the Gibb group very much for helping me realise that dream. Especially Dr. Bruce Gibb, Corinne Gibb, Yahya Ismaiel and Jenny Kim. Thank you for being so welcoming to me and helping make my time in Louisiana an experience that I will never forget.

My time studying for my PhD would not have been the same had it not been for the friends I spent so many hours with both in and outside of the lab. Dr. Promeet Saha, thank you for all of the time you spent looking out for me, pushing me and making me laugh. Every day spent with you brought something new to learn, brought new joys and without failure brought new memories that I will continue to hold dear for a long time. I'll always remember the courage you inspired in me. Juliet Barclay, thank you for reminding me to be kind to myself and for being the calming voice on the days that would never end. Not only were you there for the harder times but thank you also for the cheer you brought in all the great times we've had, and for letting me win so many

times in Mario Kart. Dr. Aisha Bismillah, thank you for your tenacity in the face of all life's challenges. The passion you bring to your work and the intensity with which you live your life will always bring a smile to my face. Thank you for all the advice you've offered me and the good times we've shared. Dr. Chris Hogg, Charlotte Bardsley, Marcus Dennington, Dr. Senthil Kumar Kabali, Dr. Burhan Hussein, Isabel Dungsworth, Luke Nicholls and all of the other great people from the McGonigal group, the Avestro group and the Walton group, past and present. You've made the time I've spent in CG233 and E214 a real pleasure, and for that I thank you. I would be remiss not mention my friends from home "The Freaks" and the friends I made in my undergraduate time at Durham University, especially James Lloyd.

I'd like to thank John, Paul, George, Ringo, Amy, Frank (both Sinatra and Ocean), Peach Pit, Arctic Monkeys, Loyle Carner, easy life, Declan McKenna, Mac Miller, The Magic Gang, Childcare, and thousands of other musicians who have been on a constant loop for the past three years.

My family, Nonno, Mum, Tom and Andy, thank you for your unwavering love and support. I wouldn't be me if it wasn't for you. I am eternally grateful for the sacrifices you've made and for the opportunities I have had as a result. I love you all and this thesis is for you.

Lastly, I would like to thank my partner, Rhapsody Yells, for believing in me enough for the both of us. For your warmth and love you show me, and for the comfort you bring me every single day, I thank you with all my heart.

List of Abbreviations

Ac	Acetyl
Acac	Acetylacetone
APCI	Atmospheric pressure chemical ionization
ASAP	Atmospheric solids analysis probe
BB	Barbaralane
BBO	Barbaralone
BDT	Bicyclo[4.2.2]deca-2,4,7,9-tetraene
Bpin	Boronic pinacol ester
BV	Bullvalene
BVO	Bullvalone
CD	Cyclodextrin
COD	Cyclooctadiene
COSY	Correlated Spectroscopy
COT	Cyclooctatriene
COTT	Cyclooctatetraene
CPD	Carbon proton decoupled
d	Doublet
DBU	1,8-Diazobicyclo(5.4.0)undec-7-ene
DCE	1,2-Dichloroethane
DFT	Density functional theory
DIBAL-H	Diisobutylaluminium hydride
DIPEA	Diisopropylethylamine
DMA	Dimethylacetamide
DME	Dimethoxyethane
DMF	Dimethylformamide
2,2-DMP	2,2-Dimethoxypropane
DMSO	Dimethylsulfoxide
DNMR	Dynamic Nuclear Magnetic Spectroscopy
DOSY	Diffusion Ordered Spectroscopy
dppe	1,2-Bis(diphenylphosphino)ethane
DVCPR	Divinylcyclopropane rearrangement
ESI	Electrospray ionization
Et	Ethyl
EVP	Exit vector plot
EXSY	Exchange spectroscopy
FBDD	Fragment Based Drug Discovery
HMBC	Heteronuclear multiple bond correlation
HMDS	Bis(trimethylsilyl)amide
HMPA	Hexamethylphosphoramide
HPLC	High-performance liquid chromatography
HR	High resolution
HSQC	Heteronuclear single quantum coherence

^{i}Bu	*iso*-Butyl
^{i}Pr	*iso*-Propyl
m	Multiplet
M.P.	Melting point
Me	Methyl
MIDA	N-methyliminodiacetic acid
MS	Mass spectrometry
NBS	N-Bromosuccinimide
^{n}Bu	*n*-Butyl
NCI	Non-covalent interactions index
NIS	N-Iodosuccinimide
NMP	N-Methyl-2-pyrrolidone
NMR	Nuclear magnetic resonance
NPR	Normal PMI ratio
NOESY	Nuclear Overhauser effect spectroscopy
NVOC	Nitroveratryloxycarbonyl
Ph	Phenyl
PMI	Principle moments of inertia
Py	Pyridyl
ROESY	Rotating-frame nuclear Overhauser effect spectroscopy
q	Quartet
s	Singlet
^{s}Bu	*sec*-Butyl
STM	Scanning tunnel miscroscopy
STMBJ	Scanning tunnel miscroscopy break junction
t	Triplet
^{t}Bu	*tert*-Butyl
TCTE	Tricyclotetraester
Tf	Trifluoromethanesulfonyl
TFA	Trifluoroacetic acid
TFE	2,2,2-Trifluoroethanol
THEH	Tetrahydro-1,8-ethenoheptalenes
THF	Tetrahydrofuran
TLC	Thin-layer chromatography
TMEDA	Tetramethylethylenediamine
TMS	Trimethylsilyl
TOCSY	Total correlation spectroscopy
TRIBAL	Triisobutylaluminium
Ts	*para*-Toluenesulfonyl
UV	Ultraviolet
VT	Variable temperature
XPhos	Dicyclohexyl[2′,4′,6′-tris(propan-2-yl)[1,1′-biphenyl]-2-yl]phosphane

General Experimental Methods

Materials: All reagents were purchased from commercial suppliers (Sigma-Aldrich, Acros Organics, Fluorochem or Alfa Aesar) and used without further purification.

Instrumentation and Analytical Techniques: Analytical thin-layer chromatography (TLC) was performed on neutral aluminum sheet silica gel plates (Fluka, 60778-25EA) and visualised under UV irradiation (254 nm). Nuclear magnetic resonance (NMR) spectra were recorded using a Bruker Advance (III)-400 (^{1}H 400.130 MHz and ^{13}C 100.613 MHz), Varian Inova-500 (^{1}H 500.130 MHz and ^{13}C 125.758 MHz), Varian VNMRS-600 (^{1}H 600.130 MHz and ^{13}C 150.903 MHz) a Varian VNMRS-700 (^{1}H 700.130 MHz and ^{13}C 176.048 MHz), Jeol ECS-400(A) (^{1}H 399.760 MHz and ^{13}C 150.903 MHz), Jeol ECS-400(D) (^{1}H 399.830 MHz and ^{13}C 100.530 MHz), or a Bruker AVIIIHD-500 (^{1}H 500.230 MHz and ^{13}C 125.782 MHz), at a constant temperature of 298 K unless otherwise stated. For variable-temperature (VT) measurements, operating temperatures were calibrated using an internal calibration solution of MeOH and glycerol. Chemical shifts (δ) are reported in parts per million (ppm) relative to the signals corresponding to residual non-deuterated solvents $CDCl_3$: δ / ppm = 7.26 or 77.16, D_2O: δ = 4.79, $(CD_3)_2CO$: δ = 2.05 or 29.84, CD_3OD: δ = 3.31 or 49.00, CD_3CD_2OD: δ = 3.56 or 56.96 or $(CD_3)_2SO$: δ = 2.50 or 39.52. Coupling constants (*J*) are reported in Hertz (Hz). ^{13}C NMR Experiments were proton-decoupled, as are ^{19}F NMR experiments which are referenced to an internal standard, hexafluorobenzene (HFB, δ = 164.99 ppm), unless otherwise stated. Assignments of ^{1}H and ^{13}C NMR signals were accomplished by two-dimensional NMR spectroscopy (COSY, NOESY, HSQC, HMBC, HSQC-TOCSY, DOSY, EXSY and ROESY). NMR spectra were processed using MestReNova version 14. Data are reported as follows: chemical shift; multiplicity; coupling constants; integral and assignment. Low-resolution atmospheric solids analysis probe (ASAP)-MS were performed using a Waters Xevo QTOF equipped with an ASAP. Atmospheric pressure chemical ionization (APCI)-MS was performed using a Bruker compact time-of-flight mass spectrometer. High-resolution electrospray (HR-ESI) and ASAP (HR-ASAP) mass spectra were measured using a Waters LCT Premier XE high resolution, accurate mass UPLC ES MS (also with ASAP ion source). Atmospheric Melting points (M.P.) were recorded using a Gallenkamp (Sanyo) apparatus and are uncorrected. The X-ray single crystal data for compound in Chapter 5 were collected at 120.0(2) K using CuKα

radiation (λ = 1.54178Å) on a Bruker D8Venture (Photon III MM C7 CPAD detector, IμS-microsource, focusing mirrors, 1° ω-scan, shutterless mode, 8-25 s variable exposure time) 3-circle diffractometer equipped with a Cryostream-700 (Oxford Cryosystems) open-flow N_2 cryostat. The structure was solved by direct method and refined by full-matrix least squares on F^2 for all data using Olex2 and SHELXTL software. All non-hydrogen atoms were refined in anisotropic approximation, hydrogen atoms were refined isotropically.

Thesis Layout

Chapter 1 introduces fluxional molecules, with a particular emphasis on bullvalenes. The discussion spans the conception of bullvalene and progress made in their synthesis up to present day methodology as well as properties and applications of bullvalene as a fluxional cage. This chapter then ends with a discussion of different categories of supramolecular hosts which may be suitable for binding bullvalene. Chapter 2 is presented in the form of a manuscript which is being prepared and is soon to be submitted. Minor rewriting and formatting alterations have been made in order to keep it consistent with the thesis style. This chapter discusses the nature of bullvalene's rearrangements, and analysis of its shape in three-dimensional space compared to other bioisosteres. Chapter 3 exhibits our ongoing attempts to synthesise tetrasubstituted bullvalenes through alterations of past methods as well as through our own novel route. Chapter 4 presents our preliminary attempts to control bullvalene isomerisation *via* encapsulation in supramolecular hosts of various types. Finally, Chapter 5 is presented in the form of a manuscript which has been prepared and is soon to be submitted. No attempt has been made to rewrite this work, but minor formatting alterations have been made in order to keep it consistent with the thesis style. This final chapter discusses correlation between the isomerisation of bullvalene with the boc-flip of an appended carbamate group.

Chapter 1 | Introduction: Bullvalenes and Supramolecular Hosts

Synopsis

This chapter begins with an introduction to the concept of fluxional molecules, and the origins of one kind of fluxional molecule in particular, bullvalene. Different syntheses from the first synthesis in 1963 up to current methodology are then discussed, both for unsubstituted and substituted bullvalenes. A discussion on the influence of older synthetic procedures on those more recently published is included. This chapter then discusses the properties of bullvalene as they have been understood at different stages throughout literature. Further, applications of bullvalene's fluxional behaviour are discussed, including those in supramolecular, material, biological and electronic chemistry. Finally, this chapter presents a number of supramolecular hosts which may be suitable for bullvalene. As part of this discussion, details regarding the effect of these hosts on the behaviour of their guests is included.

1.1. Fluxional Molecules

The sequence in which a molecule's constituent atoms are connected determines its three-dimensional shape. For most organic molecules, this sequence is fixed. Thus, alteration of a molecule's geometry is limited to bond rotations and other minor conformational changes such as bond angle bending. The fixed nature of these bonds grants a molecule stability and allows us to accurately predict their behaviour in three-dimensional space. However, these fixed bonds also limit molecules in terms of the number of different conformations which they may occupy. Fluxional molecules are exceptional in this case as they rearrange to form one of many energetically viable conformations at room temperature. The IUPAC Gold Book defines fluxional molecules as structures which "undergo rapid degenerate rearrangements (generally detectable by methods which allow the observation of the behaviour of individual nuclei in a rearranged chemical species, e.g. NMR)".[1]

The shape of molecules also determines the intermolecular interactions in which they may partake and hence, their macroscopic properties. Thus, the ability to synthesise molecules that may alter their shape significantly in response to external stimuli presents potentially ground-breaking possibilities. This thesis will focus on the synthesis and analysis of one kind of fluxional molecule, bullvalene, and its substituted derivatives to link conformational responses on the molecular scale with the macroscopic properties of a molecule. Subsequently, the aim is to manipulate these responses to control the molecules' unique properties. A fluxional molecule which can harness this ability may prove useful in a wide array of fields from biological to materials chemistry.[2]

1.2. Origins of Bullvalene

In 1963, von Eggers Doering *et al.* investigated methods through which the rate of a [3,3]-sigmatropic rearrangement of hexa-1,5-diene may be increased.[3] Typically, temperatures in the range of 150–200 °C are required to effect a Cope rearrangement.[4] This research was inspired by a 1958 report rationalising the isomerisation of 1,2-dideuterocylopropane. Rabinovitch *et al.* found that the energy barrier for C–C bond cleavage in cyclopropane is 267 kJ mol^{-1}; 80 kJ mol^{-1} lower than in ethane (347 kJ mol^{-1}). This difference was attributed to the strain experienced by the

cyclopropane ring.[5] Thus, von Eggers Doering *et al.* appended a cyclopropane ring onto the 1,5-hexadiene moiety, increasing strain in the compound. Cope rearrangement of this molecule is accompanied by strain relief, which acts as an energetic driving force. Indeed, *cis*-1,2-divinylcyclopropane **1** rapidly undergoes rearrangement to form cyclohepta-1,4-diene **2** at room temperature (Scheme 1), and at temperatures as low as −40 °C.[3,6,7]

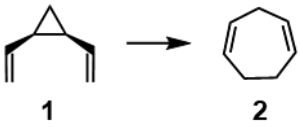

*Scheme 1: Cope rearrangement of **1** to form **2**, accompanied by strain release.*[3,6]

As a progression of this work, one of the first fluxional molecules, 3,4-homotropilidene **3**, was synthesised. Like **1**, **3** undergoes reversible Cope rearrangement at room temperature, however, unlike **1**, the product of **3**'s rearrangement is identical to its starting material (Scheme 2). This rapid interconversion of **3** between two identical structures has ramifications for its ^{1}H NMR spectrum. At −50 °C, the rate of rearrangement is sufficiently slow that seven unique proton environments are observed in a sharp, well-defined spectrum. Upon warming to room temperature, the peaks in the spectrum broaden as the Cope rearrangement occurs more rapidly resulting in faster exchange of the proton environments. Heating further to 180 °C forces the broadened peaks to converge again forming a new spectrum. At this temperature, the rearrangements are so rapid that the proton environments at positions 2 and 4 become equivalent to positions 1 and 5 respectively, and exhibit a single peak with an averaged chemical shift.[3,6]

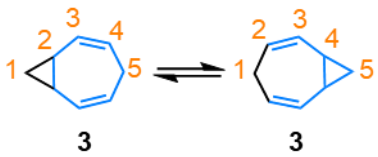

*Scheme 2: Cope rearrangement of 3,4-homotropilidene, **3**.*[3,6]

This rearrangement occurs in the "*cis*-like" conformation of **3**, and will not occur in the "*trans*-like" conformation. Yet, this conformation is disfavoured, as *cis*-**3**, experiences some transannular strain due to the proximity of the hydrogen atoms on positions 1 and 5 (Figure 1).

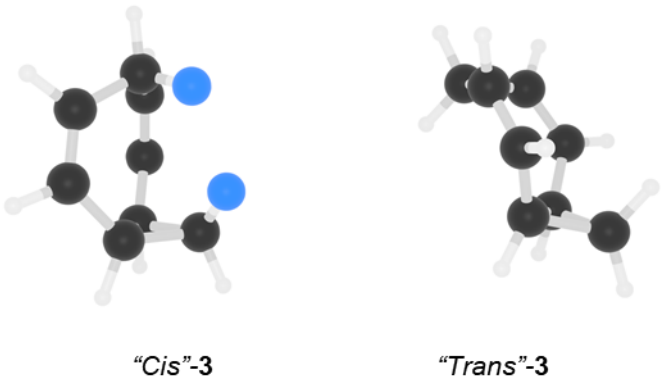

*Figure 1: Molecular structure of cis- and trans-**3**.*

Therefore, the rate of the Cope rearrangement is limited by the competing *cis/trans* isomerisation pathway. von Eggers Doering's proposed solution to this problem was to replace the two "offending hydrogen atoms" with a third *cis* alkene (Figure 2). This would fix the homotropilidene moiety in the *cis*-like conformation, favouring rearrangement. The molecule, colloquially termed "bullvalene" (**BV**), was only hypothetical at the time of publication, but was synthesised within the year by Schröder in Brussels.[8,9]

*Figure 2: Chemical structure of bullvalene (**BV**).*

The distinctive property of **BV** is that each carbon is capable of occupying any of the ten positions on the structure in any permutation. This results in a total of 1,209,600 degenerate isomers, which are constantly interconverting between one another through sequential Cope rearrangements. Each of the isomers in the case of unsubstituted **BV** are degenerate, and as such indistinguishable from one another. This degeneracy is broken when substituents are introduced to the structure.[8,10]A consequence of the fluxional character of **BV** is highly temperature-dependent ^{1}H NMR spectra (Figure 3). At low temperatures, its ^{1}H NMR spectrum is characterised by well-defined peaks for each of the four chemically inequivalent positions on the **BV** structure. As the temperature is then increased, similarly to **3**, the spectrum broadens due to the rapid Cope rearrangements and these broadened peaks begin to coalesce. Upon further heating, the spectrum exhibits only a single peak representing the average chemical shift of all chemical environments in **BV**. This single observed chemical shift is a consequence of the Cope rearrangements occurring so rapidly that

the 10 individual protons on the **BV** structure become magnetically equivalent and resonate at the same frequency. This also explains that the chemical shift of the observed peak is positioned in between that of the individual position peaks in the low temperature spectra; the single existent environment may be considered an average of the four positions on **BV**. [11,12]

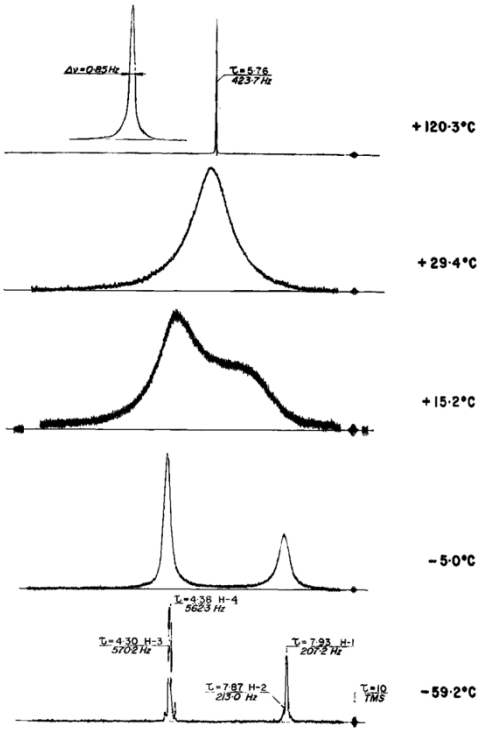

*Figure 3:Variable temperature ^{1}H NMR spectra for **BV**. Figure reproduced from publication.*[11,12]

1.3. Synthesis of Bullvalenes

The first synthetic procedure for **BV** was reported by Schröder in 1963 (Scheme 3). This synthesis involves the dimerisation of cyclooctatetraene (**COTT**) to form dimer **4**. Subsequent photolysis of **4** produces **BV** with a 6% yield over the two steps. Benzene is formed as a by-product of the reaction. This remained the only reported synthesis for three years.[8]

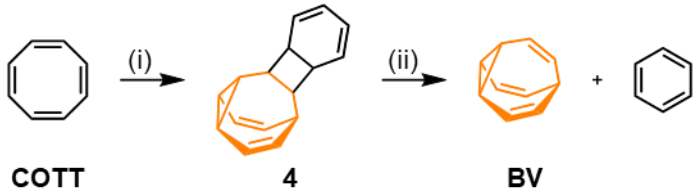

*Scheme 3: Schröder's original **BV** synthesis. (i) 100 °C, dimerisation. (ii) h ν, diethyl ether. 6% over two steps.*

Schröder also reported the first synthesis of a substituted **BV** in 1965 with a high yielding bromination–elimination reaction (Scheme 4). Elimination of **5** resulted in the formation of dehydrobullvalene **6**, which was then used in the synthesis of alkoxy bullvalenes **7**.[13]

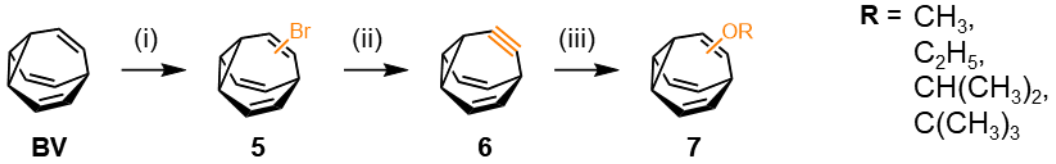

*Scheme 4: First synthesis of substituted **BV**s. (i) Br_2, KO^{t}Bu, butanol, 80–90%. (ii) KOR, DMSO. (iii) ROH, 60–90%.*

In 1966, von Eggers Doering published a new, two-step synthesis of **BV**, consisting of partial thermal decomposition of Nenitzescu's hydrocarbon **8** to form 9,10-dihydronapthalene **9** (Scheme 5). This intermediate was the subject of a photorearrangement to form **BV**.[14] The mechanism of this photorearrangement was the subject of speculation. Considering rules reported by Woodward and Hoffman in the previous year, **10** was suggested as a potential intermediate in the photorearrangement.[15]

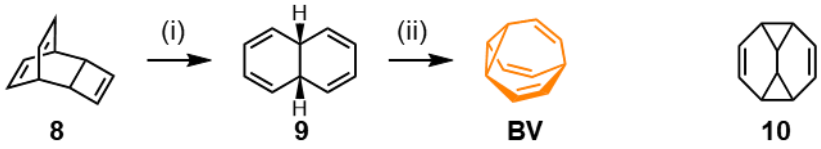

*Scheme 5: von Eggers Doering's 1966 synthesis of **BV** (i) 301 °C (ii) hν. Proposed second step intermediate **7**.*

In the same investigation von Eggers Doering *et. al* also showed that heating a sample of **BV** to 350 °C regenerated **9**, whereas heating to higher temperatures (400 °C) resulted in degradation to other products at the cost of **9**.[14] Also in 1966, Vogel *et. al* reported a remarkably similar synthesis of the first disubstituted BVs (Scheme 6). Irradiation of dimethyl *cis*-9,10-dihydronapthalenedicarboxylate **11** formed dimethyl dicarboxylate BV **12** and irradiation of *cis*-9,10-dihydronapthalenedicarboxylate anhydride **13** formed BV **14**.[16]

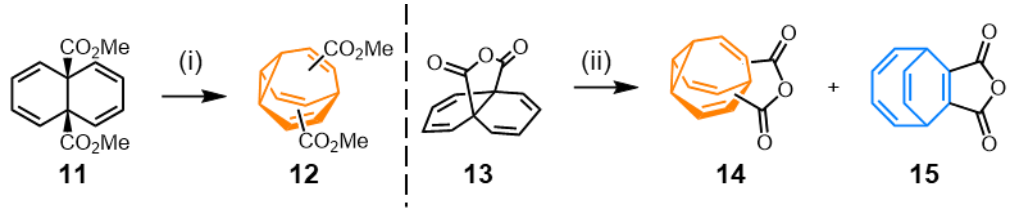

*Scheme 6: Vogel's synthesis of disubstituted BV **12**. (i) hν, MeOH, 10%. (ii) hν, Et_2O.*[16]

The side product of this second reaction was suggested to be **15**, an anhydride substituted bicyclo[4.2.2]deca-2,4,7,9-tetraene (BDT). Vogel and von Eggers Doering were the first to report this type of **BDT** structure in 1966 as a potential side-product in the synthesis **BV**, however, this structure would go on to be a key precursor for several future syntheses.[16,17]. Masamune *et al*. investigated the pyrolysis of **BDT** and discovered that hydrocarbon **10** acts as an intermediate in the isomerisation of **BDT** *via* an intramolecular Diels–Alder then a retro-Diels–Alder (Scheme 7). **10** was also presented as a precursor to **9**, which is a thermal decomposition product of both **BV** and **BDT**. [18]

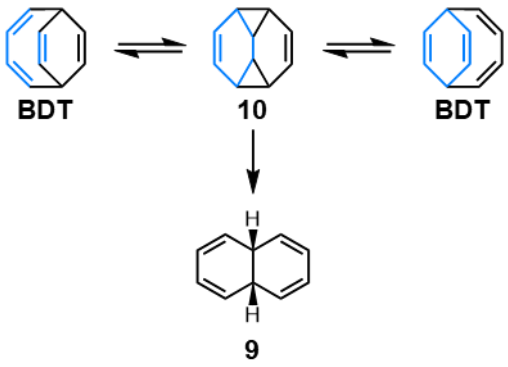

*Scheme 7: Thermal isomerisation of **BDT** and degradation to **9** via **10**.*

The first uses of **BDT** as a precursor to **BV** were published in 1967. Firstly, Scott *et al.* published an eight-step synthesis of **BV** (Scheme 8) starting with the cyclopropanation of **COTT** with methyl diazoacetate **16** to form methyl ester **17**, which was converted to the sodium salt of tosylhydrazone **18** in five steps. Thermolysis of **18** forms **BDT**, which photorearranges to yield **BV** in 64% yield. The relatively high yield of this step is the reason for the synthetic utility of **BDT**s as precursors to **BV**.[19]

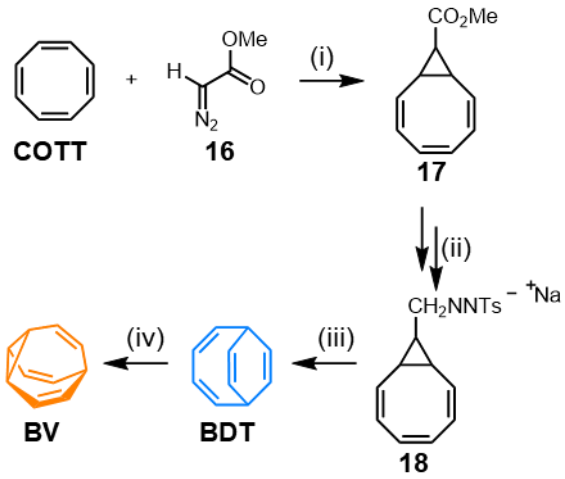

*Scheme 8: Scott et. al's 1967 synthesis of **BV** via **BDT**. (i) Cyclopropanation. (ii) five steps, via acid, acyl chloride, aldehyde and tosylhydrazone. (iii) 90–120 °C, 38%. (iv) h ν, 64%.*

This work, along with another 1970 report by Scott *et al.* hypothesised the rearrangements which occur from **18** to **BV** *via* **BDT**. Again, compound **10** was evoked as a potential intermediate in both the thermolysis of **18** and the photorearrangement of **BDT** to **BV**.[20] Krüerke's synthetic procedure (Scheme 9), also published in 1967, used the same rearrangement as its final step. Tricarbonylcyclooctatetraene iron **19** was refluxed in mesitylene with a disubstituted alkyne **20** to form BDT **21**. Photorearrangement of **21** resulted in the isolation of a viscous oil, with a temperature dependent ^{1}H NMR spectrum, which the authors stated "probably contained" BV **22**.[21]

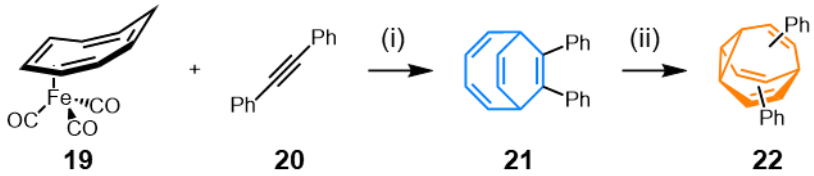

*Scheme 9: Krüerke's 1967 **BV** synthesis. (i) reflux, mesitylene, 35%. (ii) h ν, cyclohexane.*

The photorearrangement of **BDT** to form **BV** is an example of a di-π-methane rearrangement, a photochemical process which proceeds *via* a diradical transition state (Scheme 10) The mechanism of this rearrangement was first elucidated by Zimmerman *et al.*, as a rationale for the formation of semibullvalene from barrelene.[22–24]

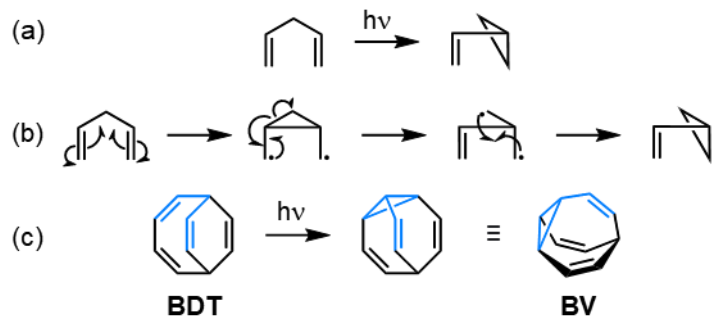

*Scheme 10: (a) Illustration of di-π-methane rearrangement. (b) Mechanism of the rearrangement. (c) Illustration of rearrangement on **BDT** to form **BV**.*[24]

The next novel synthesis of **BV** was published by von Eggers Doering *et al.* later in 1967. This involves a Buchner ring expansion on benzene using ethyl diazoacetate **23** to form cyclohepatriene ester **24** which is converted *via* the corresponding carboxylic acid and acyl chloride to α-diazoketone **25**. An intramolecular cyclopropanation is then performed to form barbaralone (**BBO**), a bistable fluxional molecule.[25–27] One-carbon homologation of **BBO** with diazomethane affords bullvalone (**BVO**) another bistable fluxional molecule. This was reduced and acetylated to give **26**. Pyrolysis of **26** at 345 °C yielded **BV** after eight synthetic steps, making this synthesis of **BV** with the most steps so far (Scheme 11).[28,29]

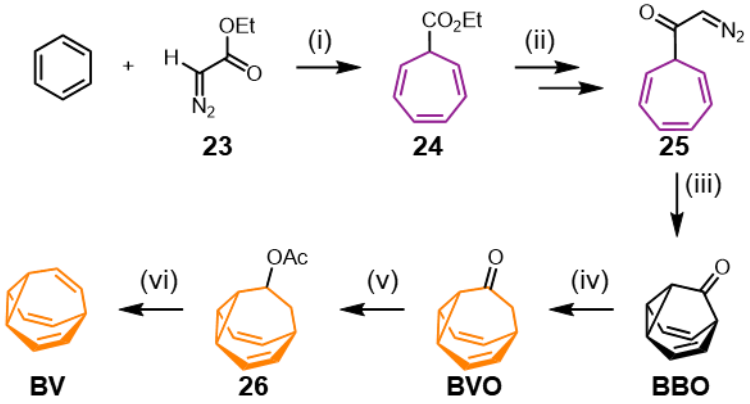

*Scheme 11: von Eggers Doering's 1967 synthesis of **BV**. (i) benzene, hν, reflux, 6–7 d. (ii)(a) H^+/ H_2O. (b) $SOCl_2$ (c) CH_2N_2, diethyl ether. (iii) $CuSO_4$, benzene/ hexane, reflux. (iv) CH_2N_2, diethyl ether, 25%. (v) (a) $NaBH_4$, diethyl ether. (b) Ac_2O, pyridine, 40%.*[28]

Schröder *et al.*'s review of **BV** chemistry in 1967 summarised much of this early research.[10] Also during this period, a substantial body of work was produced regarding the synthesis of substituted BVs, most of which rely upon bromination of **BV** followed by functional group interconversions (Scheme 12). A BV–Grignard reagent **27** was synthesised in 1971 by Schröder *et al.* and used to make carboxylic acid and ester substituted BVs **28** and **29**. Furthermore, dibullvalene **30** was synthesised by coupling **5** and **27**.[10,29,30]

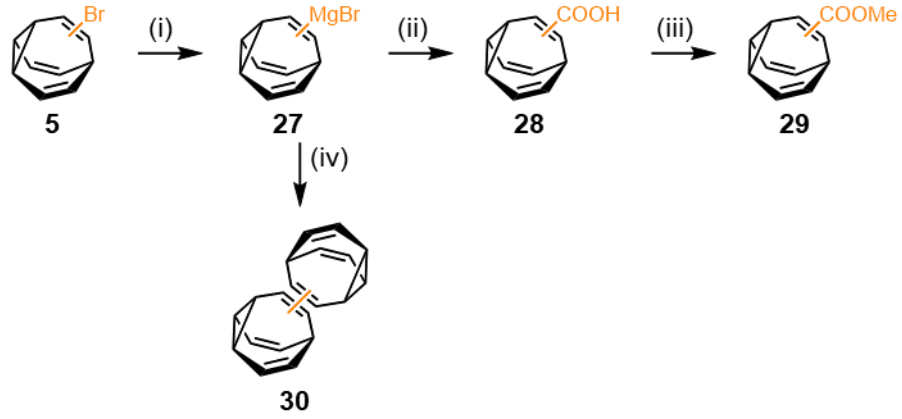

*Scheme 12: Schröder et al.'s Grignard **BV** synthesis and reactions. (i) Mg, (ii) CO_2, (iii) CH_2N_2. (iv) **5**, $CoCl_2$.*

Another Schröder report detailed the synthesis and analysis of annulated bullvalenes, formed using Diels–Alder reactions with dehydrobullvalene **6**. When tetraphenylcyclopentadienone **31** is used as the diene for the reaction, the direct Diels–Alder product, **32** was isolated (Scheme 13).

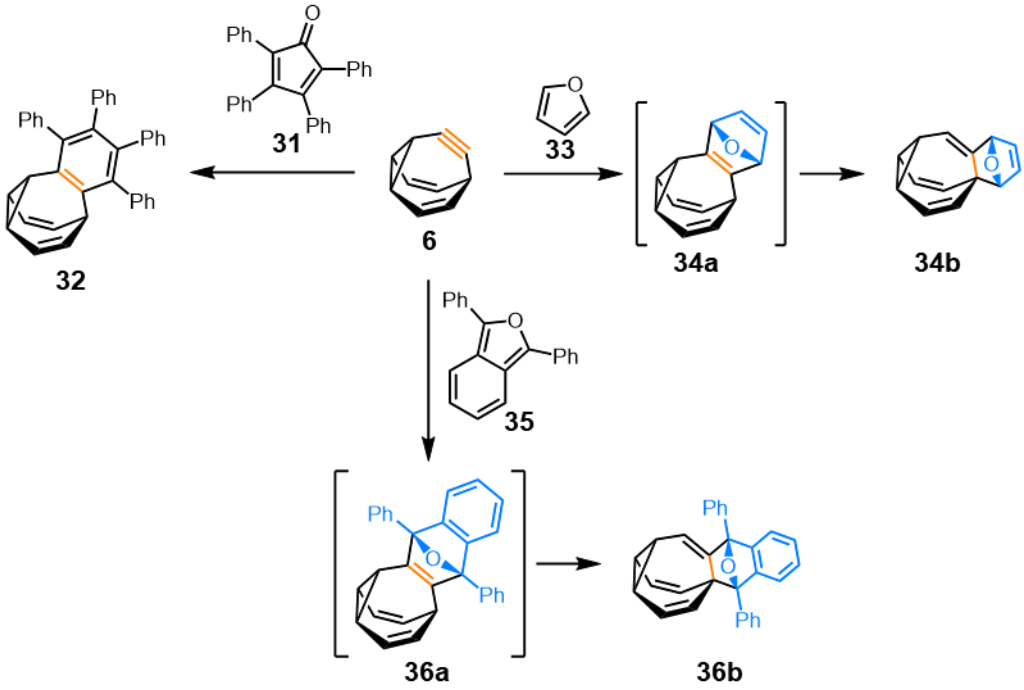

*Scheme 13: Schröder et al. synthesis of annulated BVs via Diels-Alder reactions with dehydrobullvalene **6**.*

However, when furan **33** or 1,3-diphenylisobenzofuran **35** are used instead, the direct Diels–Alders products **34a** and **36a** are not isolated due to the strain of the appended bicyclic systems. Instead, **34a** and **36a** undergo two Cope rearrangements rapidly and **34b** and **36b** are isolated as the final product. Both products exhibit temperature dependent ^{1}H NMR spectra due to rearrangements at elevated temperatures.[10,29,31]

Dibromo BV **37**, made *via* bromination–elimination of **5**, was also used to synthesise a variety of disubstituted BVs (Scheme 14). Reaction of **37** with sodium dicyanocuprate forms cyanobromo BV **38**, which may be converted to **39** over three steps. Cyanation of the other bromide on the bullvalene core results in **40**. This 1986 work exhibited some of the first heterodisubstituted BVs which have 30 isomers as opposed to 15 isomers for homodisubstituted BVs.[32]

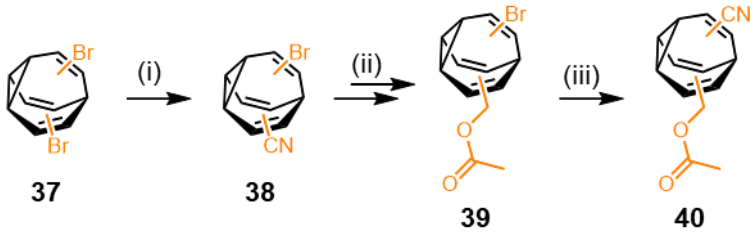

Scheme 14: Schröder et al. synthesis of heterodisubstituted BVs. (i)NaCu(CN)$_2$, DMF, 160 °C, 28%. (ii)Three steps. (a) to aldehyde, DIBAL-H, 95%. (b) to alcohol, LiAlH$_4$, −50 °C, 85%. (c) acetylation, Ac$_2$O, pyridine. (iii NaCu(CN)$_2$, DMF, 160 °C, 78%.[32]

Sequential bromination and elimination reactions have also been used to form polysubstituted BVs. Tri-, tetra-, penta-, and hexabromo BVs were all synthesised by Schröder *et al.* in 1993 as were their phenyl-substituted analogues.[33,34] Pentabromo BV underwent slower rearrangements, whereas both hexabromo and hexaphenyl BV lost their fluxional behaviour and were isolated as a single isomer, due to steric overcrowding on the BV core.[33,34]

The **BDT** intermediate, as seen in the syntheses published by Scott *et al.* and Krüerke, will serve as a cornerstone for future syntheses, as will the **BVO** and **BBO** intermediates published by von Eggers Doering *et al.*.[19,21,28] While earlier synthetic procedures rely upon rearrangements of unusual hydrocarbon structures (both thermally and photochemically induced), all synthetic pathways from 1967 onwards proceed *via* **BDT**, **BVO** or **BBO** intermediates, or some combination of the three.[2,19,21,28]

Figure 4: Structures of common intermediated BDT, BVO and BBO.

Serratosa *et al.'s* **BV** synthesis, reported in 1972 consists of diester **41** undergoing a Wittig reaction with **42** to form triester **43**. Subsequent reduction of this alkene forms the triester **44**. Hydrolysis and chlorination of **44** forms tri acyl chloride **45**, which is treated with diazomethane to form tri α-diazoketone **46**. The distinctive feature of this synthesis is the cyclisation of **46** using $CuSO_4$ and thioanisole to form **47**.

Dimerisation of α-diazoketones is well documented, but with the introduction of thioanisole, trimerization in the form of cyclopropanation also occurs readily.[35,36] Although the yield for this step was only 2%, it was increased to 4% with the use of copper chelates as a catalyst instead of $CuSO_4$.[37] Reaction of **47** with *p*-toluenesulfonyl hydrazide forms **48**, which is then subjected to a Shapiro reaction to yield **BV**. This eight-step synthesis has a total yield of 0.3% (Scheme 15).[37,38]

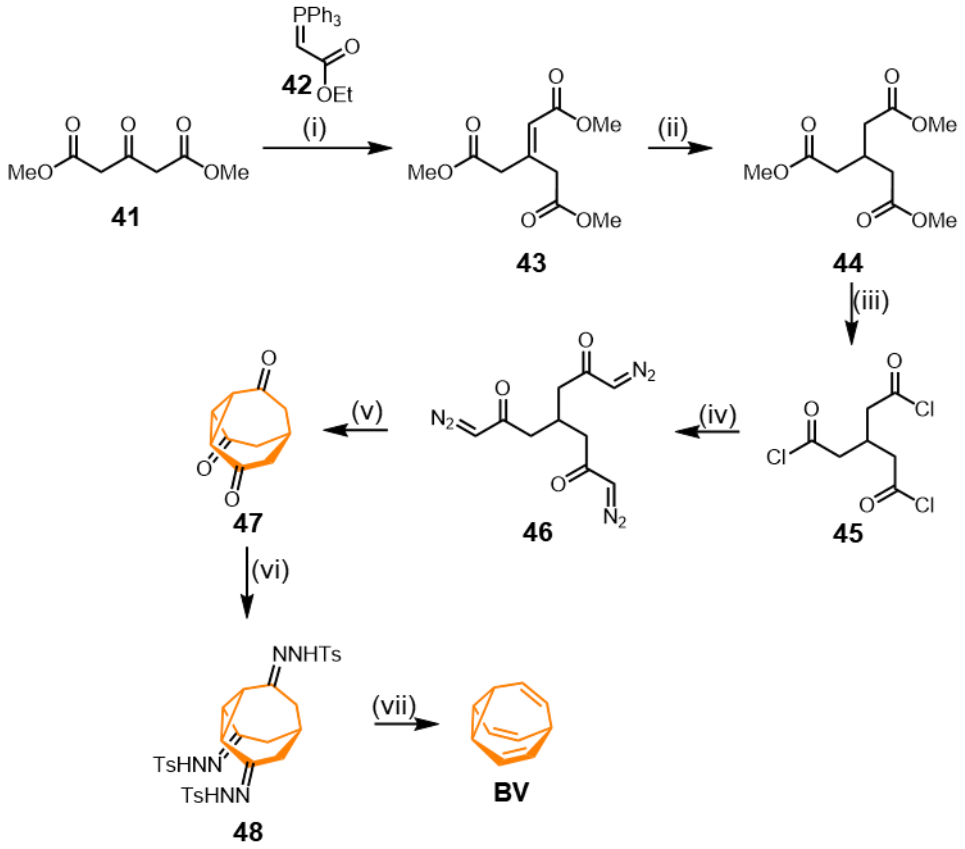

*Scheme 15: Serratosa et al. 1972 **BV** synthesis. (i) benzene, 76%. (ii) PtO_2, H_2, 92%. (iii) hydrolysis, then PCl_5, 85% over two steps. (iv) CH_2N_2, 64%. (v) Cu chelates, PhSMe, xylene, 4%. (vi) $TsNHNH_2$, AcOH. (vii) MeLi, benzene, 23 °C, 20%.*[37]

Serratosa *et al.* published another synthetic procedure in 1977 (Scheme 16). Compound **25**, a precursor in von Eggers Doering's 1967 synthesis was cyclised using Cu(acac) to form **BBO**, and a one carbon homologation with diazomethane afforded **BVO**. Both of these steps were performed in von Eggers Doering's aforementioned 1967 synthesis, however, when subjected to *p*-toluenesulfonyl hydrazide, **49** formed after an unexpected rearrangement of the carbon cage.[28,29,39] The rearranged product undergoes a Shapiro reaction, yielding **BDT**, which is subsequently irradiated to form **BV**, as in Scott's 1967 synthesis.[38,39]

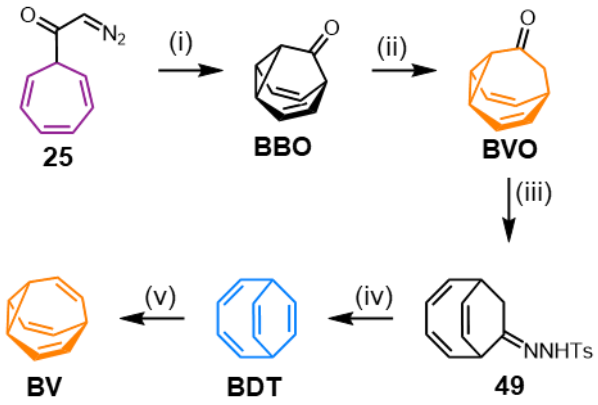

*Scheme 16: Serratosa et al.'s 1977 synthesis of **BV**. (i) Cu(acac), benzene, 80 °C, 36–48%. (ii) CH_2N_2, Et_2O, 0 −4 °C, 24%. (iii) p-$TsNHNH_2$, AcOH, 70%. (iv) MeLi, benzene, 0 °C, 36%. (v) h ν, pentane, 82%.*[39]

One might assume, from observing Serratosa's 1972 synthesis, that the intention was to form a tosylhydrazone BVO similar to **48** from **BVO**, with the possibility to perform a Shapiro to form **BV**. This is similar to the strategy from Serratosa's 1972 synthesis, forming **BV** from bullvalenetrione **47** *via* **48** (Scheme 15). However, a rearrangement yielding **49** prevented this pathway.[37,39] The proposed mechanism of this rearrangement (Scheme 17) begins with **50**, after the tosylhydrazide has attacked the **BVO**. The loss of a molecule of water allows the strain of the cyclopropane to be released, forming carbocation **51**. Compound **51** then loses a proton, with a simultaneous rearrangement to form **52**: a structure that is similar to **10,** which undergoes (Scheme 7) a retro-Diels–Alder to yield **49**.[29,39]

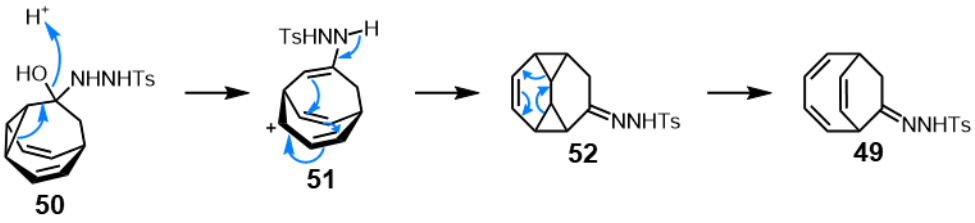

*Scheme 17:Mechanism for rearrangement of **BVO** to **49** when reacted with tosylhydrazone.*[29]

No new syntheses were published between 1977 and 2009, when Bode *et al.* published their 11-step synthetic procedure for **BV** (Scheme 18). Cycloheptanone **53** is converted in six steps to **54** in 20% yield. **54** is then reacted with sulfur ylide **55** to yield **56** which undergoes an intramolecular cyclopropanation, catalysed by polymer-bound scandium triflate. The resulting compound **57** resembles **47** from Serratosa *et al.*'s 1972 synthesis (Scheme 15). Reaction of this compound with allyl magnesium bromide results in two products, **58a** and **58b** in a 3:2 ratio. The *meso*-isomer **58a** is treated with pyridine and thionyl chloride to yield trisubstituted BVO **59**, conversely the chiral isomer **58b** is treated with diisopropylethylamine (DIPEA) and thionyl chloride, to which pyridine is added later to yield **59**. Finally, isobutyl chloroformate is used in an enolate trapping to give BV **60**, which has 860 unique isomers.[40–42]

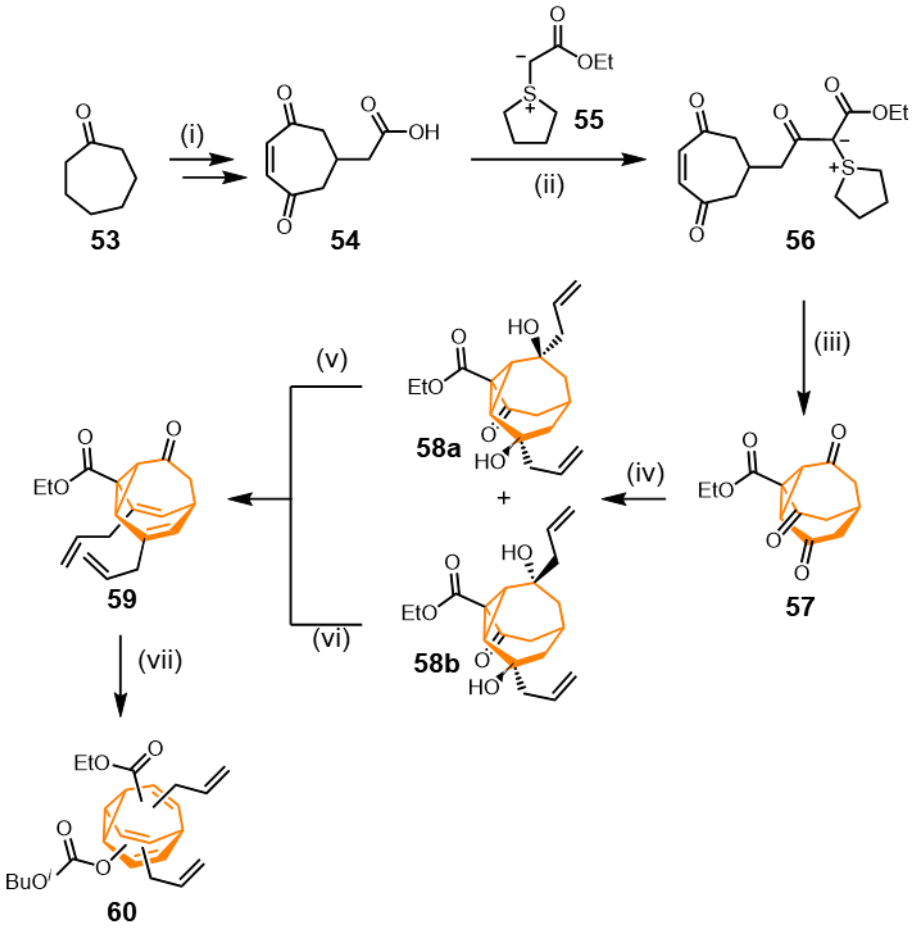

Scheme 18: Bode et al. BV synthesis. (i) six steps, 20%. (ii) ^{i}BuOCOCl, DIPEA, 77%. (iii) Sc(OTf)$_3$, PhCl, reflux, 69%. (iv) allyl magnesium bromide, CH_2Cl_2, −78 °C, 76% (3:2). (v) pyridine, $SOCl_2$, CH_2Cl_2, −78 °C, 60–70%. (vi) DIPEA, $SOCl_2$, then pyridine, CH_2Cl_2, −78 °C, 40%. (vii) ^{i}BuOCOCl, LiHMDS, THF, −78 °C to rt, 80%.

In 2011, Bode *et al.* published another similar synthesis, this time resulting in the first heterotetrasubstituted BV **64** (Scheme 19).[43,44] Phenyl magnesium bromide was added to **57** to form **61**, which was eliminated using pyridine and thionyl chloride. Allyl

magnesium bromide was then added to yield **62**, which was subsequently eliminated to form **63**. This elimination is accompanied by a Cope rearrangement in the bistable fluxional BVO cage to form the second isomer, hence the migration of the ester group. Just as in the previous example, the BVO **63** is trapped in its enolate form by the addition of isobutyl chloroformate to yield BV **64**. To date, this compound is the BV with the most unique isomers that has been synthesised (1680).[43,44]

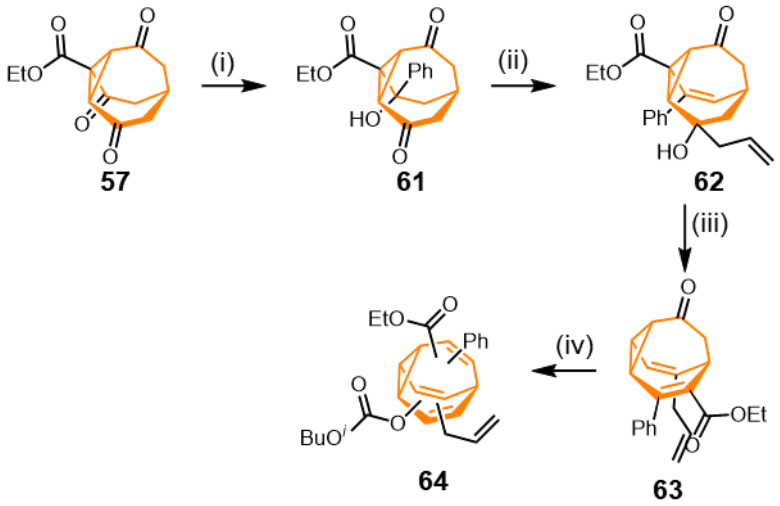

*Scheme 19: Bode et al. synthesis of heterotetrasubstituted BV **64**. (i) PhMgBr, CH_2Cl_2 −78 °C, 65%. (ii)(a) Pyridine, $SOCl_2$, CH_2Cl_2, –78 °C. (b) allyl magnesium bromide, CH_2Cl_2, −78 °C, 29% over two steps. (iii) DIPEA, $SOCl_2$, pyridine, CH_2Cl_2, –78 °C, 27%. (iv) ^{i}BuOCOCl, LiHMDS, THF, CH_2Cl_2, −78 °C to rt, 40%.*

Echavarren *et al.* published the next synthesis (Scheme 20) for BV starting from **65a**/**b** which may be synthesised from tropylium tetrafluoroborate in a single nucleophilic attack using a Grignard reagent. Gold-catalysed oxidative cyclopropanation of **65a**/**b** forms **66a**/**b**, BBOs which undergo one-carbon homologations to form BVOs **67a**/**b**. Enolate trapping of BVOs **67a/b** forms BVs **68a/b** which may be reduced with palladium catalysis in the presence of $^{n}Bu_3SnH$ to form BVs **69a**/**b**.[29,45,46]

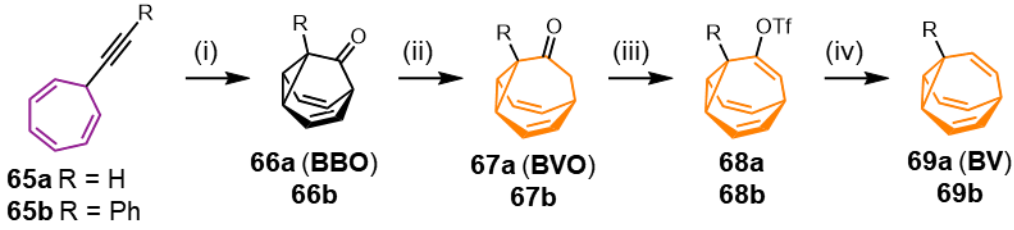

*Scheme 20: Echavarren et al.'s synthesis of **BV**. (i)$[IPrAuNCMe]^{+}[SbF_6]^{-}$, CH_2Cl_2, Ph_2SO, 23 °C, **66a** = 97% **66b** = 83%. (ii) $TMSCHN_2$, ^{n}BuLi, MeOH, SiO_2, Et_2O, THF, −78 to 23 °C, **67a** = 37% **67b** = 22%. (iii) **68a** = LiHMDS, $PhNTf_2$, THF, −78 to 0 °C. **68b** = LDA, 5-ClPyNTf$_2$, THF, −78 to 0 °C. (iv) $^{n}Bu_3SnH$, LiCl, $Pd(PPh_3)_4$, THF, 23 °C. **69a** = 44% over two steps. **69b** = 60% over two steps.*

Also detailed in this paper is the possibility for late stage functionalisation of **68b** to form disubstituted BVs (Scheme 21). **68b** is a candidate for a Stille coupling with the triflate group and three different stannanes were used to yield **22**, **70** and **71**.[46,47]

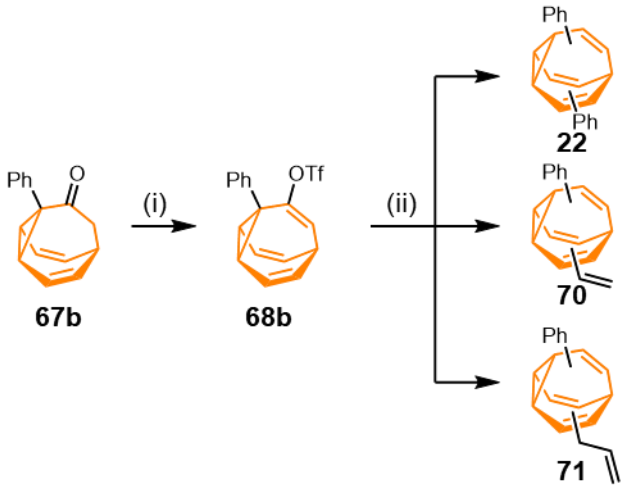

Scheme 21: Echavarren et al.'s synthesis of disubstituted BVs. (i) LDA, 5-ClPyNTf$_2$, THF, −78 to 0 °C. (ii) ^{n}Bu$_3$SnR, LiCl, Pd(PPh$_3$)$_4$, THF, 60 °C. ***22*** *R = phenyl,* ***15%*** *over two steps.* ***70*** *R = vinyl, 58% over two steps.* ***71*** *R = allyl, 37% over two steps.* [46,47]

The previous two synthetic methods from Echavarren and Bode are capable of functional group alterations on the BV at different stages of the synthetic procedure. Variation of substituents allows for addition of functionality to the BV structure which may be applied to various uses. Although, addition of this functionality has proven difficult due to the limitations of older synthetic procedures. Fallon *et. al* published a two-step synthesis of **BV** in 2018, with a wide array of substituents (Scheme 22). Firstly, a Co(I)-catalysed [6+2] cycloaddition between **COTT** and alkynes **72** forms the **BDT** framework and subsequent photorearrangement of **BDT** forms **BV**.[48,49]

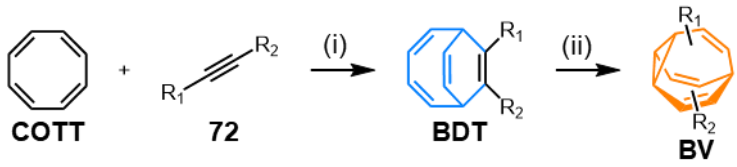

Scheme 22: Fallon et al.'s 2018 ***BV*** *synthesis.(i) CoBr$_2$(dppe) 10 mol%, ZnI$_2$ 20 mol%, Zn Dust 30 mol%, DCE or TFE, rt or 55°C, 24–48 h.63–100%. (ii) h ν, acetone, rt, 16–24 h, 35–81%.*[48,49]

This synthetic method is a significant advancement in the field, as it allows for a range mono- and disubstituted BVs as well unsubstituted **BV** to be synthesised in two simple steps with a reasonable yield. The first step is derived from work published by Buono *et. al* in which **COTT** and cyclooctatriene (**COT**) were both used in cycloadditions with alkynes **72**.[48]

The addition of ZnI_2 and Zn to the $CoBr_2$(dppe) catalyst **73** accelerates the reduction of the catalyst to its active Co(I) state **74**. This occurs *via* the formation of a Co–Zn binuclear complex **75**, which has a weaker Co–I bond and is more easily reduced to the active catalyst **74** as a dimer (Scheme 23).[48,50,51]

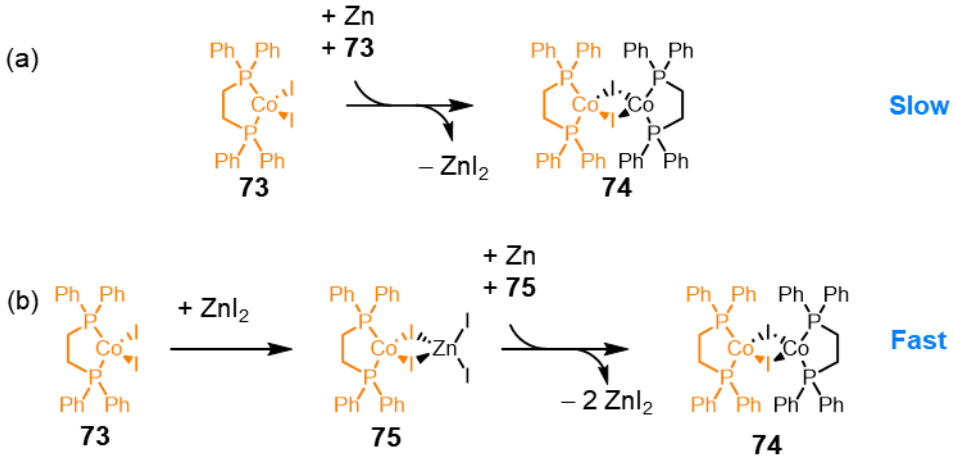

Scheme 23: Activation of Co(II) catalyst compared (a) without ZnI_2 and (b) with ZnI_2.[50]

The active Co(I) species **74** can then partake in the catalytic cycle of the [6+2] cycloaddition (Figure 5). This cycloaddition proceeds *via* either route A or route B; both mechanisms begin with the complexation of the active Co(I) catalyst **74** to **COTT**, forming $[\eta^6$-(**COTT**)$CoL_2]^+$, **76**. The two mechanisms only differ on the introduction of the alkyne. Route A suggests that complex **76** undergoes oxidative cyclometallation to form **77**. The alkyne then inserts into one of the Co–C bonds, resulting in cobaltacycle **78**. Reductive elimination yields **BDT** from **78** and restores the active form of the Co(I) catalyst. Route B differs in that it suggests that the hapticity of the Co–COTT complex changes upon addition of the alkyne, with the formation of complex **79** $[\eta^4$-(**COTT**) η^2-(alkyne)$CoL_2]^+$. The cyclometallation of **79** now involves the alkyne, yielding cobaltacycle **80**, which undergoes a 1,5-migration via σ-π-allyl complex **81**, which undergoes reductive elimination to yield **BDT** and the active catalytic species **74**.

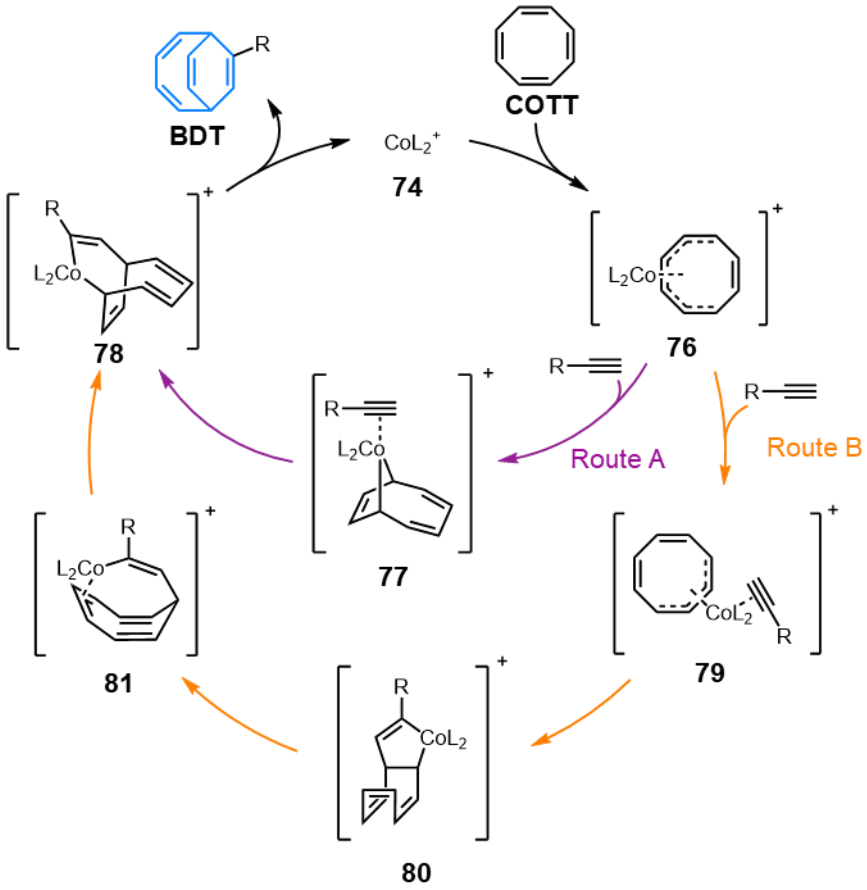

*Figure 5: The catalytic cycle for Co(I)-catalysed [6+2] cycloaddition between **COTT** and an alkyne.*[48]

In this 2018 report by Fallon *et al.*, phenylacetylene was one of the alkynes used which yielded a phenyl substituted BDT **82** in a 63% yield, however, the authors were unable to convert this BDT to phenyl-substituted BV. Instead, the photorearrangement yielded a phenyl-substituted lumibullvalene **84**. This investigation suggests that following an errant di-π-methane rearrangement phenyl "isolumibullvalene" **83** forms instead of the desired BV. Subsequently, a strain promoted Cope rearrangement occurs to yield **84** in 63% (Figure 6).[49]

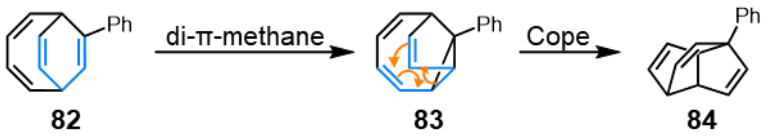

*Figure 6:Proposed degradation of phenyl BDT **82** to **84**.*

This rearrangement precludes the formation of aryl BVs from aryl alkynes in two steps and suggests that another route is necessary to synthesis aryl BVs. Fallon *et al.* reported an alternate route two years later in 2020; by including boronate esters in the

alkynes and BDT precursors. Boronate ester BVs may be used to synthesise aryl BVs *via* a Suzuki–Miyaura cross coupling, after photorearrangement.[52–54]

This publication details the use of mono-Bpin acetylene **85** to yield mono-Bpin BDT **86**, as well as bis-Bpin acetylene **87** to form bis-Bpin BDT **88**. One of these Bpin groups in **88** may also then be substituted for a B_{MIDA} group, **89** which allows for the synthesis of heterodiaryl BVs due to its decreased reactivity compared to Bpin groups.[55] Furthermore, bromination of **COTT** and subsequent borylation to **90** allows for the synthesis of tris-Bpin BDT **91**. All of these BDTs, **86**, **88**, **89** and **91** may be photorearranged to the corresponding BV, and then coupled with aryl halides to form aryl BVs (Scheme 24).[54]

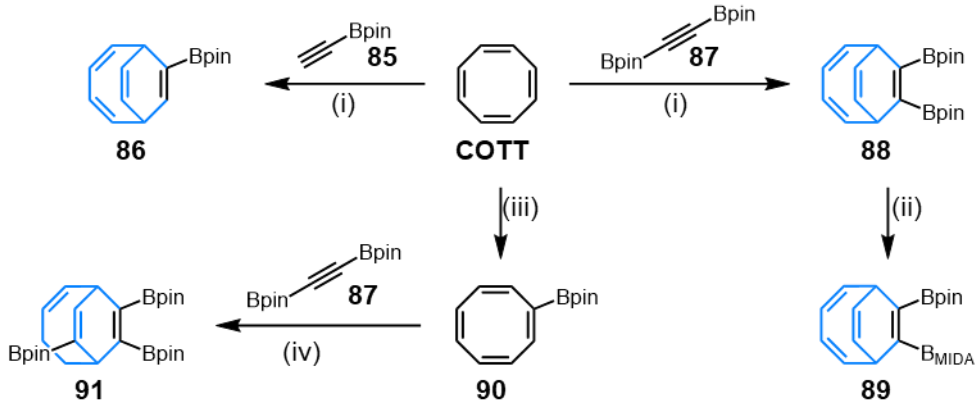

*Scheme 24:Fallon et al.'s synthesis of boronate ester BVs. (i) $CoBr_2$(dppe) 10 mol%, ZnI_2 20 mol%, Zn Dust 30 mol%, DCE, rt, 24 h. **86** = 79%. **88** = 74%. (ii) MIDA, DMSO, 120 °C, 8 h, 51%. (iii)(a) Br_2 then KO^tBu, −78 °C to rt, 94%. (b) ^{n}BuLi, then MeOBpin, −78 °C to rt, 65%. (iv) $CoBr_2$(dppe) 50 mol%, ZnI_2 100 mol%, Zn Dust 150 mol%, DCE, rt, 24 h, 36%.*[54]

The photorearrangement step in BV synthesis was also optimised in this 2020 publication. Instead of using acetone as both the solvent and a photosensitiser, the reaction was carried out in THF with thioxanthone **92** as a photosensitiser (Scheme 25). As well as more consistent, higher yields, this optimisation also increases the reaction rate, leading to completion within six hours, as opposed to 24.[54,56]

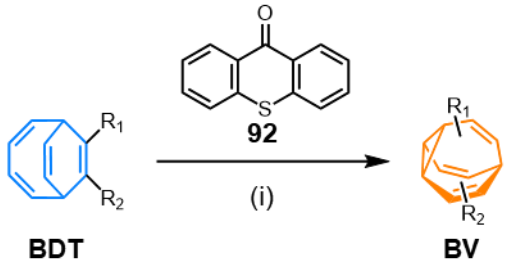

*Scheme 25: Optimised photorearrangement of **BDT** to form **BV**. (i) thioxanthone, **92** (1 mol%), THF, rt, 6 h, 55–97%.*[54]

Since 1963, BV synthesis has presented a great challenge to synthetic chemists. Many creative routes were conceptualised and performed. More recent methods involving (**BDT** and **BBO**/ **BVO** intermediates) have drawn heavy inspiration from earlier syntheses. The yields have, however, improved ten-fold since the first attempts of von Eggers Doering and Schröder. Clearly the simplicity of Fallon's synthesis compared to that of previous iterations will make BV synthesis much more facile while also potentially producing a new wave of research into properties and functions of BV.

Recently, this boronate ester BV publication has been the basis for BV synthesis in multiple papers from different groups studying BV's behaviour and uses in many different conditions. One publication, for example, served as the basis for the synthesis of the first BV embedded polymer in 2023 (Scheme 26). Bis-Bpin BV **93** was coupled with dibromide **94** to make alternating copolymer **95**, which will be discussed in section 1.6 more detail.[57]

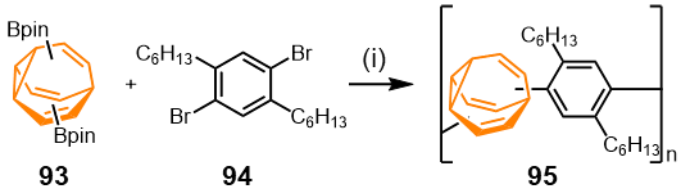

93 **94** **95**

*Scheme 26: First synthesis of BV polymer **95**. (i)XPhos Pd G3, K_3PO_4, PhMe, 60 °C.*

1.4. Bullvalene Terminology and Visualisation

BV has three different 1,5-hexadiene moieties on its three faces, which may undergo Cope rearrangements (Figure 7). This means that each isomer may rearrange to form up to three different covalent structures. Every single possible configuration of the ten methine positions on the **BV** structure are always interchangeable with one another through sequential Cope rearrangements in one network. An example of interconverting isomers is presented below.

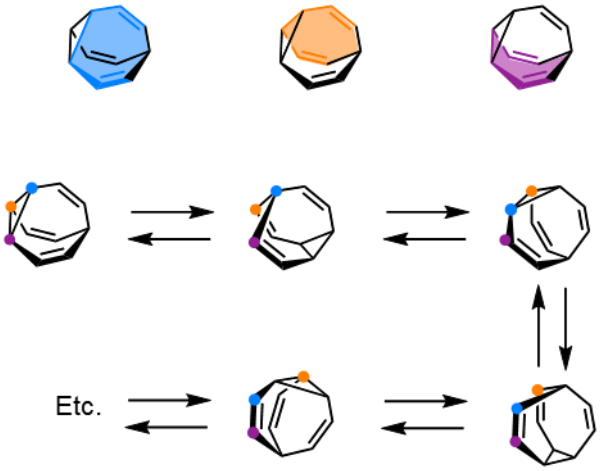

*Figure 7: **BV**'s three faces for rearrangement. An example of four sequential **BV** rearrangements interconverting isomers.*

In order to comprehend this complex fluxional system more easily, it is important that the methods of communication be clear and succinct. For this reason, appropriate conventions and terminology must be created and understood.

The first such system is Bode *et al.*'s barcode system for isomer identification (Figure 8). Introduced for the first time in 2013, these barcodes are ten-digit numbers in which each number represents an individual carbon atom on the **BV** structure. These numbers are grouped into three sets of three numbers, representing the three bridges, and one lone number representing the apical bridgehead carbon.[44]

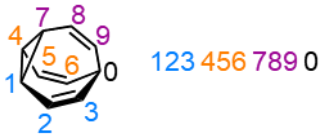

*Figure 8: Isomer barcode system for **BV**.*

When using this system to denote individual isomers, firstly the substituents should be numbered using the Cahn–Ingold–Prelog priority rules.[58] Then, using these assigned priority numbers for each substituent (and 0 for hydrogen atoms), isomers may be denoted. A key consideration in this barcode system is the C_{3v} symmetry of **BV**—a result of all three bridges being equivalent. As a result, positions 1,4 and 7 in the barcode are indistinguishable, as are positions 2, 5 and 8, and positions 3, 6 and 9. Thus, when using this barcode system for each **BV** isomer, there are three possible representations, all related to one another by a simple rotation. The code which has the lowest value is the correct code (Figure 9).[44]

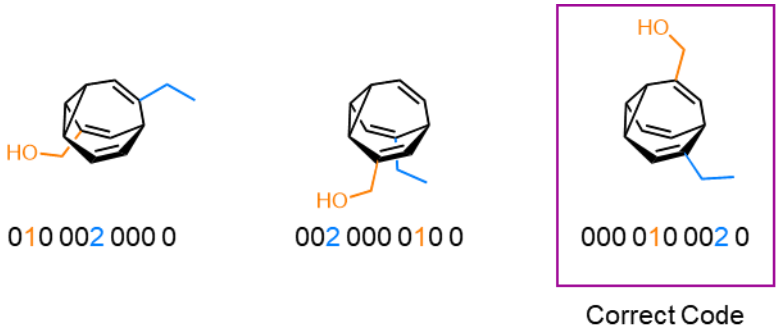

*Figure 9: An example of three possible codes for one **BV** isomer.*

Bode *et al.* refer to the advantages of this isomer barcode system in their publication: "The advantages of these codes included their capacity to (i) convert **BV** isomers to arrays of numbers that can catalogue their distinct structures, (ii) carry out Cope rearrangements *via* computer, (iii) translate numeric codes back to isomer structures, and (iv) distinguish between enantiomers." **BV** enantiomer pairs are identified in the barcode system as isomers where exactly two bridges may be swapped to give a new code (Figure 10a). This is as opposed to all three of the bridges rotating in the same direction, which does not alter the structure.

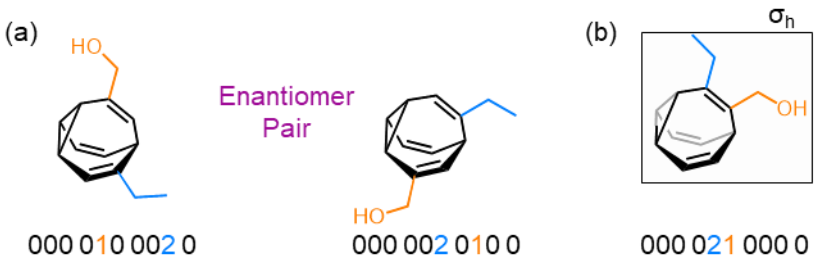

*Figure 10: Example of isomer barcodes for a pair of **BV** enantiomers*

This method of designating enantiomer pairs and finding the correct code for each isomer raises an interesting observation for **BV** in general; an isomer of **BV** can only be chiral if all three bridges are different from one another. This is a consequence of the fact that if any two of a **BV**'s bridges are identical, there will always be a mirror plane down the centre of the molecule (Figure 10b).

The topic of chirality in a **BV** molecule is explored in greater detail by Fallon *et al.* in a 2021 publication.[59] In this paper, Fallon *et al.* detail the assignment of **BV** isomers as either *P* or *M* in their helical chirality, or alternatively as achiral. Firstly, each bridge must be given a priority, 1st, 2nd and 3rd. This is done by determining which bridges have substituents closest to the cyclopropyl bridgehead. For equivalently positioned substituents, the Cahn–Ingold–Prelog priority rules are used. Subsequently, following

the rotation of the bridges from 1st to 3rd will either be a clockwise (*P*) or anti-clockwise (*M*) rotation (Figure 11).[59]

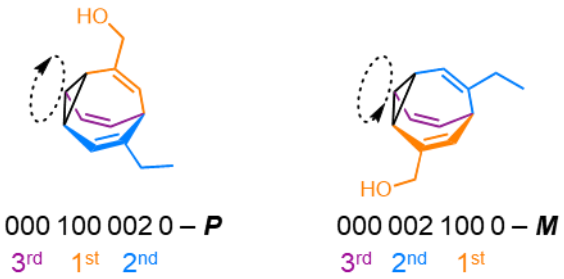

Figure 11: Assigning chirality of an example enantiomer pair.[59]

Racemisation of **BV**s is an inevitable outcome of its fluxional nature. The compounds in Figure 11 for example, are two enantiomers which are related through just three Cope rearrangements. Racemisation of a **BV** was the basis of two publications from Bode *et al.*. Due to the synthetic procedure used (Scheme 18 and Scheme 19), one specific isomer is formed first, which then equilibrates through Cope rearrangement to a distribution of different isomers at room temperature.[43,59] BV **64** was purified by preparative HPLC and other than a chiral impurity (fraction a), the rest of the fractions from the purification exhibited no signal in the circular dichroism spectrum. Furthermore, upon analysis by HPLC, each fraction exhibited a similar plot to the initial HPLC. These analyses show both that the BV isomeric distribution is racemising (resulting in no signal in the circular dichroism spectrum), and that even after separation by chromatography, the individual BV isomers are equilibrating again to the same room temperature distribution. This publication reinforces the image of BV as a rapidly rearranging, robust fluxional framework (Figure 12).[43]

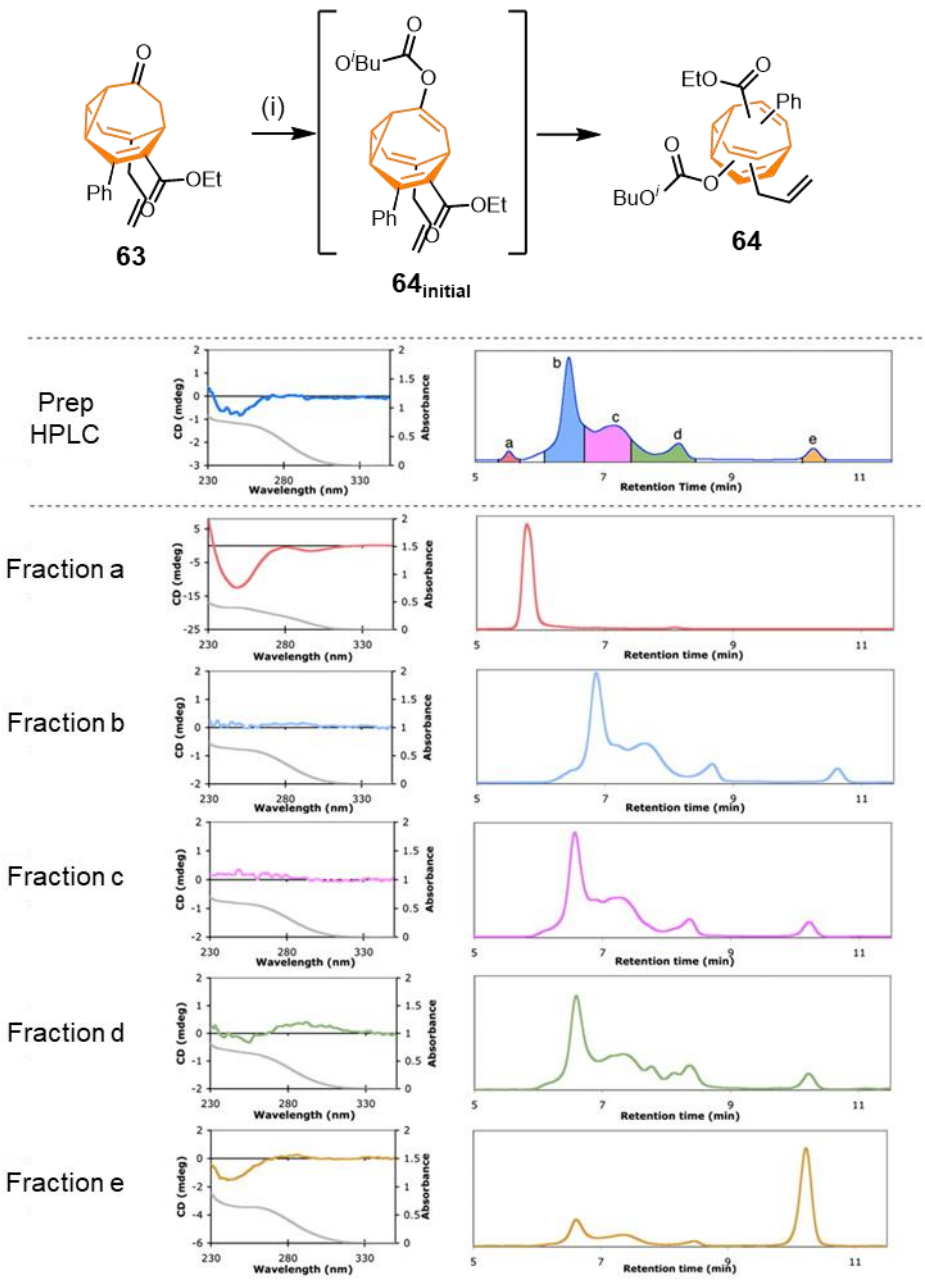

Figure 12: Bode et al. purification of BV isomer distribution. (i) ^{i}BuOCOCl, LiHMDS, THF, CH_2Cl_2, −78 °C to rt, 40%. Figure reproduced from publication.[43]

A remarkable finding in this work was that fraction e did not equilibrate after ten hours, while fractions b–d did. This is in accordance with the earlier observation that pentabromo **BV** rearranges more slowly and hexaphenyl **BV** is non-fluxional.[33,34] In a later publication, fraction e was isolated and analysed in order to elucidate which isomer it represented. Computational analysis of this compound's relative energy and that of its close relatives elucidated the three neighbouring isomers to e, all at higher energies. Furthermore, each of the six isomers which these three isomers form are less stable isomers. As a result, fraction e is in a second generation kinetic energy well, and hence has an observed half-life of 256 minutes—significantly higher than usual.[44]

This publication also emphasises the interconversion network of **64**, in order to annotate the pathway through which the initial isomer **64**$_{initial}$ rearranges to form the isomer in fraction e. Interconversion networks are a graphical illustration of BV rearrangement consisting of nodes (representing isomers), and lines between nodes (representing Cope rearrangements). The network for this system is large and complex, with 1680 isomers present. Bode *et al.* arranged them to illustrate the relationship of each node to fraction e, where each outer ring is one further Cope rearrangement away from e. The result was that 12 rearrangements must occur for the initial isomer **64**$_{initial}$ to form the isomer from fraction e, **64**$_{e}$, and that **64**$_{e}$ is related to its enantiomer through 12 further rearrangements (Figure 13).[44]

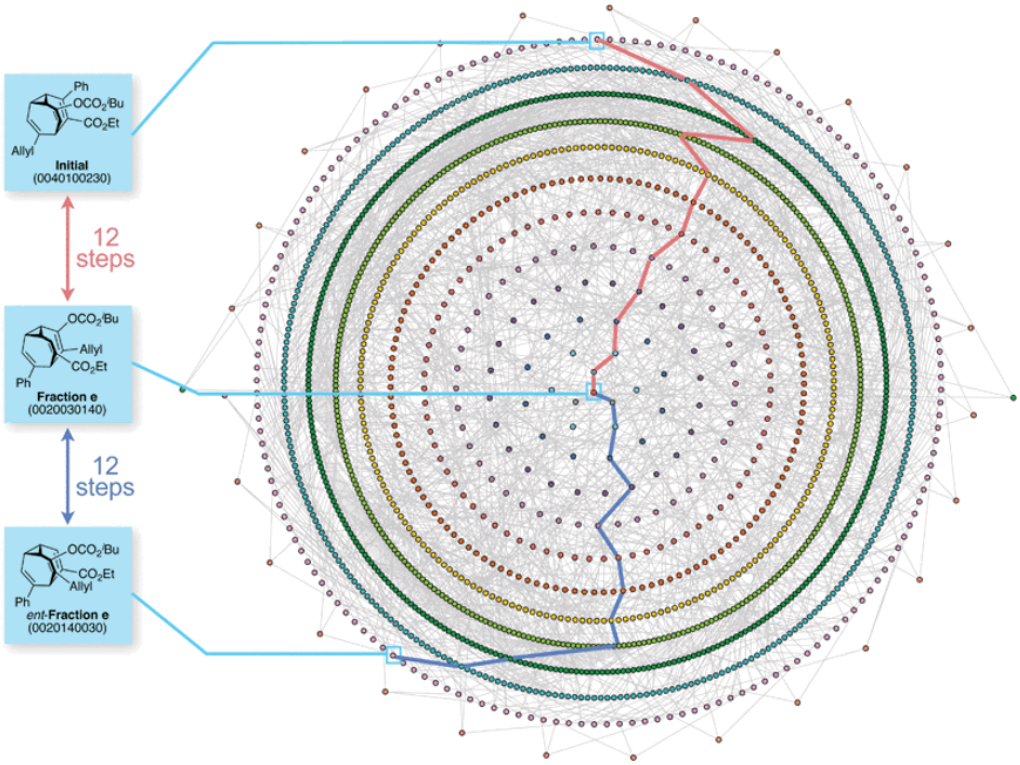

Figure 13: Bode et al. interconversion network with initial isomer, fraction e and fraction e's enantiomer labelled. Figure reproduced from publication.[44]

Whilst this example is by far the most complex interconversion network published, it is far from the first iteration of BV network analysis.[60–63] The first example of a BV interconversion network was published by Brant *et al.* in 1994. This publication illustrates interconversion networks for mono-, di-, tri- (Figure 14), tetra- and penta-substituted BVs where the substituents are identical. Further, Brant *et al.* organised the nodes in these networks such that achiral isomers are down the central mirror

plane, while the enantiomers of each isomer are related by this mirror plane, either side of the line.[60]

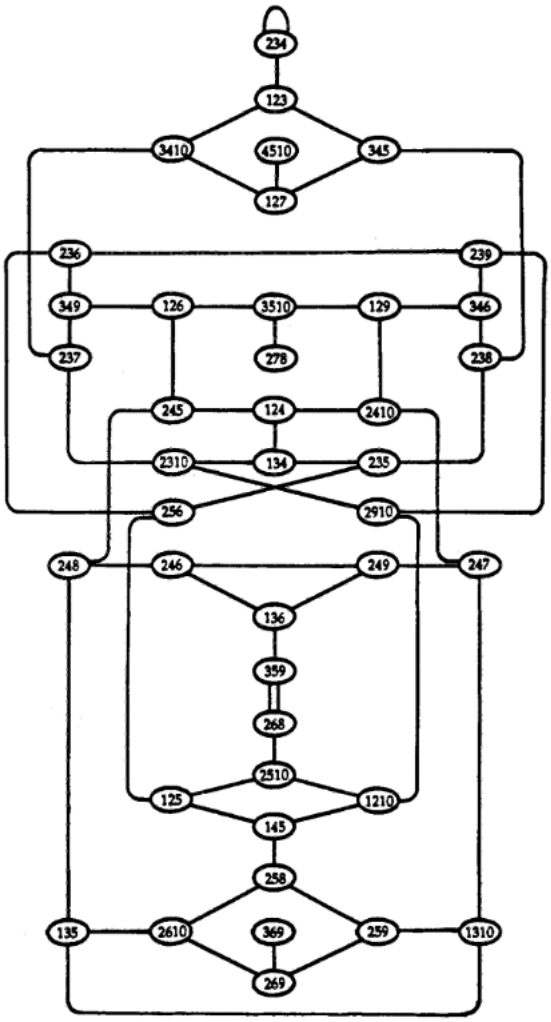

*Figure 14: Brant et al.'s interconversion network for a homo trisubstituted **BV**. Figure reproduced from publication.*[60]

Interconversion networks are an elegant method for visualising a complex natural system, and have become the standard for illustration of **BV** systems. Recently, other data regarding BVs have been included in interconversion networks, making these already intelligently designed networks more informative. An example of this can be seen in a 2019 publication from Fallon *et al.*, where the nodes and lines are colour coded to display isomers relative energies, and that of the rearrangements' transition states (Figure 15).[64]

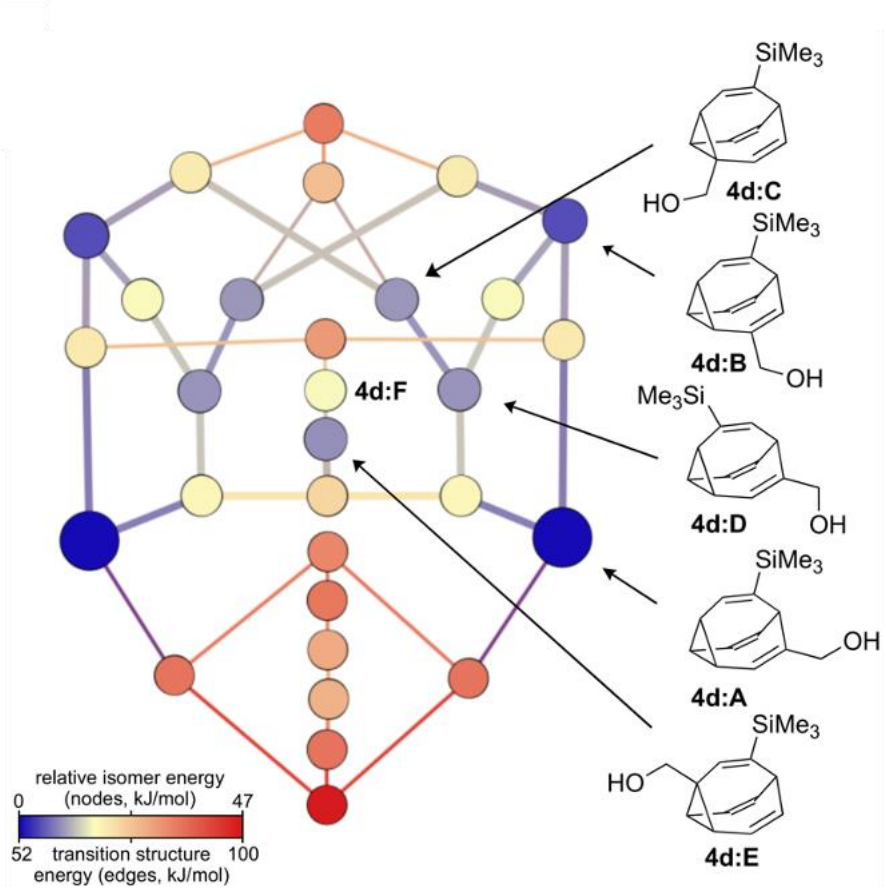

Figure 15: Fallon et al. interconversion network, including relative energies for BVs and transition states. Figure reproduced from publication.[64]

1.5. Properties of Bullvalenes

The nature of BV's rearrangements has been the topic of extensive research since its conception, such as the rate at which is rearranges with and without substituents.[65–67] One question that was posed early on is whether or not these rearrangements are limited in the solid state. Early studies measured the line width of signals in the solid-state ^{1}H NMR spectrum as a function of temperature, and found that upon increasing the temperature from −140 to 100 °C, the linewidth shortens drastically between 0 and 60 °C. This was hypothesised either as an example of BV's valence isomerism or potentially BV acting as a "plastic crystal", by displaying molecular reorientation in the crystal lattice.[68] However, two papers published slightly later suggest that the crystal lattice of BV at room temperature is too well-defined to be undergoing Cope rearrangements at this temperature.[69,70] It was only in 1985 when Earl *et al.* published a study probing the cross polarisation-magic angle spinning ^{13}C NMR spectra at varying temperatures that it was found **BV** does rearrange in the solid state.[71] At higher

temperature (358 K) one single peak was observed, which became an array of well-defined peaks at lower temperature (213 K). This single proton environment observed suggests that Cope rearrangements are still occurring in the solid state. This study also states that—due to the shift of the high temperature peaks being exactly at the weighted average of the low temperature peaks—the degeneracy of the Cope rearrangements is preserved. In conclusion, Cope rearrangement in lower temperature solid samples of **BV** are combined with rotation of the whole molecule, such that the translational symmetry of the crystal is maintained.[71] A pair of papers published in 1992 postulated that two independent dynamic processes were taking place: firstly, a symmetric threefold jump of the **BV** molecule, and secondly a combination of Cope rearrangement and molecular reorientation. These processes are aided by the globular shape of the molecule.[72,73]

Another challenge to **BV**'s rearrangements was a silver–**BV** complex formed by Gutowsky *et al.* complex using silver nitrate. This publication describes that the activation energy for the rearrangement in the presence of silver was significantly higher (15.1 ± 0.8 kcal·mol^{-1}) than that for **BV** free in solution (12.8 ± 0.1 kcal·mol^{-1}). The authors suggested, this was either due to: (i) the rearrangement of the silver-bound **BV** being less energetically favourable, or (ii) the rearrangement would not occur when bound to the metal centre, but instead proceeding *via* a dissociation, rearrangement, and reassociation pathway.[67] Paul *et al.* formed the first published crystal of a silver-**BV** complex, discovering a 1:3 ratio in the solid state with a tetrafluoroborate counterion (Figure 16). Of the three molecules of **BV**, one has two of the olefin bonds joined to the metal centre, and the other two molecules have just one olefin bound to the metal centre. In the conclusion of this publication the authors state that the slight disorder observed in the crystal structure may be due to the fact that two of the **BV** molecules in the crystal only have one olefin bound, and so may potentially still rearrange on the opposite, unbound face.[67,74,75]

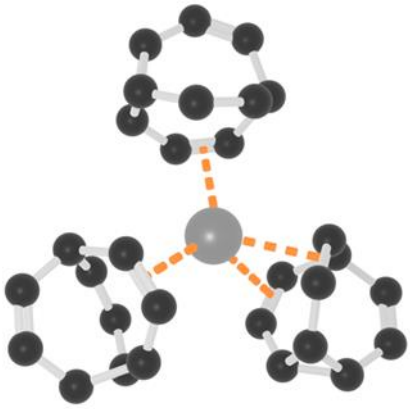

*Figure 16: Crystal structure of silver-**BV** complex.*[74]

Another feature of **BV**'s Cope rearrangement is that it passes through a bishomoaromatic C_{2v} transition state.[76,77] This is true also for related fluxional molecules semibullvalene (**SBV**), and barbaralane (**BB**), although the enthalpy of activation for Cope rearrangements in the **BV** structure are significantly higher, due to lowered strain in the ground state (Figure 17).[78,79] A new class of stable neutral 6π and 10π homoaromatic molecules was synthesised in 2023 by Teichert *et al.* based upon annulated **BBO**s (**96**). This stable homoaromatic molecule is also photoswitchable through a [1,11] sigmatropic rearrangement.[80,81]

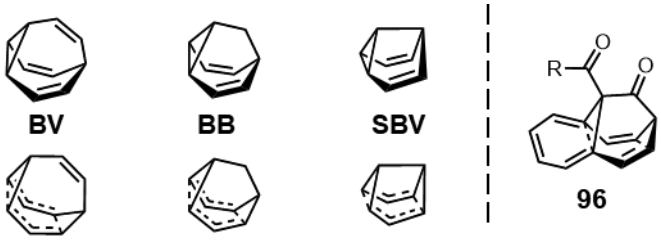

*Figure 17: Fluxional molecules and their bishomoaromatic transition states, and stable neutral homoaromatic **96**.*[80,81]

1.6. Applications of Bullvalene

The first attempt at applying **BV**'s fluxional properties was published in 1979, by Schröder *et al.* and consisted of **BV** annulation to form crown ethers bullvaleno[11–13]crown-3 **97** and bullvaleno[20–22]crown-6 **98** (Figure 18). The presence of a BV moiety in each of these crown ether moieties introduces a possibility ring size alteration, as the two crown ether substituents may be in 1,2-, 1,3- or 1,4- relative positions on the BV, resulting in a 'breathable' crown ether. Schröder then published an investigation into whether this would result in selectivity in anion binding. Unfortunately, Schröder did not observe the adaptation of this crown ether for cations of different shapes and sizes and only weak binding interactions were observed.[82,83]

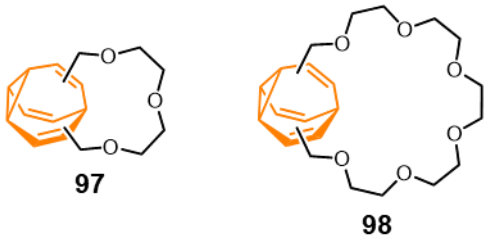

Figure 18: Structures of BV crown ethers.[82,83]

It wasn't until 2009 that another report applying BV's fluxional properties was published by Bode *et al.*. Using the synthetic method in Scheme 18, the diallyl substituted BV **60** was further functionalised by attaching porphyrin rings *via* olefin metathesis (Scheme 27). Porphyrin amine **99** underwent an amide coupling with acrylic acid to form acrylamide **100**, which was connected to BV **60** using Grubb's second-generation catalyst to form **101**.[41,84] The porphyrin rings on BV **101** were designed to act as binding groups for C_{60}. The authors hypothesised that upon addition of C_{60} to the mixture of isomers of BV **101**, the favourable interaction between the porphyrin rings and C_{60} would alter the equilibrium distribution of isomers by favouring isomers which promote the most favourable binding. However, the dynamic nature of BV presented significant challenges in analysis.

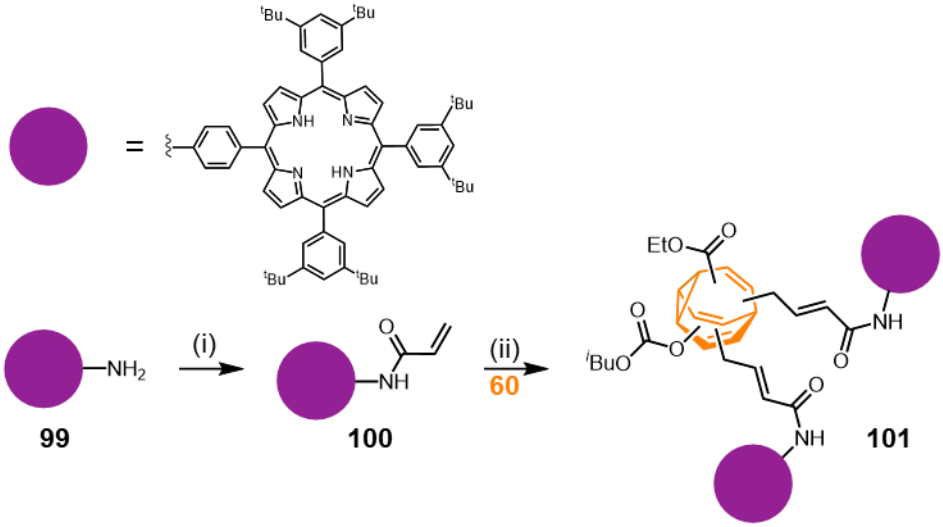

*Scheme 27: Synthesis of bisporphyrin BV **101**. (i)Acrylic acid, $SOCl_2$, DMA, 77%. (ii) Grubbs 2nd, CH_2Cl_2, 40 °C, 19%.*[41]

BV **101** was the subject of two papers, published in 2009 and 2012, which used different analytical methods to measure the binding activity of **101** to C_{60}. The former used the static bisporphyrin BVO **102** as a control to ensure that the flexibility of the linkers is not responsible for the change in binding affinity (Figure 19). The authors first attempted to use spectrophotometric titration data to analyse this binding affinity. However due to the presence of multiple binding constants in the case of BV **101**, there was not a constant isosbestic point. Instead, ^{1}H NMR spectroscopy was utilised, as the NH peak from the porphyrin rings shifts upfield upon binding to C_{60}. The result of this investigation was an increase of binding affinity with the dynamic BV molecule, thus demonstrating structurally adaptive complexation of substituted BV **101**.[41]

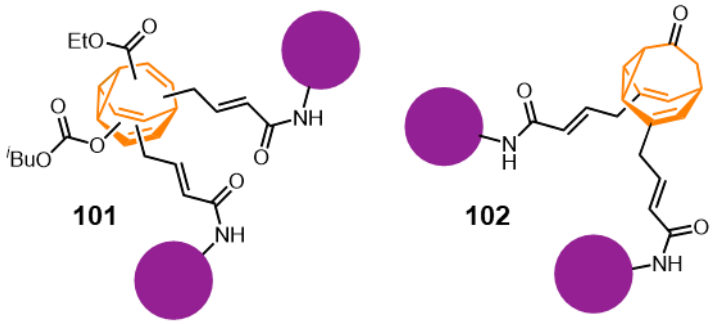

*Figure 19: BV **101** (860 isomers) and BVO **102** (2 isomers).*[41]

The next paper featuring the same BV **101** utilised a ^{13}C-labelled BV core and ^{13}C NMR spectra to identify the binding of both C_{60} and C_{70} (Figure 20). Not only were the ^{13}C NMR spectra of **101** in the presence of C_{60} different from that of **101** free in solution, but the NMR spectrum of **101** in the presence of C_{70} exhibited a third unique peak pattern, indicating **101** may act as a chemical sensor for C_{60} and C_{70} as well as having the ability differentiate the two.[85]

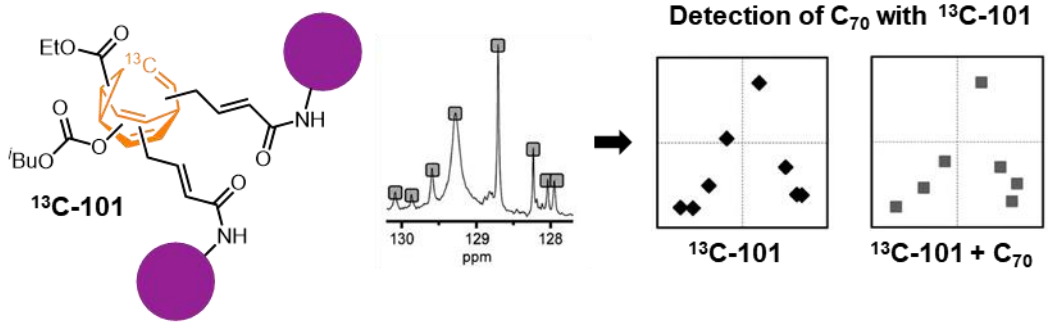

*Figure 20:^{13}C-**101** ^{13}C NMR spectra alters upon binding with C_{70}. Figure reproduced from publication.*[85]

Bode *et al.* used a similar molecule in another paper from 2010, this time with a photocleavable nitroveratryloxycarbonyl (NVOC) substituent (Figure 21). Photolysis

of the NVOC group in **103** yields bistable BVO **104**, thus creating a phototrappable BV for adaptive guest binding (Figure 21). This compound was used to bind C_{60}, with the same principle that the BV isomer distribution could be altered to favour binding. The photocleavable nature of **103** allows for the different BVO isomers **104** to be isolated and analysed.[42]

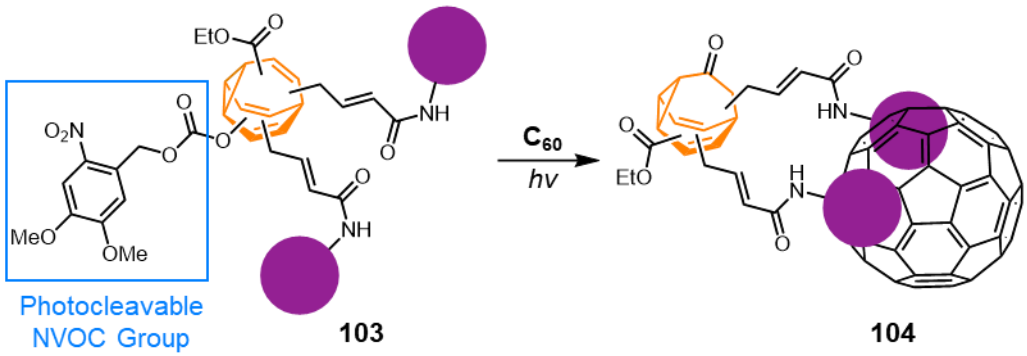

*Figure 21: Binding of C_{60} with phototrappable BV **103**.*[42]

Bode *et al.* also devised another chemical sensing bisboronic acid BV **105**, again using a ^{13}C-labelled BV core, this time to bind polyols in solution (Figure 22). **105** was synthesised using the same method from Scheme 18 altered slightly to add the triazole group, followed by a coupling to a boronic ester substituted phenyl group which is subsequently hydrolysed to the boronic acid.[86]

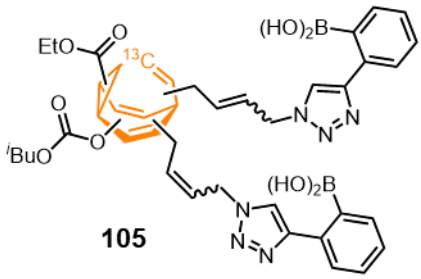

*Figure 22: Polyol-sensing boronic acid BV **105**.*[86]

In order to reduce the complexity of the ^{13}C NMR spectra, they were simplified to "NMR barcodes" which were then used to indicate any alterations in the spectra (Figure 23). The ^{13}C NMR spectra of unbound **105** and species **107** were compared in the presence of a variety of polyol compounds, such as N-acetyl neuraminic acid **106**. The conclusion of the publication was that **105** was altering its isomer distribution in order to bind to polyols.[86]

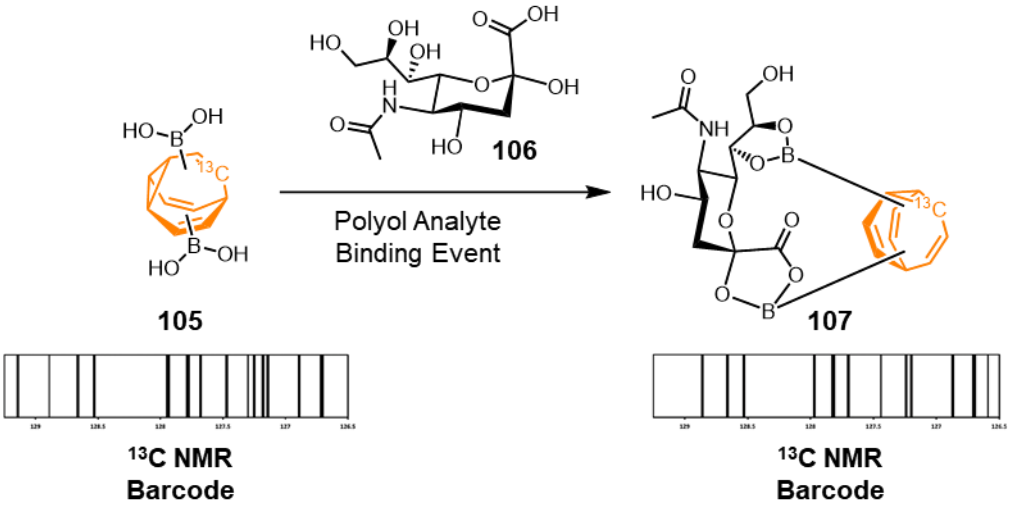

*Figure 23: Polyol binding to **105** including ^{13}C NMR barcodes. Figure reproduced from publication.*[86]

The two different binding moieties on BVs **101** and **105** demonstrate BV's ability for adaptive binding to organic compounds. These two examples were important in the establishment of BV as a potentially useful compound, exhibiting its fluxional behaviour in a new and exciting setting. However, the flexible acrylamide linkers in **101** and unsaturated carbon chains in **105** may somewhat diminish the geometric difference between BV isomers. A prospect for further study would be to synthesise functional BVs with shorter, more rigid linkers. In these cases, the difference between the different isomers will be emphasised, as opposed to the flexibility of their linkers.[2,41,86]

Bode *et al.* published their final paper on shapeshifting molecules in 2013, five years before Fallon *et al.* published their new, two-step synthesis, which made a range of BVs much more synthetically viable.[49,86] Fallon *et al.* reported the first metallo-supramolecular cage involving shapeshifting molecules in 2021, from bis-Bpin BV **108**, a Suzuki coupling yields bispyridyl BV **109**, which has an isomer ratio of 48 : 38 : 14 in free solution of its three most favourable isomers, A, B, and C (Scheme 28).[87]

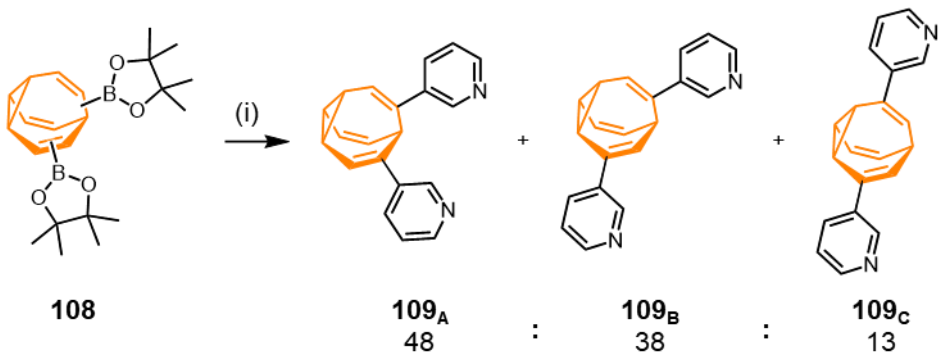

*Scheme 28: Synthesis of bispyridyl BV **109**. (i) $Pd(PPh_3)_4$ 5 mol%, NaOH, THF: H_2O, 65 °C, 92%.*[87]

Once **109** was synthesised, addition of two equivalents of $[Pd(CH_3CN)_4](BF_4)_2$ led to the formation of Pd_2**109**$_4$ (**110.BF$_4$**) as a complex mixture of isomers. These isomers were partially resolved by NMR spectroscopy at −35 °C; ^{19}F NMR spectroscopy exhibited multiple environments for encapsulation of the BF_4^- anion. Addition of one equivalent of tetrabutyl ammonium chloride resulted in complete anion exchange within the host to form **110**·Cl. Furthermore, treatment of either **110**·BF_4 or **110**·Cl with one equivalent of tetrabutyl ammonium iodide resulted in the formation of **110**·I. **110**·Cl and **110**·I. These structures were also analysed by ^{1}H NMR spectroscopy at −35 °C revealing that one isomer of **109** (**109$_B$**) was the dominant isomer in the complex, exhibiting a significant alteration of **109**'s isomer distribution upon formation of **110**·Cl and **110**·I (Scheme 29).[87]

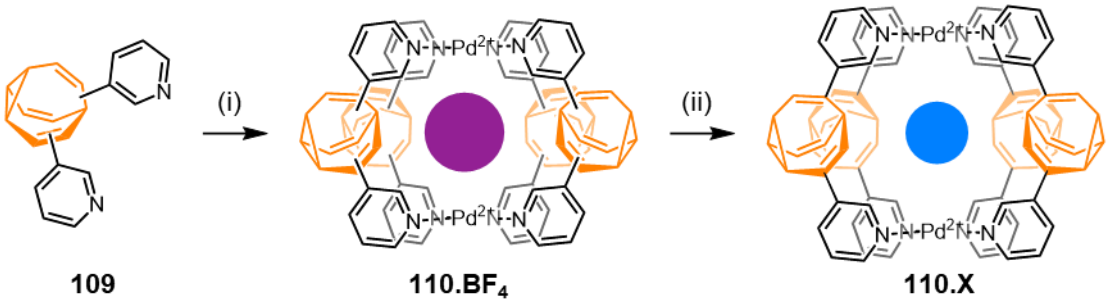

*Scheme 29:Synthesis of Pd_2L_4 complexs **110.BF$_4$** and **110.X**. **X$^-$** = Cl^- or I^-. (i) $[Pd(CH_3CN)_4](BF_4)_2$, CD_3CN, 60 °C, 10 min. (ii) NBu_4X, MeCN or DMF, 55 °C, 15 min.*

In this example, although the fluxional behaviour of the BVs involved is maintained, the isomer distribution is altered to form a complex containing only B isomers (Scheme 28) out of thousands of possible isomeric cages. This BBBB complex is isolated when each complex was analysed by single-crystal X-ray analysis. One complication in this system is that B is a chiral isomer of **109**, thus, assignment of each BV centre must be undertaken to fully assign structure. Furthermore, within the cage, **109$_B$** presents a vertical directionality, relative to an arbitrary top-view, meaning the BVs in the cage may either be up (↑) or down (↓). This means that each **109$_B$** molecule has two independent stereochemical degrees of freedom. The all B complex consists of the isomer P↑, P↓, M↓ and M↑ in that order, which may be observed from the crystal structure (Figure 24).[87]

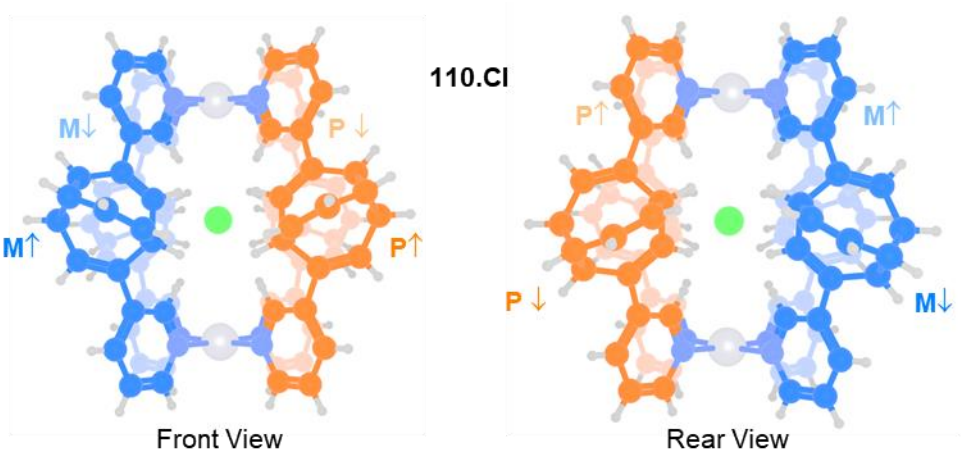

*Figure 24: Crystal structure of **110.Cl**, exhibiting P↑, P↓, M↓, M↑ pattern.*[87]

Due to the arrangement of BV centres in this complex it has a mirror plane and as such is achiral. Also, as guest exchange from **110** BF_4 to **110** Cl or **110** I results in a different isomer distribution, this system exhibits guest-dependent isomer convergence, a first for BV.[87]

Fallon *et. al* also reported the tendency of dialkenyl BVs to undergo exocyclic divinylcyclopropane rearrangements (DVCPRs), resulting in the formation of tetrahydro-1,8-ethenoheptalenes (THEHs) (Figure 25).[88] The pericyclic rearrangements occurring external to the BV framework occur *via* an ambimodal transition state. This means that the transition state may convert into more than two ground state structures, in this case, the DVCPR may occur with isomers **111A** or **111E** (which are interconverted via **112**) as a precursor to form THEH **113** *via* the same transition state, **114**.[88–90]

A variety of vinyl substituents were made for this publication, including aliphatic and aromatic ring systems, as well as methyl groups. Different substituents caused variations in the degree to which THEHs formed, as the release of the cyclopropane strain drives the formation of THEH, conjugation of the vinyl substituents into BVs olefinic system attempts to maintain the molecule's fluxional structure. Nevertheless, this publication demonstrates that there is as of yet, a lot of missing pieces in our knowledge of BV's fluxional behaviour.[88]

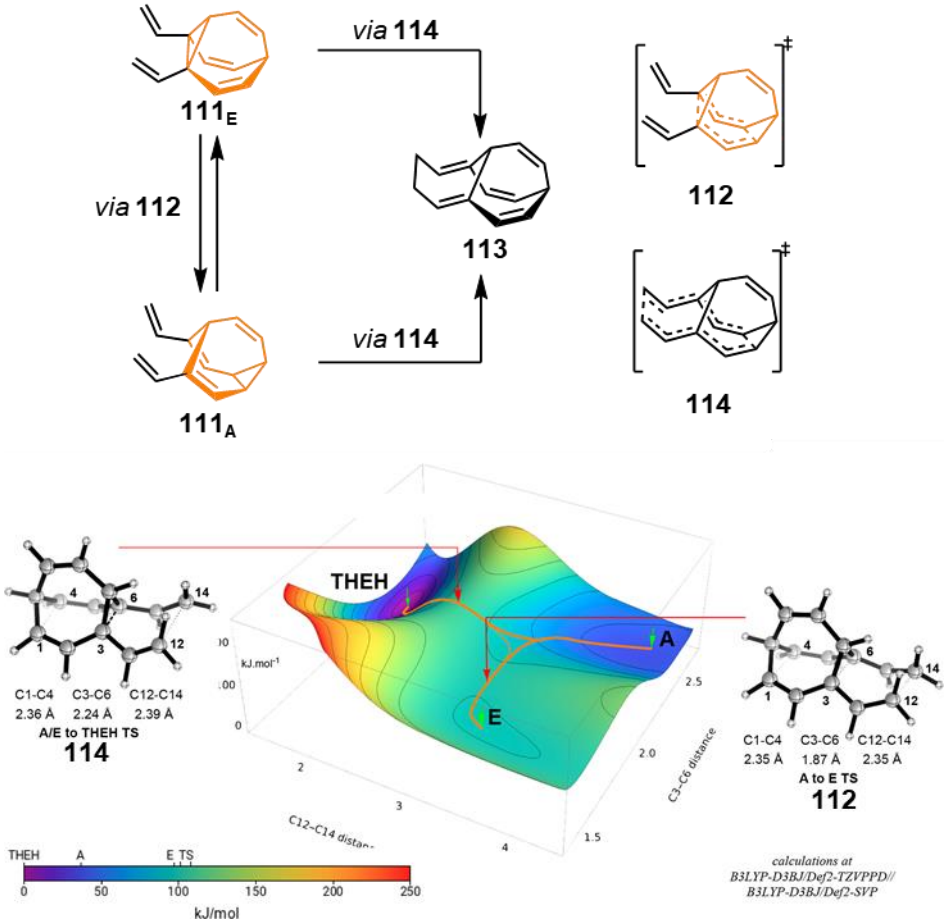

*Figure 25: Interconversion between **111** and **113**, including potential energy surface with all starting materials, products, and transition states. Figure reproduced from publication.*[88]

Also in 2022, a report by Paululat et al. detailed the synthesis and properties of fluorescent BVs. 2-Butyne-1,4-diol **115** was used to synthesise BDT **116** and irradiation formed BV **117**. **117** was reacted with diacyl chloride **118** to form BV **119**. The concept behind this work was that a transient excimer forms when the two napthoyl groups are able to interact with one another, such as in **119A**, forming an intramolecular excimer (Scheme 30).[91] Spectroscopy of dinapthoyl BV **119** showed that the λ_{max} of the emission bands resembled the fluorescence solvatochromism exhibited by other napthoates.[92,93] Next, the change in intensity of the emission peak at 450 nm was monitored upon addition of various metal ions. Lithium, calcium, barium or magnesium ions increased excimer emission intensity significantly, although this was not the case for sodium ions. These results are mirrored in the static lumibullvalene with similar substituents, so this may not be due entirely to the fluxional nature of the carbon cage.[91]

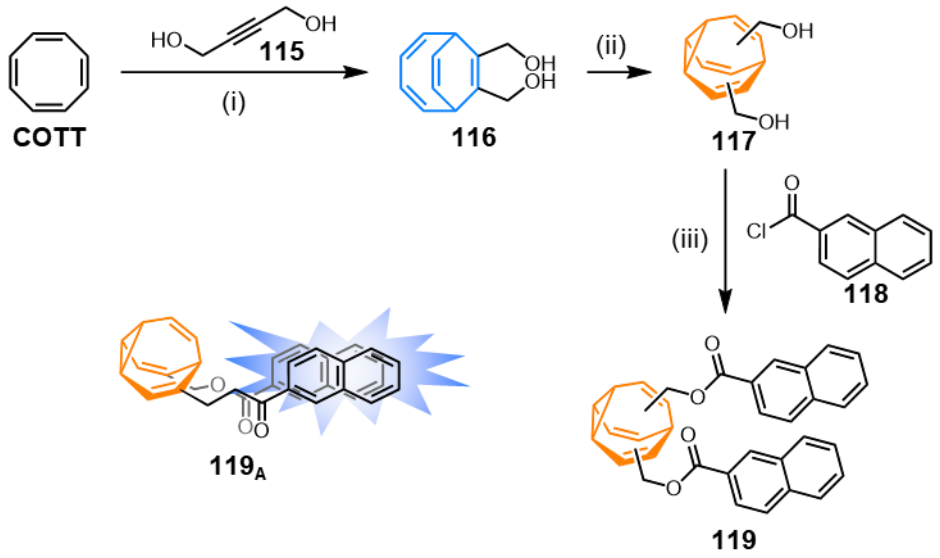

*Scheme 30: Synthesis of fluorescent BV **119**. (i) $CoBr_2$(dppe) 10 mol%, ZnI_2 20 mol%, Zn Dust 30 mol%, TFE, rt, 24 h. (ii) Thioxanthone, h ν, THF, 6 h, 46%. (iii) N-methylmorpholine, CH_2Cl_2, 0 °C to rt, 24 h, 67%.*[91]

A more fundamental discovery in this publication was the isolation of side products for the irradiation of **116** to form **117**, which also resulted in the formation of differently-substituted lumibullvalenes **120A**, **120B**, and **120C**, alongside a proposed mechanism for each of the three side products (Figure 26). The structure of lumibullvalene was first isolated in 1967 by Jones, in a publication on the photolysis of **BV**.[91,94,95]

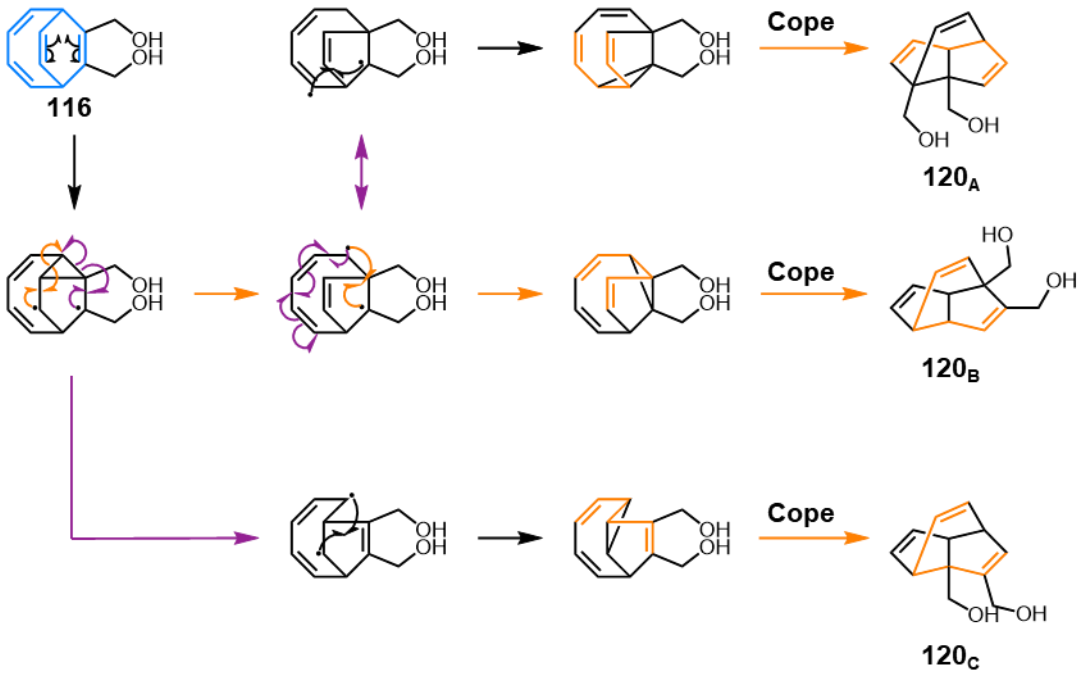

*Figure 26: Proposed mechanism of formation of lumibullvalene side products **120**.*[91]

This publication, along with early studies of BV's photolysis and thermolysis show how BV's C_{3v} symmetry, and the C_{2v} symmetry of the BDT cage both result in the potential to degrade into a variety of similarly substituted side-products.[18,20,91,94]

Early in 2023, Golder *et al.* synthesised the first polymer incorporating BV, both as an alternating copolymer **95** and also through the inclusion of bis-Bpin phenylene **121**, as a random copolymer with phenylene groups **122**. For the random copolymer, BV **93** loading (x) was altered to yield different polymeric systems (Scheme 31).[54,57]

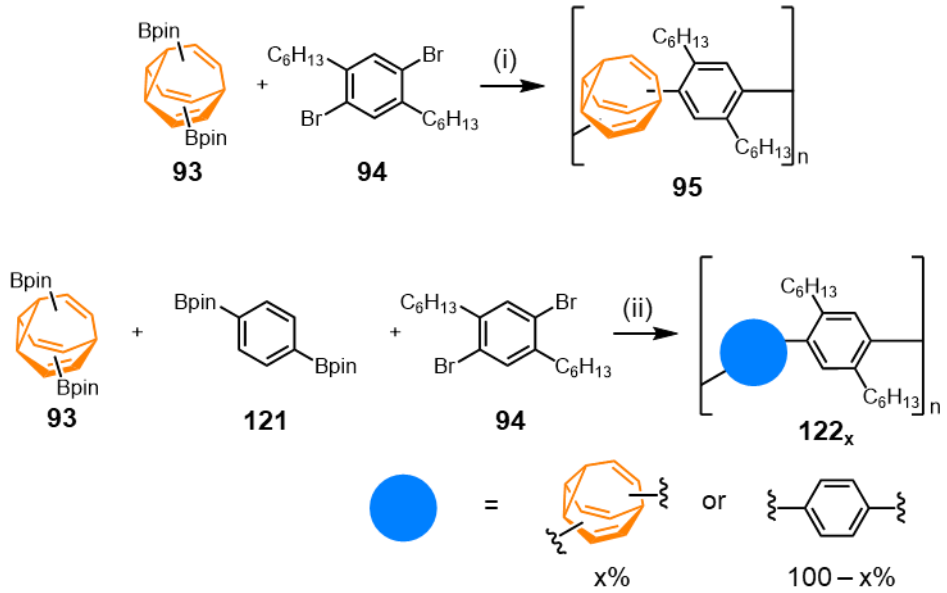

*Scheme 31: Synthesis of polymers incorporating BV structure. (i) XPhos Pd G3, K_3PO_4, PhMe, 60 °C. (ii) x = 0–34% **93**, 55–100% **121**, XPhos Pd G3, K_3PO_4, PhMe, 60 °C.*[57]

Firstly, variable temperature ^{1}H NMR spectroscopy confirmed that in the polymer chain, the BV units are still undergoing Cope rearrangements in the random copolymer $\mathbf{122_{50}}$ (with the lowest BV loading). The introduction of BV's fluxional carbon cage to an otherwise inflexible phenylene polymer backbone makes for high thermal stability, as well as tuneable solution state and thermal properties, such as T_g. The paper concludes by discussing and comparing the use of other, more rigid conjugation break spacers (such as cyclohexene, adamantane, or norbornadiene) with that of BV as a spacer in π-rich macromolecules. Not only is BV simpler to incorporate, due to the well-established Suzuki coupling reactivity, but also the fluxional nature of BVs makes for non-uniform anomalies in the polymer backbone, which is not possible with most other spacers. BV shows real promise as a new potential route for investigation of polymeric materials, due to the random, stochastic nature of its rearrangements.[57]

Another area of chemistry recently breached by BV-incorporated molecules is medicinal chemistry. A BV-linked vancomycin dimer was synthesised (Scheme 32)

and shown to be effective as an antibiotic agent against multi-drug resistant gram-positive bacteria. Starting with BDT **116**, addition of propargyl groups through nucleophilic substitution yields **123**, which is photoirradiated to form **124**. BV **124** then underwent a click reaction with benzaldehyde azide **125** to form **126**. Reductive amination of **126** with vancomycin amine **127** forms BV-linked vancomycin dimer **128**. Phenyl-linked vancomycin dimers were also synthesised as a control.[96]

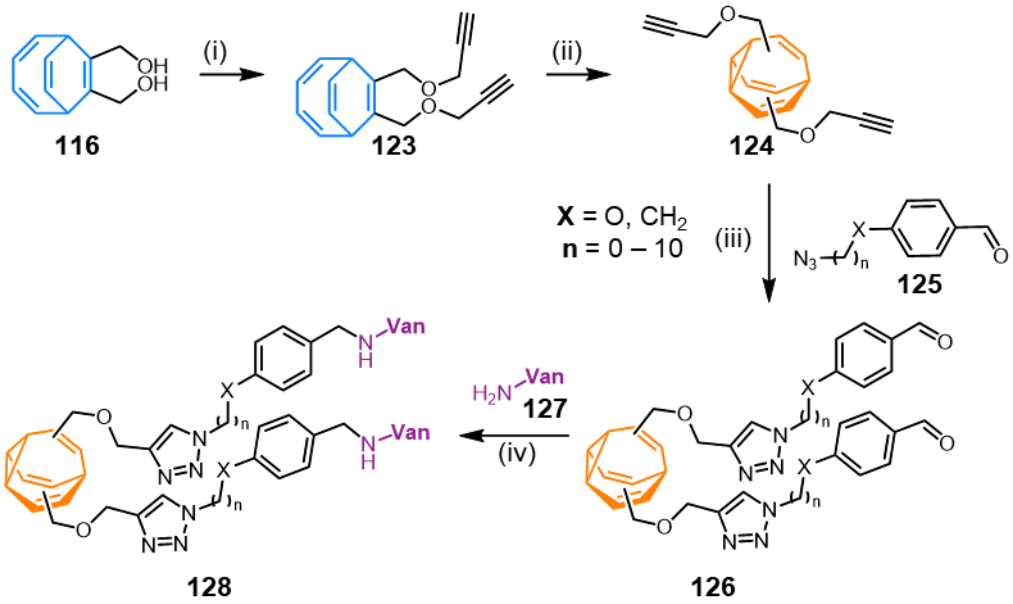

*Scheme 32: Synthesis of BV vancomycin dimer **128**. (i) Propargyl bromide, NaH, THF, 0 °C to rt, 16 h, 87%. (ii) hν, acetone, 0 °C, 16–24 h, 50%. (iii) $CuSO_4.5H_2O$, sodium ascorbate, $^tBuOH:H_2O$ 3:1, 85 °C, 16 h, 40–71%. (iv) DIPEA, MeOH: DMF 1:1, 70 °C, 2 h, then $NaCNBH_3$, 70°C, 16 h, 8–30%.*[96]

While all of the vancomycin dimers synthesised in this work exhibited some degree of antibacterial activity, the most impressive result was the increased efficacy towards vancomycin-intermediate and vancomycin-resistant bacterial strains. This is especially true for two particular BV linked vancomycin dimers, **128$_A$** (X = O, n = 3) and **128$_B$** (X = O, n = 10), which were particularly potent against vancomycin-resistant *E. faecium* and *S. aureus* respectively. Furthermore, **128$_A$** did not invoke significant resistance in bacterial strains, with the minimum inhibitory concentration doubling, as opposed to the static phenylene control compound, for which the minimum inhibitory concentration increased fourfold. This work communicates the possibility for BV as a bioisostere for different biologically active compounds in the future, and illustrates the necessity for further, varied, in depth studies to occur to gain a more developed understanding.[96]

Most recently, the rearrangement of individual BV molecules was monitored and analysed using scanning tunnel microscopy break junction (STMBJ) experiments; in these experiments, an Au STM tip is crashed into an Au (111) substrate and subsequently retracted. The conductance is measured as the distance is altered between the two electrodes (Figure 27). In this experiment, bis(thioanisole) BV **129** was synthesised and added to the STMBJ system as a solution in 1,2,4-trichlorobenzene, and bridged the two electrodes using the sulfur atoms.[97]

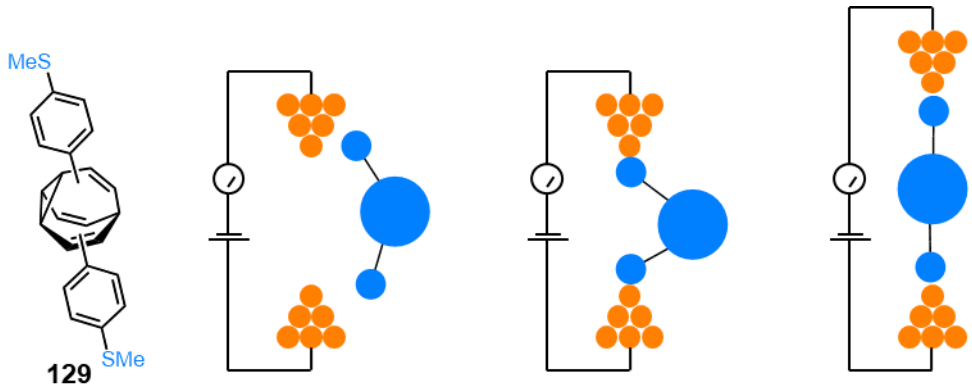

*Figure 27: BV **129** isomer alteration between two Au electrodes.*[97]

As a result of the BV bridging the gap between the two Au electrodes, piezoresistance is observed—that is, an alteration in resistance of a given system from applied stress.[98] In this system, the alteration of the distance between the tip and the surface resulted in differing levels of conductance: a consequence of different isomers bridging the gap. This is an example nanoscale electro-mechanical system displaying piezoresistance over a range of 3–9 Å, which has unique potential for detectors and sensors at the subcellular level.[97]

Finally, Fallon *et al.* also published a computational pipeline for evaluating the binding mode of BV with β- and γ-cyclodextrins (**β-** and **γ- CDs**) and exemplified this pipeline using **BV** and hydroxymethyl BV. To investigate different potential binding modes, all four isomers of hydroxymethyl BV and **BV**'s one isomer were used at different orientations, with the cyclopropane ring pointing upwards, horizontally, and downwards. In the pipeline, differently oriented bullvalenes are passed downwards through the **β-** and **γ-CD** cavity and rotated 360° simultaneously (Figure 28). The binding energies are measured throughout, producing a heat map of potential binding modes.[99]

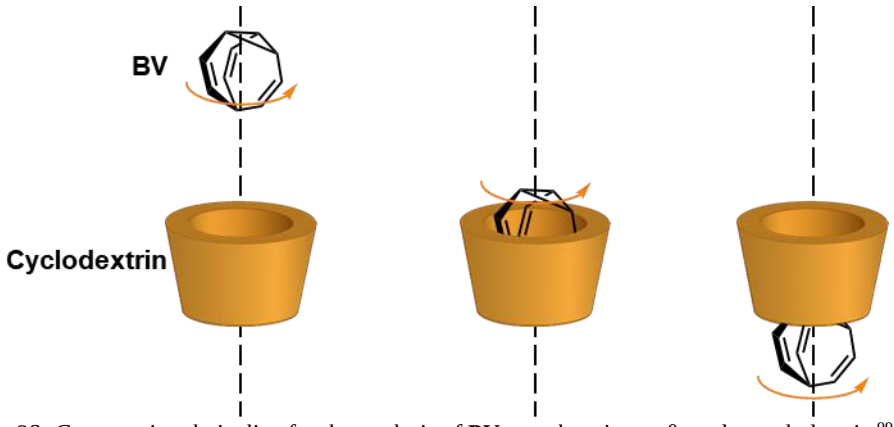

*Figure 28: Computational pipeline for the analysis of **BV** complexation to β- and γ-cyclodextrin.*[99]

Computational studies predict that while **γ-CD** did not select one binding mode preferentially to hydroxymethyl BV, **β-CD** did for each individual isomer. Fallon then used ^{1}H NMR titrations to calculate a binding energy for hydroxymethyl BV in **β-** and **γ-CD** (-18.69 ± 0.1 kJ·mol^{-1} and -13.04 ± 0.15 kJ·mol^{-1} respectively), although, no crystal structure was obtained.[99]

From its inception, BV inspired chemists to think about the vast possibilities for its applications and properties, however, challenges in synthesis prevented in depth discovery on the topic itself. Here, it has been shown that with easier synthesis, and design of substituted BVs, the potential uses for this fluxional molecule are endless, and the growing interest in the last five years have exhibited how BV is a fascinating, new area for chemists of all disciplines.

1.7. Supramolecular Hosts

In previous reports, BV's involvement in supramolecular systems has been almost exclusively to exploit its fluxional behaviour. This includes such works as Schröder *et al.*'s crown ether BVs; Bode *et al.*'s chemical sensing BV porphyrins and boronic acids; and Fallon *et al.'s* BV palladium complex.[83,85–87] There is only one report of **BV** as a molecular guest, and this work does not concern the potential alteration in **BV**'s behaviour, only potential for **BV** to act as a guest.[99] In order to gain a deeper understanding of **BV**'s fluxional behaviour, it may be beneficial to investigate how its properties are altered in limited-volume cavities, and/ or when it acts as a molecular guest. Some potential supramolecular hosts for BVs and their effects on the behaviour of different guests are discussed herein.

1.7.1. Cyclodextrin

Cyclodextrins have a long and storied history in biological and chemical sciences, which is relayed in detail in Crini's 2014 review.[100] In 1891, Villiers detailed the fermentation of potato starch using *Bacillus amylobacter* over several days resulting in the formation of dextrins—a term used at the time to describe products resulting from the degradation of starch.[100,101] This was the first discovery of cyclodextrins, and it took a long time and many erroneous predictions until the structures of the first three cyclodextrins were determined and agreed upon, work which is mainly accredited to Freudenberg and French.[100]

Cyclodextrins are water-soluble macrocycles with hydrophobic, chiral cavities. They consist of sequential glucose units linked by 1,4-glycoside bonds. The number of glucose units (6, 7, and 8 for α-, β-, and γ-cyclodextrin respectively) varies between the different cyclodextrins, and determine its properties including cavity size (Figure 29).

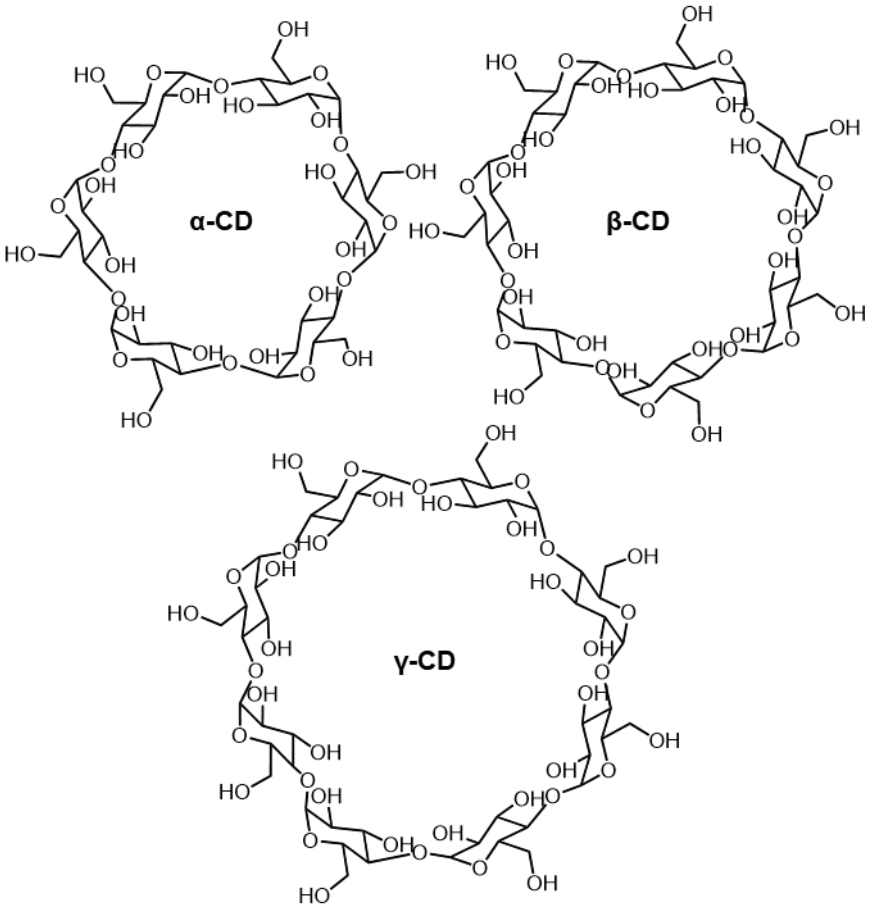

Figure 29: Chemical structures of α-, β-, and γ-cyclodextrin.

It was in 1952 that Cramer first demonstrated that **β-CD**'s shape may allow for the inclusion of different molecules inside the molecule's cavity, first using indican as a molecular guest.[100,102,103] Cramer also determined the shape of cyclodextrins to be closer to a conical frustum, as opposed to a cylinder. Thus, the two ends are differentiated by the alcohol that resides at each end.[100] The narrower end is where the 1° alcohols are present, and the wider end is where the 2° alcohols reside, which are twofold compared to the 1° alcohols.

Since this discovery, cyclodextrin's ability to act as a molecular host has been at the forefront of new research related to the molecule. Cyclodextrin complexes have exhibited useful properties in a wide array of industries, including in pharmaceuticals, food, and agriculture; usually through the alteration in behaviour of the encapsulated entity.[104–109] Cyclodextrins also exhibit useful properties within the chemical industry itself, in analytical chemistry, nanotechnology, and biomedicine.[110–113]

Cyclodextrin is not, however, limited to the formation of intermolecular complexes; intramolecular complexes are also possible *via* tethering a potential molecular guest to one of the cyclodextrin's hydroxyl groups (Figure 30).[114]

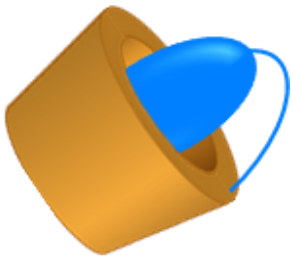

Figure 30: Example of an intramolecular complex with a tethered cyclodextrin.

Moreover, these plerotopic (self-complementary) compounds have been known to form polymeric inclusion compounds, *via* intermolecular encapsulation[115,116] The first example of a supramolecular polymer structure using cyclodextrin as a molecular host was reported in 1982 by Tabushi *et al.* utilising a ^{t}butylthiol group appended to the 1° face of a **β-CD** (**130**) (Figure 31).[117]

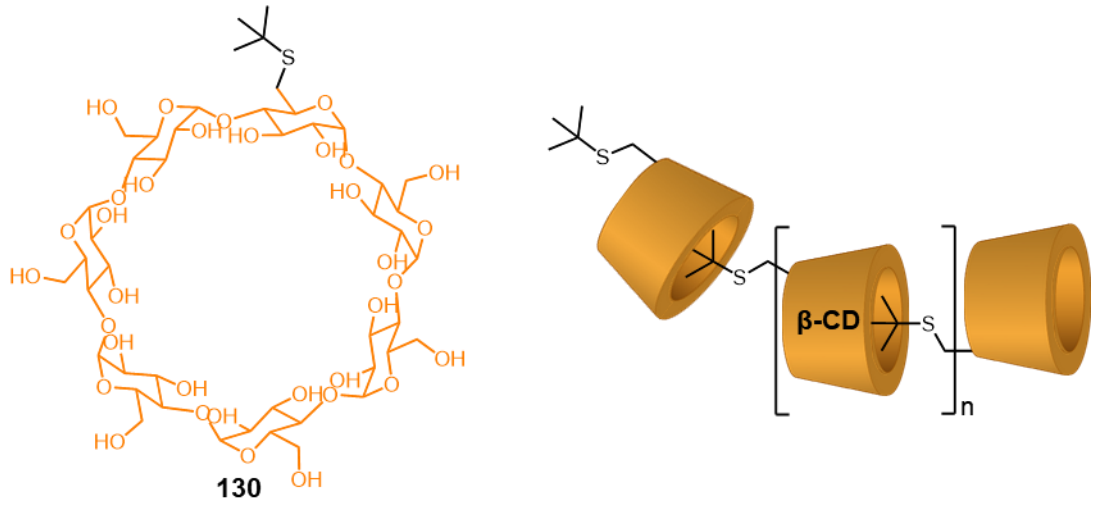

*Figure 31: Chemical structure of ᵗBu-thiol appended **β-CD**, and its self-assembled polymeric structure.*[117]

It is often the hydrophobicity of the tether which is the driving force for its inclusion, as the structures are formed in aqueous solutions. Whether these tethered compounds undergo inter- or intramolecular complexation depends upon multiple factors including concentration and the length/shape of the tether itself.[115] Furthermore, the helicity and orientation of these supramolecular polymer complexes may be tuned by exchanging the heteroatom in the tether, or by altering the length of the tether to the binding motif, as exemplified in 2003 by Inoue *et al.*.[118]

1.7.2. Cavitands

Cavitands are container-shaped molecules, capable of acting as molecular hosts to many different guests.[119,120] It is an umbrella term that covers a wide array of chemical structures and properties. Most cavitands currently studied are based upon a resorcinarene scaffold, which is characterised by sequentially linked phenolic groups forming a cyclic oligomer, typically containing four units.[121,122] The resorcinarene scaffold is synthesised in a single simple and reliable step which consists of an acid-catalysed condensation between resorcinol **131** and an aldehyde **132** to form a resorcinarene, **133** (Scheme 33).

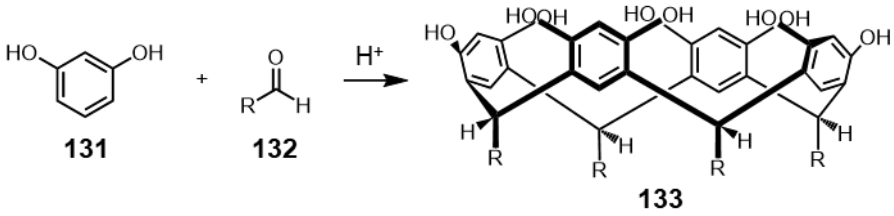

*Scheme 33: Synthesis of resorcinarene **133**.*

This reaction is often performed under thermodynamic control, at reflux over several days, for two main reasons, the first of which is the formation of the thermodynamically preferred tetramer instead of the pentameric or hexameric product.[123] Secondly, for this tetrameric species, there are four potential diastereomers which may form, one of which (rccc) is thermodynamically preferred (Figure 32). These diastereomers have a nomenclature of their own, which begins with the reference position (r), from this position, going around the macrocycle, the positions are labelled as cis (c) or trans (t) relative to this first reference position.[124]

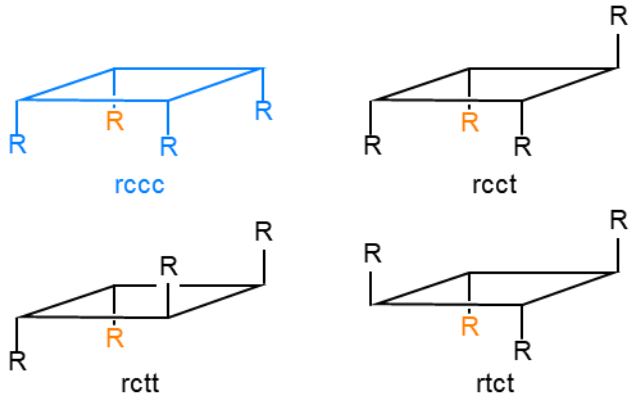

Figure 32: The four possible diastereomers of calix[4]resorcinarene, reference position labelled in orange.[124]

Moreover, there are different conformational isomers which resorcinarene **133** may occupy, including the bowl-shaped "chair" conformation, as well as the saddle and flattened-boat conformations (Figure 33). All of which have been isolated in a single crystal.[125]

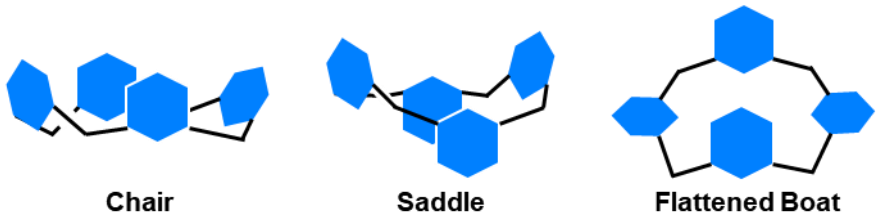

*Figure 33: Representations of the three main conformers of rccc calix[4]resorcinarene **133**.*[125]

Cavitands use this resorcinarene as a scaffold and typically build on this framework, extending and rigidifying this bowl structure to make a supramolecular host suitable for molecular encapsulation.[121]

1.7.3. Carcerands and Hemicarcerands

One of the earliest modified cavitands was synthesised in 1985 by Cram *et al*. and was based upon the calix[4]resorcinarene structure **133** (Scheme 34). These types of compounds were named carcerands, from the Latin carcer meaning "prison". This is because they are molecular capsules in which the apertures are so small that molecules inside were essentially trapped. Combination of tetrathiol **134** with tetrachloride **135** in the presence of a base, resulted in the synthesis of the first carcerand **136**.[126,127]

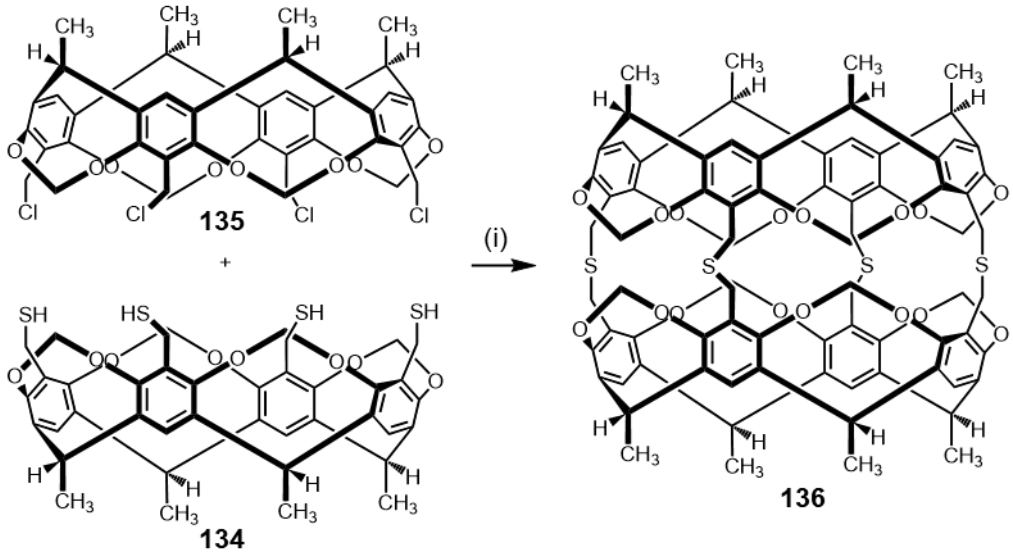

*Scheme 34: Cram et al.'s synthesis of the first carcerand **136**. (i) DMF/ THF, $CsCO_3$, 60 °C, 10 h.*

As Cram described in his Nobel lecture, "The first question to be answered was: what guest compounds would be trapped inside during the shell closure? This question is akin to asking whether two soup bowls closed rim-to-rim under the surface of a kettle of stew would net any stew. The answer was that [**136**] 'contained' essentially every kind of component of the medium present during ring closure".[128]

Using mass spectrometry, it was determined that the capsule **136** had formed, and that it contained a variety of species, including cesium chloride, DMF, and even argon from the inert environment under which the reaction occurred.[126] Cram would go on to work much further on carcerands, altering linker size between the two resorcinarene moieties. Examples include using an ether linker such as in **137**, or an imine linker , as in **138** (Figure 34). These varied linkers alter the cavity shape and allow the introduction of larger guests. Covalently-closed capsules which allow for the exchange of small molecules like these are hemicarcerands.[129–131]

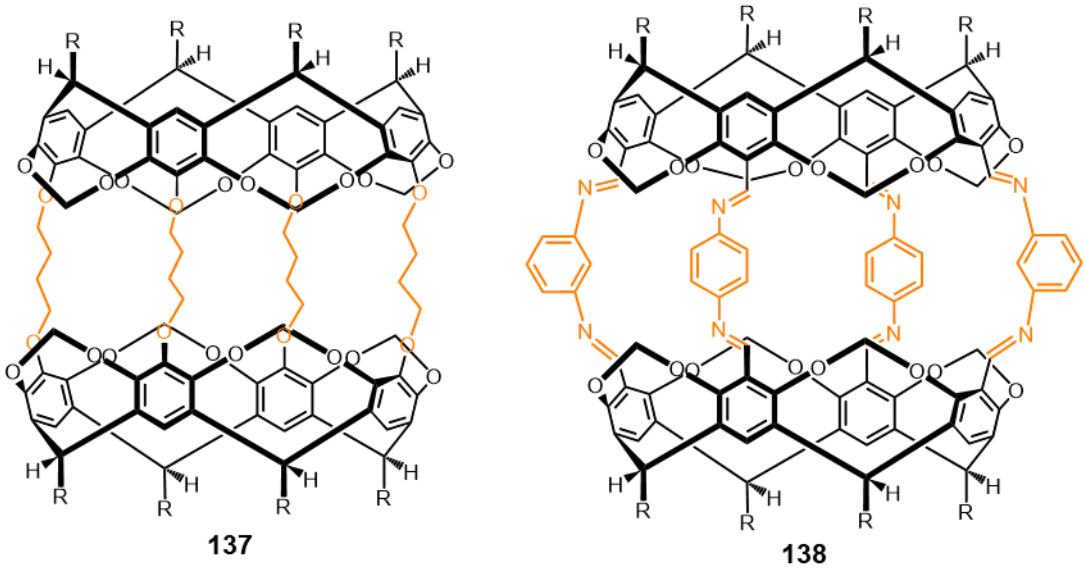

*Figure 34: An example of two of Cram's hemicarcerands, **137** and **138**.*[130,132]

1.7.4. Octa-acid Host

One example of a water soluble cavitand is the octaacid host, **139**, named for the eight carboxylic acid groups present on the periphery of its structure (Figure 35). This host was originally synthesised in 2004 by Gibb *et al.* as a host that could be used for larger organic molecules, such as steroids.[133] These cavitands are substantially augmented from the resorcinarene structure, resulting in a rigid covalent bowl with a deep, hydrophobic cavity, suitable for binding organic molecules.[133,134]

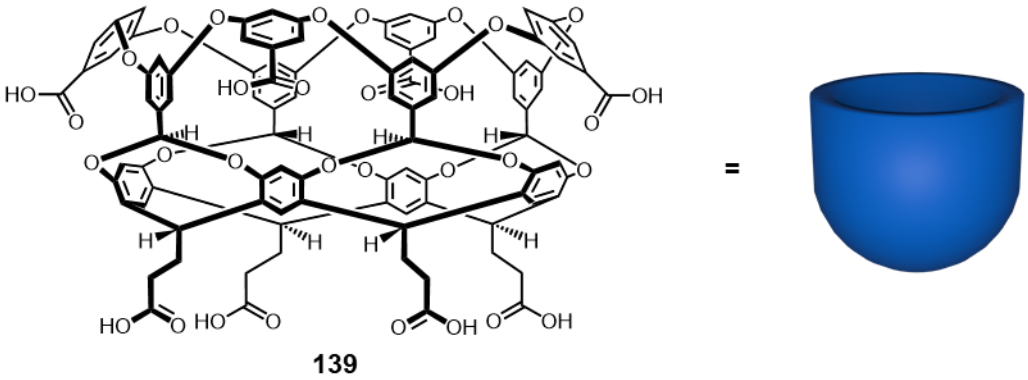

Figure 35: Chemical structure of the octaacid host, alongside a cartoon representation of the cavitand.[133]

In contrast to Cram's carcerands, these compounds are not fully sealed to entry by covalent bonds, i.e. there is an opening into the cavity, this feature results in slightly different binding possibilities for the host in aqueous solutions. The cavitand may form a dimer capsule through noncovalent interactions, creating an even larger binding pocket for hydrophobic guests. There is potential for 2:1, 2:2, and 1:1 binding motifs with this cavitand (Figure 36); the 1:1 binding motif has usually been limited to charged compounds, which may be soluble in the bulk aqueous solution.[134–137]

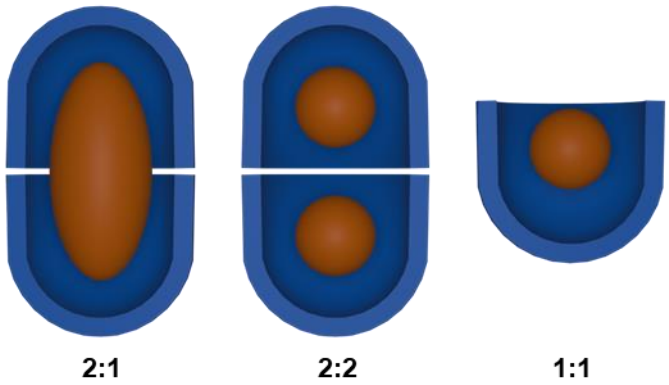

Figure 36: Cartoon representation of the different possible binding motifs for the octaacid host.[134–137]

1.8. Supramolecular Host Effects on Guests

The interior surface of cavitands often have consequences for the behaviour of encapsulated species, resulting in differing reactivity, stability or kinetics, often related to the size and shape of the cavity.[138,139] This feature of carcerands led Cram to claim in 1989 that "carcerand interiors provide a new phase of matter" in relation to the properties of encapsulated molecules.[140]

Since Cram's claim in his 1989 paper, there have been multiple examples of altered molecular properties and behaviour inside cavitands. Firstly, Cram exemplified the isolation of cyclobutadiene **140** inside hemicarcerand **141** (Figure 37).[141]

While usually susceptible to oxidation (**142**) or dimerization (**143**), **140** was synthesised, isolated and analysed inside the hemicarcerand **141**.[141–144] Cram went on again in this 1991 paper to describe the internal cavity of these hemicarcerands as a "new phase of matter" but on this occasion went further in describing the cavitands as unique when compared to clathrates or zeolites. This is due to their independence from the bulk phase: "one host molecule provides one discrete interior molecular phase". This molecular phase may exist in solid, solution or even gaseous form.[141]

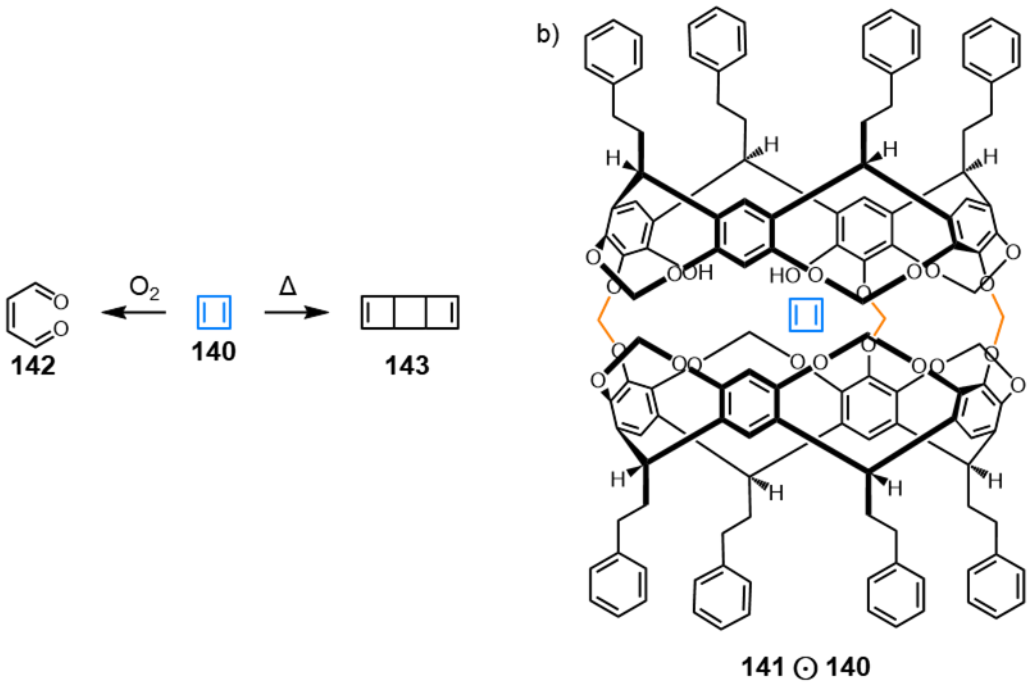

*Figure 37: a) Degradation of cyclobutadiene **140** to oxidation (**142**) or dimerization (**143**) byproducts. b) Cyclobutadiene **140** encapsulated in hemicarcerand **141**.*[141–144]

A further standout example of cavitands altering the stability of usually unstable molecules was published in 2003 by Warmuth *et al.*.[145] In this publication, the authors prepare bicyclic diazirine **144**, encapsulated in hemicarcerand **137** (Figure 38). Upon irradiation, **144** degrades, to form **145** or **146**, which free in solution would degrade *via* retro-Diels–Alder reactions to form acyclic compounds or *via* radical insertion mechanisms to form dimer products.[145] This instability is due to structures **145** and **146** being anti-Bredt, as they possess olefinic C=C bonds at the compound's bridgehead.[146,147]

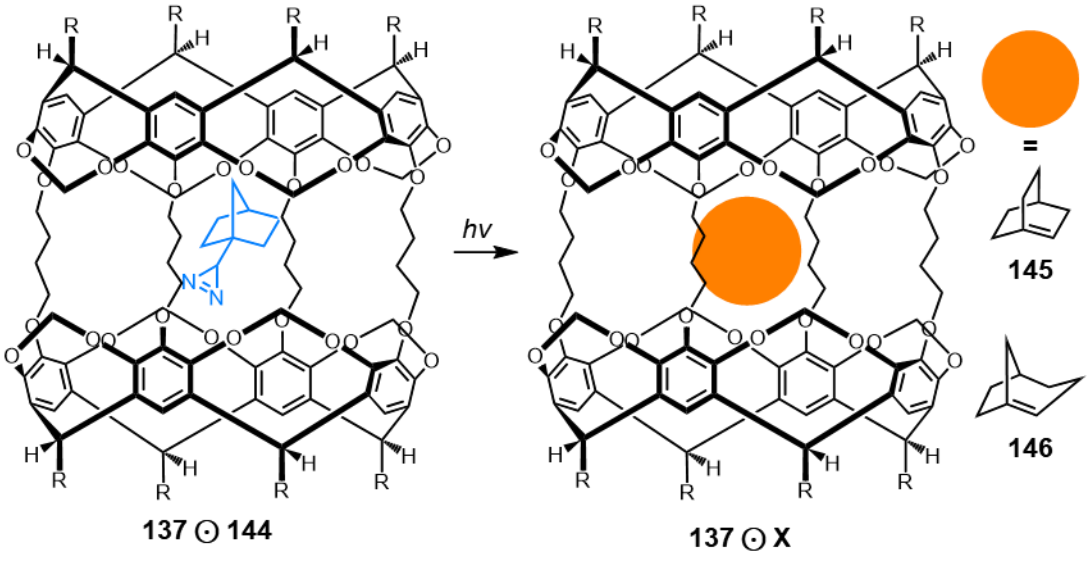

*Figure 38: Encapsulation of **144** and subsequent formation and stabilisation of anti-bredt **145** and **146** in **137**.*[145]

An intriguing element in this publication is the stabilisation of **145** and **146** not only against intermolecular degradation pathways but also against intramolecular rearrangement. The exceptionally high barrier to decomposition by retro Diels–Alder is most likely due to steric constraints imposed by the host molecule.[145]

One final example of substrate control by cavitands is in their ability to impose constraints upon conformational mobility. This was first demonstrated in a publication from Rebek *et al.* in which the activation energy ($\Delta G^{\ddagger}$) of a cyclohexane ring flip (10.25 kcal mol^{-1} free in solution) was increased by encapsulation in a reversible capsule to 10.55 kcal·mol^{-1} in capsule.[148] The authors suggest in this publication that this increase in activation energy occurs as a result of favourable host–guest interactions lowering ground state energies as opposed to steric constraints imposed upon transition state structures.[148]

A subsequent publication from Sherman *et al.* in 2000 reported a similar result, this time using carcerand **147** instead of a reversible macrocyclic host to investigate the effect on the ring flip kinetics of thioxane **148** and dioxane **149** (Figure 39).[149] In this publication, the difference in the activation energy for ring flipping is significantly larger than for that in Rebek's aforementioned paper ($\Delta\Delta G^{\ddagger}$ = 1.8 kcal mol^{-1} and 1.6 kcal mol^{-1} for **148** and **149** respectively). As a result, it is suggested by the authors that the more rigid carceplexes may experience thermodynamic control *via* stabilisation of both conformations or kinetic control *via* steric constraints imposed on the transition state structures or possibly a combination of both.[149]

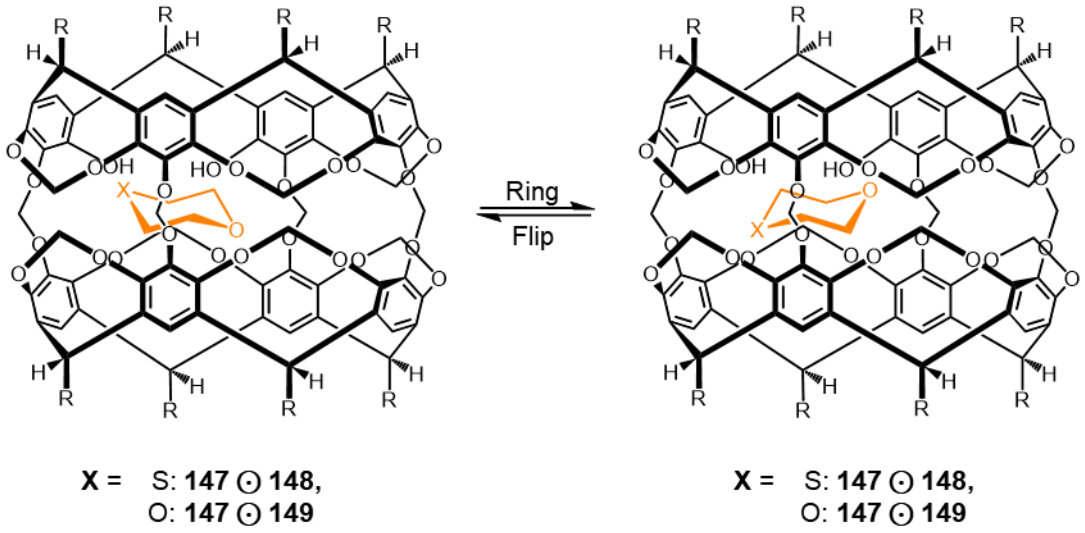

*Figure 39: Depiction of ring flip of thioxane **148** and dioxane **149** in hemicarcerand **147**.*[149]

In both Rebek and Sherman's papers, the authors used variable temperature NMR spectroscopy in order to investigate the rate at which the ring flip occurs. This may be achieved due to the fact that as the ring flip occurs, protons in axial positions become equatorial protons and *vice versa*. As a result, when low temperature NMR spectroscopy is performed these protons appear as two peaks as the conformers are "frozen out" in the cavitand. The $\Delta\delta$ of these two peaks and the spectrometer frequency may be used to calculate the peak separation, $\Delta\nu$, in Hz. This may be used to calculate the rate constant k_c using Equation 1.[148]

$$k_c = \frac{2\pi}{\sqrt{2}}\,\Delta\nu$$

Equation 1: Calculating rate constant, k_c from $\Delta\nu$.[148]

Once the rate constant is known, the temperature of coalescence, T_c, may then be used in the Eyring equation (Equation 2) to calculate the activation energy of the conformational change.[148–150]

$$\Delta G^{\ddagger} = 4.58\ T_c\ (10.32+\log(\frac{T_c}{k_c}))$$

Equation 2: Calculating activation energy from rate constant, k_c and temperature of coalescence, T_c.[148,150]

1.9. Summary and Outlook

BV's rearrangements have captivated organic chemists since its conception in 1963, however, it was not until recently that their synthesis became more viable. In becoming more synthetically attainable, much more work has been published regarding **BV** and potential applications of its unique properties. Thus far, investigations into the fundamental nature of **BV** and its rearrangements are limited. This includes the use of BV as a supramolecular guest, despite the large potential impact on its fluxional behaviour. This thesis explores the fundamental principles of BV's behaviour and how these principles may be modified by alterations on the BV core, or by encapsulation of BV molecule in limited volume cavities.

References

1 P. Muller, *Pure Appl. Chem.*, 1994, **66**, 1077–1184.

2 A. N. Bismillah, B. M. Chapin, B. A. Hussein and P. R. McGonigal, *Chem. Sci.*, 2020, **11**, 324–332.

3 W. von Eggers Doering and W. R. Roth, *Angew. Chem. Int. Ed. Engl.*, 1963, **2**, 115–122.

4 R. P. Lutz, *Chem. Rev.*, 1984, **84**, 205–247.

5 B. S. Rabinovitch, E. W. Schlag, K. B. Wiberg and J. Chem Phys, *J. Chem. Phys.*, 1958, **28**, 504–505.

6 W. von Eggers Doering and W. R. Roth, *Tetrahedron*, 1963, **19**, 715–737.

7 J. M. Brown, B. T. Golding and J. J. Stofko, *J. Chem. Soc., Chem. Commun.*, 1973, 319b.

8 G. Schröder, *Angew. Chem. Int. Ed. Engl.*, 1963, **2**, 481–482.

9 A. Ault, *J. Chem. Educ.*, 2001, **78**, 924.

10 G. Schröder and J. F. M. Oth, *Angew. Chem. Int. Ed. Engl.*, 1967, **6**, 414–423.

11 R. Merényi, J. F. M. Oth and G. Schröder, *Chem. Ber.*, 1964, **97**, 3150–3161.

12 J. F. M. Oth, K. Müllen, J.-M. Gilles and G. Schröder, *Helv. Chim. Acta.*, 1974, **57**, 1415–1433.

13 J. F. M. Oth, R. Merényi, J. Nielsen and G. Schröder, *Chem. Ber.*, 1965, **98**, 3385–3400.

14 W. von E. Doering and J. W. Rosenthal, *J. Am. Chem. Soc.*, 1966, **88**, 2078–2079.

15 R. Hoffmann and R. B. Woodward, *J. Am. Chem. Soc.*, 1965, **87**, 2046–2048.

16 E. Vogel, W. Grimme, W. Meckel, H. J. Riebel and J. F. M. Oth, *Angew. Chem. Int.l Ed. Engl.*, 1966, **5**, 590.

17 W. von E. Doering and J. W. Rosenthal, *Tetrahedron Lett.*, 1967, **8**, 349–350.

18 R. T. Seidner, N. Nakatsuka and S. Masamune, *Can. J. Chem.*, 1970, **48**, 187–192.

19 M. Jones and L. T. Scott, *J. Am. Chem. Soc.*, 1967, **89**, 150–151.

20 M. Jones, S. D. Reich and L. T. Scott, *J. Am. Chem. Soc.*, 1970, **92**, 3118–3126.

21 U. Krüerke, *Angew. Chem. Int.l Ed. Engl.*, 1967, **6**, 79.

22 H. E. Zimmerman and G. L. Grunewald, *J. Am. Chem. Soc.*, 1966, **88**, 183–184.

23 H. E. Zimmerman, R. W. Binkley, R. S. Givens and M. A. Sherwin, *J. Am. Chem. Soc.*, 1967, **89**, 3932–3933.

24 H. E. Zimmerman and D. Armesto, *Chem. Rev.*, 1996, **96**, 3065–3112.

25 J. B. Lambert, *Tetrahedron Lett.*, 1963, **4**, 1901–1906.

26 J. C. Barborak, S. Chari and P. v. R. Schleyer, *J. Am. Chem. Soc.*, 1971, **93**, 5275–5277.

27 M. Sanz-Novo, M. Mato, Í. León, A. M. Echavarren and J. L. Alonso, *Angew. Chem. Int. Ed. Engl.*, 2022, **61**, e202117045

28 W. von Eggers Doering, B. M. Ferrier, E. T. Fossel, J. H. Hartenstein, M. Jones, G. Klumpp, R. M. Rubin and M. Saunders, *Tetrahedron*, 1967, **23**, 3943–3963.

29 S. Ferrer and A. M. Echavarren, *Synthesis*, 2019, **51**, 1037–1048.

30 J. F. M. Oth, S. Eckhard, H. Röttele and G. Schröder, *Justus. Liebigs. Ann. Chem.*, 1971, **745**, 112–123.

31 J. F. M. Oth, R. Merényi, H. Röttele and G. Schröder, *Chem. Ber.*, 1967, **100**, 3538–3550.

32 K. Sarma, W. Witt and G. Schröder, *Chem. Ber.*, 1986, **119**, 2339–2349.

33 K. Rebsamen and G. Schröder, *Chem. Ber.*, 1993, **126**, 1425–1427.

34 K. Rebsamen, H. Röttele and G. Schröder, *Chem. Ber.*, 1993, **126**, 1429–1433.

35 C. Grundmann, *Justus Liebigs Ann. Chem.*, 1938, **536**, 29–36.

36 F. Serratosa and J. Quintana, *Tetrahedron Lett.*, 1967, **8**, 2245–2249.

37 J. Font, F. López and F. Serratosa, *Tetrahedron Lett.*, 1972, **13**, 2589–2590.

38 R. H. Shapiro and M. J. Heath, *J. Am. Chem. Soc.*, 1967, **89**, 5734–5735.

39 J. S. Casas and F. Serratosa, *An. Quim.*, 1977, **73**, 300–302.

40 A. R. Lippert, J. Kaeobamrung and J. W. Bode, *J. Am. Chem. Soc.*, 2006, **128**, 14738–14739.

41 A. R. Lippert, V. L. Keleshian and J. W. Bode, *Org. Biomol. Chem.*, 2009, **7**, 1529–1532.

42 A. R. Lippert, A. Naganawa, V. L. Keleshian and J. W. Bode, *J. Am. Chem. Soc.*, 2010, **132**, 15790–15799.

43 M. He and J. W. Bode, *Proc. Natl. Acad. Sci. U.S.A*, 2011, **108**, 14752.

44 M. He and J. W. Bode, *Org. Biomol. Chem.*, 2013, **11**, 1306–1317.

45 P. R. McGonigal, C. de León, Y. Wang, A. Homs, C. R. Solorio-Alvarado and A. M. Echavarren, *Angew. Chem. Int. Ed. Engl.*, 2012, **51**, 13093–13096.

46 S. Ferrer and A. M. Echavarren, *Angew. Chem. Int. Ed. Engl.*, 2016, **55**, 11178–11182.

47 J. K. Stille, *Angew. Chem. Int. Ed. Engl.*, 1986, **25**, 508–524.

48 M. Achard, M. Mosrin, A. Tenaglia and G. Buono, *J. Org. Chem.*, 2006, **71**, 2907–2910.

49 O. Yahiaoui, L. F. Pašteka, B. Judeel and T. Fallon, *Angew. Chem. Int. Ed. Engl.*, 2018, **57**, 2570–2574.

50 B. Ma and J. K. Snyder, *Organometallics*, 2002, **21**, 4688–4695.

51 J. Charpentier, F. Voirol, F. Flachsmann, S. Tanner, N. Aeberli, G. Brunner and A. Goeke, *Helv. Chim. Acta.*, 2020, **103**, e2000175.

52 N. Miyaura and A. Suzuki, *J. Chem. Soc., Chem. Commun.*, 1979, 866.

53 N. Miyaura, K. Yamada and A. Suzuki, *Tetrahedron Lett.*, 1979, **20**, 3437–3440.

54 H. D. Patel, T.-H. Tran, C. J. Sumby, L. F. Pašteka and T. Fallon, *J. Am. Chem. Soc.*, 2020, **142**, 3680–3685.

55 D. Aich, P. Kumar, D. Ghorai, K. Kanti Das and S. Panda, *Chem. Commun.*, 2022, **58**, 13298–13316.

56 N. F. Nikitas, P. L. Gkizis and C. G. Kokotos, *Org. Biomol. Chem.*, 2021, **19**, 5237–5253.

57 M. N. Pomfret, P. B. Sun, Z. Huang, A. C. Freund, T. Miyoshi, and M. R. Golder, *Angew. Chem. Int. Ed. Engl.*, 2023, **62**, e202301695.

58 R. S. Cahn, C. Ingold and V. Prelog, *Angew. Chem. Int. Ed. Engl.*, 1966, **5**, 385–415.

59 O. Yahiaoui, H. D. Patel, K. S. Chinner, L. F. Pašteka and T. Fallon, *Org. Lett.*, 2020, **23**, 1157–1162.

60 B. M. Gimarc and A. R. Brant, *J. Chem. Inf. Comput. Sci.*, 1994, **34**, 1167–1173.

61 E. K. Lloyd and G. A. Jones, *Acta. Appl. Math.*, 1998, **52**, 121–147.

62 J. Brocas, *J. Math. Chem.*, 1994, **15**, 389–395.

63 M. H. Klin, S. S. Tratch and N. S. Zefirov, *J. Math. Chem.*, 1991, **7**, 135–151.

64 O. Yahiaoui, L. F. Pašteka, C. J. Blake, C. G. Newton and T. Fallon, *Org. Lett.*, 2019, **21**, 9574–9578.

65 M. Saunders, *Tetrahedron Lett.*, 1963, **4**, 1699–1702.

66 G. Schröder, J. F. M. Oth and R. Merényi, *Angew. Chem. Int. Ed. Engl.*, 1965, **4**, 752–761.

67 A. Allerhand and H. S. Gutowsky, *J. Am. Chem. Soc.*, 1965, **87**, 4092–4096.

68 J. D. Graham and E. R. Santee, *J. Am. Chem. Soc.*, 1966, **88**, 3453–3454.

69 S. M. Johnson, J. S. McKechnie, B. T. S. Lin and I. C. Paul, *J. Am. Chem. Soc.*, 1967, **89**, 7123–7123.

70 A. Amit, R. Huber and W. Hoppe, *Acta Crystallogr. B*, 1968, **24**, 865–869.

71 B. H. Meier and W. L. Earl, *J. Am. Chem. Soc.*, 1985, **107**, 5553–5555.

72 J. J. Titman, Z. Luz and H. W. Spiess, *J. Am. Chem. Soc.*, 1992, **114**, 3765–3771.

73 S. Schlick, Z. Luz, R. Poupko and H. Zimmermann, *J. Am. Chem. Soc.*, 1992, **114**, 4315–4320.

74 M. G. Newton and I. C. Paul, *J. Am. Chem. Soc.*, 1966, **88**, 3161–3162.

75 J. S. McKechnie, M. Gary. Newton and I. C. Paul, *J. Am. Chem. Soc.*, 1967, **89**, 4819–4825.

76 D. A. Hrovat, E. C. Brown, R. V. Williams, H. Quast and W. T. Borden, *J. Org. Chem.*, 2005, **70**, 2627–2632.

77 R. V. Williams, *Chem. Rev.*, 2001, **101**, 1185–1204.

78 T. Rozgonyi, A. Bartók-Pártay and A. Stirling, *J. Phys. Chem. A*, 2010, **114**, 1207–1211.

79 R. V. Williams, *Eur. J. Org. Chem.*, 2001, **2001**, 227–235.

80 T. Tran Ngoc, N. Grabicki, E. Irran, O. Dumele and J. F. Teichert, *Nat. Chem.*, 2023, **15**, 377–385.

81 T. Tran Ngoc, J. van der Welle, T. Rüffer and J. F. Teichert, *Synthesis*, 2023, **55**, 2658–2669.

82 G. Schröder and W. Witt, *Angew. Chem. Int. Ed. Engl.*, 1979, **18**, 311–312.

83 K. Sarma, W. Witt and G. Schröder, *Chem. Ber.*, 1983, **116**, 3800–3812.

84 M. Scholl, S. Ding, C. W. Lee and R. H. Grubbs, *Org. Lett.*, 1999, **1**, 953–956.

85 K. K. Larson, M. He, J. F. Teichert, A. Naganawa and J. W. Bode, *Chem. Sci.*, 2012, **3**, 1825–1828.

86 J. F. Teichert, D. Mazunin and J. W. Bode, *J. Am. Chem. Soc.*, 2013, **135**, 11314–11321.

87 A. P. Birvé, H. D. Patel, J. R. Price, W. M. Bloch and T. Fallon, *Angew. Chem. Int. Ed. Engl.*, 2022, **61**, e202115468

88 H. D. Patel, S. Gaggl, L. F. Pašteka and T. Fallon, *Org. Lett.*, 2022, **24**, 319–323.

89 S. R. Hare and D. J. Tantillo, *Pure Appl. Chem.*, 2017, **89**, 679–698.

90 D. H. Ess, S. E. Wheeler, R. G. Iafe, L. Xu, N. Çelebi-Ölçüm and K. N. Houk, *Angew. Chem. Int. Ed. Engl.*, 2008, **47**, 7592–7601.

91 C. Dohmen, H. Ihmels and T. Paululat, *Eur. J Org Chem*, 2022, **45**, e202201172

92 Y. L. Chow and C. I. Johansson, *J. Photochem. Photobiol.*, 1993, **74**, 171–180.

93 İ. Sidir and Y. G. Sidir, *J. Mol. Liq.*, 2016, **221**, 972–985.

94 M. Jones, *J. Am. Chem. Soc.*, 1967, **89**, 4236–4238.

95 L. A. Paquette and M. J. Kukla, *J. Am. Chem. Soc.*, 1972, **94**, 6874–6875.

96 A. Ottonello, J. A. Wyllie, O. Yahiaoui, S. Sun, R. A. Koelln, J. A. Homer, R. M. Johnson, E. Murray, P. Williams, J. R. Bolla, C. V. Robinson, T. Fallon, T. P. Soares da Costa and J. E. Moses, *Proc. Natl. Acad. Sci. U.S.A.*, 2023, **120**, e2208737120

97 J. R. Reimers, T. Li, A. P. Birvé, L. Yang, A. C. Aragonès, T. Fallon, D. S. Kosov and N. Darwish, *Nat. Commun.*, 2023, **14**, 6089.

98 P. M. Winter, G. M. Lanza, S. A. Wickline, M. Madou, C. Wang, P. B. Deotare, M. Loncar, Y. K. Yap, J. Rose, M. Auffan, O. Proux, V. Niviere, J.-Y. Bottero, Z. L. Wang, Y. Liu, R. G. Polcawich, J. S. Pulskamp, R. M. Proie, W.-T. Park, S. V. Kalinin, B. J. Rodriguez, A. L. Kholkin, G. L. Liu, J. Lagemaat, L. Valdevit, J. W. Hutchinson, S. Oh, M. Madou, K. Tonisch, E. De Rosa, J. Fernandez-Moure, E. Tasciotti, D. Gebauer, B. E. O'Neill and K. C. Li, in *Encyclopedia of Nanotechnology*, Springer Netherlands, Dordrecht, 2012, pp. 2111–2117.

99 Z. Shadfar, O. Yahiaoui, T. A. Collier, T. Fallon and J. R. Allison, *J. Chem. Phys.*, 2021, **154**, 154105.

100 G. Crini, *Chem. Rev.*, 2014, **114**, 10940–10975.

101 A. Villiers, *Bull. Soc. Chim. Fr.*, 1891, **45**, 468.

102 F. Cramer, *Angew. Chem.*, 1952, **64**, 136–136.

103 L. Szente and J. Szemán, *Anal. Chem.*, 2013, **85**, 8024–8030.

104 G. Astray, C. Gonzalez-Barreiro, J. C. Mejuto, R. Rial-Otero and J. Simal-Gándara, *Food Hydrocoll.*, 2009, **23**, 1631–1640.

105 A. Gonzalez Pereira, M. Carpena, P. García Oliveira, J. C. Mejuto, M. A. Prieto and J. Simal Gandara, *Int. J. Mol. Sci.*, 2021, **22**, 1339.

106 O. Bekers, E. V. Uijtendaal, J. H. Beijnen, A. Bult and W. J. M. Underberg, *Drug Dev. Ind. Pharm.*, 1991, **17**, 1503–1549.

107 G. Tiwari, R. Tiwari and A. Rai, *J. Pharm. Bioallied Sci.*, 2010, **2**, 72.

108 Z. Liu, W. Xu, E. G. Kovaleva, J. Cheng and H. Li, *Adv. Agrochem.*, 2022, **1**, 89–99.

109 N. Morin-Crini, S. Fourmentin, É. Fenyvesi, E. Lichtfouse, G. Torri, M. Fourmentin and G. Crini, *Environ. Chem. Lett.*, 2021, **19**, 2581–2617.

110 D. D. Gadade and S. S. Pekamwar, *Adv. Pharm. Bull.*, 2020, **10**, 166–183.

111 Z. Juvancz and J. Szejtli, *Trends Anal.Chem.*, 2002, **21**, 379–388.

112 X. Wang, J. Wu, X. Liu, X. Qiu, L. Cao and Y. Ji, *ACS Appl. Mater. Interfaces*, 2022, **14**, 25928–25936.

113 E. Bilensoy, Ed., *Cyclodextrins in Pharmaceutics, Cosmetics, and Biomedicine*, Wiley, 2011.

114 R. A. Dunbar and F. V. Bright, *Supramol. Chem.*, 1994, **3**, 93–99.

115 J. Rotzler and M. Mayor, *Chem. Soc. Rev.*, 2013, **42**, 44–62.

116 P. R. Ashton, I. Baxter, S. J. Cantrill, M. C. T. Fyfe, P. T. Glink, J. F. Stoddart, A. J. P. White and D. J. Williams, *Angew. Chem. Int. Ed. Engl.*, 1998, **37**, 1294–1297.

117 K. Hirotsu, T. Higuchi, K. Fujita, T. Ueda, A. Shinoda, T. Imoto and I. Tabushi, *J. Org. Chem.*, 1982, **47**, 1143–1144.

118 Y. Liu, Z. Fan, H.-Y. Zhang, Y.-W. Yang, F. Ding, S.-X. Liu, X. Wu, T. Wada and Y. Inoue, *J. Org. Chem.*, 2003, **68**, 8345–8352.

119 D. J. Cram, *Science*, 1983, **219**, 1177–1183.

120 G. Montà-González, F. Sancenón, R. Martínez-Máñez and V. Martí-Centelles, *Chem. Rev.*, 2022, **122**, 13636–13708.

121 A. Wishard and B. C. Gibb, *Calixarenes and Beyond*, Springer International Publishing, 2016, pp. 195–234.

122 P. Timmerman, W. Verboom and D. N. Reinhoudt, *Tetrahedron*, 1996, **52**, 2663–2704.

123 H. Konishi, T. Nakamura, K. Ohata, K. Kobayashi and O. Morikawa, *Tetrahedron Lett.*, 1996, **37**, 7383–7386.

124 C. R. Pfeiffer, K. A. Feaster, S. J. Dalgarno and J. L. Atwood, *Cryst. Eng. Comm.*, 2016, **18**, 222–229.

125 D. Moore, G. W. Watson, T. Gunnlaugsson and S. E. Matthews, *New J. Chem.*, 2008, **32**, 994.

126 D. J. Cram, S. Karbach, Y. H. Kim, L. Baczynskyj and G. W. Kallemeyn, *J. Am. Chem. Soc.*, 1985, **107**, 2575–2576.

127 R. Warmuth, *Supramolecular Chemistry*, Wiley, 2012.

128 D. J. Cram, *J. Incl. Phenom. Macro.*, 1988, **6**, 397–413.

129 D. J. Cram, R. Jaeger and K. Deshayes, *J. Am. Chem. Soc.*, 1993, **115**, 10111–10116.

130 M. L. C. Quan and D. J. Cram, *J. Am. Chem. Soc.*, 1991, **113**, 2754–2755.

131 J. C. Sherman, D. J. Cram, J. A. Bryant, T Blanda, M. Vincenti and C. B. Knobler, *J. Am. Chem. Soc.*, 1991, **113**, 7717–7727.

132 J. Yoon, C. Sheu, K. N. Houk, C. B. Knobler and D. J. Cram, *J. Org. Chem.*, 1996, **61**, 9323–9339.

133 C. L. D. Gibb and B. C. Gibb, *J. Am. Chem. Soc.*, 2004, **126**, 11408–11409.

134 K. Wang and B. C. Gibb, *J. Org. Chem.*, 2017, **82**, 4279–4288.

135 C. L. D. Gibb and B. C. Gibb, *J. Am. Chem. Soc.*, 2006, **128**, 16498–16499.

136 C. L. D. Gibb and B. C. Gibb, *J. Am. Chem. Soc.*, 2011, **133**, 7344–7347.

137 H. S. Ashbaugh, B. C. Gibb and P. Suating, *J. Phys. Chem. B*, 2021, **125**, 3253–3268.

138 B. W. Purse and J. Rebek, *Proc. Natl. Acad. Sci. U.S.A*, 2005, **102**, 10777–10782.

139 X. Cai, R. Kataria and B. C. Gibb, *J. Am. Chem. Soc.*, 2020, **142**, 8291–8298.

140 J. C. Sherman and D. J. Cram, *J. Am. Chem. Soc.*, 1989, **111**, 4527–4528.

141 D. J. Cram, M. E. Tanner and R. Thomas, *Angew. Chem. Int. Ed. Engl.*, 1991, **30**, 1024–1027.

142 M. Avram, G. Mateescu, I. G. Dinulescu, E. Marica and C. D. Nenitzescu, *Tetrahedron Lett.*, 1961, **2**, 21–26.

143 M. Avram, I. G. Dinulescu, E. Marica, G. Mateescu, E. Sliam and C. D. Nenitzescu, *Chem. Ber.*, 1964, **97**, 382–389.

144 E. Hedaya, R. D. Miller, D. W. McNeil, P. F. D'Angelo and P. Schissel, *J. Am. Chem. Soc.*, 1969, **91**, 1875–1877.

145 P. Roach and R. Warmuth, *Angew. Chem. Int. Ed. Engl.*, 2003, **42**, 3039–3042.

146 J. Bredt, *Justus Liebigs Ann. Chem.*, 1924, **437**, 1–13.

147 J. Bredt, Jos. Houben and P. Levy, *Chem. Ber.*, 1902, **35**, 1286–1292.

148 B. M. O'Leary, R. M. Grotzfeld and J. Rebek, *J. Am. Chem. Soc.*, 1997, **119**, 11701–11702.

149 R. G. Chapman and J. C. Sherman, *J. Org. Chem.*, 2000, **65**, 513–516.

150 H. Eyring, *J. Chem. Phys.*, 1935, **3**, 107–115.

Chapter 2 |

A Guide to Bullvalene Stereodynamics

Manuscript to be submitted as ‘A Guide to Bullvalene Stereodynamics’ William Maturi, Robert A. Ives, Matthew Gill, Conor D. Rankine, and Paul R. McGonigal.

Abstract

Herein we outline a simple set of rules for bullvalene's rearrangement process, including a new positional naming system (α, β, γ, and δ) and an equation that may be used to calculate the number of isomers for a given bullvalene system. Furthermore, we perform principle moments of inertia and exit vector analysis on three substituted bullvalenes and compare its results to commonly used ring systems in medicinal chemistry. We find that bullvalene's 3-D shape makes it comparable to other bioisosteres currently used to replace planar aromatic ring systems in drug discovery. Moreover, bullvalene's valence isomerisation presents a unique opportunity for medicinal chemists, with numerous shapes and substituent relationships attainable as a concentration-independent dynamic covalent library from a single compound.

Acknowledgments

The following people are gratefully acknowledged for their contribution to this chapter: Robert Ives for contributions to editing the text and contribution to computational work. Dr. Matthew Gill for contributions to editing the text. Dr. Connor Rankine for helping to develop the bullviso tool for isomer generation and performing computational work.

2.1 Introduction

The $C_{10}H_{10}$ hydrocarbon cage bullvalene (BV) fluctuates between 1,209,600 degenerate isomers through rapid and reversible strain-promoted Cope rearrangements (Figure 1).[1–3] There are now several useful synthetic methods available to prepare substituted derivatives of BV,[4–7] which fluctuate between nondegenerate constitutional isomers with distinct shapes. This 'shapeshifting' property of BVs and other fluxional molecules has presented opportunities for their inclusion as dynamic structural units in functional molecules and materials, [8] such as chemical sensors,[7,9,10] fluorophores,[11] metal complexes,[12,13] components of electro-mechanical systems,[14] rigid-rod polymers,[15,16] and antibiotics.[17]

BVs have the seemingly contradictory characteristics of being both highly dynamic molecules, while also being rigid 3D structures. Their tricyclic hydrocarbon skeletons are shape-persistent structures with the substituents projecting outwards at well-defined angles. Building blocks with rigid 3D structures are key components of materials, such as metal-organic frameworks[18,19] and other porous networks.[20,21] In the context of medicinal chemistry research and particularly fragment-based drug discovery (FBDD) libraries,[22] there has been growing concern that drug candidates based on flat or rod-like molecules offer limited shape diversity.[23]

Consequently, there is a desire for a greater number of diverse 3-D fragments to be included within these libraries to cover more chemical space and to escape the 'flatland'.[24] One way that this objective can be achieved is by exploring and employing more exotic hydrocarbon frameworks as fragments; particularly as the molecular core is considered the key factor in shape diversity.[23,25] It has also been suggested that increasing the 3-dimensionality of drug leads can result in enhanced biological activity.[23,25] Herein, we discuss the 3-D shape diversity accessible from BVs and how their fluxional behaviour allows BVs to be used to explore new areas of chemical space. Designing effective materials based on BV derivatives requires understanding of their stereodynamics, i.e., their overall 3D shapes, the relative orientations that are accessible to appended substituents, and the relative energies of the isomers at equilibrium. We provide a concise guide to the rearrangement processes of substituted BVs and apply computational modelling to categorize and quantify their stereodynamics. To do so, we perform energy-weighted principal moment of inertia (PMI)[26] and exit vector (EV)[27,28] analyses. Much of the analysis can be automated

using a new computational tool we have developed, bullviso, that generates all the isomers of a given substituted BV, and the input files needed to compute relative energy levels of each isomer. To demonstrate its utility, we apply bullviso to examine di-, tri- and tetramethyl BVs. The analysis illustrates that shapeshifting mixtures of BV derivatives not only dynamically sample different areas of chemical space from a single starting compound, but they also position their substituents at a range of angles, extending beyond those typically found in *cis*-1,3- and *cis*-1,4-disubstituted rings. Moreover, BV systems maintain a higher degree of sphericity than most common ring systems found in biologically active molecules.

2.2 Bullvalene's Structure

Given the large number of possible BV isomers, a method for naming them is essential for any discussion involving their interconversion. Bode and coworkers developed a barcode labelling system by numbering each position on the BV as shown in Figure 1a. The number in the barcode depends on the group at that position, enabling each isomer to be described with a unique numeric code.[29] Importantly, this system enables isomer information to be parsed in computer algorithms to construct a full network map for interconversion of all the non-degenerate isomers of a substituted BV – a task that is otherwise impractical to do by hand. Whilst this model is a helpful guide to understanding the interconversion of BV isomers by concisely and comprehensibly describing the positions of all substituents in any given isomer, its inherent complexity makes reference to individual positions challenging.

In order to describe and discuss the elementary steps of BV rearrangements and make reference to distinct positions in the structure, we suggest the use of Greek letter locants as positional labels. The threefold rotational symmetry of the BV core reduces its number of chemically inequivalent positions to four. Therefore, we label these positions as α–δ (Figure 1b), starting from α as the apical bridgehead position to δ as the cyclopropyl position. The olefin positions, which are typically the energetically favoured sites for any non-hydrogen substituents are labelled as β and γ. Prime and double prime labels distinguish the different 'arms' of the BV.

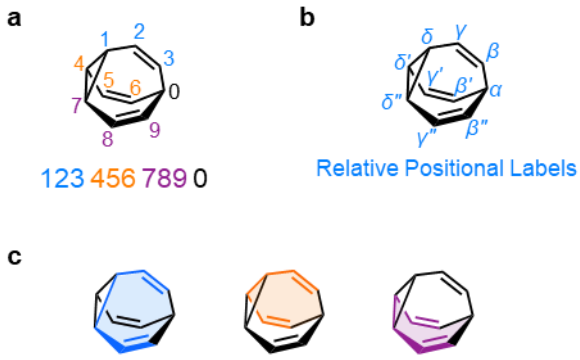

Figure 1: (a) The BV isomer barcode labelling system and (b) relative positional labels. (c) The three faces of BV that can each participate in a Cope rearrangement highlighted in different colours.

2.3 The Elementary Bullvalene Rearrangement Steps

Each BV rearrangement occurs on one of the three 'faces' (Figure 1c), which all present a 1,5-hexadiene motif, constituting two arms of the BV. The positions of the BV that are part of the 1,5-hexadiene undergoing a given Cope rearrangement can be referred to as participating sites (P), while the other four positions are non-participating sites (NP). Whether a substituent is located on a P or a NP site determines its resulting position on the BV following isomerization. The α is always on an NP site and thus has only one positional outcome for rearreangements. On the other hand, for each of the other sites (β, γ and δ), there exist two potential positional outcomes following a single rearrangement step, even though there are three possible 1,5-hexadiene moieties that can undergo Cope rearrangement.

These positional outcomes can be determined using mono-substituted BV as a model. Firstly, the α position has only one positional outcome, as demonstrated in Figure 2ai, the α position will always migrate to a newly formed δ position. There are two noteworthy elements to this first rearrangement: (i) The α substituent exchanges positions to a δ substituent on the NP arm. (ii) This rearrangement is reversible, thus a δ substituent on a NP position will migrate to the α position. Conversely, a substituent on the δ position on a P site will migrate, reversibly, to the β position (Figure 2aii). Figure 2aiii demonstrates the reversible migration of a β substituent to

the γ position when in a NP position. Finally, a γ substituent in a P position remains in the γ position, due to symmetry in the transition state for BV (Figures 2aiv and 2b).

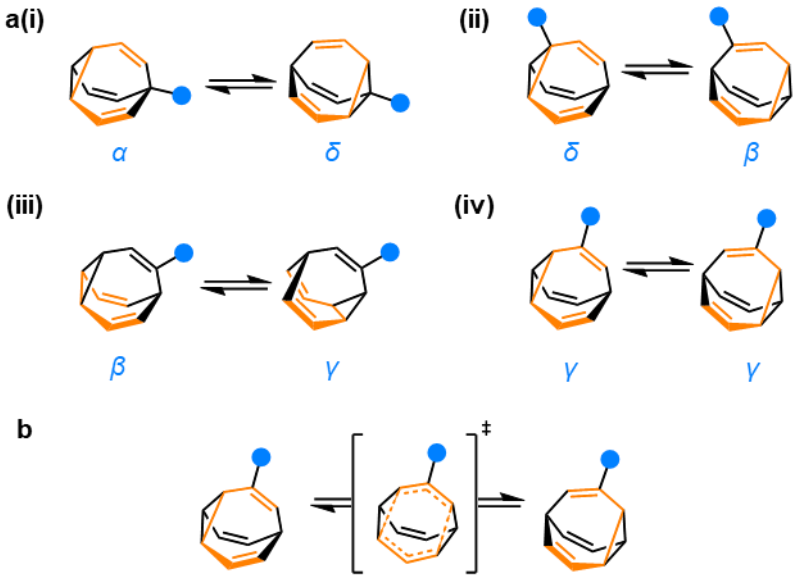

Figure 2 (a)(i–iv) Rearrangement process of each BV position (α, β, γ and δ) showing the isomer that is formed directly. (b) Illustration of the higher symmetry in a transition state relative to its ground state.

To summarize, the elementary steps that govern the outcome of any BV rearrangement are:

(a) $\alpha_{NP} \rightleftharpoons \delta_{NP}$

(b) $\delta_{P} \rightleftharpoons \beta_{P}$

(c) $\beta_{NP} \rightleftharpoons \gamma_{NP}$

(d) $\gamma_{P} \rightleftharpoons \gamma_{P}$

These elementary steps apply equally to every BV substituent in every isomer, regardless of the total number of substituents or their relative positions. Therefore, they may be used to predict and describe the movement of groups on BV and determine the relationship between all BV isomers. These rules are summarised schematically in Figure 3.

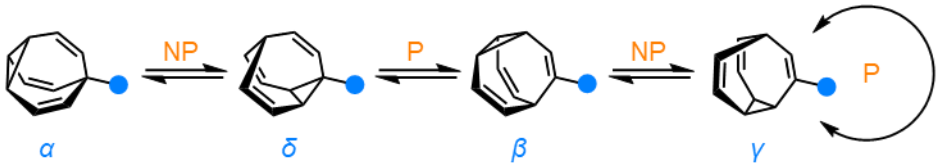

Figure 3 The simplest isomer network of a BV (i.e., a monosubstituted BV) showing the migration of a substituent following Cope rearrangements. Full isomerisation requires sequential Cope rearrangement steps that include the substituent in the 1,5-hexadiene unit (P = participating) or exclude it (NP = non-participating).[30]

2.4 Calculating the Number of BV Isomers

Calculating the number of unique BV isomers is one of the most important considerations for the construction of a BV interconversion network. When Bode *et al.* reported their method for generating codes for BV isomers, they also provided a Matlab code to calculate the number of unique BV isomers.[29] We present *Equation 1* which provides an intuitive "back of the envelope" method for calculating the number of isomers for a given BV system where:

- N_{iso} is the number of unique non-degenerate isomers of the BV (enantiomers are considered to be unique isomers).
- $\prod_{a=1}^{A} N_a!$ is calculated by multiplying together a term for each unique type of substituent (including H). The term is the factorial of the number of incidences of that substituent appended to the BV.
- S is a correction value that accounts for the C_{3v} symmetry of BV and has a value of 0, 1, 3 or 6.
- The 1/3 multiplier accounts for the C_{3v} symmetry of BV as identical isomers will be represented three times in all of the combinations.

$$N_{iso} = \frac{1}{3}\left(\frac{10!}{\prod_{a=1}^{A} N_a!} + 2S\right)$$

Equation 1: Equation for calculating the number of nondegenerate isomers within a given BV system.

This equation treats each substituent as one number within a group of ten numbers, similarly to the isomer barcode system. For example, a BV with three unique substituents, **1**, is represented as 0000000123 (Figure 4a), or a BV with three identical substituents, **2**, and one unique substituent is represented as 0000001112. The equation then uses combinatorics to calculate the total number of ways in which these substituents can be ordered. For example, for **1** there are three substituents that occur once in the BV and a fourth "substituent" (H) that occurs 7 times, therefore, the denominator of the equation becomes 1! × 1! × 1! × 7!. Whereas, for **2** there is one substituent that occurs once, one substituent that occurs 3 times and H that occurs 6 times, therefore, the denominator of the equation becomes 1! × 3! × 6!.

This number is then divided by three due to the C_{3v} symmetry of BV's core. An issue arises from the 1/3 term in the equation and that is that not every isomer will be repeated three times; BV isomers that have three identically substituted arms will only be represented once each in the combinatoric calculation. As such, a correction is

required and the term 2*S* must be introduced to account for duplicates before dividing by three. *S* is the number of ways that the substituents can be arranged around the BV to provide C_{3v} symmetry, or in other words where all three arms of the BV possess identical substitution patterns. For example, the substituents on **1** cannot be arranged in any way such that it possesses C_{3v} symmetry, hence $S = 0$ (Figure 4a). However, in the case of **2**, three of the substituents are the same and thus there are three different ways in which they can be arranged such that the BV possesses C_{3v} symmetry (Figure 4b). The three identical isomers are possible only when the unique substituent is at the α position. They are thus present where the three similar substituents are all on the β position, all on the γ position or all on the δ position; as a result, for **2** the term $S = 3$. Therefore, with the correction introduced the equation for N_{iso} of **1** gives 240 and for **2** it gives 282 unique isomers.

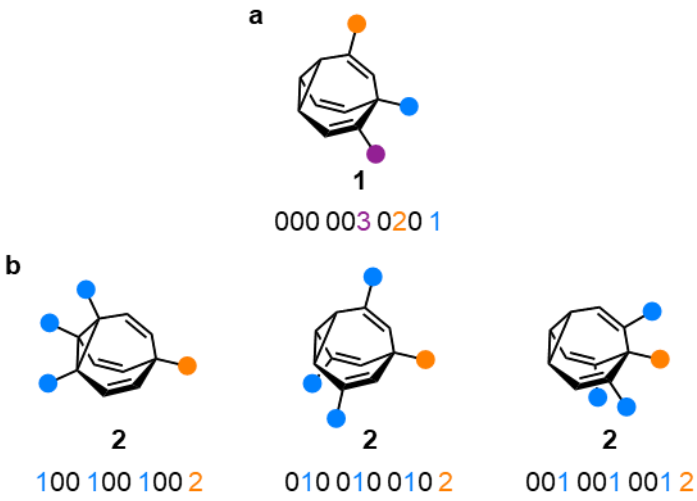

Figure 4: (a) Structural depiction of an isomer of BV 1 and (b) the three isomers of BV 2 with C_{3v} symmetry and respective isomer codes using Bode's isomer code system.

For the 42 possible BV substituent systems, $S = 0$ for 35 of them. The only cases where $S \neq 0$ are where the ten substituents can be grouped into three groups of three similar substituents, with one 'extra' substituent. For example, in the case of **2** the substituents may be grouped as 000, 000, 111, and 2, whereas this is not possible for **1**. The only cases where $S = 1$ are where there is a single substituent (as the single substituent can sit in the α position) or where there are no substituents. An example of a system where $S = 6$ is where there are two unique substituents which are in groups of three, such as a 0001112223 system. This is because isomers 012 012 012 3, 021 021 021 3, 102 102 102 3, 120 120 120 3, 201 201 201 3 and 210 210 210 3, all have identical arms.

2.5 Generating Bullvalene Isomers (bullviso)

bullviso[31] is an in-house-developed Python3 code [publicly available under the GNU Public License (GPLv3) on GitLab] that interfaces with RDKit[32,33] to generate Cartesian coordinates for substituted BVs. *bullviso* generates exhaustively all possible isomer barcodes for a *K*-substituted [*K* = 1–10] BV and filters out the non-unique isomer barcodes according to the protocol outlined by Bode *et al.*[29] Cartesian coordinates sampling the constitutional isomers of the substituted BV are generated by grafting a given substituent (supplied as a SMILES string) onto a BV to produce a unique substituted BV corresponding to each isomer barcode. *bullviso* can generate up to *N* configurational/conformational isomers according to the experimental-torsion distance geometry (ETDG) with 'basic knowledge' (+K) embedding approach (ETKDGv3)[34,35] as implemented in RDKit; these configurational/conformational isomers are then (pre-)optimized using the Universal Force Field (UFF)[36] and the *M* lowest-energy isomers are returned. Cartesian coordinates can be outputted in *xyz* file format or, alternatively, as pre-prepared inputs for Gaussian (G09; G16)[37] or Orca (> v5).[38–40]

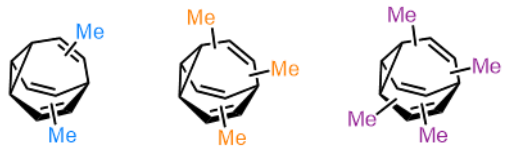

3 **4** **5**

*Figure 5: Compounds Me_2BV (**3**), Me_3BV (**4**) and Me_4BV (**5**).*

2.6 Principal Moments of Inertia Analysis

Principal moments of inertia (PMI) plots, as developed by Saur and Schwartz,[26] have been used as a straightforward and quantitative method to assess the shape diversity of potential pharmaceutical molecules.[41,42] Typical PMI plots present either the lowest energy conformer of any given compound to compare the inherent shapes of an array of molecules;[43,44] or a range of conformers to gain insight into conformational diversity of a limited number of molecules.[24] The lowest energy conformer determined by DFT calculations for each isomer of the BVs **3**–**5** (Figure 5) was used to examine shape diversity within the substituted BV networks. This approach, using methyl substituted BVs, allows us to emphasise the properties of the BV scaffold and the impact of its valence isomerisation.

Density functional theory (DFT) calculations using the PBE0[45–47] functional with Grimme's D3 dispersion correction[48] and the def2-SV(P)[49] basis set were deemed suitable for modelling the energetics of BV systems. Using this level of theory, we modelled all the isomers populations of **3**, **4** and **5** (15, 42, and 72 isomers respectively). For these isomers, we calculated the three principal moments of inertia (I_1, I_2 and I_3 in ascending order) using a KNIME[50] Vernalis[51] chemoinformatic protocol, to calculate normal PMI ratios (NPRs) for all isomers (Equations 2 and 3).

$$(\mathbf{a})\ \mathrm{NPR1} = \frac{I_1}{I_3} \qquad (\mathbf{b})\ \mathrm{NPR2} = \frac{I_2}{I_3}$$

Equation 2: (a) For calculating NPR1; and (b) For calculating NPR2, where I_1, I_2 and I_3 represent the three principal moments of inertia in ascending order.

Calculated NPR values were then plotted onto a 2-D PMI plot (Figure 6a–c, NPR1 vs NPR2), following the standard layout with vertices defined by values associated with rod-like [0,1], disk-like [0.5, 0.5] and spherical [1,1] geometry, analogous to alkyne, benzene and adamantane structures respectively (Figure 7a). Parallel lines on the PMI plot correspond to ΣNPR values (ΣNPR = NPR1 + NPR2) between 1.0 and 2.0. The points that lie furthest from the rod-disc axis (ΣNPR = 1.0) are indicative of greater 3-D character.

The PMI plot of Me_2BV (**3**) (Figure 6ai) shows the structural diversity in the population of constitutional isomers, which are located in the range $1.44 \leq \Sigma\mathrm{NPR} \leq 1.57$. The isomers are labelled alphabetically (A–O) in ascending order. Darker labelled points (**3**$_{B/C}$ / **3**$_{E/F}$ / **3**$_{H/I}$) indicate the overlap in PMI coordinates for the three enantiomeric pairs of **3**. In addition, we present the energy-weighted PMI plots (Figure 6aii) by scaling the data point size according to the Boltzmann population at 298 K. Figure 6aii shows that the four lowest energy isomers of Me_2BV (**3**$_{A–D}$) have good 3-D coverage; the vast majority (>90%) of the population will exist as one of these constitutional isomers free in solution at 298 K.

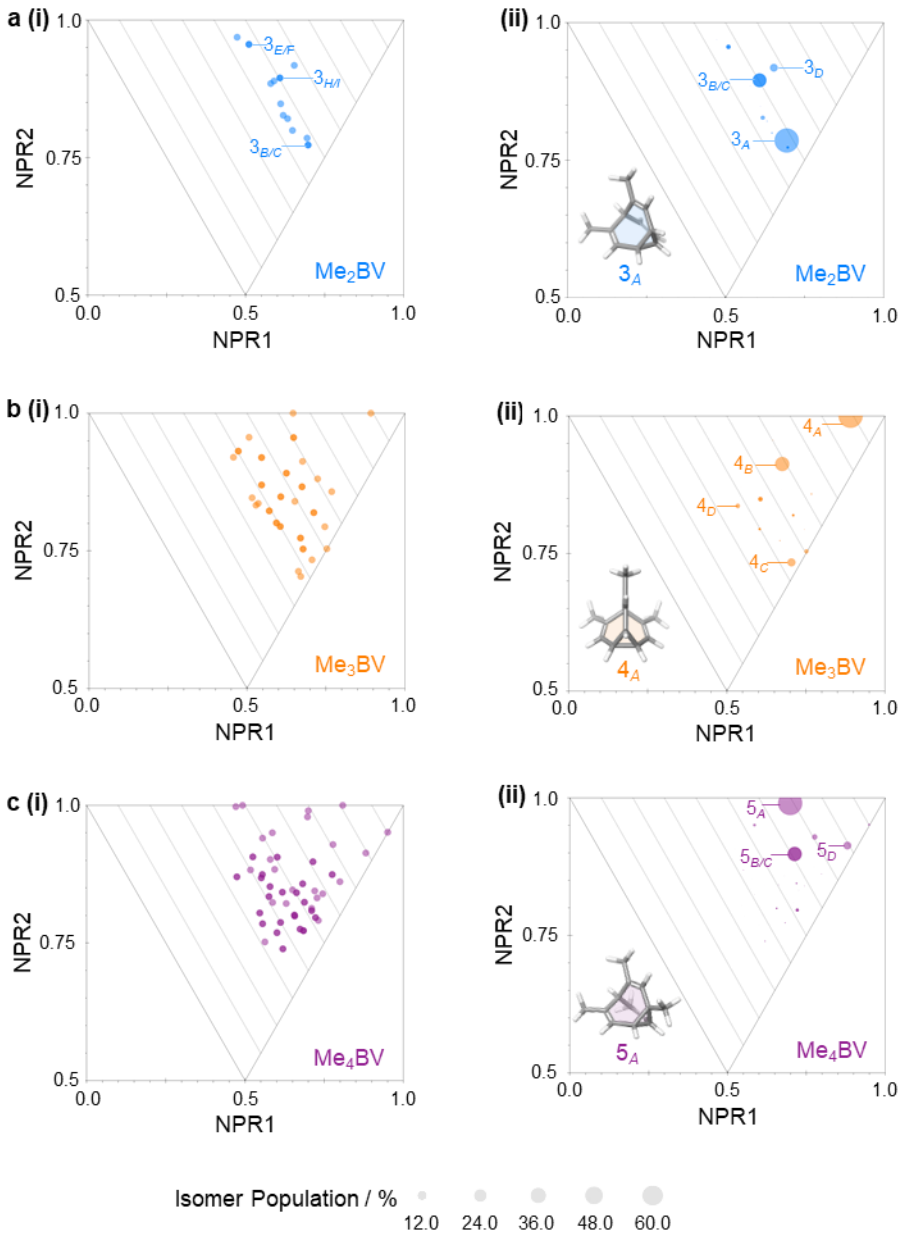

*Figure 6: (a)(i) Me_2BV (**3**) PMI plot highlighting enantiomeric pairs (**$3_{B/C}$** / **$3_{E/F}$** / **$3_{H/I}$**), (ii) Me_2BV (**3**) PMI plot adjusted by Boltzmann distribution at 298 K. The lowest energy isomer, **3_A**, is depicted, with the four lowest energy isomers, **$3_{A–D}$**, highlighted. (b)(i) Me_3BV (**4**) PMI plot, (ii) Me_3BV (**4**) PMI plot adjusted by Boltzmann distribution at 298 K. The lowest energy isomer, **4_A**, is depicted, and **$4_{A–D}$** highlighted. (c)(i) Me_4BV (**5**) PMI plot, (ii) Me_4BV (**5**) PMI plot adjusted by Boltzmann distribution at 298 K. The lowest energy isomer **5_A** is depicted, with **$5_{A–D}$** highlighted.*

The introduction of further substituents to the BV scaffold (**4** and **5**) results in increased 3-D variety (Figure 6b and 6c) with a greater proportion of more spherical structures where ΣNPR ≥ 1.7 (maxima of 1.89 and 1.90 for **4** and **5**, respectively). In both cases, the PMI distributions are markedly broader than that of **3**, spanning 1.3 ≤ ΣNPR ≤ 1.9. Similarly to **3**, only a small number of **4** and **5**'s constitutional isomers are energetically favorable in solution (Figure 6bii and 6cii). Despite this, even the

most energetically favourable isomers exhibit large shape diversity. Nonetheless, favourable binding interactions may compensate for the difference in energy between the less favourable isomers, as BV frequently adapts to its environment in supramolecular systems.[7,9,12,13] As a result, isomers which are not favourable free in solution may still be present in binding motifs.

In order to understand how BVs coverage of chemical space compares to commonly used ring systems, a small representative library of rings prominent in pharmaceuticals was compared to methyl substituted BVs (Figure S1).[52,53] PMI analysis demonstrates the lack of 3-D diversity in currently used ring systems (Figure 7).[52,53] Notably, no BV scaffolds are located close to the rod-disc axis (ΣNPR ≤ 1.3) whereas many of the prevalent rings are. Compounds **6**, **7** and **8** are the most comparable common structures substituted BVs in terms of space coverage. Many recent works have utilized adamantane and cubane scaffolds as bioisosteres for planar systems due to their 3-D, rigid structures. [54–56] However, each constitutional isomer of adamantane and cubane must be synthesised in an independent process, whereas BV can access all of its constitutional isomers through energetically accessible Cope rearrangements.

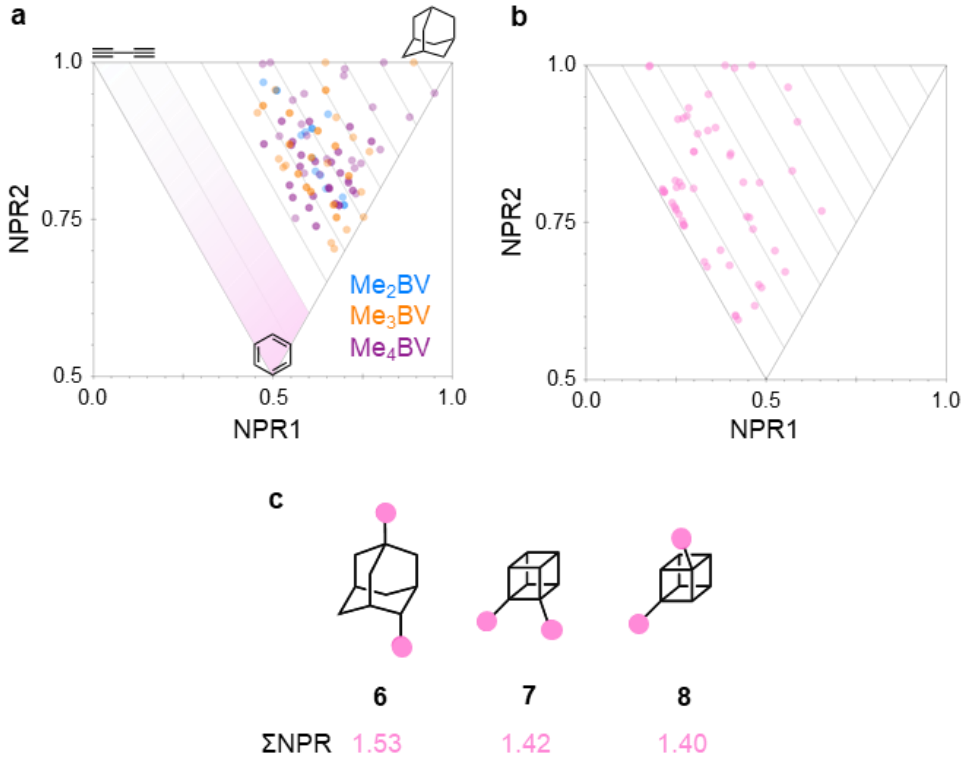

*Figure 7: (a) PMI plot showing space coverage of Me_2BV (**3**), Me_3BV (**4**) and Me_4BV (**5**) isomers away from the rod-disc axis (pink region). (b) PMI plot for common ring systems. (c) Structures of compounds 1,4-Me_2 adamantane (**6**), 1,2-Me_2 cubane (**7**) and 1,4-Me_2 cubane (**8**). ΣNPR values for compounds **6**–**8** are shown.*

2.7 Exit Vector Analysis

Exit vector (EV) plots analyse the 3-D relationship between two substituents, these plots are useful to compare the geometry of ring systems in bioisostere studies.[28] The EV plot for a single molecule will possess only one data point if a compound is conformationally rigid and multiple points if it is conformationally flexible or possesses multiple isomers, as is the case with BV. Usually, multiple compounds are shown in a single plot for comparison. The relative orientation of two exit vectors (v_1 and v_2), appended to a central scaffold, can be described by four geometric parameters: the distance between the appended carbons (r); the dihedral angle of the vectors (θ) and the plane angles of each vector (φ_1 and φ_2) (Figure 8a and 8b).[27,28] These values were calculated computationally for all isomers of methyl substituted BVs **3**, **4** and **5**. Typically, EV plots are constructed using θ = 0°–180°; as there is no convention for dihedral angle directionality, so each θ is a positive value. In most systems, negative θ values are not necessary other than to directly compare enantiomers. In the case of BV, it is important to consider the enantiomers as they are in dynamic equilibrium with the rest of the constitutional isomers, making them inseparable from the mixture. As a result, exclusion of negative θ values would disregard the full structural diversity of the BV scaffold. In addition, because of the spherical nature of BVs, the dihedral angle is always between –60° and 60°. Consequently, plotting θ from –90° to +90° is more useful for BVs instead of the convention.

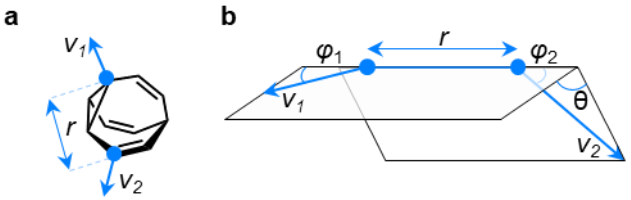

*Figure 8: (a) Illustration of the vectors, v_1 and v_2 (compound **3**'s scaffold used as an example). b) Definition of geometric parameters r, φ_1, φ_2, and θ.*

For Me_2BV **3,** there are 15 constitutional isomers shown by the EV plot to be confined to two distinct regions, with the majority at θ ~ 0° and some other peaks around θ ~ ±30°. The points in the former region spanning a range of r ~ 1.3–3.1 Å (Figure 9ai). This small distribution occurs due to the intrinsic planarity of appended carbon atoms within the BV scaffold. The data points at θ ~ 0° are a result of when the two methyl groups are either on the same arm of the BV or placed at the same type of position on BV, i.e. both on the β position, on different 'arms'. The four points located at θ ~ ±30°

correspond to two of the three enantiomer pairs of the isomers with differently substituted arms (**3**$_{B/C}$ and **3**$_{E/F}$). For the final enantiomer pair, **3**$_{H/I}$, θ = ±0.5°.

An energy-weighted EV plot was constructed for **3** to account for the Boltzmann population of isomers at 298 K in solution (Figure 9aii). The two major data points correspond to **3**$_A$ (r = 2.52, θ = 0°, p = 53%) and enantiomer pair ***3***$_{B/C}$ (r ~ 3.10 Å, θ ~ 30°, p = 17% for each enantiomer) which exhibit a significant alteration in EVs.

As the absolute geometry of the BV core is well defined, we would expect compounds **4** and **5** to exhibit similar characteristics to **3**. This is true when the Boltzmann distribution of isomers energetically accessible in solution is considered, with the most favourable isomers appearing at θ ~ 0° and θ ~ ±30° (Figures 9aii, 9bii and 9cii). However, for the complete isomer network, different relationships are present as a broader distribution of dihedral angles between –60° and 60° is observed (Figures 9ai, 9bi and 9ci). The greater spread of dihedral angles for compounds **4** and **5** compared to **3** can be attributed to an increase in steric hindrance as a result of the introduction of additional substituents.

For **3** and **4**, the substituents may be arranged such that all the groups are in the β position, which is typically the most favourable position, resulting in the lowest energy and thus most populated isomer. However, in the case of **5** it is not possible for all of the methyl groups to be in the β position and thus the fourth methyl group will be in one of the other three positions which gives rise to new spatial relationships for lower energy isomers. As a result, there are six data points in the θ ~ ±30° region for Me_4BV **5**, which are significantly populated at 298 K in solution (Figure 9cii).

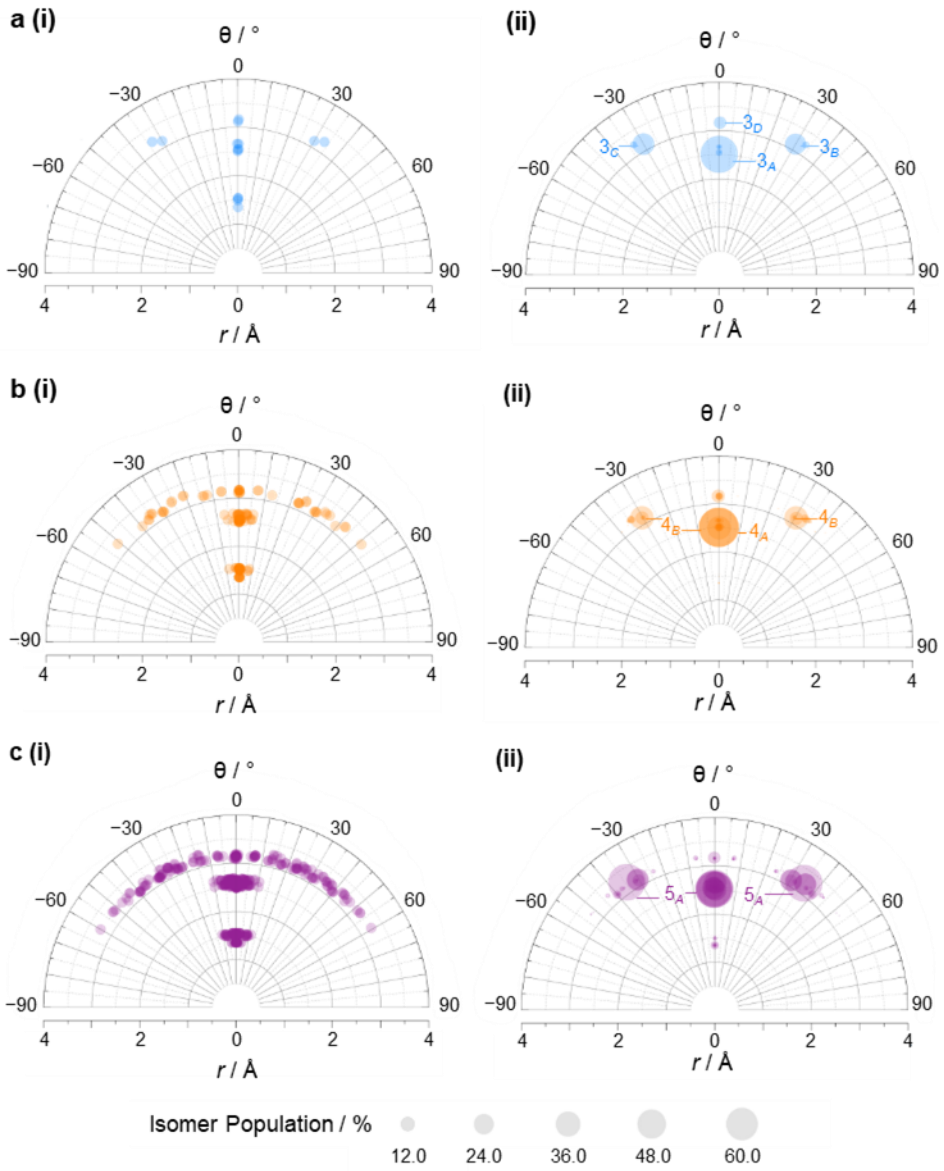

*Figure 9: (a)298 K. (b)(i) Me₃BV (**4**) EVP for 42 isomers; (ii) Me₃BV (**4**) EVP adjusted by Boltzmann distribution at 298 K. (c)(i) Me₄BV (**5**) EVP for 72 isomers; (ii) Me₄BV (**5**) EVP adjusted by Boltzmann distribution at 298 K.*

Figure 10a illustrates four defined regions, *a–d*, determined by Grygorenko *et al.*, which encompass the common exit vectors of disubstituted cycloalkanes.[28,56,57] This plot was constructed by extensive analysis of compounds in the Cambridge Structural Database and calculating the exit vectors of the two substituents. The plot shows the areas of chemical space that can be accessed with common aliphatic ring systems and which systems give access to such regions. For example, region *a* is populated with 1,2-disubstituted aliphatic rings whereas region *b* typically corresponds to 1,3- and *cis*-1,4-disubstituted cyclohexanes.

Figure 10b shows this same plot overlaid with data from Figure 9 so that the exit vectors of the substituted BVs **3–5** can be compared to common aliphatic ring systems.

For the methyl substituted BVs, a proportion of data points from each compound fall within the *a* or *b* region. Grygorenko *et al.* state that substituents which are present around θ = 0° in region *a* correspond specifically to *cis*-1,2-disubstituted cyclopropyl compounds.[28] The presence of BV data points in this region is expected, as the structure of BV contains a cyclopropyl ring which can only contain *cis*-substituents. The range of data points that lie outside of regions *a* and *b* represent an area of chemical space that cannot be easily accessed with standard disubstituted cycloalkanes.

Figure 10c shows the same data points as in Figure 10b adjusted for the Boltzmann distribution of isomers energetically accessible in solution and, therefore, depicts the regions of space that compounds **3**, **4** and **5** will cover at 298 K when free in solution. For compounds **3** and **4**, the isomers in region *a* disappear entirely due to the fact that having two substituents on the cyclopropyl ring is energetically unfavourable compared to other isomers. However, data points in this region do not completely disappear for compound **5**, because as previously mentioned, the introduction of the fourth substituent results in increased variation in substituent position for the lower energy isomers.

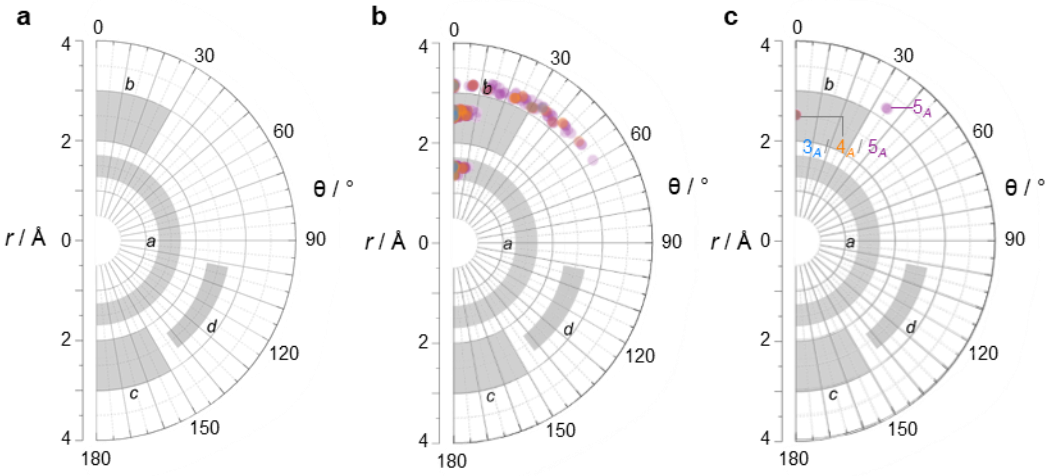

*Figure 10: (a) EVP for disubstituted cycloalkanes, showing regions (a, b, c and d) that correspond to common scaffolds.[28] (b) EVP comparison of entire population of **3**, **4** and **5** with common scaffolds. (c) EVP comparison of lowest energy isomer of **3**, **4** and **5** with common scaffolds.*

It is important to note that, particularly in a pharmaceutical context, the binding of a substituted BV to a target may result in the BV adopting a constitutional isomer that may be less energetically favourable in the solution state. Adaptation of BV's

constitutional isomers for preferential binding in supramolecular systems is well established.[9,12,58] Therefore, it is important not to dismiss isomers that with a low population at 298 K, as they may still be accessible or even preferred when bound to a target. Each of the points plotted on the non-energy-weighted plots may present a potential binding motif.

Collectively, these plots demonstrate the potential that substituted BV has to act as a 3-D scaffold in medicinal chemistry, particularly in the field of FBDD. We have demonstrated through PMI plots that these substituted BVs exhibit persistent 3-D character, lying in the ~1.30 ≤ ΣNPR ≤ ~1.90 region, which is underrepresented in common pharmaceuticals.[24,52,53,56] This has also shown that the substituted BVs share similarities to adamantane and cubane which are used as bioisosteres for planar, linear compounds in FBDD.[59–61] We have also shown through exit vector plots that substituted BVs cover regions of chemical space that are not populated by prevalent cyclic aliphatic compounds.[28]

Most importantly, these investigations have shown that using BV as a 3-D scaffold has the benefit of being able to take advantage of a wide variety of constitutional isomers in just one isolatable compound. As such, the BV scaffold has the ability to access multiple different regions of chemical space and possess varying exit vectors simply by virtue of its internal Cope rearrangements and, even at 298 K, several of these different geometries are adopted. This dynamic property of BV offers an advantage over classical 3-D fragments and hit-to-lead screening.

2.8 Conclusions

The rearrangement processes of BV have been described in detail, accompanied by our proposed naming system. In addition, a simple equation has been developed for calculating the number of BV isomers by hand. Building upon these methods, a BV isomer generation software (bullviso) has been written which then allowed us to perform 3-D shape analysis. Subsequently, PMI and EV analyses have shown that BVs have potential as bioisosteres similar to other rigid 3-D structures currently in use. Critically, the dynamic properties of BV mean that multiple different geometries are accessible from a single compound. These investigations lend insight into the potential for BV to be used as a unique 3-D scaffold for fragment based drug discovery.

Experimental

Isomer Generation

All initial sets of Cartesian coordinates sampling the constitutional isomers of **3**, **4**, and **5** were generated *via* the in-house-developed *bullviso*[31] code. *bullviso* is publicly available under the GNU Public License (GPLv3) on GitLab. All constitutional isomers were subsequently (pre-)optimized at the GFN2-xTB[62,63] (extended tight binding; xTB) level of theory using *xtb* (v6.4.1).[64] An SCF convergence criterion of 1.0×10^{-6} a.u. was used with convergence criteria of 5.0×10^{-6} and 1.0×10^{-3} a.u. for the energy change and gradient, respectively, in all geometry optimizations. All constitutional isomers verified at the GFN2-xTB level of theory were progressed to DFT geometry optimization.

DFT Geometry Optimization

All DFT geometry optimizations and energy evaluations of the constitutional isomers of **3**, **4**, and **5** were carried out at the PBE0-D3 level of theory (*i.e.* with the PBE0[45–47]density functional of Adamo and Barone coupled with the D3[48] dispersion correction of Grimme *et al.*) using ORCA (v5.0.2).[38–40] All calculations were carried out under the resolution-of-identity (RI) approximation for the Coulomb integrals (RIJONX). A tightened SCF convergence criterion of 1.0×10^{-9} a.u. was used in all calculations; convergence criteria of 2.0×10^{-7} and 3.0×10^{-5} a.u. were used for the energy change and gradient, respectively, in all geometry optimizations. The def2-SV(P)[49] basis set of Weigend and Ahlrichs was coupled with the def2/J[65] auxilliary basis set; the two were used together throughout. The proper convergence of all geometry optimizations to real minima was verified *via* vibrational frequency inspection.

*Table S1: Isomer codes, Energy (E) and Relative energies (E_{rel}), Dipole moment (μ) and Geometric parameters r, φ_1, φ_2, and θ for Me_2BV **(3)**. I and J correspond to the appended carbon atom number on BV scaffold.*

Isomer	E / Hartree	E_{rel} / kJ·mol^{-1}	*I*	*J*	*r* / Å	φ_1 / °	φ_2 / °	θ / °	*μ* / D
000 000 001 1	−464.735969	20.59	β	α	1.537	61.0	67.4	−0.2	0.311
000 000 010 1	−464.738464	14.04	γ	α	2.554	30.4	45.6	0.2	0.755
000 000 011 0	−464.737758	15.89	γ	β	1.353	56.0	55.1	−0.1	0.477
000 000 100 1	−464.736512	19.16	δ	α	3.122	12.4	16.9	−0.1	0.609
000 000 101 0	−464.740612	8.40	δ	β	2.544	42.0	31.3	−0.2	0.302
000 000 110 0	−464.736491	19.22	δ	γ	1.494	63.8	63.0	−0.3	0.727
000 001 001 0	−464.743810	0.00	β′	β	2.509	53.8	53.7	−0.2	0.126

000 001 010 0	−464.742721	2.86	β′	γ	3.14	34.1	26.6	30.0	0.399
000 001 100 0	−464.740664	8.26	β′	δ	3.237	15.1	23.4	33.4	0.258
000 010 001 0	−464.742780	2.70	γ′	β	3.139	26.8	34.1	−30.0	0.399
000 010 010 0	−464.741728	5.47	γ′	γ	3.166	32.5	32.7	0.2	0.774
000 010 100 0	−464.739697	10.80	γ′	δ	2.662	45.0	44.7	−0.5	0.654
000 100 001 0	−464.740682	8.21	δ′	β	3.236	23.5	15.1	−33.3	0.257
000 100 010 0	−464.739675	10.86	δ′	γ	2.662	44.7	45.1	0.2	0.656
000 100 100 0	−464.733729	26.47	δ′	δ	1.542	61.3	61.4	0.0	0.566

Table S2: Isomer codes, Energy (E) and Relative energies (E_{rel}), Dipole moment (μ) and Geometric parameters r, φ_1, φ_2, and θ for Me_3BV ***(4)****. I and J correspond to the appended carbon atom number on BV scaffold.*

Isomer	**E / Hartree**	**E_{rel} / kJ·mol^{-1}**	***I***	***J***	***r* / Å**	**φ_1 / °**	**φ_2 / °**	**θ / °**	**μ / D**
000 000 011 1	−503.968652	43.80	γ	β	1.357	59.0	59.3	−0.4	0.544
000 000 011 1	−503.968652	43.80	γ	α	2.544	28.3	40.4	0.4	0.544
000 000 011 1	−503.968652	43.80	β	α	1.542	63.3	67.1	0.7	0.544
000 000 101 1	−503.974248	29.11	δ	β	2.561	42.6	34.6	−0.2	0.365
000 000 101 1	−503.974248	29.11	δ	α	3.114	13.2	12.2	0.1	0.365
000 000 101 1	−503.974248	29.11	β	α	1.535	61.1	67.2	0.2	0.365
000 000 110 1	−503.973677	30.61	δ	γ	1.492	63.6	63.1	0.1	0.833
000 000 110 1	−503.973677	30.61	δ	α	3.12	8.8	17.8	0.1	0.833
000 000 110 1	−503.973677	30.61	γ	α	2.569	33.7	46.2	−0.2	0.833
000 000 111 0	−503.970754	38.29	δ	γ	1.505	63.8	65.9	0.2	0.549
000 000 111 0	−503.970754	38.29	δ	β	2.534	37.6	25.7	0.0	0.549
000 000 111 0	−503.970754	38.29	γ	β	1.356	58.7	54.9	−0.1	0.549
000 001 001 1	−503.972914	32.61	β'	β	2.492	52.6	52.4	−0.2	0.209
000 001 001 1	−503.972914	32.61	β'	α	1.539	61.1	68.6	−7.8	0.209
000 001 001 1	−503.972914	32.61	β	α	1.539	61.1	68.6	7.6	0.209
000 001 010 1	−503.976285	23.76	β'	γ	3.143	32.1	27.4	23.2	0.457
000 001 010 1	−503.976285	23.76	β'	α	1.536	60.9	67.4	0.9	0.457
000 001 010 1	−503.976285	23.76	γ	α	2.563	30.8	47.7	5.9	0.457
000 001 011 0	−503.979301	15.85	β'	γ	3.132	35.3	25.4	39.4	0.318
000 001 011 0	−503.979301	15.85	β'	β	2.524	54.2	56.9	−2.6	0.318
000 001 011 0	−503.979301	15.85	γ	β	1.353	56.0	55.2	−0.3	0.318
000 001 100 1	−503.974363	28.81	β'	δ	3.258	16.7	23.6	−21.0	0.316
000 001 100 1	−503.974363	28.81	β'	α	1.536	61.0	67.3	−0.6	0.316

000 001 100 1	−503.974363	28.81	δ	α	3.134	12.2	19.4	−13.9	0.316
000 001 101 0	−503.982174	8.30	β'	δ	3.221	15.5	23.6	−34.0	0.179
000 001 101 0	−503.982174	8.30	β'	β	2.504	53.4	53.8	−0.2	0.179
000 001 101 0	−503.982174	8.30	δ	β	2.54	41.8	31.1	0.4	0.179
000 001 110 0	−503.978096	19.01	β'	δ	3.248	15.1	24.2	42.6	0.471
000 001110 0	−503.978096	19.01	β'	γ	3.15	34.1	28.4	23.0	0.471
000 001 110 0	−503.978096	19.01	δ	γ	1.493	63.7	63.0	0.2	0.471
000 010 001 1	−503.976318	23.68	γ'	β	3.144	27.3	32.3	23.0	0.457
000 010 001 1	−503.976318	23.68	γ'	α	2.563	30.8	47.6	5.6	0.457
000 010 001 1	−503.976318	23.68	β	α	1.536	60.9	67.5	0.6	0.457
000 010 010 1	−503.978773	17.23	γ'	γ	3.151	32.7	32.8	0.0	0.892
000 010 010 1	−503.978773	17.23	γ'	α	2.55	30.1	45.6	0.8	0.892
000 010 010 1	−503.978773	17.23	γ	α	2.55	30.1	45.6	−0.6	0.892
000 010 011 0	−503.978373	18.28	γ'	γ	3.18	32.4	34.7	7.1	0.560
000 010 011 0	−503.978373	18.28	γ'	β	3.161	26.2	36.1	−36.2	0.560
000 010 011 0	−503.978373	18.28	γ	β	1.352	55.9	55.1	0.1	0.560
000 010 100 1	−503.976846	22.29	γ'	δ	2.658	44.8	44.6	−0.8	0.762
000 010 100 1	−503.976846	22.29	γ'	α	2.55	30.3	45.4	0.8	0.762
000 010 100 1	−503.976846	22.29	δ	α	3.11	12.1	16.8	−0.5	0.762
000 010 101 0	−503.981157	10.97	γ'	δ	2.655	44.6	44.7	−0.9	0.408
000 010 101 0	−503.981157	10.97	γ'	β	3.124	26.6	34.2	−29.8	0.408
000 010 101 0	−503.981157	10.97	δ	β	2.54	41.9	31.0	0.4	0.408
000 010 110 0	−503.976996	21.90	γ'	δ	2.673	45.3	46.5	3.2	0.828
000 010 110 0	−503.976996	21.90	γ'	γ	3.158	33.5	31.5	−6.8	0.828
000 010 110 0	−503.976996	21.90	δ	γ	1.494	63.8	62.9	0.4	0.828
000 011 001 0	−503.979298	15.85	γ'	β'	1.352	56.0	55.1	0.2	0.310
000 011 001 0	−503.979298	15.85	γ'	β	3.134	25.2	35.0	−39.6	0.310
000 011 001 0	−503.979298	15.85	β'	β	2.527	56.8	53.9	2.4	0.310
000 011 010 0	−503.978334	18.38	γ'	β'	1.352	55.9	55.1	0.3	0.560
000 011 010 0	−503.978334	18.38	γ'	γ	3.18	34.7	32.3	7.0	0.560
000 011 010 0	−503.978334	18.38	β'	γ	3.161	36.0	26.2	−36.4	0.560
000 011 100 0	−503.976206	23.97	γ'	β'	1.352	56.1	55.0	0.3	0.456
000 011 100 0	−503.976206	23.97	γ'	δ	2.679	48.6	45.3	2.7	0.456
000 011 100 0	−503.976206	23.97	β'	δ	3.241	13.7	24.3	−50.8	0.456
000 100 001 1	−503.974408	28.69	δ'	β	3.258	23.6	16.6	−20.7	0.315
000 100 001 1	−503.974408	28.69	δ'	α	3.134	12.2	19.5	−13.5	0.315

000 100 001 1	−503.974408	28.69	β	α	1.536	61.0	67.3	−0.9	0.315
000 100 010 1	−503.976816	22.37	δ'	γ	2.657	44.7	44.9	−0.8	0.763
000 100 010 1	−503.976816	22.37	δ'	α	3.11	12.1	16.8	0.2	0.763
000 100 010 1	−503.976816	22.37	γ	α	2.55	30.2	45.4	0.5	0.763
000 100 011 0	−503.976229	23.91	δ'	γ	2.68	45.3	48.6	−2.7	0.457
000 100 011 0	−503.976229	23.91	δ'	β	3.241	24.3	14.0	51.1	0.457
000 100 011 0	−503.976229	23.91	γ	β	1.352	56.1	55.0	0.0	0.457
000 100 100 1	−503.971059	37.48	δ'	δ	1.54	61.4	61.4	−0.1	0.670
000 100 100 1	−503.971059	37.48	δ'	α	3.132	15.3	16.7	12.5	0.670
000 100 100 1	−503.971059	37.48	δ	α	3.133	15.4	16.7	−12.3	0.670
000 100 101 0	−503.975111	26.85	δ'	δ	1.54	61.2	61.5	−0.1	0.324
000 100 101 0	−503.975111	26.85	δ'	β	3.228	20.1	16.1	−25.8	0.324
000 100 101 0	−503.975111	26.85	δ	β	2.554	44.6	31.5	−5.3	0.324
000 100 110 0	−503.969699	41.05	δ'	δ	1.548	61.1	63.4	−2.7	0.750
000 100 110 0	−503.969699	41.05	δ'	γ	2.645	40.2	42.5	3.6	0.750
000 100 110 0	−503.969699	41.05	δ	γ	1.498	65.7	62.8	6.7	0.750
000 101 001 0	−503.982160	8.34	δ'	β'	2.54	41.8	31.2	−0.2	0.183
000 101 001 0	−503.982160	8.34	δ'	β	3.22	23.7	15.7	34.1	0.183
000 101 001 0	−503.982160	8.34	β'	β	2.504	53.7	53.6	0.0	0.183
000 101 010 0	−503.981121	11.07	δ'	β'	2.539	41.9	31.0	−0.4	0.407
000 101 010 0	−503.981121	11.07	δ'	γ	2.655	44.8	44.6	1.1	0.407
000 101 010 0	−503.981121	11.07	β'	γ	3.124	34.3	26.5	29.8	0.407
000 101 100 0	−503.975151	26.74	δ'	β'	2.554	44.6	31.6	5.0	0.323
000 101 100 0	−503.975151	26.74	δ'	δ	1.539	61.5	61.2	−0.1	0.323
000 101 100 0	−503.975151	26.74	β'	δ	3.229	15.9	20.2	25.3	0.323
000 110 001 0	−503.978071	19.07	δ'	γ'	1.493	63.7	63.0	0.3	0.470
000 110 001 0	−503.978071	19.07	δ'	β	3.249	24.2	15.0	42.2	0.470
000 110 001 0	−503.978071	19.07	γ'	β	3.151	28.3	34.0	22.9	0.470
000 110 010 0	−503.976989	21.91	δ'	γ'	1.493	63.8	62.9	0.3	0.830
000 110 010 0	−503.976989	21.91	δ'	γ	2.673	46.5	45.4	3.5	0.830
000 110 010 0	−503.976989	21.91	γ'	γ	3.156	31.6	33.7	−6.8	0.830
000 110 100 0	−503.969765	40.88	δ'	γ'	1.498	65.7	62.9	6.6	0.750
000 110 100 0	−503.969765	40.88	δ'	δ	1.548	63.4	61.1	−2.6	0.750
000 110 100 0	−503.969765	40.88	γ'	δ	2.645	42.5	40.1	3.6	0.750
001 001 001 0	−503.985336	0.00	β"	β'	2.513	53.6	53.5	−0.2	0.248
001 001 001 0	−503.985336	0.00	β"	β	2.515	53.3	53.3	0.0	0.248

001 001 001 0	−503.985336	0.00	β'	β	2.513	53.5	53.6	0.1	0.248
001 001 010 0	−503.984343	2.61	β"	β'	2.504	54.2	54.1	0.1	0.144
001 001 010 0	−503.984343	2.61	β"	γ	3.143	33.8	26.5	30.4	0.144
001 001 010 0	−503.984343	2.61	β'	γ	3.142	33.9	26.6	−30.3	0.144
001 001 100 0	−503.982227	8.16	β"	β'	2.51	53.8	54.0	0.4	0.051
001 001 100 0	−503.982227	8.16	β"	δ	3.236	14.7	23.2	−34.2	0.051
001 001 100 0	−503.982227	8.16	β'	δ	3.237	14.3	23.3	33.3	0.051
001 010 010 0	−503.983260	5.45	β"	γ'	3.137	34.5	27.1	30.6	0.505
001 010 010 0	−503.983260	5.45	β"	γ	3.136	34.7	27.0	−30.3	0.505
001 010 010 0	−503.983260	5.45	γ'	γ	3.166	32.6	32.7	−0.2	0.505
001 010 100 0	−503.981171	10.93	β"	γ'	3.143	34.1	26.4	29.9	0.380
001 010 100 0	−503.981171	10.93	β"	δ	3.233	15.3	23.5	−35.1	0.380
001 010 100 0	−503.981171	10.93	γ'	δ	2.663	44.9	44.7	0.0	0.380
001 100 010 0	−503.981155	10.98	β"	δ'	3.233	15.3	23.5	35.4	0.380
001 100 010 0	−503.981155	10.98	β"	γ	3.143	34.1	26.3	−30.0	0.380
001 100 010 0	−503.981155	10.98	δ'	γ	2.663	44.8	45.0	−0.2	0.380
001 100 100 0	−503.975147	26.75	β"	δ'	3.248	15.3	26.2	25.3	0.296
001 100 100 0	−503.975147	26.75	β"	δ	3.247	15.3	26.2	−25.5	0.296
001 100 100 0	−503.975147	26.75	δ'	δ	1.544	61.4	61.4	0.1	0.296
010 010 010 0	−503.982133	8.41	γ"	γ'	3.166	33.1	33.0	0.1	0.876
010 010 010 0	−503.982133	8.41	γ"	γ	3.165	33.2	33.0	0.0	0.876
010 010 010 0	−503.982133	8.41	γ'	γ	3.163	33.3	33.3	0.0	0.876
010 010 100 0	−503.980126	13.68	γ"	γ'	3.172	32.2	32.4	−0.1	0.761
010 010 100 0	−503.980126	13.68	γ"	δ	2.663	45.2	44.9	−0.4	0.761
010 010 100 0	−503.980126	13.68	γ'	δ	2.663	45.1	44.9	0.1	0.761
010 100 100 0	−503.974214	29.20	γ"	δ'	2.668	45.4	45.8	6.2	0.696
010 100 100 0	−503.974214	29.20	γ"	δ	2.669	45.2	45.7	−6.6	0.696
010 100 100 0	−503.974214	29.20	δ'	δ	1.545	61.4	61.4	0.1	0.696
100 100 100 0	−503.965015	53.35	δ"	δ'	1.541	61.0	61.0	0.1	0.609
100 100 100 0	−503.965015	53.35	δ"	δ	1.541	61.0	61.0	0.0	0.609
100 100 100 0	−503.965015	53.35	δ'	δ	1.541	61.1	61.0	0.1	0.609

Table S3: Isomer codes, Energy (E) and Relative energies (E_{rel}), Dipole moment (μ) and Geometric parameters r, φ_1, φ_2, and θ for Me_4BV ***(5)****. I and J correspond to the appended carbon atom number on BV scaffold.*

Isomer	E / Hartree	E_{rel} / kJ·mol^{-1}	v_1	v_2	r / Å	φ_1 / °	φ_2 / °	θ / °	μ / D
000 000 111 1	−543.201058	59.60	δ	γ	1.505	63.3	67.6	−0.5	0.6261
000 000 111 1	−543.201058	59.60	δ	β	2.558	37.8	29.0	−0.2	0.6261
000 000 111 1	−543.201058	59.60	δ	α	3.097	8.0	11.0	−0.5	0.6261
000 000 111 1	−543.201058	59.60	γ	β	1.363	58.6	57.4	0.3	0.6261
000 000 111 1	−543.201058	59.60	γ	α	2.559	28.2	39.9	0.7	0.6261
000 000 111 1	−543.201058	59.60	β	α	1.546	65.8	66.4	0.1	0.6261
000 001 011 1	−543.205509	47.92	β'	γ	3.118	35.5	27.6	−27.2	0.4404
000 001 011 1	−543.205509	47.92	β'	β	2.500	52.7	56.4	0.3	0.4404
000 001 011 1	−543.205509	47.92	β'	α	1.538	60.8	69.2	8.6	0.4404
000 001 011 1	−543.205509	47.92	γ	β	1.357	58.5	59.5	3.4	0.4404
000 001 011 1	−543.205509	47.92	γ	α	2.552	28.1	42.2	−10.2	0.4404
000 001 011 1	−543.205509	47.92	β	α	1.544	63.6	68.4	−10.7	0.4404
000 001 101 1	−543.211306	32.70	β'	δ	3.231	19.4	24.2	22.7	0.2501
000 001 101 1	−543.211306	32.70	β'	β	2.489	52.2	52.3	0.0	0.2501
000 001 101 1	−543.211306	32.70	β'	α	1.538	61.0	68.6	−7.3	0.2501
000 001 101 1	−543.211306	32.70	δ	β	2.559	42.3	35.2	−2.5	0.2501
000 001 101 1	−543.211306	32.70	δ	α	3.127	13.1	14.8	21.5	0.2501
000 001 101 1	−543.211306	32.70	β	α	1.537	61.2	68.5	7.3	0.2501
000 001 110 1	−543.211751	31.53	β'	δ	3.272	16.1	24.2	−28.7	0.5216
000 001 110 1	−543.211751	31.53	β'	γ	3.158	31.5	28.7	−16.5	0.5216
000 001 110 1	−543.211751	31.53	β'	α	1.534	60.7	67.4	−2.1	0.5216
000 001 110 1	−543.211751	31.53	δ	γ	1.490	63.4	63.1	−0.5	0.5216
000 001 110 1	−543.211751	31.53	δ	α	3.132	8.7	20.3	−13.6	0.5216
000 001 110 1	−543.211751	31.53	γ	α	2.578	34.0	48.3	−5.0	0.5216
000 001 111 0	−543.212477	29.63	β'	δ	3.225	15.3	24.8	−47.3	0.3858
000 001 111 0	−543.212477	29.63	β'	γ	3.150	35.3	26.3	−30.9	0.3858
000 001 111 0	−543.212477	29.63	β'	β	2.515	53.8	58.5	3.0	0.3858
000 001 111 0	−543.212477	29.63	δ	γ	1.503	63.7	65.9	−0.6	0.3858
000 001 111 0	−543.212477	29.63	δ	β	2.531	37.5	25.7	1.6	0.3858
000 001 111 0	−543.212477	29.63	γ	β	1.356	58.6	55.0	1.2	0.3858
000 010 011 1	−543.209119	38.44	γ'	γ	3.156	32.9	33.1	5.5	0.6033
000 010 011 1	−543.209119	38.44	γ'	β	3.161	27.1	32.1	−29.4	0.6033
000 010 011 1	−543.209119	38.44	γ'	α	2.559	30.4	48.5	−6.4	0.6033
000 010 011 1	−543.209119	38.44	γ	β	1.357	58.8	59.3	0.7	0.6033

000 010 011 1	−543.209119	38.44	γ	α	2.540	28.0	40.4	−2.5	0.6033
000 010 011 1	−543.209119	38.44	β	α	1.541	63.1	67.3	−2.3	0.6033
000 010 101 1	−543.214680	23.84	γ'	δ	2.642	44.5	44.5	−0.9	0.4750
000 010 101 1	−543.214680	23.84	γ'	β	3.126	27.4	32.7	−22.7	0.4750
000 010 101 1	−543.214680	23.84	γ'	α	2.560	30.7	47.4	−5.5	0.4750
000 010 101 1	−543.214680	23.84	δ	β	2.557	42.5	34.4	0.0	0.4750
000 010 101 1	−543.214680	23.84	δ	α	3.103	13.0	12.2	−0.8	0.4750
000 010 101 1	−543.214680	23.84	β	α	1.535	61.0	67.3	−0.2	0.4750
000 010 110 1	−543.214078	25.42	γ'	δ	2.668	45.3	46.4	−3.4	0.9506
000 010 110 1	−543.214078	25.42	γ'	γ	3.145	33.5	31.5	6.7	0.9506
000 010 110 1	−543.214078	25.42	γ'	α	2.542	29.8	45.3	−1.2	0.9506
000 010 110 1	−543.214078	25.42	δ	γ	1.492	63.7	63.0	−0.4	0.9506
000 010 110 1	−543.214078	25.42	δ	α	3.109	8.6	17.7	−0.1	0.9506
000 010 110 1	−543.214078	25.42	γ	α	2.566	33.4	46.2	0.9	0.9506
000 010 111 0	−543.211407	32.43	γ'	δ	2.667	44.5	47.5	−3.2	0.6007
000 010 111 0	−543.211407	32.43	γ'	γ	3.185	32.6	32.1	−0.5	0.6007
000 010 111 0	−543.211407	32.43	γ'	β	3.139	25.8	36.8	39.0	0.6007
000 010 111 0	−543.211407	32.43	δ	γ	1.504	63.9	65.8	−1.3	0.6007
000 010 111 0	−543.211407	32.43	δ	β	2.530	37.6	25.5	−1.4	0.6007
000 010 111 0	−543.211407	32.43	γ	β	1.356	58.5	54.9	0.4	0.6007
000 011 001 1	−543.205524	47.88	γ'	β'	1.357	58.5	59.5	−3.7	0.4384
000 011 001 1	−543.205524	47.88	γ'	β	3.118	27.6	35.3	27.4	0.4384
000 011 001 1	−543.205524	47.88	γ'	α	2.551	28.0	42.3	10.3	0.4384
000 011 001 1	−543.205524	47.88	β'	β	2.498	56.7	52.6	0.2	0.4384
000 011 001 1	−543.205524	47.88	β'	α	1.544	63.6	68.4	11.2	0.4384
000 011 001 1	−543.205524	47.88	β	α	1.537	60.8	69.1	−8.4	0.4384
000 011 010 1	−543.209146	38.37	γ'	β'	1.357	58.9	59.3	0.0	0.6116
000 011 010 1	−543.209146	38.37	γ'	γ	3.156	33.5	33.0	−5.0	0.6116
000 011 010 1	−543.209146	38.37	γ'	α	2.540	28.1	40.5	1.3	0.6116
000 011 010 1	−543.209146	38.37	β'	γ	3.156	33.3	27.3	28.4	0.6116
000 011 010 1	−543.209146	38.37	β'	α	1.541	63.1	67.3	0.8	0.6116
000 011 010 1	−543.209146	38.37	γ	α	2.558	30.4	48.4	6.7	0.6116
000 011 011 0	−543.215144	22.62	γ'	β'	1.351	55.7	55.1	−0.5	0.4003
000 011 011 0	−543.215144	22.62	γ'	γ	3.197	34.2	34.1	0.0	0.4003
000 011 011 0	−543.215144	22.62	γ'	β	3.154	24.8	37.2	45.4	0.4003
000 011 011 0	−543.215144	22.62	β'	γ	3.153	37.3	24.7	−45.2	0.4003

000 011 011 0	−543.215144	22.62	β'	β	2.541	57.1	57.0	0.1	0.4003
000 011 011 0	−543.215144	22.62	γ	β	1.351	55.7	55.1	0.5	0.4003
000 011 100 1	−543.207151	43.61	γ'	β'	1.357	58.9	59.0	−1.8	0.5159
000 011 100 1	−543.207151	43.61	γ'	δ	2.675	46.9	45.1	−2.1	0.5159
000 011 100 1	−543.207151	43.61	γ'	α	2.540	28.1	40.3	1.1	0.5159
000 011 100 1	−543.207151	43.61	β'	δ	3.262	13.6	24.2	28.6	0.5159
000 011 100 1	−543.207151	43.61	β'	α	1.541	63.3	67.1	2.8	0.5159
000 011 100 1	−543.207151	43.61	δ	α	3.117	11.7	20.3	16.9	0.5159
000 011 101 0	−543.217729	15.84	γ'	β'	1.352	56.0	55.1	0.0	0.2993
000 011 101 0	−543.217729	15.84	γ'	δ	2.673	48.3	45.3	3.0	0.2993
000 011 101 0	−543.217729	15.84	γ'	β	3.117	25.4	35.2	39.3	0.2993
000 011 101 0	−543.217729	15.84	β'	δ	3.226	14.1	24.3	−51.0	0.2993
000 011 101 0	−543.217729	15.84	β'	β	2.520	56.3	54.1	−3.1	0.2993
000 011 101 0	−543.217729	15.84	δ	β	2.531	41.5	30.7	−0.6	0.2993
000 011 110 0	−543.213770	26.23	γ'	β'	1.351	55.9	54.9	0.2	0.5898
000 011 110 0	−543.213770	26.23	γ'	δ	2.691	48.9	47.0	−1.0	0.5898
000 011 110 0	−543.213770	26.23	γ'	γ	3.175	35.3	30.7	13.6	0.5898
000 011 110 0	−543.213770	26.23	β'	δ	3.255	13.5	25.0	−59.4	0.5898
000 011 110 0	−543.213770	26.23	β'	γ	3.176	35.6	27.4	−28.9	0.5898
000 011 110 0	−543.213770	26.23	δ	γ	1.491	63.7	62.7	−1.7	0.5898
000 100 011 1	−543.207204	43.47	δ'	γ	2.674	45.0	46.6	−1.9	0.5204
000 100 011 1	−543.207204	43.47	δ'	β	3.256	24.2	15.4	31.5	0.5204
000 100 011 1	−543.207204	43.47	δ'	α	3.114	11.8	20.0	17.3	0.5204
000 100 011 1	−543.207204	43.47	γ	β	1.357	59.1	59.2	0.1	0.5204
000 100 011 1	−543.207204	43.47	γ	α	2.541	28.3	40.3	0.3	0.5204
000 100 011 1	−543.207204	43.47	β	α	1.541	63.2	67.1	0.3	0.5204
000 100 101 1	−543.209013	38.72	δ'	δ	1.538	61.0	61.5	0.2	0.3850
000 100 101 1	−543.209013	38.72	δ'	β	3.249	20.2	17.7	14.0	0.3850
000 100 101 1	−543.209013	38.72	δ'	α	3.145	15.2	19.1	0.6	0.3850
000 100 101 1	−543.209013	38.72	δ	β	2.570	45.1	34.9	4.7	0.3850
000 100 101 1	−543.209013	38.72	δ	α	3.126	16.1	12.2	12.2	0.3850
000 100 101 1	−543.209013	38.72	β	α	1.533	61.1	67.1	0.0	0.3850
000 100 110 1	−543.206971	44.08	δ'	δ	1.547	61.0	63.3	2.7	0.8614
000 100 110 1	−543.206971	44.08	δ'	γ	2.641	40.0	42.4	−3.4	0.8614
000 100 110 1	−543.206971	44.08	δ'	α	3.118	16.0	16.4	17.5	0.8614
000 100 110 1	−543.206971	44.08	δ	γ	1.497	65.6	63.0	−6.6	0.8614

000 100 110 1	−543.206971	44.08	δ	α	3.133	12.1	17.6	−20.8	0.8614
000 100 110 1	−543.206971	44.08	γ	α	2.566	34.5	45.9	3.1	0.8614
000 100 111 0	−543.203636	52.84	δ'	δ	1.546	60.6	64.4	−3.6	0.5379
000 100 111 0	−543.203636	52.84	δ'	γ	2.665	40.3	46.5	3.3	0.5379
000 100 111 0	−543.203636	52.84	δ'	β	3.224	19.5	13.5	45.5	0.5379
000 100 111 0	−543.203636	52.84	δ	γ	1.509	65.8	65.6	9.3	0.5379
000 100 111 0	−543.203636	52.84	δ	β	2.545	40.4	26.1	5.9	0.5379
000 100 111 0	−543.203636	52.84	γ	β	1.356	59.6	55.0	−4.1	0.5379
000 101 001 1	−543.211278	32.77	δ'	β'	2.559	42.4	35.1	3.0	0.2609
000 101 001 1	−543.211278	32.77	δ'	β	3.230	24.1	19.7	−23.3	0.2609
000 101 001 1	−543.211278	32.77	δ'	α	3.126	13.1	14.7	−21.4	0.2609
000 101 001 1	−543.211278	32.77	β'	β	2.485	52.6	52.5	0.2	0.2609
000 101 001 1	−543.211278	32.77	β'	α	1.537	61.2	68.4	−7.6	0.2609
000 101 001 1	−543.211278	32.77	β	α	1.538	61.1	68.5	7.8	0.2609
000 101 010 1	−543.214731	23.71	δ'	β'	2.557	42.4	34.4	0.1	0.4743
000 101 010 1	−543.214731	23.71	δ'	γ	2.642	44.5	44.5	−0.8	0.4743
000 101 010 1	−543.214731	23.71	δ'	α	3.103	12.9	12.3	−1.3	0.4743
000 101 010 1	−543.214731	23.71	β'	γ	3.126	32.6	27.4	−22.7	0.4743
000 101 010 1	−543.214731	23.71	β'	α	1.535	61.0	67.4	−0.4	0.4743
000 101 010 1	−543.214731	23.71	γ	α	2.560	30.7	47.4	−5.4	0.4743
000 101 011 0	−543.217733	15.83	δ'	β'	2.531	41.5	30.7	0.9	0.2959
000 101 011 0	−543.217733	15.83	δ'	γ	2.673	45.2	48.3	−3.1	0.2959
000 101 011 0	−543.217733	15.83	δ'	β	3.225	24.2	14.4	51.2	0.2959
000 101 011 0	−543.217733	15.83	β'	γ	3.119	35.0	25.2	−39.5	0.2959
000 101 011 0	−543.217733	15.83	β'	β	2.520	54.0	56.5	2.6	0.2959
000 101 011 0	−543.217733	15.83	γ	β	1.352	56.0	55.1	0.4	0.2959
000 101 100 1	−543.209013	38.72	δ'	β'	2.570	45.1	34.8	−4.4	0.3837
000 101 100 1	−543.209013	38.72	δ'	δ	1.538	61.5	61.0	−0.1	0.3837
000 101 100 1	−543.209013	38.72	δ'	α	3.126	16.1	12.2	−12.6	0.3837
000 101 100 1	−543.209013	38.72	β'	δ	3.249	17.5	20.3	−13.7	0.3837
000 101 100 1	−543.209013	38.72	β'	α	1.534	61.1	67.1	−0.3	0.3837
000 101 100 1	−543.209013	38.72	δ	α	3.145	15.2	19.2	−0.6	0.3837
000 101 101 0	−543.216658	18.65	δ'	β'	2.551	44.4	31.5	−5.3	0.1730
000 101 101 0	−543.216658	18.65	δ'	δ	1.538	61.3	61.2	0.0	0.1730
000 101 101 0	−543.216658	18.65	δ'	β	3.213	20.2	16.3	26.0	0.1730
000 101 101 0	−543.216658	18.65	β'	δ	3.214	16.2	20.2	−25.5	0.1730

000 101 101 0	−543.216658	18.65	β'	β	2.481	53.7	53.9	−0.1	0.1730
000 101 101 0	−543.216658	18.65	δ	β	2.551	44.4	31.5	5.6	0.1730
000 101 110 0	−543.211289	32.74	δ'	β'	2.551	45.2	31.3	6.0	0.4899
000 101 110 0	−543.211289	32.74	δ'	δ	1.546	61.2	63.1	2.6	0.4899
000 101 110 0	−543.211289	32.74	δ'	γ	2.638	40.1	42.1	−3.3	0.4899
000 101 110 0	−543.211289	32.74	β'	δ	3.242	15.8	19.6	36.8	0.4899
000 101 110 0	−543.211289	32.74	β'	γ	3.107	34.8	31.2	22.6	0.4899
000 101 110 0	−543.211289	32.74	δ	γ	1.497	65.7	62.8	−6.3	0.4899
000 110 001 1	−543.211756	31.52	δ'	γ'	1.490	63.4	63.1	−0.4	0.5248
000 110 001 1	−543.211756	31.52	δ'	β	3.271	24.2	16.4	−29.3	0.5248
000 110 001 1	−543.211756	31.52	δ'	α	3.132	8.7	20.3	−13.5	0.5248
000 110 001 1	−543.211756	31.52	γ'	β	3.156	28.9	31.9	−16.4	0.5248
000 110 001 1	−543.211756	31.52	γ'	α	2.578	34.0	48.2	−5.2	0.5248
000 110 001 1	−543.211756	31.52	β	α	1.534	60.7	67.4	−1.7	0.5248
000 110 010 1	−543.214090	25.39	δ'	γ'	1.492	63.7	63.0	0.4	0.9505
000 110 010 1	−543.214090	25.39	δ'	γ	2.668	46.3	45.3	3.3	0.9505
000 110 010 1	−543.214090	25.39	δ'	α	3.109	8.6	17.7	−0.5	0.9505
000 110 010 1	−543.214090	25.39	γ'	γ	3.144	31.5	33.5	−6.7	0.9505
000 110 010 1	−543.214090	25.39	γ'	α	2.566	33.4	46.2	−1.0	0.9505
000 110 010 1	−543.214090	25.39	γ	α	2.542	29.9	45.3	1.4	0.9505
000 110 011 0	−543.213744	26.30	δ'	γ'	1.491	63.7	62.7	−1.1	0.5930
000 110 011 0	−543.213744	26.30	δ'	γ	2.690	46.9	48.8	−1.0	0.5930
000 110 011 0	−543.213744	26.30	δ'	β	3.253	24.9	13.8	−60.0	0.5930
000 110 011 0	−543.213744	26.30	γ'	γ	3.173	31.1	35.3	13.7	0.5930
000 110 011 0	−543.213744	26.30	γ'	β	3.173	27.8	36.0	−29.3	0.5930
000 110 011 0	−543.213744	26.30	γ	β	1.351	55.9	54.8	−0.1	0.5930
000 110 100 1	−543.206983	44.05	δ'	γ'	1.497	65.6	62.9	−7.0	0.8593
000 110 100 1	−543.206983	44.05	δ'	δ	1.547	63.3	61.0	2.7	0.8593
000 110 100 1	−543.206983	44.05	δ'	α	3.133	12.1	17.6	−20.9	0.8593
000 110 100 1	−543.206983	44.05	γ'	δ	2.640	42.6	40.0	−3.8	0.8593
000 110 100 1	−543.206983	44.05	γ'	α	2.566	34.5	45.9	3.7	0.8593
000 110 100 1	−543.206983	44.05	δ	α	3.118	16.0	16.4	17.7	0.8593
000 110 101 0	−543.211245	32.86	δ'	γ'	1.497	65.6	62.8	6.2	0.4884
000 110 101 0	−543.211245	32.86	δ'	δ	1.546	63.1	61.2	−2.8	0.4884
000 110 101 0	−543.211245	32.86	δ'	β	3.243	19.6	15.7	−36.7	0.4884
000 110 101 0	−543.211245	32.86	γ'	δ	2.638	42.0	40.1	3.1	0.4884

000 110 101 0	−543.211245	32.86	γ'	β	3.109	31.1	34.6	−22.6	0.4884
000 110 101 0	−543.211245	32.86	δ	β	2.551	45.3	31.3	−5.6	0.4884
000 110 110 0	−543.205433	48.12	δ'	γ'	1.498	66.3	62.6	−8.4	0.9068
000 110 110 0	−543.205433	48.12	δ'	δ	1.557	63.0	63.0	−0.2	0.9068
000 110 110 0	−543.205433	48.12	δ'	γ	2.655	41.1	43.2	10.3	0.9068
000 110 110 0	−543.205433	48.12	γ'	δ	2.655	43.0	41.0	−10.3	0.9068
000 110 110 0	−543.205433	48.12	γ'	γ	3.086	36.4	36.6	0.0	0.9068
000 110 110 0	−543.205433	48.12	δ	γ	1.498	66.3	62.7	8.8	0.9068
000 111 001 0	−543.212485	29.60	δ'	γ'	1.503	63.7	65.9	0.3	0.3864
000 111 001 0	−543.212485	29.60	δ'	β'	2.531	37.5	25.6	−1.3	0.3864
000 111 001 0	−543.212485	29.60	δ'	β	3.224	24.8	15.4	47.1	0.3864
000 111 001 0	−543.212485	29.60	γ'	β'	1.356	58.6	54.9	−0.7	0.3864
000 111 001 0	−543.212485	29.60	γ'	β	3.148	26.6	35.3	31.1	0.3864
000 111 001 0	−543.212485	29.60	β'	β	2.514	58.4	53.8	−3.2	0.3864
000 111 010 0	−543.211438	32.35	δ'	γ'	1.504	63.9	65.8	1.0	0.6048
000 111 010 0	−543.211438	32.35	δ'	β'	2.530	37.6	25.5	0.9	0.6048
000 111 010 0	−543.211438	32.35	δ'	γ	2.666	47.4	44.6	3.7	0.6048
000 111 010 0	−543.211438	32.35	γ'	β'	1.356	58.6	54.9	−0.5	0.6048
000 111 010 0	−543.211438	32.35	γ'	γ	3.181	32.3	32.9	0.8	0.6048
000 111 010 0	−543.211438	32.35	β'	γ	3.136	37.0	26.2	−38.9	0.6048
000 111 100 0	−543.203646	52.81	δ'	γ'	1.509	65.8	65.6	−9.2	0.5395
000 111 100 0	−543.203646	52.81	δ'	β'	2.545	40.3	26.1	−5.6	0.5395
000 111 100 0	−543.203646	52.81	δ'	δ	1.546	64.4	60.4	3.5	0.5395
000 111 100 0	−543.203646	52.81	γ'	β'	1.356	59.6	55.0	4.2	0.5395
000 111 100 0	−543.203646	52.81	γ'	δ	2.665	46.5	40.2	−3.3	0.5395
000 111 100 0	−543.203646	52.81	β'	δ	3.225	13.4	19.3	−45.1	0.5395
001 001 001 1	−543.207757	42.02	β"	β'	2.521	49.2	49.4	0.4	0.2054
001 001 001 1	−543.207757	42.02	β"	β	2.516	49.7	49.7	−0.1	0.2054
001 001 001 1	−543.207757	42.02	β"	α	1.544	60.9	70.4	0.4	0.2054
001 001 001 1	−543.207757	42.02	β'	β	2.521	49.3	49.2	−0.3	0.2054
001 001 001 1	−543.207757	42.02	β'	α	1.544	60.9	70.5	0.1	0.2054
001 001 001 1	−543.207757	42.02	β	α	1.544	60.9	70.4	−0.5	0.2054
001 001 010 1	−543.213382	27.25	β"	β'	2.486	53.1	53.1	0.1	0.1735
001 001 010 1	−543.213382	27.25	β"	γ	3.162	29.2	26.6	23.4	0.1735
001 001 010 1	−543.213382	27.25	β"	α	1.538	61.0	68.8	8.5	0.1735
001 001 010 1	−543.213382	27.25	β'	γ	3.161	29.3	26.7	−23.5	0.1735

001 001 010 1	−543.213382	27.25	β'	α	1.538	61.0	68.6	−8.3	0.1735
001 001 010 1	−543.213382	27.25	γ	α	2.577	31.3	50.3	−0.2	0.1735
001 001 011 0	−543.220959	7.36	β"	β'	2.510	54.1	54.1	−0.2	0.2382
001 001 011 0	−543.220959	7.36	β"	γ	3.137	34.9	25.0	39.9	0.2382
001 001 011 0	−543.220959	7.36	β"	β	2.531	53.8	56.4	−2.6	0.2382
001 001 011 0	−543.220959	7.36	β'	γ	3.136	34.7	25.0	−40.0	0.2382
001 001 011 0	−543.220959	7.36	β'	β	2.530	53.7	56.5	2.4	0.2382
001 001 011 0	−543.220959	7.36	γ	β	1.352	55.9	55.2	0.0	0.2382
001 001 100 1	−543.211517	32.15	β"	β'	2.489	53.0	52.7	−0.2	0.1368
001 001 100 1	−543.211517	32.15	β"	δ	3.267	14.6	22.9	−14.4	0.1368
001 001 100 1	−543.211517	32.15	β"	α	1.538	61.1	68.5	−8.7	0.1368
001 001 100 1	−543.211517	32.15	β'	δ	3.266	14.9	22.9	15.0	0.1368
001 001 100 1	−543.211517	32.15	β'	α	1.538	61.0	68.5	8.3	0.1368
001 001 100 1	−543.211517	32.15	δ	α	3.150	11.9	22.1	−0.1	0.1368
001 001 101 0	−543.223761	0.00	β"	β'	2.514	53.7	53.5	−0.4	0.2654
001 001 101 0	−543.223761	0.00	β"	δ	3.220	14.7	23.3	−34.4	0.2654
001 001 101 0	−543.223761	0.00	β"	β	2.510	53.0	53.5	−0.5	0.2654
001 001 101 0	−543.223761	0.00	β'	δ	3.219	15.1	23.4	35.0	0.2654
001 001 101 0	−543.223761	0.00	β'	β	2.508	53.2	53.5	0.2	0.2654
001 001 101 0	−543.223761	0.00	δ	β	2.536	41.5	31.0	−0.1	0.2654
001 001 110 0	−543.219802	10.39	β"	β'	2.509	54.4	54.2	0.2	0.2058
001 001 110 0	−543.219802	10.39	β"	δ	3.250	14.1	24.0	42.6	0.2058
001 001 110 0	−543.219802	10.39	β"	γ	3.157	33.3	28.1	23.8	0.2058
001 001 110 0	−543.219802	10.39	β'	δ	3.249	14.3	24.0	−42.9	0.2058
001 001 110 0	−543.219802	10.39	β'	γ	3.154	33.5	28.4	−23.8	0.2058
001 001 110 0	−543.219802	10.39	δ	γ	1.492	63.6	62.8	0.1	0.2058
001 010 010 1	−543.216707	18.52	β"	γ'	3.140	32.8	27.7	−23.6	0.5755
001 010 010 1	−543.216707	18.52	β"	γ	3.140	32.9	27.7	23.4	0.5755
001 010 010 1	−543.216707	18.52	β"	α	1.535	60.8	67.5	0.0	0.5755
001 010 010 1	−543.216707	18.52	γ'	γ	3.157	32.2	32.2	0.2	0.5755
001 010 010 1	−543.216707	18.52	γ'	α	2.559	30.5	47.7	−6.7	0.5755
001 010 010 1	−543.216707	18.52	γ	α	2.559	30.5	47.7	6.6	0.5755
001 010 011 0	−543.220027	9.80	β"	γ'	3.142	34.4	27.1	31.7	0.3118
001 010 011 0	−543.220027	9.80	β"	γ	3.130	35.7	25.7	−39.7	0.3118
001 010 011 0	−543.220027	9.80	β"	β	2.519	54.6	57.5	2.1	0.3118
001 010 011 0	−543.220027	9.80	γ'	γ	3.185	32.2	34.3	7.3	0.3118

001 010 011 0	−543.220027	9.80	γ'	β	3.168	25.9	35.3	−37.3	0.3118
001 010 011 0	−543.220027	9.80	γ	β	1.352	55.8	55.1	0.7	0.3118
001 010 100 1	−543.214856	23.38	β"	γ'	3.144	32.5	27.2	−23.0	0.4453
001 010 100 1	−543.214856	23.38	β"	δ	3.255	16.8	23.5	22.7	0.4453
001 010 100 1	−543.214856	23.38	β"	α	1.536	60.8	67.4	0.1	0.4453
001 010 100 1	−543.214856	23.38	γ'	δ	2.658	44.6	44.4	0.2	0.4453
001 010 100 1	−543.214856	23.38	γ'	α	2.559	30.7	47.5	−6.0	0.4453
001 010 100 1	−543.214856	23.38	δ	α	3.123	12.0	19.4	13.7	0.4453
001 010 101 0	−543.222765	2.61	β"	γ'	3.147	33.7	26.1	−30.3	0.1435
001 010 101 0	−543.222765	2.61	β"	δ	3.217	15.6	23.7	35.6	0.1435
001 010 101 0	−543.222765	2.61	β"	β	2.500	53.8	54.1	0.1	0.1435
001 010 101 0	−543.222765	2.61	γ'	δ	2.655	44.7	44.7	0.0	0.1435
001 010 101 0	−543.222765	2.61	γ'	β	3.125	26.9	34.1	30.5	0.1435
001 010 101 0	−543.222765	2.61	δ	β	2.536	41.6	30.9	−0.5	0.1435
001 010 110 0	−543.218583	13.59	β"	γ'	3.142	34.7	26.7	−30.8	0.5476
001 010 110 0	−543.218583	13.59	β"	δ	3.247	14.8	24.2	43.9	0.5476
001 010 110 0	−543.218583	13.59	β"	γ	3.153	34.1	28.4	23.6	0.5476
001 010 110 0	−543.218583	13.59	γ'	δ	2.675	45.1	46.5	−3.5	0.5476
001 010 110 0	−543.218583	13.59	γ'	γ	3.158	33.4	31.8	7.1	0.5476
001 010 110 0	−543.218583	13.59	δ	γ	1.492	63.7	62.8	0.2	0.5476
001 011 010 0	−543.219986	9.91	β"	γ'	3.131	35.4	25.6	39.8	0.3101
001 011 010 0	−543.219986	9.91	β"	β'	2.520	54.3	57.2	−2.3	0.3101
001 011 010 0	−543.219986	9.91	β"	γ	3.139	34.7	27.3	−31.4	0.3101
001 011 010 0	−543.219986	9.91	γ'	β'	1.352	55.8	55.1	−0.3	0.3101
001 011 010 0	−543.219986	9.91	γ'	γ	3.186	34.3	32.1	−7.1	0.3101
001 011 010 0	−543.219986	9.91	β'	γ	3.166	35.6	25.9	36.7	0.3101
001 011 100 0	−543.217838	15.55	β"	γ'	3.137	35.1	25.0	−39.6	0.2536
001 011 100 0	−543.217838	15.55	β"	β'	2.528	54.0	56.9	2.4	0.2536
001 011 100 0	−543.217838	15.55	β"	δ	3.229	14.8	23.0	37.8	0.2536
001 011 100 0	−543.217838	15.55	γ'	β'	1.352	56.0	55.1	0.4	0.2536
001 011 100 0	−543.217838	15.55	γ'	δ	2.681	48.5	45.2	2.4	0.2536
001 011 100 0	−543.217838	15.55	β'	δ	3.241	13.3	24.0	−51.9	0.2536
001 100 010 1	−543.214790	23.55	β"	δ'	3.254	17.1	23.7	−23.3	0.4444
001 100 010 1	−543.214790	23.55	β"	γ	3.147	32.2	27.0	23.0	0.4444
001 100 010 1	−543.214790	23.55	β"	α	1.536	60.8	67.4	0.3	0.4444
001 100 010 1	−543.214790	23.55	δ'	γ	2.657	44.3	44.7	0.2	0.4444

001 100 010 1	−543.214790	23.55	δ'	α	3.123	11.9	19.4	−14.3	0.4444
001 100 010 1	−543.214790	23.55	γ	α	2.560	30.7	47.5	5.7	0.4444
001 100 011 0	−543.217797	15.66	β"	δ'	3.229	14.7	23.0	38.1	0.2536
001 100 011 0	−543.217797	15.66	β"	γ	3.135	35.1	25.1	−39.6	0.2536
001 100 011 0	−543.217797	15.66	β"	β	2.527	54.1	56.9	2.4	0.2536
001 100 011 0	−543.217797	15.66	δ'	γ	2.682	45.3	48.4	2.5	0.2536
001 100 011 0	−543.217797	15.66	δ'	β	3.241	24.1	13.3	−52.2	0.2536
001 100 011 0	−543.217797	15.66	γ	β	1.352	56.0	55.0	0.3	0.2536
001 100 100 1	−543.208991	38.78	β"	δ'	3.268	16.9	26.1	13.7	0.3588
001 100 100 1	−543.208991	38.78	β"	δ	3.268	17.1	26.2	−14.0	0.3588
001 100 100 1	−543.208991	38.78	β"	α	1.535	61.0	67.2	0.1	0.3588
001 100 100 1	−543.208991	38.78	δ'	δ	1.541	61.3	61.3	0.1	0.3588
001 100 100 1	−543.208991	38.78	δ'	α	3.145	15.3	19.2	25.5	0.3588
001 100 100 1	−543.208991	38.78	δ	α	3.145	15.3	19.2	−25.7	0.3588
001 100 101 0	−543.216676	18.60	β"	δ'	3.247	14.5	25.9	25.3	0.1146
001 100 101 0	−543.216676	18.60	β"	δ	3.231	15.9	26.3	−26.4	0.1146
001 100 101 0	−543.216676	18.60	β"	β	2.507	53.4	53.4	0.2	0.1146
001 100 101 0	−543.216676	18.60	δ'	δ	1.541	61.2	61.6	−0.2	0.1146
001 100 101 0	−543.216676	18.60	δ'	β	3.228	19.8	15.4	−25.9	0.1146
001 100 101 0	−543.216676	18.60	δ	β	2.551	44.4	31.5	−4.3	0.1146
001 100 110 0	−543.211294	32.73	β"	δ'	3.247	15.4	26.8	−26.1	0.4697
001 100 110 0	−543.211294	32.73	β"	δ	3.263	14.9	27.4	33.7	0.4697
001 100 110 0	−543.211294	32.73	β"	γ	3.172	33.3	26.2	19.0	0.4697
001 100 110 0	−543.211294	32.73	δ'	δ	1.551	61.2	63.4	−2.7	0.4697
001 100 110 0	−543.211294	32.73	δ'	γ	2.646	40.2	42.6	4.4	0.4697
001 100 110 0	−543.211294	32.73	δ	γ	1.497	65.6	62.8	7.2	0.4697
001 101 010 0	−543.222754	2.64	β"	δ'	3.218	15.6	23.7	35.6	0.1343
001 101 010 0	−543.222754	2.64	β"	β'	2.499	53.8	54.3	0.3	0.1343
001 101 010 0	−543.222754	2.64	β"	γ	3.145	33.8	26.6	−30.6	0.1343
001 101 010 0	−543.222754	2.64	δ'	β'	2.536	41.7	30.9	−0.9	0.1343
001 101 010 0	−543.222754	2.64	δ'	γ	2.656	44.7	44.4	0.5	0.1343
001 101 010 0	−543.222754	2.64	β'	γ	3.129	33.7	26.4	30.2	0.1343
001 101 100 0	−543.216628	18.73	β"	δ'	3.231	15.9	26.3	−26.5	0.1159
001 101 100 0	−543.216628	18.73	β"	β'	2.508	53.5	53.4	0.2	0.1159
001 101 100 0	−543.216628	18.73	β"	δ	3.248	14.5	25.8	25.6	0.1159
001 101 100 0	−543.216628	18.73	δ'	β'	2.551	44.5	31.5	−4.4	0.1159

001 101 100 0	−543.216628	18.73	δ'	δ	1.541	61.6	61.3	−0.1	0.1159
001 101 100 0	−543.216628	18.73	β'	δ	3.229	15.4	19.9	−26.0	0.1159
001 110 010 0	−543.21860	13.55	β"	δ'	3.246	15.0	24.2	43.8	0.5507
001 110 010 0	−543.21860	13.55	β"	γ'	3.150	34.3	28.7	23.5	0.5507
001 110 010 0	−543.21860	13.55	β"	γ	3.144	34.4	26.4	−30.7	0.5507
001 110 010 0	−543.21860	13.55	δ'	γ'	1.492	63.8	62.8	−0.1	0.5507
001 110 010 0	−543.21860	13.55	δ'	γ	2.674	46.5	45.3	−3.8	0.5507
001 110 010 0	−543.21860	13.55	γ'	γ	3.157	31.6	33.6	6.8	0.5507
001 110 100 0	−543.211265	32.81	β"	δ'	3.263	14.8	27.5	33.4	0.4679
001 110 100 0	−543.211265	32.81	β"	γ'	3.175	33.1	25.7	18.7	0.4679
001 110 100 0	−543.211265	32.81	β"	δ	3.248	15.6	26.9	−26.2	0.4679
001 110 100 0	−543.211265	32.81	δ'	γ'	1.497	65.6	62.8	7.8	0.4679
001 110 100 0	−543.211265	32.81	δ'	δ	1.551	63.3	61.1	−2.8	0.4679
001 110 100 0	−543.211265	32.81	γ'	δ	2.644	42.9	40.2	4.9	0.4679
010 010 010 1	−543.219091	12.26	γ"	γ'	3.152	33.1	33.1	−0.1	1.0082
010 010 010 1	−543.219091	12.26	γ"	γ	3.152	33.0	33.1	−0.1	1.0082
010 010 010 1	−543.219091	12.26	γ"	α	2.547	29.8	45.7	0.1	1.0082
010 010 010 1	−543.219091	12.26	γ'	γ	3.152	33.1	33.0	0.0	1.0082
010 010 010 1	−543.219091	12.26	γ'	α	2.546	29.8	45.6	0.1	1.0082
010 010 010 1	−543.219091	12.26	γ	α	2.546	29.8	45.6	0.0	1.0082
010 010 011 0	−543.218926	12.69	γ"	γ'	3.167	33.6	33.4	−0.1	0.6330
010 010 011 0	−543.218926	12.69	γ"	γ	3.182	32.5	34.7	7.0	0.6330
010 010 011 0	−543.218926	12.69	γ"	β	3.158	26.4	36.7	−36.4	0.6330
010 010 011 0	−543.218926	12.69	γ'	γ	3.180	32.8	35.0	−6.9	0.6330
010 010 011 0	−543.218926	12.69	γ'	β	3.159	26.5	36.4	36.9	0.6330
010 010 011 0	−543.218926	12.69	γ	β	1.351	55.8	55.0	−0.3	0.6330
010 010 100 1	−543.217194	17.24	γ"	γ'	3.158	32.4	32.5	0.3	0.8848
010 010 100 1	−543.217194	17.24	γ"	δ	2.658	45.1	44.7	0.0	0.8848
010 010 100 1	−543.217194	17.24	γ"	α	2.547	30.0	45.4	−0.6	0.8848
010 010 100 1	−543.217194	17.24	γ'	δ	2.659	44.9	44.6	0.1	0.8848
010 010 100 1	−543.217194	17.24	γ'	α	2.547	30.1	45.5	0.2	0.8848
010 010 100 1	−543.217194	17.24	δ	α	3.099	11.9	16.7	0.4	0.8848
010 010 101 0	−543.221662	5.51	γ"	γ'	3.170	32.8	32.6	−0.2	0.4925
010 010 101 0	−543.221662	5.51	γ"	δ	2.657	44.6	44.8	−0.6	0.4925
010 010 101 0	−543.221662	5.51	γ"	β	3.123	26.7	34.5	−30.3	0.4925
010 010 101 0	−543.221662	5.51	γ'	δ	2.656	44.7	45.0	0.5	0.4925

010 010 101 0	−543.221662	5.51	γ'	β	3.122	26.9	34.8	30.3	0.4925
010 010 101 0	−543.221662	5.51	δ	β	2.535	41.7	30.8	0.2	0.4925
010 010 110 0	−543.217491	16.46	γ"	γ'	3.178	32.2	32.6	−0.2	0.9150
010 010 110 0	−543.217491	16.46	γ"	δ	2.674	45.5	46.5	−4.2	0.9150
010 010 110 0	−543.217491	16.46	γ"	γ	3.153	34.3	32.3	6.8	0.9150
010 010 110 0	−543.217491	16.46	γ'	δ	2.674	45.4	46.7	3.6	0.9150
010 010 110 0	−543.217491	16.46	γ'	γ	3.158	33.8	31.7	−6.9	0.9150
010 010 110 0	−543.217491	16.46	δ	γ	1.493	63.9	62.8	0.4	0.9150
010 011 100 0	−543.216860	18.12	γ"	γ'	3.189	32.0	34.1	7.0	0.5222
010 011 100 0	−543.216860	18.12	γ"	β'	3.165	25.8	36.0	−36.8	0.5222
010 011 100 0	−543.216860	18.12	γ"	δ	2.665	45.1	44.8	−1.3	0.5222
010 011 100 0	−543.216860	18.12	γ'	β'	1.352	55.9	55.0	0.0	0.5222
010 011 100 0	−543.216860	18.12	γ'	δ	2.680	48.7	45.4	−2.0	0.5222
010 011 100 0	−543.216860	18.12	β'	δ	3.236	14.3	24.2	52.7	0.5222
010 100 011 0	−543.216835	18.18	γ"	δ'	2.665	45.0	44.8	−1.5	0.5229
010 100 011 0	−543.216835	18.18	γ"	γ	3.188	31.9	34.1	7.2	0.5229
010 100 011 0	−543.216835	18.18	γ"	β	3.163	25.9	36.4	−36.0	0.5229
010 100 011 0	−543.216835	18.18	δ'	γ	2.681	45.4	48.7	−2.1	0.5229
010 100 011 0	−543.216835	18.18	δ'	β	3.240	24.2	13.8	52.5	0.5229
010 100 011 0	−543.216835	18.18	γ	β	1.352	55.9	55.0	−0.4	0.5229
010 100 100 1	−543.211495	32.20	γ"	δ'	2.662	45.4	45.4	5.8	0.8106
010 100 100 1	−543.211495	32.20	γ"	δ	2.663	45.0	45.6	−6.9	0.8106
010 100 100 1	−543.211495	32.20	γ"	α	2.546	30.2	45.2	0.9	0.8106
010 100 100 1	−543.211495	32.20	δ'	δ	1.544	61.4	61.4	−0.2	0.8106
010 100 100 1	−543.211495	32.20	δ'	α	3.122	15.2	16.5	−11.6	0.8106
010 100 100 1	−543.211495	32.20	δ	α	3.121	15.2	16.6	12.2	0.8106
010 100 101 0	−543.215660	21.27	γ"	δ'	2.669	45.3	45.7	5.9	0.4270
010 100 101 0	−543.215660	21.27	γ"	δ	2.662	44.9	45.8	−6.8	0.4270
010 100 101 0	−543.215660	21.27	γ"	β	3.130	26.1	33.6	−30.0	0.4270
010 100 101 0	−543.215660	21.27	δ'	δ	1.543	61.1	61.6	0.0	0.4270
010 100 101 0	−543.215660	21.27	δ'	β	3.226	20.0	16.0	26.7	0.4270
010 100 101 0	−543.215660	21.27	δ	β	2.550	44.4	31.4	5.4	0.4270
010 100 110 0	−543.210233	35.52	γ"	δ'	2.671	45.6	46.3	−7.3	0.8431
010 100 110 0	−543.210233	35.52	γ"	δ	2.682	45.6	48.1	3.2	0.8431
010 100 110 0	−543.210233	35.52	γ"	γ	3.182	32.4	28.1	7.3	0.8431
010 100 110 0	−543.210233	35.52	δ'	δ	1.552	61.1	63.4	2.5	0.8431

010 100 110 0	−543.210233	35.52	δ'	γ	2.646	40.2	42.8	−4.7	0.8431
010 100 110 0	−543.210233	35.52	δ	γ	1.497	65.7	62.8	−7.3	0.8431
010 101 100 0	−543.215670	21.24	γ"	δ'	2.662	44.9	45.8	−6.9	0.4272
010 101 100 0	−543.215670	21.24	γ"	β'	3.132	26.0	33.5	−30.3	0.4272
010 101 100 0	−543.215670	21.24	γ"	δ	2.669	45.3	45.6	5.8	0.4272
010 101 100 0	−543.215670	21.24	δ'	β'	2.550	44.5	31.3	5.6	0.4272
010 101 100 0	−543.215670	21.24	δ'	δ	1.543	61.6	61.2	0.0	0.4272
010 101 100 0	−543.215670	21.24	β'	δ	3.225	16.2	20.1	27.0	0.4272
010 110 100 0	−543.210282	35.39	γ"	δ'	2.682	45.8	48.2	−3.1	0.8410
010 110 100 0	−543.210282	35.39	γ"	γ'	3.180	32.7	28.2	−7.4	0.8410
010 110 100 0	−543.210282	35.39	γ"	δ	2.672	45.5	46.2	7.7	0.8410
010 110 100 0	−543.210282	35.39	δ'	γ'	1.497	65.8	62.8	7.4	0.8410
010 110 100 0	−543.210282	35.39	δ'	δ	1.552	63.3	61.1	−2.6	0.8410
010 110 100 0	−543.210282	35.39	γ'	δ	2.645	42.7	40.2	4.6	0.8410
011 100 100 0	−543.210698	34.30	γ"	β"	1.351	56.1	54.9	0.3	0.4735
011 100 100 0	−543.210698	34.30	γ"	δ'	2.686	48.9	46.3	8.3	0.4735
011 100 100 0	−543.210698	34.30	γ"	δ	2.686	48.8	46.3	−8.8	0.4735
011 100 100 0	−543.210698	34.30	β"	δ'	3.252	13.8	26.9	−43.0	0.4735
011 100 100 0	−543.210698	34.30	β"	δ	3.251	14.1	26.9	43.2	0.4735
011 100 100 0	−543.210698	34.30	δ'	δ	1.548	61.4	61.4	0.0	0.4735
100 100 100 1	−543.202482	55.87	δ"	δ'	1.541	60.8	61.0	0.2	0.7129
100 100 100 1	−543.202482	55.87	δ"	δ	1.541	61.0	61.0	0.0	0.7129
100 100 100 1	−543.202482	55.87	δ"	α	3.147	17.8	16.5	−0.5	0.7129
100 100 100 1	−543.202482	55.87	δ'	δ	1.541	60.9	60.9	0.0	0.7129
100 100 100 1	−543.202482	55.87	δ'	α	3.148	17.7	16.4	0.0	0.7129
100 100 100 1	−543.202482	55.87	δ	α	3.147	17.8	16.4	0.2	0.7129
100 100 101 0	−543.206421	45.52	δ"	δ'	1.543	61.0	61.0	0.0	0.3467
100 100 101 0	−543.206421	45.52	δ"	δ	1.540	60.8	61.2	0.1	0.3467
100 100 101 0	−543.206421	45.52	δ"	β	3.239	22.9	15.8	16.6	0.3467
100 100 101 0	−543.206421	45.52	δ'	δ	1.540	60.7	61.1	0.0	0.3467
100 100 101 0	−543.206421	45.52	δ'	β	3.239	22.9	15.6	−16.0	0.3467
100 100 101 0	−543.206421	45.52	δ	β	2.565	46.9	31.9	0.2	0.3467
100 100 110 0	−543.199442	63.85	δ"	δ'	1.540	60.7	60.7	−0.1	0.7632
100 100 110 0	−543.199442	63.85	δ"	δ	1.547	61.0	63.5	−2.4	0.7632
100 100 110 0	−543.199442	63.85	δ"	γ	2.657	41.2	40.6	−4.9	0.7632
100 100 110 0	−543.199442	63.85	δ'	δ	1.548	60.9	63.4	2.4	0.7632

100 100 110 0	−543.199442	63.85	δ'	γ	2.657	41.1	40.6	4.7	0.7632
100 100 110 0	−543.199442	63.85	δ	γ	1.504	67.5	62.6	−0.1	0.7632

Isomer Populations

*Table S4: Energy (E), Relative energies (E_{rel}), and Boltzmann distribution population percentage (P / %) for Me_2BV **(3)**.*

Isomer	E / Hartree	E_{rel} / kJ·mol^{-1}	*P / %*
000 000 001 1 *(N)*	−464.735969	20.59	0
000 000 010 1 *(J)*	−464.738464	14.04	0
000 000 011 0 *(K)*	−464.737758	15.89	0
000 000 100 1 *(L)*	−464.736512	19.16	0
000 000 101 0 *(G)*	−464.740612	8.40	2
000 000 110 0 *(M)*	−464.736491	19.22	0
000 001 001 0 *(A)*	−464.74381	0.00	53
000 001 010 0 *(C)*	−464.742721	2.86	17
000 001 100 0 *(F)*	−464.740664	8.26	2
000 010 001 0 *(B)*	−464.742780	2.70	17
000 010 010 0 *(D)*	−464.741728	5.47	6
000 010 100 0 *(H)*	−464.739697	10.80	1
000 100 001 0 *(E)*	−464.740682	8.21	2
000 100 010 0 *(I)*	−464.739675	10.86	1
000 100 100 0 *(O)*	−464.733729	26.47	0

*Table S5: Energy (E), Relative energies (E_{rel}), and Boltzmann distribution population percentage (P / %) for Me_3BV **(4)**.*

Isomer	*E* / Hartree	E_{rel} / kJ·mol^{-1}	*P / %*
000 000 011 1	−503.968652	43.80	0
000 000 101 1	−503.974248	29.11	0
000 000 110 1	−503.973677	30.61	0
000 000 111 0	−503.970754	38.29	0
000 001 001 1	−503.972914	32.61	0
000 001 010 1	−503.976285	23.76	0
000 001 011 0	−503.979301	15.85	0
000 001 100 1	−503.974363	28.81	0
000 001 101 0	−503.982174	8.3	2

000 001 110 0	−503.978096	19.01	0
000 010 001 1	−503.976318	23.68	0
000 010 010 1	−503.978773	17.23	0
000 010 011 0	−503.978373	18.28	0
000 010 100 1	−503.976846	22.29	0
000 010 101 0	−503.981157	10.97	1
000 010 110 0	−503.976996	21.9	0
000 011 001 0	−503.979298	15.85	0
000 011 010 0	−503.978334	18.38	1
000 011 100 0	−503.976206	23.97	0
000 100 001 1	−503.974408	28.69	0
000 100 010 1	−503.976816	22.37	0
000 100 011 0	−503.976229	23.91	0
000 100 100 1	−503.971059	37.48	0
000 100 101 0	−503.975111	26.85	0
000 100 110 0	−503.969699	41.05	0
000 101 001 0	−503.98216	8.34	2
000 101 010 0	−503.981121	11.07	1
000 101 100 0	−503.975151	26.74	0
000 110 001 0	−503.978071	19.07	0
000 110 010 0	−503.976989	21.91	0
000 110 100 0	−503.969765	40.88	0
001 001 001 0	−503.985336	0	60
001 001 010 0	−503.984343	2.61	21
001 001 100 0	−503.982227	8.16	2
001 010 010 0	−503.98326	5.45	7
001 010 100 0	−503.981171	10.93	1
001 100 010 0	−503.981155	10.98	1
001 100 100 0	−503.975147	26.75	0
010 010 010 0	−503.982133	8.41	2
010 010 100 0	−503.980126	13.68	0
010 100 100 0	−503.974214	29.2	0
100 100 100 0	−503.965015	53.35	0

*Table S6: Energy (E), Relative energies (E_{rel}), and Boltzmann distribution population percentage (P / %) for Me_4BV **(5)**.*

Isomer	E / Hartree	E_{rel} / kJ·mol^{-1}	P / %
000 000 111 1	−543.201058	59.60	0
000 001 011 1	−543.205509	47.92	0
000 001 101 1	−543.211306	32.70	0
000 001 110 1	−543.211751	31.53	0
000 001 111 0	−543.212477	29.63	0
000 010 011 1	−543.209119	38.44	0
000 010 101 1	−543.21468	23.84	0
000 010 110 1	−543.214078	25.42	0
000 010 111 0	−543.211407	32.43	0
000 011 001 1	−543.205524	47.88	0
000 011 010 1	−543.209146	38.37	0
000 011 011 0	−543.215144	22.62	0
000 011 100 1	−543.207151	43.61	0
000 011 101 0	−543.217729	15.84	0
000 011 110 0	−543.21377	26.23	0
000 100 011 1	−543.207204	43.47	0
000 100 101 1	−543.209013	38.72	0
000 100 110 1	−543.206971	44.08	0
000 100 111 0	−543.203636	52.84	0
000 101 001 1	−543.211278	32.77	0
000 101 010 1	−543.214731	23.71	0
000 101 011 0	−543.217733	15.83	0
000 101 100 1	−543.209013	38.72	0
000 101 101 0	−543.216658	18.65	0
000 101 110 0	−543.211289	32.74	0
000 110 001 1	−543.211756	31.52	0
000 110 010 1	−543.21409	25.39	0
000 110 011 0	−543.213744	26.30	0
000 110 100 1	−543.206983	44.05	0
000 110 101 0	−543.211245	32.86	0
000 110 110 0	−543.205433	48.12	0
000 111 001 0	−543.212485	29.60	0
000 111 010 0	−543.211438	32.35	0
000 111 100 0	−543.203646	52.81	0
001 001 001 1	−543.207757	42.02	0

001 001 010 1	−543.213382	27.25	0
001 001 011 0	−543.220959	7.36	3
001 001 100 1	−543.211517	32.15	0
001 001 101 0	−543.223761	0.00	52
001 001 110 0	−543.219802	10.39	1
001 010 010 1	−543.216707	18.52	0
001 010 011 0	−543.220027	9.80	1
001 010 100 1	−543.214856	23.38	0
001 010 101 0	−543.222765	2.61	18
001 010 110 0	−543.218583	13.59	0
001 011 010 0	−543.219986	9.91	1
001 011 100 0	−543.217838	15.55	0
001 100 010 1	−543.21479	23.55	0
001 100 011 0	−543.217797	15.66	0
001 100 100 1	−543.208991	38.78	0
001 100 101 0	−543.216676	18.60	0
001 100 110 0	−543.211294	32.73	0
001 101 010 0	−543.222754	2.64	18
001 101 100 0	−543.216628	18.73	0
001 110 010 0	−543.2186	13.55	0
001 110 100 0	−543.211265	32.81	0
010 010 010 1	−543.219091	12.26	0
010 010 011 0	−543.218926	12.69	0
010 010 100 1	−543.217194	17.24	0
010 010 101 0	−543.221662	5.51	6
010 010 110 0	−543.217491	16.46	0
010 011 100 0	−543.21686	18.12	0
010 100 011 0	−543.216835	18.18	0
010 100 100 1	−543.211495	32.20	0
010 100 101 0	−543.21566	21.27	0
010 100 110 0	−543.210233	35.52	0
010 101 100 0	−543.21567	21.24	0
010 110 100 0	−543.210282	35.39	0
011 100 100 0	−543.210698	34.30	0
100 100 100 1	−543.202482	55.87	0
100 100 101 0	−543.206421	45.52	0

100 100 110 0	−543.199442	63.85	0

Principal Moments of Inertia Generation

3-D structures of compounds were generated using Vernalis KNIME nodes v1.34.1 and RDKit v4.5.0 in KNIME v4.4.1, based upon the Vernalis example workflow (https://hub.knime.com/vernalis/spaces/Public/latest/PMI%20Plotting%20Example~zuyv2AxB_dFVs0Ym, accessed November 2022). DFT optimised (ωB97M-V functional, def2-SV(P) basis set) were imported into the KNIME workflow *via* an SDF reader. A maximum of 30 conformers were generated for each molecule, using experimental torsions and 'basic knowledge' – i.e. flat rings etc. The geometry of each was optimised using MMFF94 force field with 1000 iterations. Prior to calculation, explicit hydrogens were added. Post calculation, explicit hydrogens were kept and the lowest energy conformer of each molecule was selected. Normalised principal moments of inertia (PMI) values (NPR1 and NPR2) were then derived and plotted on a 2D PMI plot in Microsoft Excel 2023.

Table S7: PMI generation of normalised principal moments of inertia (NPR1 and NPR2) for Me_2BV ***(3)***.

Isomer	NPR1	NPR2
000 000 001 1 (*N*)	0.579451568	0.884053394
000 000 010 1 (*J*)	0.648490572	0.798908463
000 000 011 0 (*K*)	0.633008369	0.820297516
000 000 100 1 (*L*)	0.473739491	0.968402290
000 000 101 0 (*G*)	0.619009668	0.826640516
000 000 110 0 (*M*)	0.611689113	0.847342749
000 001 001 0 (*A*)	0.694590202	0.785185086
000 001 010 0 (*C*)	0.609014942	0.894473552
000 001 100 0 (*F*)	0.510598953	0.955380037
000 010 001 0 (*B*)	0.609010310	0.894471363
000 010 010 0 (*D*)	0.654156352	0.917353765
000 010 100 0 (*H*)	0.698308763	0.772691736
000 100 001 0 (*E*)	0.510591262	0.955397691
000 100 010 0 (*I*)	0.698304702	0.772702604
000 100 100 0 (*O*)	0.590581046	0.888824493

Table S8: PMI generation of normalised principal moments of inertia (NPR1 and NPR2) for Me_3BV ***(4)***.

Isomer	NPR1	NPR2
000 000 011 1	0.662971310	0.712488254
000 000 101 1	0.516496035	0.846370614
000 000 110 1	0.528833382	0.832863467
000 000 111 0	0.670738372	0.703398101
000 001 001 1	0.652346910	0.839580720
000 001 010 1	0.625540139	0.890769526
000 001 011 0	0.669654028	0.773255566
000 001 100 1	0.473135465	0.930891427
000 001 101 0	0.607636684	0.848361464
000 001 110 0	0.546430483	0.919287752
000 010 001 1	0.625540963	0.890759877
000 010 010 1	0.746792262	0.793448936
000 010 011 0	0.647718778	0.955680574
000 010 100 1	0.593820861	0.800836680
000 010 101 0	0.711872896	0.819256412
000 010 110 0	0.674476176	0.866517628
000 011 001 0	0.669658721	0.773251710
000 011 010 0	0.647723374	0.955691226
000 011 100 0	0.570785225	0.822385486
000 100 001 1	0.473128508	0.930888432
000 100 010 1	0.593814445	0.800843681
000 100 011 0	0.570770626	0.822386315
000 100 100 1	0.457564827	0.919742134
000 100 101 0	0.546856878	0.869661457
000 100 110 0	0.677790124	0.753007295
000 101 001 0	0.607639268	0.848363075
000 101 010 0	0.711872514	0.819246991
000 101 100 0	0.546848992	0.869664043
000 110 001 0	0.546438566	0.919289540
000 110 010 0	0.674467592	0.866524433
000 110 100 0	0.677798780	0.753011319
001 001 001 0	0.892975057	0.999995568
001 001 010 0	0.676531071	0.912325595
001 001 100 0	0.536304976	0.836139627
001 010 010 0	0.706239380	0.733588598

001 010 100 0	0.605649669	0.794098332
001 100 010 0	0.605648288	0.794101934
001 100 100 0	0.507145821	0.956196177
010 010 010 0	0.753482798	0.753485031
010 010 100 0	0.768961471	0.857654514
010 100 100 0	0.723964861	0.880883726
100 100 100 0	0.646586940	0.999996888

Table S9: PMI generation of normalised principal moments of inertia (NPR1 and NPR2) for Me_4BV ***(5)***.

Isomer	NPR1	NPR2
000 000 111 1	0.563051215	0.751696738
000 001 011 1	0.674686669	0.775069595
000 001 101 1	0.555183858	0.873884216
000 001 110 1	0.524845860	0.906436938
000 001 111 0	0.612853060	0.786923960
000 010 011 1	0.687754380	0.824019790
000 010 101 1	0.630662518	0.821485164
000 010 110 1	0.656495218	0.800477250
000 010 111 0	0.710933870	0.808541740
000 011 001 1	0.674685300	0.775066330
000 011 010 1	0.687750916	0.824010651
000 011 011 0	0.650410620	0.846078320
000 011 100 1	0.555926360	0.784486640
000 011 101 0	0.684549860	0.772347480
000 011 110 0	0.601847940	0.905901900
000 100 011 1	0.555921690	0.784492220
000 100 101 1	0.474779760	0.869858100
000 100 110 1	0.546817392	0.804077475
000 100 111 0	0.600965544	0.768555240
000 101 001 1	0.555190288	0.873874502
000 101 010 1	0.684566608	0.772346810
000 101 011 0	0.684562483	0.772343273
000 101 100 1	0.474779337	0.869866035
000 101 101 0	0.587400463	0.823499121
000 101 110 0	0.618288850	0.841957250
000 110 001 1	0.524854429	0.906432500

000 110 010 1	0.656492730	0.800476170
000 110 011 0	0.601839460	0.905906190
000 110 100 1	0.546813110	0.804079130
000 110 101 0	0.618282800	0.841953650
000 110 110 0	0.731480740	0.790645070
000 111 001 0	0.612864740	0.786922310
000 111 010 0	0.710928400	0.808529240
000 111 100 0	0.600962510	0.768545750
001 001 001 1	0.809209990	0.999993550
001 001 010 1	0.697889580	0.979044680
001 001 011 0	0.777979461	0.928502653
001 001 100 1	0.517980060	0.882348820
001 001 101 0	0.700049140	0.989860770
001 001 110 0	0.587054020	0.950107760
001 010 010 1	0.727553751	0.831528016
001 010 011 0	0.723262451	0.795699963
001 010 100 1	0.579461478	0.852400313
001 010 101 0	0.714882263	0.897453794
001 010 110 0	0.657390165	0.798637152
001 011 010 0	0.723267062	0.795699518
001 011 100 0	0.620258594	0.739152709
001 100 010 1	0.579467520	0.852404580
001 100 011 0	0.620257270	0.739153250
001 100 100 1	0.471633060	0.997681370
001 100 101 0	0.551907470	0.868170480
001 100 110 0	0.575908430	0.834141260
001 101 010 0	0.714899330	0.897457410
001 101 100 0	0.551914366	0.868172360
001 110 010 0	0.657386370	0.798639360
001 110 100 0	0.575907431	0.834135051
010 010 010 1	0.950846377	0.950854008
010 010 011 0	0.720698637	0.844085604
010 010 100 1	0.745382690	0.839053390
010 010 101 0	0.881862400	0.912984280
010 010 110 0	0.799755990	0.861150800
010 011 100 0	0.663252290	0.841042480

010 100 011 0	0.663252420	0.841039070
010 100 100 1	0.594341440	0.883316360
010 100 101 0	0.682183630	0.857493310
010 100 110 0	0.775420660	0.874045650
010 101 100 0	0.682188570	0.857492320
010 110 100 0	0.775414600	0.874038310
011 100 100 0	0.579943440	0.901650508
100 100 100 1	0.492922242	0.999997408
100 100 101 0	0.555813522	0.939994105
100 100 110 0	0.710702857	0.812443988

Table 10. PMI generation of normalised principal moments of inertia (NPR1 and NPR2) for 3-D and common ring systems

Compound	NPR1	NPR2
1,4-dimethyladamantane	0.560813614	0.965283098
1,2-dimethylcubane	0.654554766	0.768061524
1,4-dimethylcubane	0.386724171	0.999990450
p-xylene	0.216879256	0.797921538
o-xylene	0.416028907	0.600580363
m-xylene	0.336329337	0.679090911
1,4-dimethylpiperazine	0.248330953	0.816390622
(1*S*,2*S*)-1,2-dimethylcyclobutane	0.479827723	0.650785997
(1*R*,3*R*)-1,3-dimethylcyclobutane	0.279549544	0.919459774
(1*R*,2*S*)-1,2-dimethylcyclobutane	0.553180758	0.671158082
(1*S*,3*S*)-1,3-dimethylcyclobutane	0.255843764	0.914094127
(1*R*,4*R*,6*R*)-2,6-dimethylbicyclo[2.2.1]hept-2-ene	0.482384578	0.813203336
1,3-dimethylazetidine	0.268972148	0.915622214
1,2-dimethylazetidine	0.487557647	0.646360335
2,5-dimethylpyridine	0.216330750	0.798840434
2,3-dimethylpyridine	0.422075200	0.594999842
2,4-dimethylpyridine	0.328569016	0.687151837
3,4-dimethylpyridine	0.414936199	0.601949465
1,4-dimethylpiperidine	0.259618894	0.813581832
2,6-dimethyl-2-azaspiro[3.3]heptane	0.174720498	0.998096293
2,5-dimethyloctahydrocyclopenta[*c*]pyrrole	0.285180132	0.931848441
3,6-dimethyl-3-azabicyclo[3.1.0]hexane	0.412421426	0.995728438

1,5-dimethylazocane	0.437109773	0.813556375
2,6-dimethyl-2,6-diazaspiro[3.3]heptane	0.177391885	0.999617791
1,6-dimethyl-1,6-diazaspiro[3.3]heptane	0.309926511	0.891222204
(*R*)-1,7-dimethyl-1,7-diazaspiro[4.4]nonane	0.359787851	0.901014064
2,5-dimethyl-2,5-diazaspiro[3.4]octane	0.338226173	0.895946912
(1*S*,4*S*)-2,5-dimethyl-2,5-diazabicyclo[2.2.1]heptane	0.587353006	0.910167407
(1*S*,3*S*)-1,3-dimethylcyclohexane	0.453685408	0.758132605
(1*R*,2*R*)-1,2-dimethylcyclopropane	0.299772204	0.862461341
(1*s*,4*s*)-1,4-dimethylcyclohexane	0.400440242	0.856168260

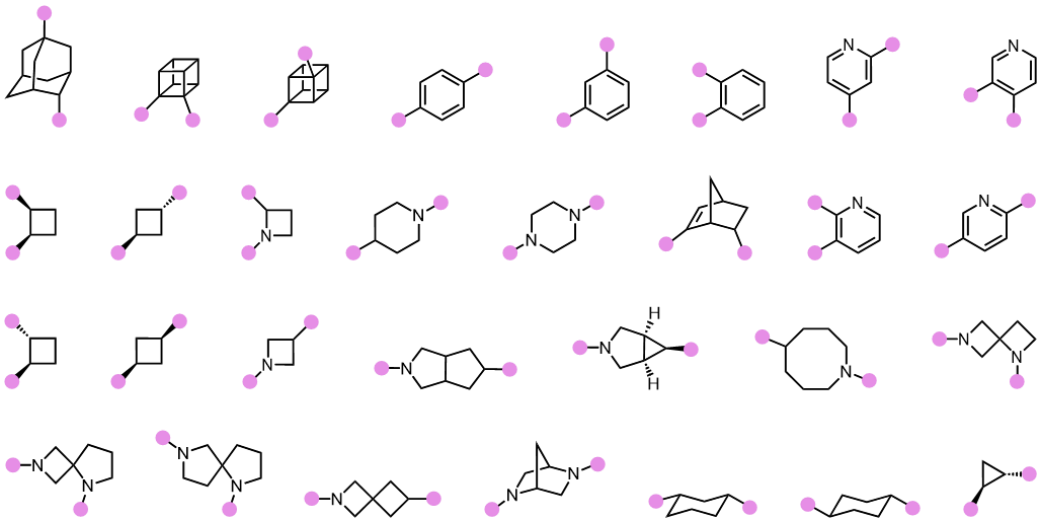

*Figure S1: Selection of commonly used ring systems in medicinal chemistry for comparison to **3**, **4**, and **5**.*

References

1 W. von Eggers Doering and W. R. Roth, *Tetrahedron*, 1963, **19**, 715–737.

2 A. N. Bismillah, B. M. Chapin, B. A. Hussein and P. R. McGonigal, *Chem. Sci.*, 2020, **11**, 324–332.

3 S. Ferrer and A. M. Echavarren, *Synthesis*, 2019, **51**, 1037–1048.

4 O. Yahiaoui, L. F. Pašteka, B. Judeel and T. Fallon, *Angew. Chem. Int. Ed. Engl.*, 2018, **57**, 2570–2574.

5 O. Yahiaoui, L. F. Pašteka, C. J. Blake, C. G. Newton and T. Fallon, *Org. Lett.*, 2019, **21**, 9574–9578.

6 H. D. Patel, T.-H. Tran, C. J. Sumby, L. F. Pašteka and T. Fallon, *J. Am. Chem. Soc.*, 2020, **142**, 3680–3685.

7 J. F. Teichert, D. Mazunin and J. W. Bode, *J. Am. Chem. Soc.*, 2013, **135**, 11314–11321.

8 A. Sanchez, A. Gurajapu, W. Guo, W.-Y. Kong, C. J. Laconsay, N. S. Settineri, D. J. Tantillo and T. J. Maimone, *J. Am. Chem. Soc.*, 2023, **145** 13452–13461

9 A. R. Lippert, V. L. Keleshian and J. W. Bode, *Org. Biomol. Chem.*, 2009, **7**, 1529–1532.

10 A. R. Lippert, A. Naganawa, V. L. Keleshian and J. W. Bode, *J. Am. Chem. Soc.*, 2010, **132**, 15790–15799.

11 C. Dohmen, H. Ihmels and T. Paululat, *Eur. J. Org. Chem.*, 2022, **2022**, e202201172.

12 A. P. Birvé, H. D. Patel, J. R. Price, W. M. Bloch and T. Fallon, *Angew. Chem. Int. Ed. Engl.*, 2022, **61**, e202115468.

13 C. Dohmen, T. Paululat and H. Ihmels, *Chem. Eur. J.*, DOI:10.1002/chem.202304311.

14 J. R. Reimers, T. Li, A. P. Birvé, L. Yang, A. C. Aragonès, T. Fallon, D. S. Kosov and N. Darwish, *Nat. Commun.*, 2023, **14**, 6089.

15 M. N. Pomfret, P. B. Sun, Z. Huang, A. C. Freund, T. Miyoshi and M. R. Golder, *Angew. Chem. Int. Ed. Engl.*, 2023, **62**, e202301695

16 D. J. Tantillo and R. Hoffmann, *Acc. Chem. Res.*, 2006, **39**, 477–486.

17 A. Ottonello, J. A. Wyllie, O. Yahiaoui, S. Sun, R. A. Koelln, J. A. Homer, R. M. Johnson, E. Murray, P. Williams, J. R. Bolla, C. V. Robinson, T. Fallon, T.

P. Soares da Costa and J. E. Moses, *Proc. Natl. Acad. Sci. U.S.A.*, 2023, **120**, e2208737120

18 A. E. Baumann, D. A. Burns, B. Liu and V. S. Thoi, *Commun. Chem.*, 2019, **2**, 86.

19 V. F. Yusuf, N. I. Malek and S. K. Kailasa, *ACS Omega*, 2022, **7**, 44507–44531.

20 R.-B. Lin and B. Chen, *Chem*, 2022, **8**, 2114–2135.

21 K. Geng, T. He, R. Liu, S. Dalapati, K. T. Tan, Z. Li, S. Tao, Y. Gong, Q. Jiang and D. Jiang, *Chem. Rev.*, 2020, **120**, 8814–8933.

22 D. A. Erlanson, S. W. Fesik, R. E. Hubbard, W. Jahnke and H. Jhoti, *Nat. Rev. Drug Discov.*, 2016, **15**, 605–619.

23 A. W. Hung, A. Ramek, Y. Wang, T. Kaya, J. A. Wilson, P. A. Clemons and D. W. Young, *Proc. Natl. Acad. Sci. U.S.A.*, 2011, **108**, 6799–6804.

24 T. D. Downes, S. P. Jones, H. F. Klein, M. C. Wheldon, M. Atobe, P. S. Bond, J. D. Firth, N. S. Chan, L. Waddelove, R. E. Hubbard, D. C. Blakemore, C. De Fusco, S. D. Roughley, L. R. Vidler, M. A. Whatton, A. J. A. Woolford, G. L. Wrigley and P. O'Brien, *Chem. Eur. J.*, 2020, **26**, 8969–8975.

25 W. R. J. D. Galloway, A. Isidro-Llobet and D. R. Spring, *Nat. Commun., 2010 1:1*, 2010, **1**, 1–13.

26 W. H. B. Sauer and M. K. Schwarz, *J. Chem. Inf. Comput. Sci.*, 2003, **43**, 987–1003.

27 O. O. Grygorenko, D. Demenko, D. M. Volochnyuk and I. V Komarov, *New. J. Chem.*, 2018, **42**, 8355.

28 O. O. Grygorenko, P. Babenko, D. M. Volochnyuk, O. Raievskyi and I. V. Komarov, *RSC Adv.*, 2016, **6**, 17595–17605.

29 M. He and J. W. Bode, *Org. Biomol. Chem.*, 2013, **11**, 1306–1317.

30 G. Schröder, J. F. M. Oth and R. Merényi, *Angew. Chem. Int. Ed. Engl.*, 1965, **4**, 752–761.

31 bullviso, 2024, https://gitlab.com/conor.rankine/bullviso.

32 RDKit: Open-Source Cheminformatics. https://rdkit.org.

33 RDKit, 2023, https://github.com/rdkit/rdkit.

34 S. Riniker and G. A. Landrum, *J. Chem. Inf. Model.*, 2015, **55**, 2562–2574.

35 S. Wang, J. Witek, G. A. Landrum and S. Riniker, *J. Chem. Inf. Model.*, 2020, **60**, 2044–2058.

36 A. K. Rappe, C. J. Casewit, K. S. Colwell, W. A. Goddard and W. M. Skiff, *J. Am. Chem. Soc.*, 1992, **114**, 10024–10035.

37 M. J. Frisch, G. W. Trucks, H. B. Schlegel, G. E. Scuseria, M. A. Robb, J. R. Cheeseman, G. Scalmani, V. Barone, G. A. Petersson, H. Nakatsuji, X. Li, M. Caricato, A. V. Marenich, J. Bloino, B. G. Janesko, R. Gomperts, B. Mennucci, H. P. Hratchian, J. V. Ortiz, A. F. Izmaylov, J. L. Sonnenberg, D. Williams-Young, F. Ding, F. Lipparini, F. Egidi, J. Goings, B. Peng, A. Petrone, T. Henderson, D. Ranasinghe, V. G. Zakrzewski, J. Gao, N. Rega, G. Zheng, W. Liang, M. Hada, M. Ehara, K. Toyota, R. Fukuda, J. Hasegawa, M. Ishida, T. Nakajima, Y. Honda, O. Kitao, H. Nakai, T. Vreven, K. Throssell, J. A. Montgomery, Jr., J. E. Peralta, F. Ogliaro, M. J. Bearpark, J. J. Heyd, E. N. Brothers, K. N. Kudin, V. N. Staroverov, T. A. Keith, R. Kobayashi, J. Normand, K. Raghavachari, A. P. Rendell, J. C. Burant, S. S. Iyengar, J. Tomasi, M. Cossi, J. M. Millam, M. Klene, C. Adamo, R. Cammi, J. W. Ochterski, R. L. Martin, K. Morokuma, O. Farkas, J. B. Foresman, and D. J. Fox, Gaussian, Inc., Wallingford CT, 2016..

38 F. Neese, *Wiley Interdiscip. Rev. Comp. Mol. Sci.*, 2012, **2**, 73–78.

39 F. Neese, *Wiley Interdiscip. Rev. Comp. Mol. Sci.*, 2018, **8**, e1327

40 F. Neese, F. Wennmohs, U. Becker and C. Riplinger, *J. Chem. Phys.*, 2020, **152**, 224108

41 A. D. Morley, A. Pugliese, K. Birchall, J. Bower, P. Brennan, N. Brown, T. Chapman, M. Drysdale, I. H. Gilbert, S. Hoelder, A. Jordan, S. V. Ley, A. Merritt, D. Miller, M. E. Swarbrick and P. G. Wyatt, *Drug Discov. Today*, 2013, **18**, 1221–1227.

42 B. Over, S. Wetzel, C. Grütter, Y. Nakai, S. Renner, D. Rauh and H. Waldmann, *Nat. Chem.*, 2013, **5**, 21–28.

43 S. P. Jones, J. D. Firth, M. C. Wheldon, M. Atobe, R. E. Hubbard, D. C. Blakemore, C. De Fusco, S. C. C. Lucas, S. D. Roughley, L. R. Vidler, M. A. Whatton, A. J. A. Woolford, G. L. Wrigley and P. O'Brien, *RSC Med. Chem.*, 2022, **13**, 1614–1620

44 P. Garner, P. B. Cox, U. Rathnayake, N. Holloran and P. Erdman, *ACS Med. Chem. Lett.*, 2019, **10**, 815.

45 C. Adamo and V. Barone, *J. Chem. Phys.*, 1999, **110**, 6158–6170.

46 J. P. Perdew, K. Burke and M. Ernzerhof, *Phys. Rev. Lett.*, 1997, **78**, 1396–1396.

47 J. P. Perdew, K. Burke and M. Ernzerhof, *Phys. Rev. Lett.*, 1996, **77**, 3865–3868.

48 S. Grimme, J. Antony, S. Ehrlich and H. Krieg, *J. Chem. Phys.*, 2010, **132**, 154104

49 F. Weigend and R. Ahlrichs, *Phys. Chem. Chem. Phys.*, 2005, **7**, 3297.

50 N. and D. F. and G. T. R. and K. T. and M. T. and O. P. and S. C. and T. K. and W. B. Berthold Michael R. and Cebron, in *Data Analysis, Machine Learning and Applications*, ed. H. and S.-T. L. and D. R. Preisach Christine and Burkhardt, Springer Berlin Heidelberg, Berlin, Heidelberg, 2008, pp. 319–326.

51 S. D. Roughley, *Curr. Med. Chem.*, 2018, **27**, 6495–6522.

52 R. D. Taylor, M. MacCoss and A. D. G. Lawson, *J. Med. Chem.*, 2014, **57**, 5845–5859.

53 J. Shearer, J. L. Castro, A. D. G. Lawson, M. MacCoss and R. D. Taylor, *J. Med. Chem.*, 2022, **65**, 8699–8712.

54 B. A. Chalmers, H. Xing, S. Houston, C. Clark, S. Ghassabian, A. Kuo, B. Cao, A. Reitsma, C. E. P. Murray, J. E. Stok, G. M. Boyle, C. J. Pierce, S. W. Littler, D. A. Winkler, P. V. Bernhardt, C. Pasay, J. J. De Voss, J. McCarthy, P. G. Parsons, G. H. Walter, M. T. Smith, H. M. Cooper, S. K. Nilsson, J. Tsanaktsidis, G. P. Savage and C. M. Williams, *Angew. Chem. Int. Ed. Engl.*, 2016, **55**, 3580–3585.

55 L. Wanka, K. Iqbal and P. R. Schreiner, *Chem. Rev.*, 2013, **113**, 3516–3604.

56 T. A. Reekie, C. M. Williams, L. M. Rendina and M. Kassiou, *J. Med. Chem.*, 2018, **62**, 1078–1095.

57 K. C. Nicolaou, J. Yin, D. Mandal, R. D. Erande, P. Klahn, M. Jin, M. Aujay, J. Sandoval, J. Gavrilyuk and D. Vourloumis, *J. Am. Chem. Soc.*, 2016, **138**, 1698–1708.

58 G. Schröder and W. Witt, *Angew. Chem. Int. Ed. Engl.*, 1979, **18**, 311–312.

59 E. G. Tse, S. D. Houston, C. M. Williams, G. Paul Savage, L. M. Rendina, I. Hallyburton, M. Anderson, R. Sharma, G. S. Walker, R. Scott Obach and M. H. Todd, *J. Med. Chem.*, 2020, **63**, 11585–11601.

60 P. K. Mykhailiuk, *Org. Biomol. Chem.*, 2019, **17**, 2839–2849.

61 M. A. M. Subbaiah and N. A. Meanwell, *J. Med. Chem.*, 2021, **64**, 14046–14128.

62 S. Grimme, C. Bannwarth and P. Shushkov, *J. Chem. Theory Comput.*, 2017, **13**, 1989–2009.

63 C. Bannwarth, S. Ehlert and S. Grimme, *J. Chem. Theory Comput.*, 2019, **15**, 1652–1671.

64 C. Bannwarth, E. Caldeweyher, S. Ehlert, A. Hansen, P. Pracht, J. Seibert, S. Spicher and S. Grimme, *Wiley Interdiscip. Rev. Comp. Mol. Sci.*, 2021, **11**, e1493.

65 F. Weigend, *Phys. Chem. Chem. Phys.*, 2006, **8**, 1057.

Chapter 3 | Towards Tetrasubstituted Bullvalenes

Abstract

Recent advances in bullvalene synthesis have made substituted fluxional molecules more synthetically attainable than ever before. However, current synthetic methodology limit bullvalene to di- and trisubstitution. The only reported route for tetrasubstituted bullvalenes are limited by eleven or more step syntheses and do not install four similar substituents. This chapter exhibits our ongoing attempts to synthesise tetrasubstituted bullvalenes in order to make bullvalene cross-linked polymers. Currently, our research indicates that pursuing cycloadditions with substituted cyclooctatetraene starting materials do not afford any target bullvalenes, most likely due to limitations imposed by steric hindrance. Alternatively, a new synthetic method for bullvalene has been proposed and researched extensively, with much more promise. The limits of this new methodology are in forming stable dialdehydes for Weiss–Cook condensations which result eventually in the formation of a fluxional core.

Acknowledgments

The following people are gratefully acknowledged for their contribution to this chapter: Dr. Senthil Kumar Kabali for contribution in the synthesis of tetrasubstituted cyclooctatetraene derivatives **28** and **29**. Ho Chi Wong, for synthesis and formation of a crystal of **36**. Dr. Matthew Gill contributed to the synthesis of **47**, and synthesised of **48**, attempted synthesis of dialdehydes **54**, **62**, **64**, **65** and **66**. Dr. Aisha Bismillah contributed to the analysis of isomer mixture **47**. Dr. Paul McGonigal made attempts to synthesise **50**.

3.1 Introduction

Cross-linking polymer chains (Figure 1a) gives rise to thermosets, which are particularly durable polymeric materials. Unlike thermoplastics, whose discrete polymer chains are associated through relatively weak noncovalent bonding interactions, covalent bonds must be cleaved in order to break the structure of a thermoset. An idealised thermoset structure has a simple mesh-like topology in which the polymer chains connect a network of cross-linking nodes with a regular structure.[1] However, cross-linking reactions are typically kinetically controlled processes that inevitably trap defects in the networks, such as tangled polymer chains (Figure 1a). Knots in polymer chains have been shown to be the weakest part of the structure and the site of breakage when the material is subjected to mechanical stress.[2,3]

Dynamic polymers (Figure 1b) on the other hand, are capable of reproducing these same properties, but are also processable. This is due to their ability to make and break these cross-links under certain conditions.[4] 'Dynamers' of this kind were proposed in the 1990s by Lehn, and now are a fast-emerging area of chemistry, allowing for unique transformative behaviour.[5,6] Vitrimers exhibit the same strength and durability of traditional thermosets, but with the added recyclability, as well as self-healing, shape memory, and other exciting properties.[7] Many of these kinds of materials use external stimuli such as thermal, photochemical, or chemical triggers in order to exhibit these exciting properties.

Bullvalene (BV) is a fluxional molecule which may undergo rapid Cope rearrangements at room temperature due to internal molecular strain imposed by its structure. BV has been included in a linear polymer, resulting in a polymer with high thermal stability and tunable properties.[8] BV's rearrangements present a fascinating opportunity as a polymer cross-link junction (Figure 1c). In this setting, a polymer may be tangled or untangled simply through Cope rearrangements which are constantly occurring, even in the solid state.[9] Similarly to vitrimers, these compounds may exhibit the ability to be reprocessed, as well as being highly durable. However, unlike vitrimers, these compounds would be able to be reprocessed with no stimuli at all, due to the constantly occurring Cope rearrangements in the BV core.

This means that for a cross-linked polymer which may incorporate a BV scaffold as a cross-linking junction, the result would be a polymer which has both dynamic topology, but also the stability of fixed covalent connectivity. Here, we investigate

synthetic methods to achieve tetrasubstituted BVs, in order to synthesise a polymer system which contains BV cross-links.

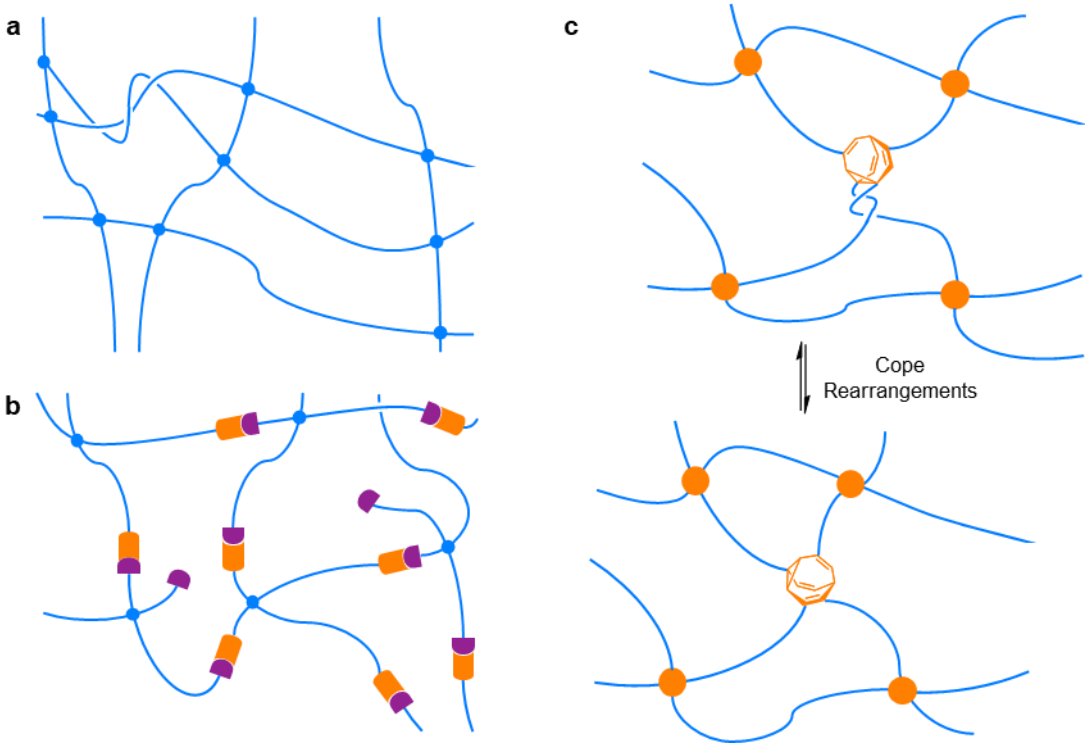

Figure 1: Illustrations of (a) Cross-linked polymer systems. (b) Dynamic polymer systems. (c) Our proposed bullvalene cross-linked polymer.

3.2 Tetrasubstituted BVs for Polymerisation

Before undertaking experimental investigation of this proposed phenomenon, we performed thought experiments to understand how the low-barrier pericyclic rearrangements at BV cross-links could lead to dynamic topology, i.e., spontaneous covalent tangling and untangling. Firstly, we observe that a tetrasubstituted BV is necessary and a trisubstituted BV will not suffice. This is a topological question; trisubstituted BVs will indeed tangle simply through accessible Cope rearrangements just as a tetrasubstituted BVs will, however, a trisubstituted BV will be able to undo this twist through single-bond rotations. This would give this polymer properties that would presumably be similar to any other cross-linked polymer with trivalent cross-links e.g. 1,3,5-trisubstituted benzene rings. In contrast, rotation at a tangled tetrasubstituted BV junction will not undo the tangle, but simply translate the tangle to a different part of the polymeric structure (Figure 2).

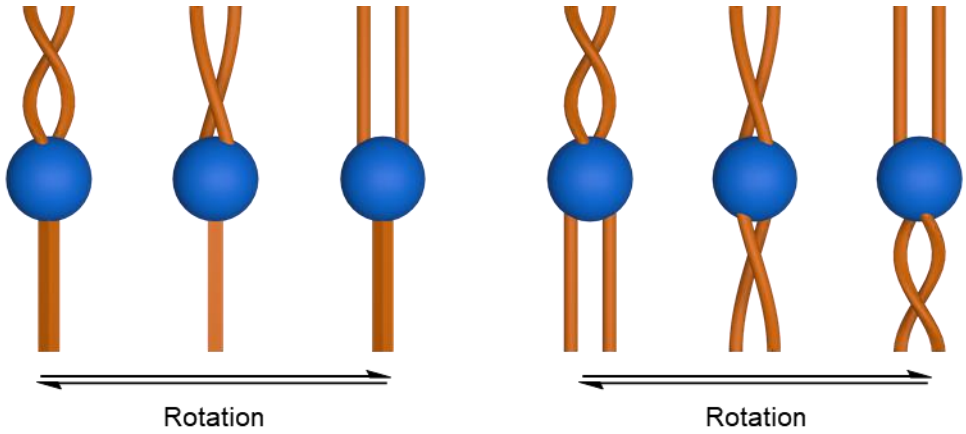

Figure 2: Rotation of tangled bullvalene cross-linked polymers.

The tangling of the polymer chains may be demonstrated using a network analysis (Chapter 1) for a tetrasubstituted BV and picking two isomers to form a "loop", which will see two substituents rotate around one another. One key element of this "loop" is that the other two substituents should remain in place such as not to undo the tangling of the initial two substituents (Figure 3).

Figure 3: Isomer A and isomer B represent two isomers of a bullvalene in a cross-linked polymer.

When using the network analysis to establish the relationship between these two isomers, two routes of rearrangement connecting them were found. These routes were the same length, and saw substituents 2 and 3 rotate 180° around one another in opposite directions. Therefore, if we use Cope rearrangements to transform isomer A into isomer B via route one, and return to isomer A using the route two, we expect to see a 360 ° tangling of two polymer chains, resulting in a new tangle in the cross-linked polymer (Figure 4). This was then simulated and animated using Blender software to demonstrate that a tangle in this kind of cross-linked polymer is in fact, possible (BV polymer tangle video).

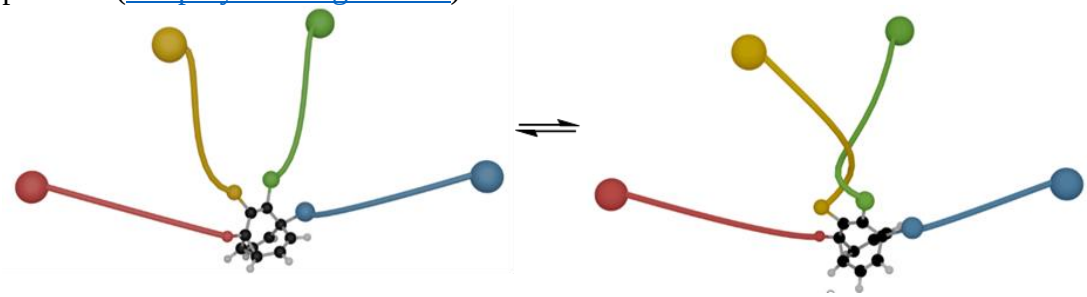

Figure 4: Both bullvalene cross-linked polymers display Isomer A here, after having rearranged via Isomer B.

The route of tangling and untangling for this polymer was deciphered through the construction of a network analysis and identification of the relevant isomers. Amongst the 1680 isomers, there are multiple routes which will result in the tangling of the fluxional polymer. The one that was chosen is the shortest that exemplifies the tangling action, and is shown below (Figure 5).

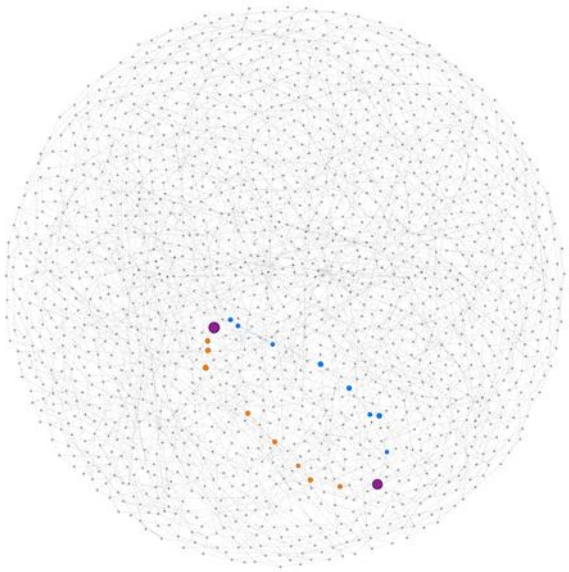

Figure 5: Network analysis for the fluxional polymer This network analysis was made using the computer program GePhi.

3.3 Using Disubstituted COTT with Fallon's BDT Method

The first method through which the synthesis of tetrasubstituted BVs was attempted is using a modified version of Fallon's two-step synthesis (Scheme 1).[10] The first step of this synthesis is a cobalt (I) catalysed [6+2] cycloaddition between cyclooctatetraene (**COTT**) and an alkyne to form a bicyclo[4.2.2]deca-2,4,7,9-tetraene (BDT) intermediate. This step was first established by Buono *et al.* in 2006.[11] Once this BDT has been formed, photoexcitation causes a di-π-methane rearrangement to occur, resulting in the formation of the BV structure in reasonable yields. This second step is a component of multiple different **BV** syntheses, firstly by Jones and Scott in 1967, just a year after the rearrangement had been established by Zimmerman *et al.*.[12–15]

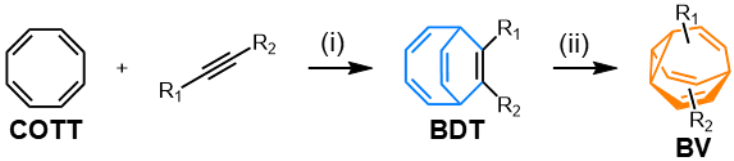

*Scheme 1: Fallon et al.'s 2018 and 2022 **BV** synthesis.(i) $CoBr_2$(dppe) 10 mol%, ZnI_2 20 mol%, Zn Dust 30 mol%, DCE or TFE, rt or 55°C, 24–48 h.63–100%. (ii) h ν, thioxanthone, THF, rt, 6 h, 55–97%.* [10,15]

Fallon *et al.* used the same methodology with a monosubstituted COTT, such as **2**, resulting in a trisubstituted BVs.[15,16] A TMS group was installed on the COTT *via* bromination of **COTT** to form monobromo COTT **1**, followed by bromine-lithium exchange and nucleophilic attack on trimethylsilyl chloride (Scheme 2).

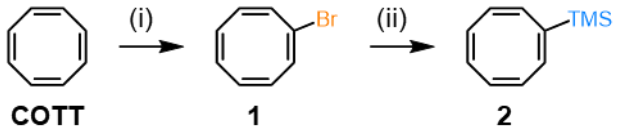

*Scheme 2: Fallon's synthesis of monosubstituted COTT **2**. (i) (a) Br_2, CH_2Cl_2, −78°C to rt. (b) KO^{t}Bu, THF, 3 h, −78°C to rt, 85%. (ii) ^{n}BuLi in hexanes, TMS-Cl, THF, −78°C, 2 h, 78%.*

Fallon's methodology is the basis of a lot of work undertaken in this chapter, firstly hoping to synthesise disubstituted COTTs, and then performing cycloadditions to form tetrasubstituted BDTs and then BVs. The yields for cycloaddition with a substituted COTT are significantly lower than those for unsubstituted **COTT**, but the desired products are still isolated in sufficient amounts for further work. (Scheme 3 and Table 1). This demonstrates the challenge to overcome steric hindrance in the cycloaddition reaction.

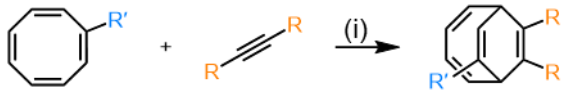

Scheme 3: General synthesis of trisubstituted BDTs, yield detailed in Table 1. (i) $COBr_2$(dppe), ZnI_2, Zn Dust, TFE or DCE, 55 °C or rt.

Table 1: Yields for Co(I) cycloaddition with substituted COTT vs unsubstituted COTT.

COTT Substituent (R′)	Alkyne Substituents (R)	Yield / %
H	CH_2OH	80[10]
TMS	CH_2OH	43[16]
H	Boronate Pinacol Ester	74[15]
Boronate Pinacol Ester[a]	Boronate Pinacol Ester[a]	36[15]

[a]Performed with increased catalyst loading.

3.3.1 Disubstituted COTT—Bromination

Initial attempts to yield a disubstituted COTT were by sequential brominations to yield dibromo COTT **3**, which may then be functionalised before cycloaddition. The involvement of zinc dust in the cycloaddition reaction precludes the presence of an alkyl halide, which may result in a Frankland reaction; a radical reaction which forms zinc bromide and alkyl zinc compounds.[17,18] Konz *et al.* performed this dibromination

pathway in 1970, reporting a yield upwards of 92%[19] but this has not been reproduced in literature since (Scheme 4).

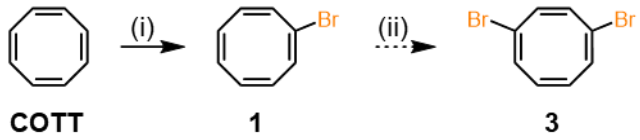

Scheme 4: Attempted dibromination of COTT. (i) (a) Br_2, CH_2Cl_2, −78°C to rt. (b) KO^{t}Bu, THF, 3 h, −78°C to rt, 81%. (ii) (a) Br_2, CH_2Cl_2, −78°C to rt. (b) KO^{t}Bu, THF, 3 h, −78°C to rt, product not obtained.

Compound **1** was obtained in an 81% yield, however, further bromination resulted in a mixture of **1** and **3**, which could not be separated by distillation or chromatography. The ^{1}H NMR spectrum of **3** has never been reported, as Konz *et al.* instead provided the spectrum of the Diels–Alder adduct with 4-methyl-1,2,4-triazoline-3,5-dione. The ^{1}H NMR spectrum of the mixture of **3** and **1** appears as though there are two product isomers present, although 1,4-substitution is reportedly the only product which forms during this reaction. This can be rationalised by the fact that COTT's ground state is a D_{2d} tub-shape (**3** and **3′**), which may isomerise and invert first *via* a D_{4h} planar ring (**3a** and **3a′**) followed by a planar D_{8h} bond-switching transition state (**3b**) (Figure 6).[20] All ^{13}C environments in the tub-shaped D_{2d} ground-state structure of **1** are inequivalent, so its ^{13}C NMR spectrum is expected to show eight signals (as opposed to five as would be expected of a planar ring system).[16]

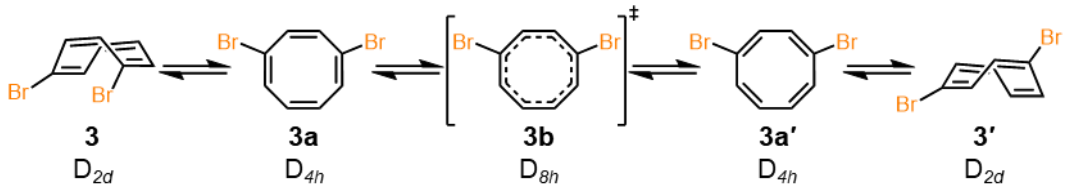

Figure 6: An illustration of the isomerisation of 1,4-disubstituted COTT.

The main objection from pursuing this route in more depth was the irreproducible nature of the second bromination, along with difficulties experienced in purification. Furthermore, the cost of **COTT** and difficulties experienced in purifying **3** made significantly scaling up this reaction ineffectual. Instead another, more reliable and reproducible method was sought to reduce wasted **COTT**.

3.3.2 Disubstituted COTT – Sulfonation

Gottesfeld *et al.* had outlined simply the equilibrium between the 1,4- and 1,6-isomers of disubstituted COTT molecules in a paper from 1992.[21] Gottesfeld *et al.* did not achieve their disubstituted COTTs through bromination but instead through sulfonation of **COTT** to form a cyclooctatriene (COT)–sulfone adduct **4** (Scheme 5).

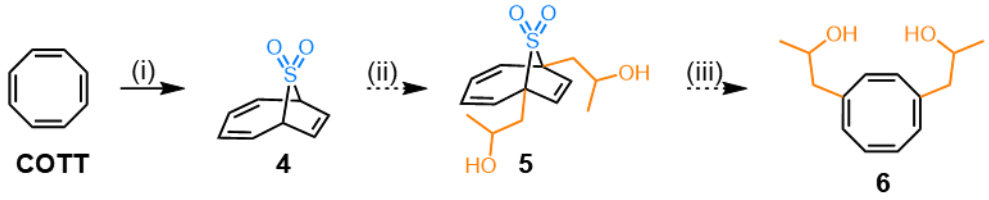

Scheme 5: Gottesfeld's synthesis of diol COTT. (i) SbF_5, SO_2 (l), −70 °C, 24 h, 18%. (ii) (a) ^{n}BuLi, THF, −78 °C. (b) propylene oxide, $BF_3.Et_2O$, −78 °C. Product not obtained. (iii) hv, reaction not attempted.

This synthetic method was originally developed by Paquette *et al.* and uses antimony pentafluoride as a catalyst in liquid SO_2 to form **4**.[22] Antimony pentafluoride acts as a Lewis acid in this reaction, and is soluble in SO_2. Without an SO_2 tank available to use, the gas was instead condensed from the reaction of sodium sulfite with conc. sulfuric acid, after bubbling through a container of sodium hydroxide pellets to absorb any water from the gas formation. SO_2 condenses at temperatures from −10 °C and freezes at −72 °C, so a dry ice–acetonitrile cooling tower (T = −41 °C) was used.

Addition of ^{n}BuLi to **4** causes lithiation of the bridgehead positions. Nucleophilic attack on ethylene oxide results in an ethyl alcohol-functionalised COT–sulfone. Subsequent irradiation releases SO_2 gas in a chelotropic rearrangement, yielding a 1,4-diol COTT. A similar reaction was attempted, instead using propylene oxide to form **5**.

Preliminary attempts at forming **4** were low-yielding, but enough material was isolated for a small-scale attempt at the second step. Mass spectrometry confirmed the formation of trace amounts of **5**. The challenge of bringing material through this low-yielding route was exacerbated by irreproducibility of the sulfonation of **COTT**. The literature preparation for COT sulfone **4** was "treating **COTT** with antimony pentafluoride in liquid SO_2 yielded product", with no analysis or further information present.[21]

The result of these attempts was another reaction that was unreliable and deemed a waste of our limited supply of **COTT**. Other channels were therefore explored, particularly ones that did not involve **COTT** as a starting material, so as to reduce cost of the reaction.

3.3.3 Disubstituted COTT – Lithiation of COD

The third synthetic strategy for tetrasubstituted BVs does not use **COTT** as a starting material but instead uses cyclooctadiene (**COD**), which is a much more readily available, stable and cheaper starting material. Based upon a synthesis by Burton *et al.* (Scheme 6), **COD** is deprotonated with ^{n}BuLi in the presence of TMEDA to form a dilithyl cycloctatetraenide salt **7**, which may then perform a nucleophilic attack on trimethylsilyl chloride to form bis-TMS COT **8**.[23] This compound may then be deprotonated with ^{n}BuLi again, and the resultant dilithyl cycloctatetraenide salt **9** oxidised using mercuric chloride to form di-TMS COTT **10** as the final product.

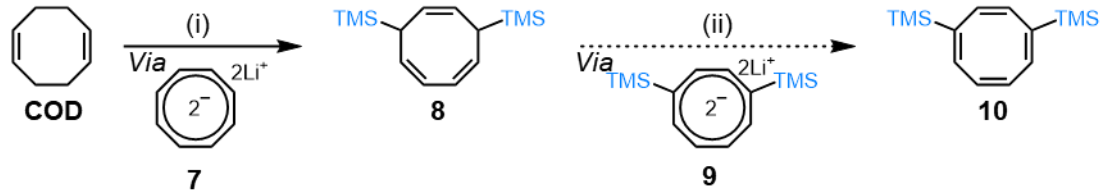

Scheme 6: Burton's synthesis of a disubstituted COTT (i) (a) ^{n}BuLi, TMEDA, pentane, 0 °C to reflux, 24 h (b) TMS-Cl, THF, −30 °C, 18 h, 3%. (ii) (a) ^{n}BuLi, THF, −78 °C, 2 h. (b) Oxidising agent, THF, rt, 18 h, no product obtained.

In the first attempts of the lithiation step, yields were low, but enough material was obtained to attempt the second step on a small scale. It was desirable to avoid the use of hazardous mercuric chloride in the second step, thus, other oxidising agents were trialled in the reaction. Manganese oxide and chloranil were the two oxidising agents initially used, neither of which yielded any product **10**. More recently, in March 2022, Konig *et al.* published a similar synthesis, using silver nitrate as the oxidant in the reaction, affording **10** in 55% yield over the two steps from **COD**, a significant improvement on the yields reported by Burton *et al.* (37% over two steps).[23,24]

This synthetic procedure would have been attempted in the lab had it been published slightly earlier, as it was only a short time after work on this synthesis had stopped. This was in favour of a new method which proved to have an advantage over the previous three attempted.

3.3.4 Disubstituted COTT – Alkyne Ester

Grovenstein *et al.* developed a series of disubstituted COTTs using irradiation of an ester alkyne **11** with benzene, the result of which is **12**, a strained bicyclic compound. The cyclobutene formed then cleaves to form heterodisubstituted COTT **13** (Figure 7).[25] This chemistry was developed further by Paquette *et al.* with a variety of substrates.[26]

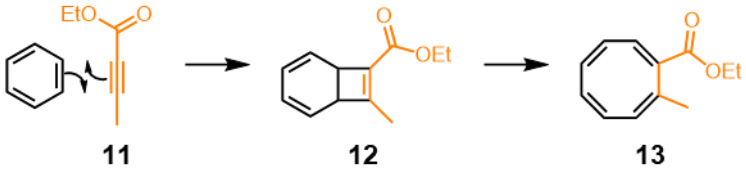

Figure 7: Mechanism of Paquette's substituted COTT synthesis.

This reaction was initially undertaken using but-2-yn-1,4-diol **14** as a starting material for the synthesis of alkynic ester **15**,[27] which was irradiated with 254 nm ultraviolet light in benzene (Scheme 6).

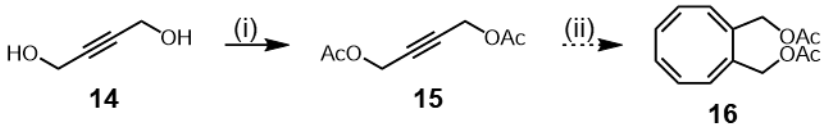

Scheme 7: Attempted synthesis of diacetyl COTT. (i) Acetyl chloride, CH_2Cl_2, rt, 18 h, 88%. (ii) 254 nm, benzene, rt, 5 d, no product obtained.

The second step in this reaction did not proceed at all, with no disubstituted COTT **16** present in the crude reaction mixture after days of irradiation. As such, the literature was revisited. It was noted that in order for the photoaddition to occur, the alkyne used must be conjugated with the esters present, as stated by Bryce-Smith *et al.* in 1970.[28] Acetylene dicarboxylic acid diethyl ester **17** was used instead, and the reaction proceeded to yield **18** (Scheme 7).

This reaction is carried out over three to five days and requires the vessel to be washed once a day in order to remove an orange polymer coating that builds up from polymerisation of the starting materials. This is a simple, single step synthesis, using relatively cheap, and recoverable starting materials which also allows for the synthesis of multiple grams of disubstituted COTT **18** at once, unlike the previously attempted synthetic strategies.[26] As a result, investigation on other synthetic routes was stopped in favour of this one.

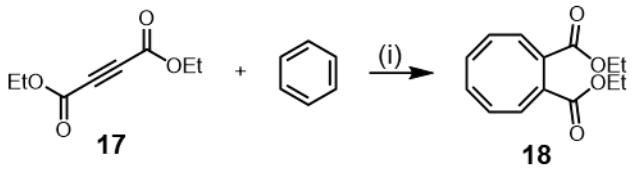

Scheme 8: Synthesis of disubstituted COTT by photoaddition of alkyne with benzene. (i) 254 nm, rt, 5 d, 36%.

Another difference between this COTT synthesis compared to the previous strategies is the formation of a 1,2-disubstituted species as opposed to the 1,4-disubstituted species. This may be an advantage due to the fact that the limiting factor in the cobalt-catalysed cycloaddition will most likely be steric hindrance from the COTT substituents, thus, having the substituents vicinal to one another is optimal.

When Buono *et al.* developed the synthetic methodology for the cobalt-catalysed cycloaddition, both **COTT** and **COT** were used as starting materials.[11] In the proposed mechanism for this cycloaddition (Figure 8) **COT** acts as a hexa- and tetrahaptic ligand (**19** and **20** respectively), at most donating six electrons. Thus, the vicinal substituted positions do not have to be involved in the binding to the Co(I) centre and, the 1,2-disubstituted COTT should impose less steric constraint on the cycloaddition compared to 1,4-disubstituted COTTs.

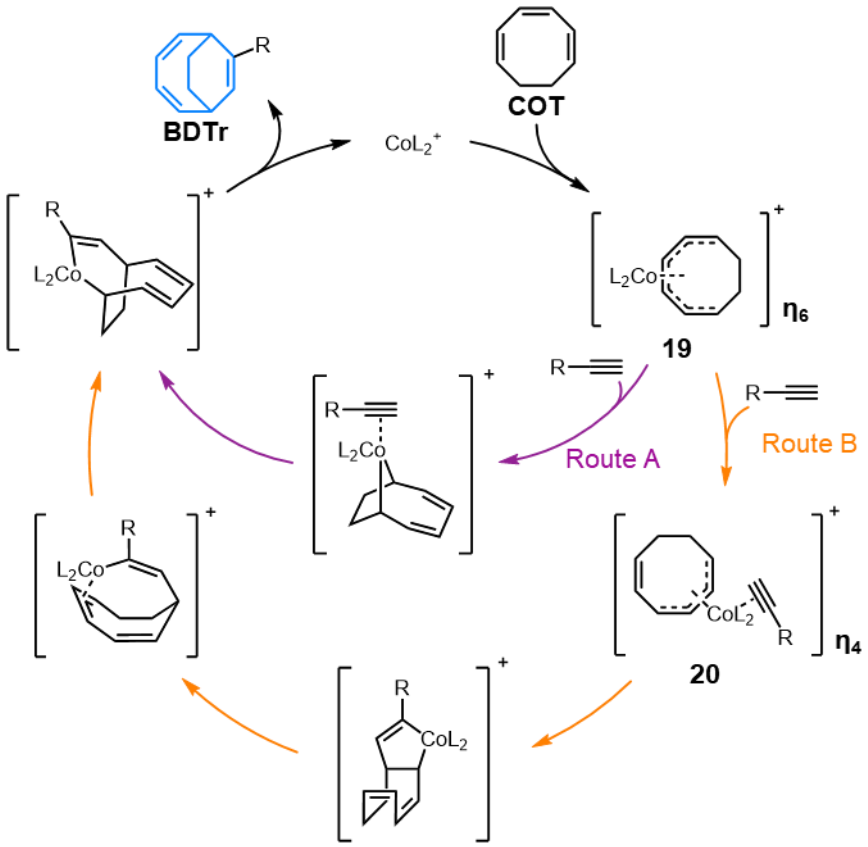

Figure 8: Proposed mechanism for Co(I) catalysed cycloaddition of COT with substituted alkyne.

Another advantage of this synthesis is that the substituents are simple synthetic handles. Esters can be reduced to alcohols and aldehydes, resulting in the possibility of forming a wide array of disubstituted COTTs (Scheme 9). A range of disubstituted COTTs were made, with the esters of **18** first being reduced to form vicinal diol **21**. This diol **21** was then acetal protected, forming **22**, with the hope of reducing any coordinating behaviour from the lone pairs of **21**.

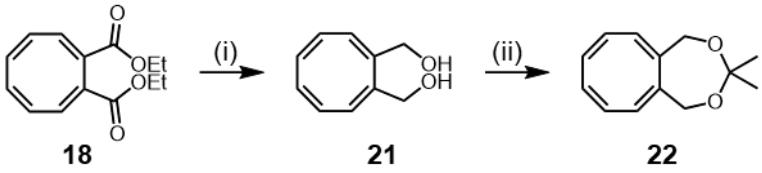

Scheme 9: Functional group interconversion of diethylester COTT. (i) DIBAL, CH_2Cl_2, −78 to 0 °C, 2 h, 71%. (ii) 2,2-DMP, p-toluenesulfonic acid, CH_2Cl_2, rt, 3 h, 59%.

In Buono's original report, the cycloadditions are performed in one of two solvents—trifluoroethanol (TFE) for more polar alkynes and 1,2-dichloroethane (DCE) for less polar alkynes. These reaction solvents also use different temperatures: 55 °C and 40 °C respectively although Fallon *et al.* use 55 °C and rt.[11]

These transformations were performed in order to probe a potential alteration in behaviour of COTTs **18**, **21** and **22** in cycloaddition reactions. Initially this was to change the steric effects of the substituents, however there was another significant effect on the [8]annulene when these substituents are altered.

It can be observed from ^{1}H NMR spectroscopy that the electronics of the ring are predictably altered by the substituents attached (Figure 9). If we directly compare the chemical shifts of the protons on **COTT** to those of each of these substituted COTTs, we see a pattern appear. The diester COTT **18**'s conjugation with the ring shifts the peaks for the ring protons downfield. As such, both the electron density on the ring and its ability to bind to the Co(I) centre is lowered. When the ester is reduced, the diol COTT **21** shows chemical shifts closer to that of **COTT**, however due to the inductive effect of the alcohol groups, there is still a smaller downfield shift. Finally, the acetal protected COTT diol **22** shows shifts much closer to that of unsubstituted **COTT**, and hence is electronically the most similar substituted COTT. It was the hope that this behaviour may translate to binding and reactivity during the cycloaddition.

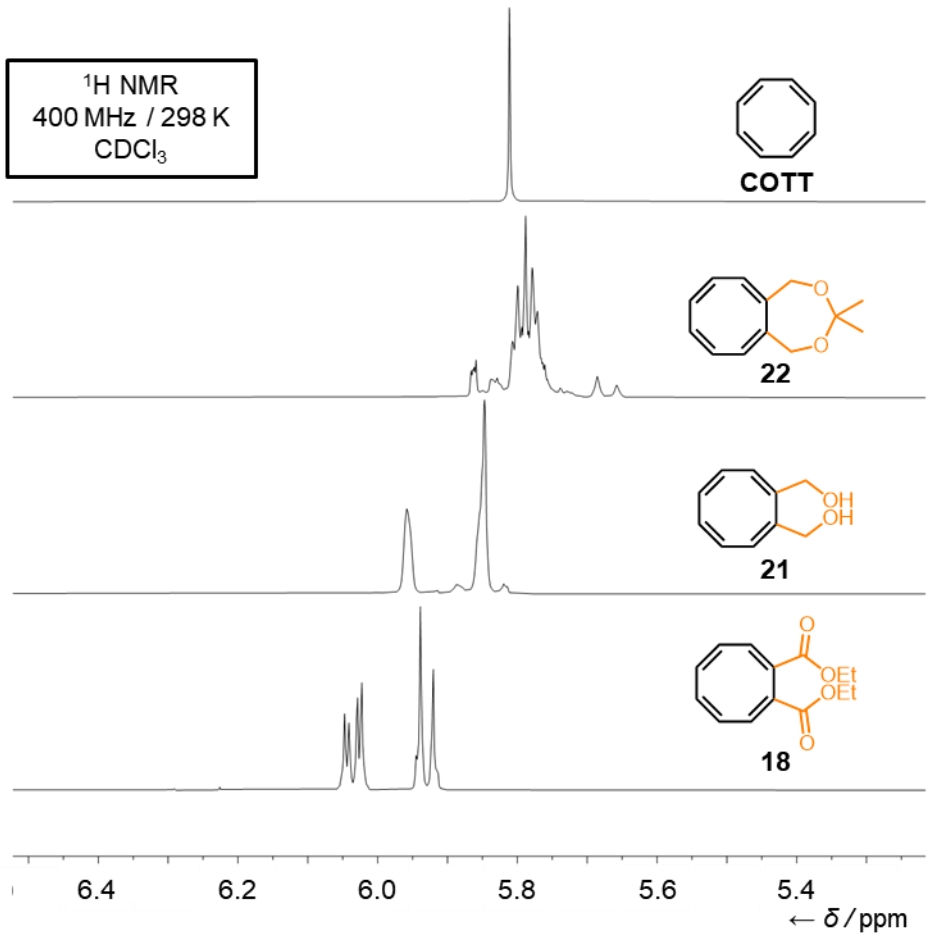

Figure 9: Partial ^{1}H NMR Spectra for COTT and substituted equivalents.

Each of these three molecules has been used in attempted Co(I) catalysed cycloadditions using monosubstituted alkyne **23** for coupling, and none showed any product formation (Scheme 10). Established strategies to increase the yield of metal-catalysed [6+2] cycloadditions, such as slow addition of the alkyne to the reaction mixture[29] or altering the catalyst loading used in the reaction were attempted.[15,30] Also, performing these reactions at a higher temperature is a potential route of exploration for each COTT to overcome steric hindrance in the reaction (Table 2).

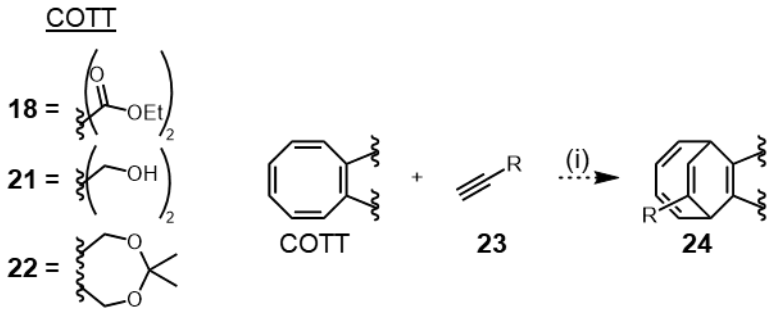

*Scheme 10: Attempted BDT formation with substituted COTTs **18**, **21** and **22** and alkyne **23**. (i) $CoBr_2$(dppe) 10–20%, ZnI_2 20–40%, Zn Dust 30–60%, DCE/TFE, rt to 75 °C no reaction observed.*

*Table 2: Conditions screened for the cycloaddition of substituted COTTs with alkyne **23**.*

COTT	23, R =	Solvent	T / °C	$CoBr_2$(dppe) Loading[a]	Slow Addition
18	TMS	DCE	rt	10%	N
18	TMS	DCE	50	10%	Y
21	CH_2OH	TFE	55	10%	N
21	CH_2OH	TFE	55	10%	Y
21	CH_2OH	TFE	75	10%	Y
21	CH_2OH	TFE	75	20%	Y
22	CH_2OH	TFE	55	10%	Y
22	CH_2OH	TFE	75	10%	Y
22	CH_2OH	TFE	75	20%	Y

[a]$CoBr_2$(dppe), ZnI_2 and Zn Dust were present in a 1:2:3 ratio.

If **23** had undergone a cycloaddition with **18**, **21** or **22**, this would still only lead to a trisubstituted BDT **24**, and correspondingly a trisubstituted BV. It would only be on the occasion that a disubstituted alkyne underwent this reaction that a tetrasubstituted BV may be formed; as such, this is not a viable synthetic route.

In the synthesis of these disubstituted COTTs, it was observed that the ^{1}H NMR spectrum for the acetal protected COTT **22** exhibits unusual properties as a result of the ring flipping action described previously in Figure 6. At first what seemed to be an impurity, instead was determined to be the presence of a conformational isomer of the vicinal diol acetal **22**. Just as with dibromo COTT **3**, the isomers may interconvert between the D_{2d} COTT tub-shaped conformations (**22** and **22′**) via a flat D_{4h} isomer **22a**, and then via excitation to the bond-shifting D_{8h} COTT conformation **22b**. The resulting isomers, **22** and **22′** are not planar (Figure 10).

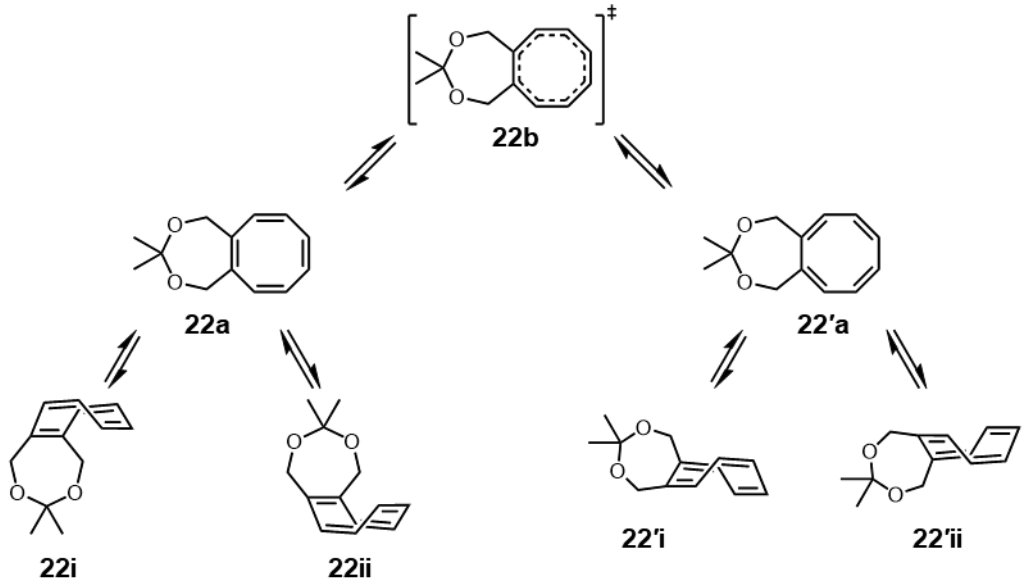

*Figure 10: Conformational change of COTT acetal **22**.*

During the fluttering between **22i** and **22ii**, the acetal methyl groups alternate environments, which results in a single averaged peak in the ^{1}H NMR spectrum at 1.34 ppm. In contrast, the isomers **22′i** and **22′ii** do not have this same property, as one methyl group will always be closer to the central COTT ring whilst the other always points further away, resulting in two individual singlet peaks in the ^{1}H NMR spectrum at 1.41 and 1.44 ppm (Figure 10). The relative integral for these peaks connotes an isomer ratio of 4:1 (**22**:**22′**).

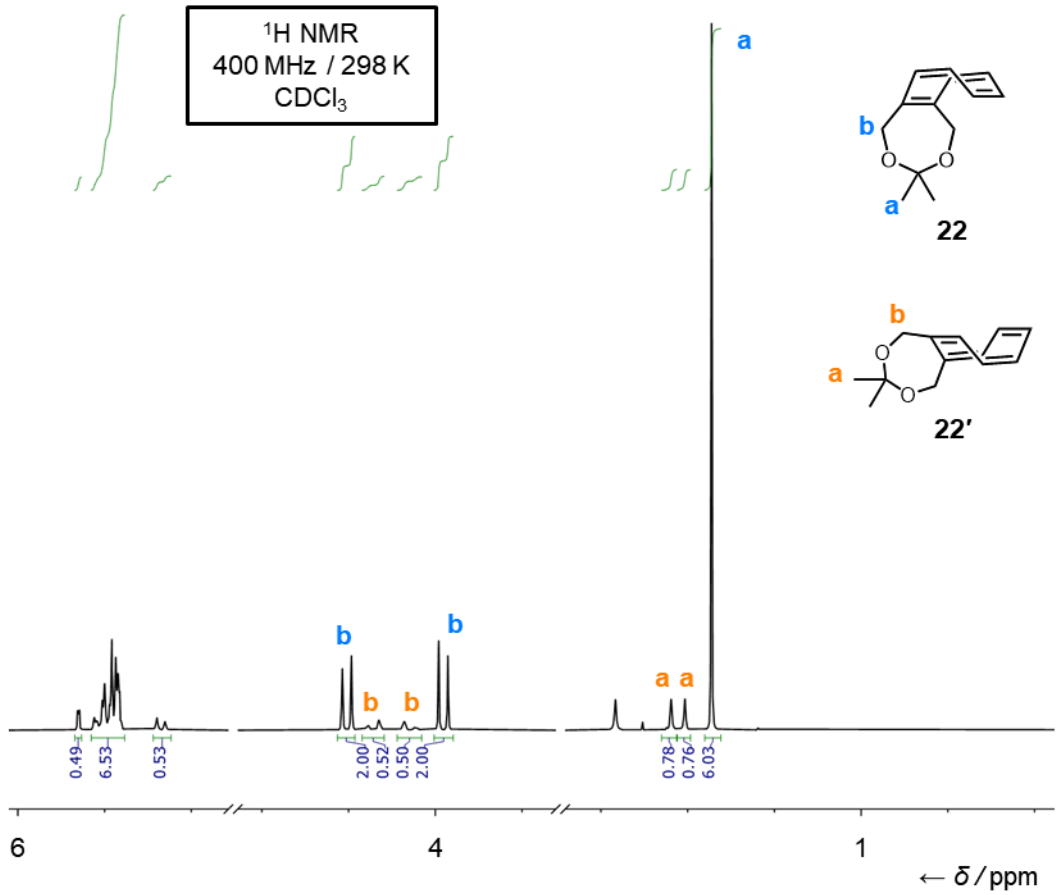

*Figure 11: Partial ¹H NMR Spectrum of **22**, exhibiting peak differences due to fluttering behaviour.*

3.4 Using Substituted COTTs in Older Syntheses

As mentioned in Chapter 1, Fallon's synthetic method is the most efficient, high yielding synthetic procedure for the formation of BVs, however, it was not the first synthetic procedure to use **COTT** as a starting material. In fact, the first ever published synthesis of BV from 1963 proceeded by the thermal dimerization of **COTT**.[31]

Due to the proposed mechanism of this dimerisation, if it were successful between two disubstituted COTTs **25**, the product **26** would still not necessarily go on to form a tetrasubstituted BV, but instead may form a disubstituted BV **27** (Scheme 11).

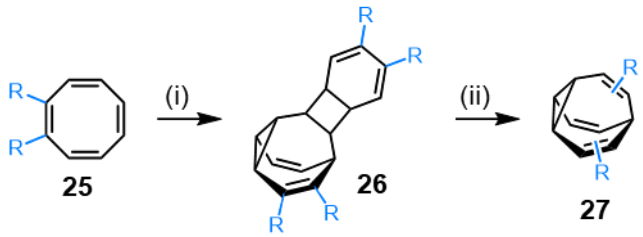

*Scheme 11: Hypothetical synthesis of **BV** with dimerisation of disubstituted COTT.*

Appropriately, this route would require the synthesis of a tetrasubstituted COTT. Through the tetramerization of propargyl alcohol **23** with (DME)$NiBr_2$ as a catalyst, a mixture of tetrasubstituted COTTs formed (Scheme 12).[32] This mixture includes 1,2,5,6-cyclooctatetraene **28** which may be separated from the mixture by acetal protection. As the only tetraol COTT that can be fully acetal protected, the acetal product, **29** may be separated from the mixture by washing the crude reaction precipitate with chloroform.

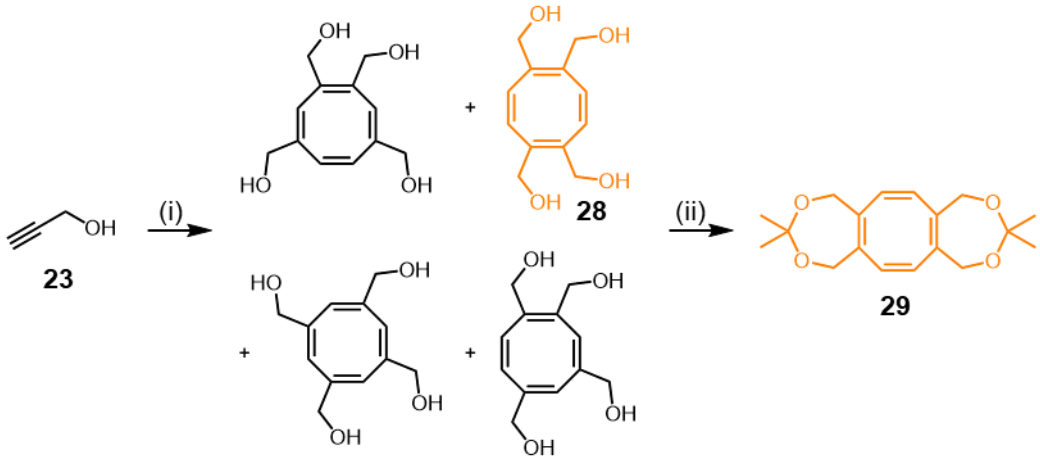

*Scheme 12: Synthesis of tetrol COTT **29** via tetramerisation and acetal protection. (i) (DME)$NiBr_2$, $NaBH_4$, rt, 3 h. (ii) 2,2-DMP, p-toluenesulfonic acid, MeOH, rt, 18 h, 15% over two steps.*

Once **29** has been separated from the mixture of COTT structures, it may be deprotected again to form pure tetrol **28** (Scheme 13).

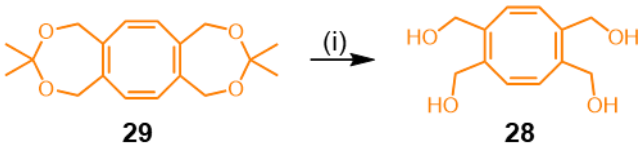

*Scheme 13: Deprotection of **29** to form tetrol COTT **28**. (i) p-toluenesulfonic acid, MeOH: H_2O (1:10), 50 °C, 3 h, 92%.*

Preliminary attempts to dimerise **29** resulted in deprotection of the acetal groups to form **28**, so **28** was made the main focus of this method. First, **28** was heated in a microwave vial to 100 °C, the temperature at which **COTT** dimerised in Schröder *et al.*'s 1963 synthesis, but no reaction was observed, so the temperature was increased incrementally, without change until 180 °C at which a glass-like insoluble black solid was formed. Diphenylether was therefore used as an inert solvent with a high boiling point to prevent degradation of the starting material but no product formation was observed at 180 °C. In the original dimerization, of the final ten carbons which constitute the **BV** cage eight are from one **COTT** molecule, and the other two are from

a second molecule of **COTT**. This means that with our hypothetical method, a tetra- penta- or hexa- substituted BV may form, depending on the orientation of the dimerising molecules. However, as the dimerization did not proceed, an alternative attempt at using substituted COTTs to synthesise a tetrasubstituted BV was explored. The final method attempted was based upon Jones *et al*'s 1967 synthesis in which ethyl diazoacetate is used to form a bicyclic ester **30** which is converted to the tosyl hydrazine **31**, over five steps and then thermally decomposed to BDT **32** (Scheme 14).[12,33] As well as attempting the Jones synthesis with their original $CuSO_4$ catalyst, other conditions, using a rhodium acetate dimer catalyst—such as Buchner ring expansions—were also used.[34]

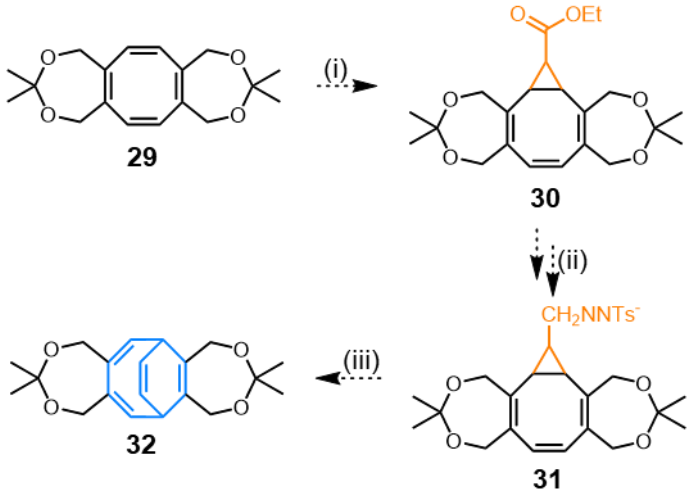

*Scheme 14: Attempted synthesis of tetrasubstituted BV from **29** using Jones et al's 1967 method. (i) $CuSO_4$/ $Rh_2(OAc)_4$, CH_2Cl_2. No product obtained. (ii) Five functional group interconversions. (iii) Thermolysis.*

Both cyclopropanation conditions returned no product on multiple attempts, varying equivalents and increasing temperature. As a result of no product formation in any attempted route, it was determined that the use of substituted COTTs in the pursuit of tetrasubstituted BVs was not viable.

3.5 Tricyclotetraester (TCTE) Method for Bullvalene Synthesis

3.5.1 Benzobullvalene

A Knoevenagel condensation was attempted between 2,3-anthracenedicarboxaldehyde **33** and diethyl 1,3-acetonedicarboxylate **34** to form tropone **35** as part of a different research project by another PhD student. In this reaction a side product had formed from a Weiss–Cook reaction, a reaction similar to the Knoevenagel which features a second nucleophilic attack as opposed to an olefin-

forming dehydration. This side product was isolated during the purification process (Scheme 15).

The side product **36** crystallised and the structure notably had similarities with the structure of **BV**, fused with an anthracene group. A single bond linking the two bridged cyclic structures would result in a bistable fluxional molecule.

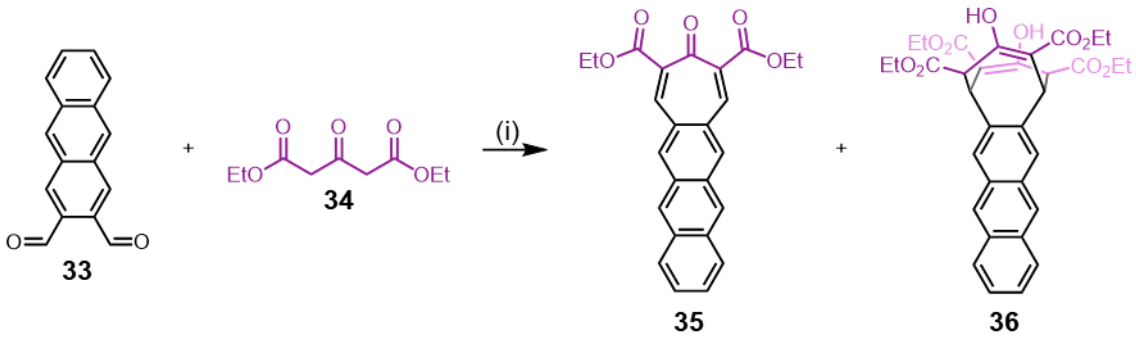

Scheme 15: Attempted tropone synthesis, resulting in side product. (i) AcOH/ piperidine,

As a result, a Weiss–Cook condensation was performed using phthaldialdehyde (**37**), with 1,3-acetonedicarboxylate **34**.[35,36] Compounds **37** and **34** were mixed with diethylamine in ethanol at room temperature and stirred overnight. The reaction was kept at −18 °C for three days to induce precipitation of the desired product **38** (Scheme 16).[37] In this structure, a single bond linking the two bridged cyclic structures would result in a fluxional "benzobullvalene" compound. This benzobullvalene would interconvert between two similar structures *via* a single Cope rearrangement, like barbaralane. Intermediate **38** will herein be referred to as the tricyclotetraester (TCTE) intermediate **38**.

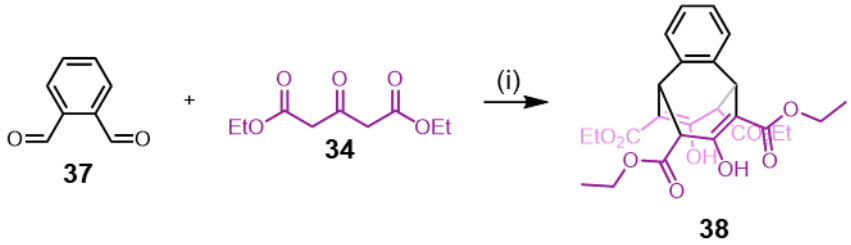

*Scheme 16: Synthesis of the TCTE intermediate **38** (i) $HNEt_2$, EtOH, rt, 16 h, 35%.*

Once TCTE **38** formed, strategies were investigated for the formation of a single cyclopropane group through the linking of the two adjacent bridges. Monobromination of one of the enol groups was attempted to introduce a leaving group which then may be eliminated.

Halogenations were attempted with one equivalent of bromine, NBS and NIS, but this resulted only in a mixture of dihalo-TCTE **39** and starting material **38**. No singly-

halogenated product was isolated at any point. NBS was identified as the most efficient reagent used to synthesise **39** (Scheme 17).

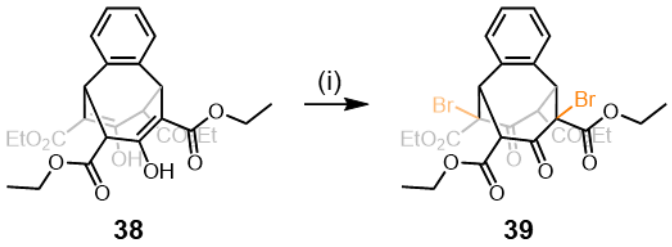

*Scheme 17: Bromination of **38**. (i) NBS, $CHCl_3$, rt, 18 h, 49%.*

In further experiments, triethylamine and sodium hydride were added in order to promote elimination and isolate the benzobullvalene before a second halogenation occurred. Still no desired product was formed, instead, starting material remained alongside a dicyclopropyl (TCTE-Cpr_2) **40**. With **39** in hand, reactions were performed in the presence of different bases, such as triethylamine and sodium hydride, all of which resulted in elimination to **40**. Finally, zinc dust was added to a solution of **39** in THF in an attempt to initiate a radical elimination that would result in a benzobullvalene. However, protodehalogenation occurred instead, resulting in the initial TCTE **38** (Scheme 18).

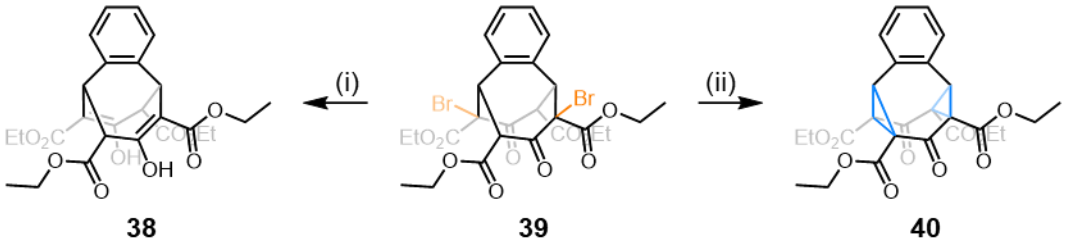

*Scheme 18: Reactions of **39**. (i) Zn dust, THF. (ii) Base, THF.)*

There are two methods in the literature, which approach the conversion of barbaralane-like and semibulvalene-like analogues of this TCTE-CPr_2 **40** to a fluxional molecule.[38,39] As such, we set out to develop efficient conditions for the synthesis of **40** and its subsequent conversion to a benzobullvalene. This involved bromination with NBS in chloroform, followed by filtration of the insoluble succinimide byproduct. The crude bromide mixture was then added to sodium hydride in THF to yield **40** (Scheme 19).

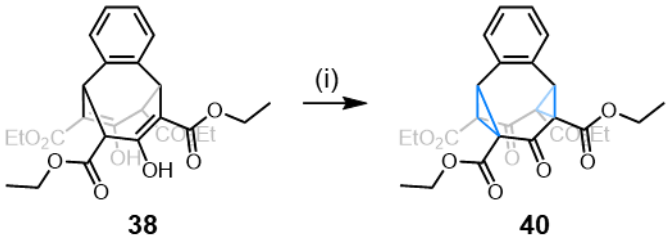

*Scheme 19: Synthesis of **40** from **39**. (i) (a) NBS, $CHCl_3$, rt, 18 h. (b) NaH, THF, 6 h, 75%.*

The first attempts at converting **40** into a benzobullvalene are based on an analogous reaction published by Gompper *et al.* to make a semibullvalene. Using sodium naphthalenide as a single electron reducing agent, **41** is reduced and the intermediate enolate trapped using acetyl chloride to form a bistable fluxional molecule: octasubstituted semibullvalene **42** (Scheme 20).[38]

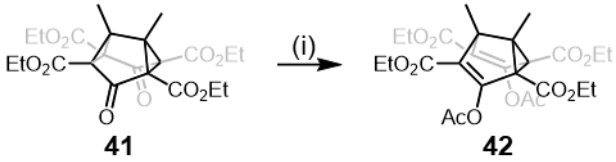

*Scheme 20: Single electron reduction of **33** with sodium naphthalenide to yield semibullvalene **34**. (i) (a) $NaC_{10}H_8$, THF. (b) AcCl, 25%*

Sodium naphthalenide was used first as a single electron reducing agent in attempts to form **43**. Used *in situ*, sodium metal is stirred in THF with naphthalene, which results in a deep green colour. This colour is due to the presence of the radical anion in solution.[38,40] In the first attempts, no conversion was achieved at all, and starting material was recovered, contaminated with naphthalene. A few attempts performed after the initial attempts exhibited new peaks in ^{1}H NMR spectrum of the crude mixtures. Purification by chromatography was attempted on this crude mixture although it was noted that the signals in the aromatic region of the ^{1}H NMR spectra were no longer present, suggesting potential dearomatisation by the single electron reducing agent. Aromatic peaks had disappeared. No single identifiable product was obtained, instead after the attempted purification, each fraction seemed still to consist of a complex mixture of unknown compounds.

Another single electron reducing agent, samarium (II) iodide, also known as Kagan's reagent was used in the same reaction. In this case, the samarium enolate should be the intermediate product, which would then again be trapped by the acetyl chloride to form benzobullvalene **43**. However, the ^{1}H NMR spectra of the crude mixtures following these attempts resembled those of the sodium naphthlenide attempts. A

complicated mixture of dearomatised products was obtained. These results may be due to Gompper *et al.*'s analogue not including an aromatic group, so the phenylene ring in **40** may be intervening in this reaction (Scheme 21).[41,42]

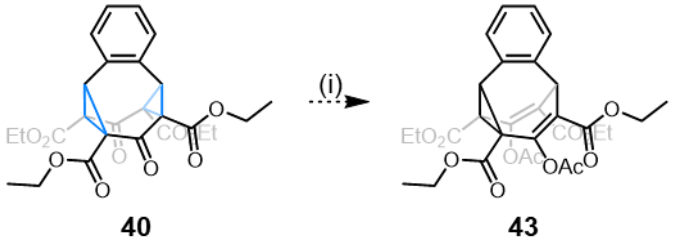

*Scheme 21: Attempted single electron reduction of **40** to form **43**. (i) Single electron reducing agent, THF.*

The second pathway which was attempted to form a bistable fluxional molecule from this route is based upon a 1994 publication by Grohmann *et al.*.[39] In this work, the dicyclopropyl compound **44** was reduced using triisobutyl aluminium (TRIBAL) to selectively form the *exo,exo*-diol **45**. This *cis*-diol was then reduced using diphosphorus tetraiodide (P_2I_4) to yield bistable barbaralane **46** (Scheme 22). P_2I_4 is a deoxygenating agent which has exhibited proficiency in forming iodo compounds or olefinic bonds from a variety of substrates such as alcohols and epoxides. This reaction is owed partially to phosphorus's high affinity for oxygen.[43]

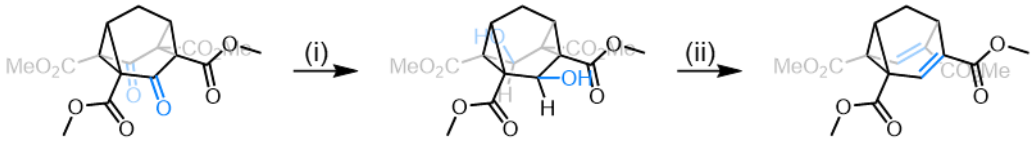

*Scheme 22: Grohmann et al.'s 1966 synthesis of barbaralane **46**. (i) Al(^{i}Bu)$_3$, Toluene, 5 °C, 2.5 h, 79%. (ii) P_2I_4, pyridine, 80 °C, overnight, 36%.*

A solution of TRIBAL in toluene was added to TCTE-CPr$_2$, **40**, in an attempt to selectively form *exo,exo*-diol **47** as in Grohmann's preparation. It was immediately clear that when TRIBAL was used at 0 °C for the reduction, a mixture of products formed, most likely the *exo,exo*-, *exo,endo*- and *endo,endo*- isomers. This was unexpected as Grohmann's reported yield was 79%, a highly efficient and selective reaction. This may be due to the fact that the third bridge on **44** is a methylene unit, as opposed to a significantly bulkier phenylene bridge. Subsequently, the reactions were repeated using TRIBAL at lower temperatures, in the hope of the formation of the kinetic product, *exo,exo*-**47**; however, at −78 °C, the reaction did not proceed at all. When the reaction was then attempted at −50 °C and −30 °C, it only proceeded slowly and revealed the same mixture of isomers as observed at 0 °C.

The considerable difference in the shapes of **44** and **40** clearly has ramifications for its reactivity. As a result, other reducing agents, DIBAL, $NaCNBH_3$ and $NaBH_4$ were also used with **44**, in order to explore the reactivity of each species and their outcomes. It was discovered that while DIBAL showed similar results to TRIBAL and $NaCNBH_3$ exhibited very little reaction at all, the reaction with $NaBH_4$ appeared clearly to produce two main constituent species (Scheme 23).

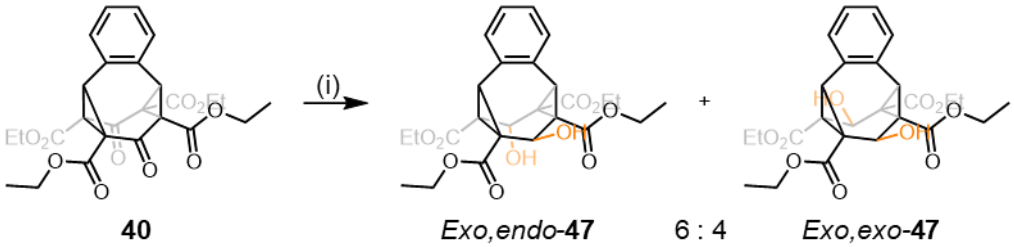

*Scheme 23:Reduction of **40** to form two diastereomers of **47**. (i) $NaBH_4$, EtOH, rt, 20 h, 45%.*

*Table 3: Outcome of attempted reductions on **40**.*

Reducing Agent	T / °C	t / h	Conversion[a]	Outcome
TRIBAL	0	2.5	95	Undecipherable Mixture A
TRIBAL	−78	6	<5	Little to no reaction
TRIBAL	−30	6	90	Undecipherable Mixture A
DIBAL	0	18	100	Undecipherable Mixture B
$NaCNBH_3$	rt	4	0	No reaction
$NaBH_4$	rt	4	100	Mixture of two isomers.

[a] Determined by ratio of starting material to crude mixture.

There are three isomers which may form as a result of this reduction. These are the *exo,endo-*, *exo,exo-* and *endo,endo*-isomers. It was determined by the NOESY NMR correlation of the protons geminal to the alcohols (a and b) that in this reaction, *exo,endo*-**47** and *exo,exo*-**47** were the two isomers which formed. Only *exo*-protons should exhibit a NOESY correlation to the phenylene protons in any of the three isomers. The COSY NMR spectrum demonstrates only two constituent species in the crude mixture, and of these mixtures, only a single species indicates this kind of NOESY coupling. The minor isomer present does not show any correlation to phenylene rings and so is determined to be *exo,exo*-**47**, this isomer comprises 40% of the crude mixture. Also, for the major isomer, which makes up 60% of the mixture only has this NOESY correlation to one of the geminal peaks, and thus is decidedly *exo,endo*-**47**.

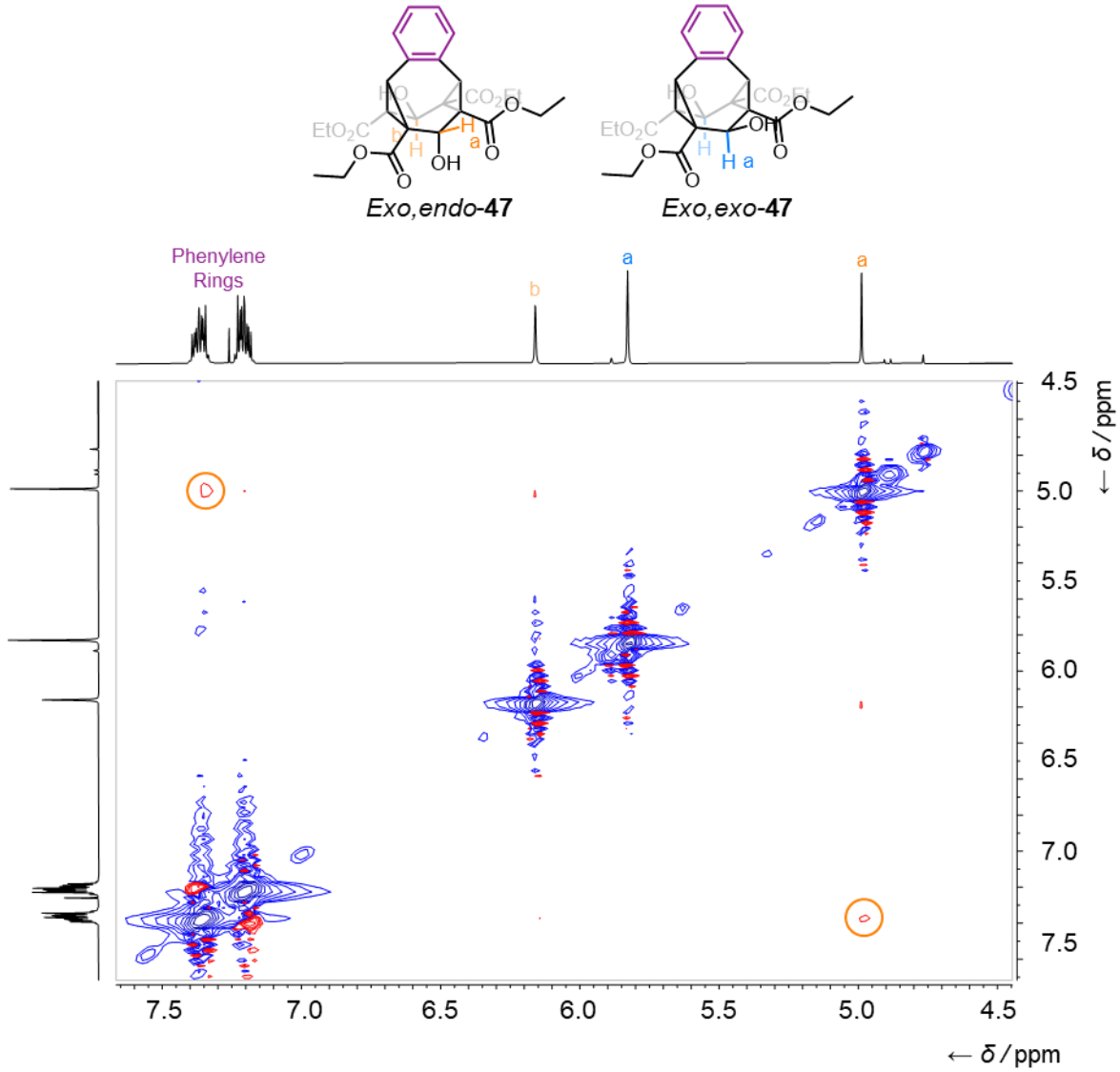

*Figure 12: NOESY Spectrum for crude mixture of exo,endo-**47** and exo,exo-**47**.*

Once the presence of *exo, exo*-**47** had been established, the final step of the procedure could be undertaken. The literature conditions use pyridine however the use of lutidine resulted in a significantly higher yield. For this reaction, two experiments were carried out on the 30:70 *exo, exo*; *exo, endo* **47** crude mixture resulting in yields of 11% and 22% using pyridine and lutidine respectively (Scheme 24).[39,44]

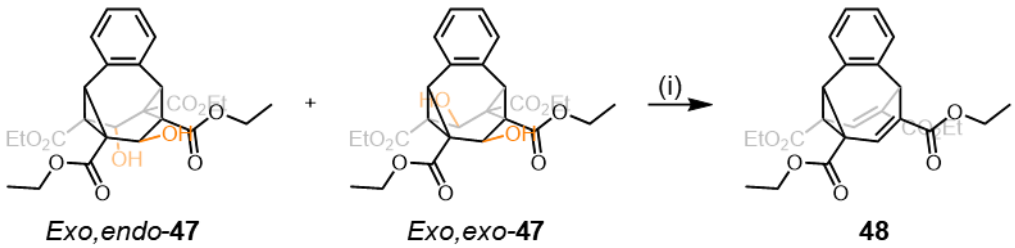

*Scheme 24: Synthesis of benzobullvalene **48**. (i) 2,6-lutidine, P_2I_4, 80 °C, 22%.*

Compound **48** is a benzobullvalene, a bistable fluxional molecule which may undergo a Cope rearrangement on one face to interconvert between two identical isomers. The synthesis of **48** is a significant step towards eventually synthesising a tetrasubstituted BV. This route is short, four step synthesis, and although some of the steps are low yielding they are as of yet unoptimised. Due to the fact that this is a bistable fluxional isomer, there is no way that it may undergo the sequential Cope rearrangements necessary for dynamic tangling/untangling of a polymer network.

Compound **48** may still be of some use if the rearrangement equilibrium may be biased towards one of the isomers. In order to bias this equilibrium, an element of asymmetry should be introduced, such that the two isomers become inequivalent. A substituent present on any one of the positions of the phenylene ring would work as a possibility to desymmetrise **48**. Alternatively, if one of the ester groups could be selectively cleaved, this would also work to bias the equilibrium.

The double bond at the top bridge of **48** will not partake in Cope rearrangements such as to maintain the aromaticity of the aryl ring. Selectively cleaving the phenylene ring on **48** would not be a viable synthetic option, as such, another potential route is required to replace the phthaldialdehyde **37** used in the first step of this synthesis (Scheme 16). Replacing **37** with a different dialdehyde species that may be more easily cleaved or altered would allow for the installation of a third olefinic bridge and thus, a tetraester BV. This compound would be capable of undergoing Cope rearrangements on all three faces. The development of this route remains a great progression towards the eventual synthesis of a tetrasubstituted BV.

3.5.2 Alternative Starting Materials

Work started to determine what kind of functional group could possibly replace the phenylene ring in **48**. An olefin group either substituted or unsubstituted, or alternatively some other functional group which may be converted into an alkene is required for the synthesis of a BV. Substitution at the alkene positions is not necessary, because the four ester groups present the possibility for functionalisation and polymerisation. Furthermore, installation of more substituents may even be detrimental to the BV's rearrangement, resulting in rate decelerations, as observed with penta- and hexa-substituted BVs in 1993.[45,46]

Thus far, several alternatives have been attempted to yield a tetrasubstituted BV, the first uses 2,5-dimethoxy-2,5-dihydrofuran **49** in the condensation step, which would install an alkene in the TCTE intermediate. This has been used as a substitute for the unstable maleic dialdehyde in different reactions.[47] However, ^{1}H NMR spectroscopy only identified the trace presence of what was potentially the tropone species **50**, a result of the Knoevenagel condensation but not of the equivalent TCTE species (Scheme 25).[48] The reaction temperature was increased significantly, from 60 °C to 120 °C in a microwave reactor in an attempt to force a Weiss–Cook condensation, but still no product was obtained. Different conditions, including those used to synthesise the previous anthracenyl and benzyl TCTE (**36** and **38**, Scheme 15 and Scheme 16), were also trialled but to no avail.

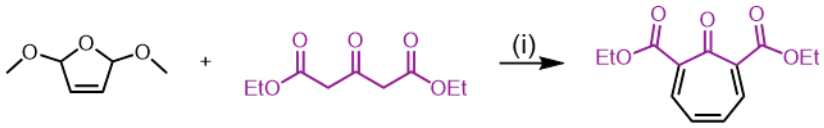

49 **34** **50**

*Scheme 25: Attempted condensation attempts with dihydrofuran **49**. (i) MeOH, NH_4Cl, 60 °C. 8 h, trace product observed.*

Whilst **49** would be the most straightforward starting material, as the olefin bridge is already installed, this also gives rise to potential competitive, unwanted 1,6-addition as well as the desired 1,4-addition which will likely give rise to a mixture of products. Furthermore, the presence of the extra olefinic position in **50** may result in complications during the bromination step. Therefore, we sought to identify alternative substrates that would be used in place of **49** and would allow the formation of an olefin group in the later stages of the synthesis. Related compounds were synthesised from **49** which may be hydrolysed to form dialdehyde products (Scheme 26). Oxidation of **49** with potassium permanganate results in the formation of tetrahydrofuran **51**, which may subsequently be silyl protected to form **52**.[49]

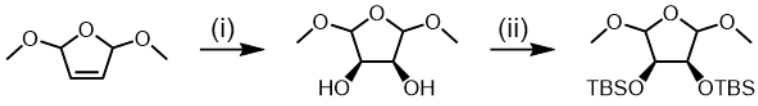

49 **51** **52**

*Scheme 26: Synthesis of tetrahydrofurans **51** and **52**. (i) MnO_4, $MgSO_4.7H_2O$, H_2O, EtOH, 0 °C, 4 h, 50%. (ii) Imidazole, TBDMSCl, DMF, 0 °C, 1 h, 30%.*

Both **51** and **52** were subjected to hydrolysis in order to obtain their dialdehyde analogues **53** and **54** respectively (Figure 13). This was attempted according to previous procedures under acidic conditions.[49]

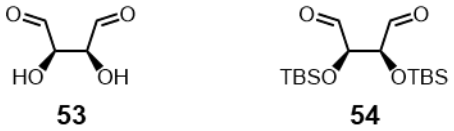

53 **54**

*Figure 13: Structure of dialdehyde analogues **53** and **54**.*

Upon stirring in 0.2 M sulfuric acid, neither substrate **53** nor **54** were present according to ^{1}H NMR spectroscopy. It was considered possible that any product that might have formed may be cyclising back to starting material due to instability of the aldehdye. As a result, immediately following hydrolysis in sulfuric acid, crude mixtures were combined with **34** under a variety of basic conditions, according to the literature. These included combination with diethylamine in ethanol, using a pH 8.0 aqueous phosphate buffer, a pH 9.0 aqueous borate buffer and sodium hydroxide solutions in methanol.[50,51] None of these attempts produced any desired product, as a result, one last attempt was undertaken in order to prove the formation of the aldehyde **54**. **52** was stirred in 6 M hydrochloric acid at 80 °C for four hours. Still no aldehyde product was observed by ^{1}H NMR spectroscopy or mass spectrometry, so other routes were considered.

The hypothesis for this route was to eventually deprotect the hydroxyl groups to form bistable fluxional molecule **55** which may then undergo a Corey–Winters to form the desired BV **56** (Scheme 27). Alternatively, there is potential for the P_2I_4 step to form an olefinic bridge and the fluxional compound simultaneously by reacting with all four hydroxyl groups in **57**.[39]

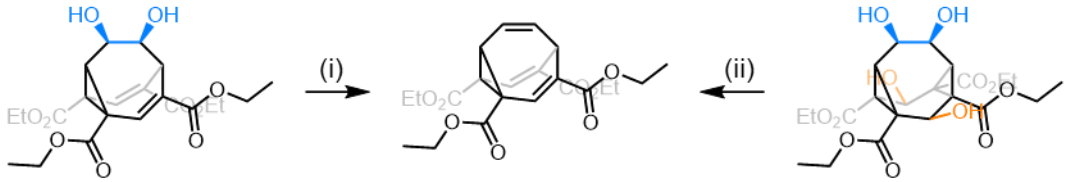

55 **56** **57**

*Scheme 27: Proposed synthesis of tetrasubstituted BV **56**. (i) Corey-Winters olefination. (ii) P_2I_4 reduction.*

Another related route proceeds *via* ribose **58** and the corresponding acetal protected **59**. According to Garcia Martinez *et al.*, treatment of **59** with sodium periodate in water results in the formation of unstable dialdehyde **60**, which may react before degradation (Scheme 28). The aim for this route would be to form an acetal protected alternative to **55** or **57** which may be deprotected and go on to form **56**.[52]

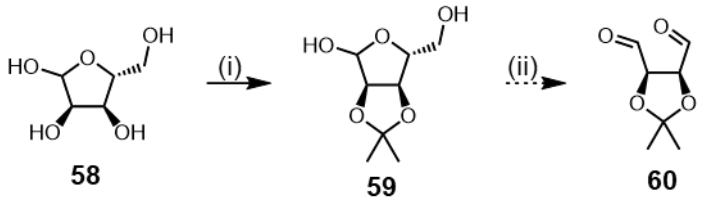

*Scheme 28: Synthesis of potential TCTE intermediate **60**. (i) conc. H_2SO_4, acetone, rt, 4 h, 81%. (ii) $NaIO_4$, H_2O, rt, 20 h.*

Similarly to substrates **53** and **54**, no reaction was observed when combined with **34** in various conditions. Moreover, no evidence of dialdehyde **60** formation was observed at all by ^{1}H NMR spectroscopy or mass spectrometry.

Another alternative attempted was the oxidation of 1,4-butanediol **61** to form 1,4-butandial **62**. This was attempted using a Swern oxidation, which proceeded well. Evidence of the dialdehyde was observed in the ^{1}H NMR spectra of crude mixtures. However, due to the instability of this compound, it had to be used *in situ*. The result of the attempted Weiss–Cook condensation was unfortunately a complex mess when monitored by ^{1}H NMR spectroscopy; possibly arising as a result of self-condensation of the enolisable dialdehyde under the reaction conditions. Mass spectrometry did provide evidence of some product **63** formation but none was isolated (Scheme 29).

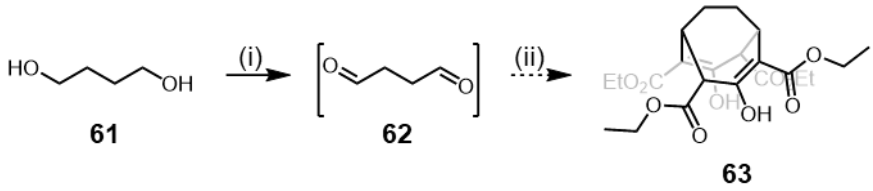

*Scheme 29: Attempted synthesis of **63**. (i) $(COCl)_2$, DMSO, NEt_3, −78 °C. (ii) $HNEt_2$, EtOH, rt, 18 h.*

3.5.3 Ongoing Work in the Group

Since these attempts, more work on a few different synthetic routes incorporating different ideas is ongoing, hopefully finally to yield a tetrasubstituted BV (Figure 14). There are three new synthetic methods which will be briefly discussed, and are still ongoing. The first involves an epoxide aldehyde **64**. P_2I_4 will reduce epoxides to

alkenes, and so this method may potentially be used in concert with the reduction of the *exo,exo*-diol to yield BV **56**.[53,54]

Secondly, using a phenanthrene dialdehyde such as **65** to synthesise a fluxional molecule will result in a molecule that does not have the same constraints as benzo bullvalene **48**. This is because in the phenanthrene motif, the central ring present does not have the same strong aromatic character as the external rings.[55] Exploratory computational results have suggested therefore that the bond will partake in Cope rearrangements. Hence, although geometric constraints may limit the two BV carbons involved to be vicinal to one another, the result would be a fluxional molecule with more than two possible states.

Finally, the use of aldehyde **66** would possibly introduce a photocleavable group to the intermediate molecules which may be selectively removed at any point during the synthesis through removal of the silyl protecting group and irradiation with ultraviolet light to form an olefinic bond and anthracene as a by-product *via* a retro Diels–Alder reaction.

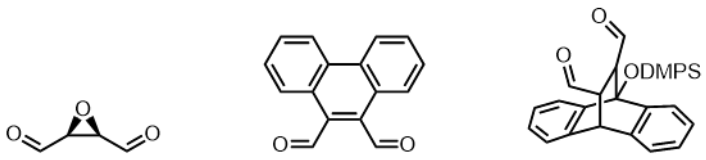

64 **65** **66**

Figure 14: New proposed synthetic strategies for tetrasubstituted BVs.

3.6 Conclusions and Future Work

The synthesis of homotetrasubstituted BVs *via* a simple, short synthetic procedure remains a difficult endeavour. The use of substituted COTTs in previously reported routes has failed to yield any target BV; as steric hindrance imposed by the appendant groups seems insurmountable. Instead, the pursuit of new strategies may be necessary to achieve this goal.

A five-step route initiated by a Weiss–Cook condensation, and subsequent modification by bromination, elimination and two reductions has yielded the fluxional benzobullvalene **48**. This route has been identified as a possible means to yield a homotetrasubstituted BV. Synthesis of the target would require substitution of phthaldialdehyde starting material **37** with another aldehyde which may subsequently be exchanged for a third olefinic bridge. Multiple dialdehydes (**49**, **53**, **54**, **60** and **62**) have been trialled to no avail, however, new routes using dialdehydes **64**–**66** have

proved promising in preliminary experiments. We are currently studying their ability to undergo Weiss–Cook condensations, however their enhanced stability relative to those previously attempted aldehydes is encouraging.

Experimental

Bromocyclooctatetraene (1)

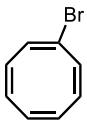

Cyclooctatetraene (3.0 g, 29.0 mmol) and anhydrous CH_2Cl_2 (25 mL) were added to an oven-dried round-bottomed flask under an inert atmosphere. The mixture was cooled to −78 °C and a solution of bromine (4.6 g, 29.0 mmol) in anhydrous CH_2Cl_2 (18 mL) was added dropwise over 1 h. The reaction mixture was stirred at −78 °C for a further 1 h. To the reaction mixture, a solution of KO^{t}Bu (3.90 g, 34.8 mmol) in anhydrous THF (18 mL) was added dropwise over 1 h and the reaction mixture stirred at −78 °C for a further 2 h. The reaction was quenched with a saturated aqueous solution of NH_4Cl (20 mL), and the mixture was extracted with CH_2Cl_2 (25 mL). The organic fraction was washed with H_2O (50 mL) then brine (50 mL), and dried over $MgSO_4$. The solvent was evaporated under reduced pressure to yield the title compound as a brown oil (4.3 g, 23.5 mmol, 81%). **^{1}H NMR** (599 MHz, $CDCl_3$) δ 6.22 (s, 1H), 5.97–5.74 (m, 5H), 5.68–5.60 (m, 1H). **^{13}C NMR** (151 MHz, $CDCl_3$) δ 133.4 (CH), 133.3 (CH), 132.9 (CH), 132.5 (CH), 132.2 (CH), 131.0 (CH), 131.0 (CH), 121.5 (C). **HR-ASAP-MS** *m/z*: $[M+H]^+$ 182.9785 (calculated $C_8H_8Br^+$ = 182.9809). Analysis is in agreement with literature reports.[15]

9-Thiabicyclo[4.2.1]nona-2,4,7-triene 9,9-dioxide (4)

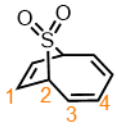

Conc. sulfuric acid was added dropwise to solid Na_2SO_3, leading to the generation of gaseous SO_2, which was passed over NaOH pellets and condensed using a cold finger at −70 °C to form liquid SO_2 (1.5 mL). To the liquid SO_2, cyclooctatetraene (210 mg, 2.00 mmol) and antimony pentafluoride (436 mg, 2.00 mmol) were added, and the reaction mixture was stirred at −70 °C for 18 h. The reaction mixture was warmed to rt, the SO_2 was allowed to evaporate and the remaining solid was diluted with H_2O (10 mL). The aqueous layer was extracted with CH_2Cl_2 (2 × 10 mL). The combined organic fractions were dried over $MgSO_4$, and the solvent was removed under reduced pressure. The remaining black solid was suspended in diethyl ether (100 mL), stirred for 15 min and filtered. The solvent was removed under reduced pressure, and the crude residue was purified by column chromatography (Teledyne Isco CombiFlash Rf+ system, 12 g SiO_2, hexanes–EtOAc, gradient elution) to yield the title compound as an off-white solid (60 mg, 0.36 mmol, 18%). **M.P.** 190–192 °C. **^{1}H NMR** (700 MHz, $CDCl_3$) δ 6.09 (2H, dd, *J* = 9.0, 3.3

Hz, H_4), 6.01 (2H, dd, J = 2.5, 1.3 Hz, H_1), 5.89 (2H, ddd, *J* = 9.0, 8.1, 3.3 Hz, H_3), 3.90 (2H, ddd, *J* = 8.0, 2.5, 1.3 Hz, H_2). **^{13}C NMR** (176 MHz, $CDCl_3$) δ 128.4 (C_4), 126.7 (C_3), 123.1 (C_1), 61.9 (C_2). **HR-ASAP-MS**: $[M+H]^+$ = 169.0304 (calculated $C_8H_9SO_2^+$ = 169.0320).

1,4-Bis(trimethylsilyl)cycloocta-2,5,7-triene (8)

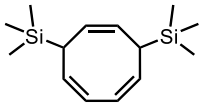

^{n}BuLi (2.5 M in hexane, 9.7 mL, 24.0 mmol, 3.0 eq.) was added to a solution of cycloocta-1,5-diene (0.99 mL, 8.0 mmol, 1.0 eq.) in anhydrous pentane (8 mL) at 0 °C in an oven-dried round-bottomed flask under an inert atmosphere. To this mixture, TMEDA (3.64 mL, 24.0 mmol, 3.0 eq.) was added and the reaction was stirred at rt for 16 h, then at reflux for 24 h. The mixture was cooled to −30 °C and chlorotrimethylsilane (2.05 mL, 16.0 mmol, 2.0 eq.) was added dropwise. The mixture was stirred at room temperature for 18 h, then hydrolysed by pouring onto ice water (10 mL). The organic layer separated, washed with water (6 × 10 mL) and dried over $MgSO_4$. The solvent was removed under reduced pressure, leaving a residue. Methanol was added, and the mixture was cooled to −20 °C for 18 h. The resulting precipitate was filtered and dried under reduced pressure to yield the title compound as a yellow solid (60 mg, 0.24 mmol, 3%). **^{1}H NMR** (400 MHz, $CDCl_3$) δ 5.84–5.76 (m, 2H, ring CH), 5.59–5.44 (m, 4H, ring CH), 2.86–2.74 (m, 2H, ring CH), 0.02 (s, 18H, $SiMe_3$). Spectroscopic data is in agreement with literature reports.[23] No further analysis was undertaken due to small quantities and instability.[24]

2-Butyn-1,4-diol diacetate (15)

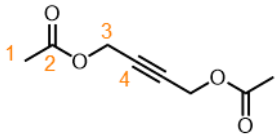

A solution of acetyl chloride (4.01 g, 50.6 mmol) in anhydrous CH_2Cl_2 (10 mL) was added dropwise to a stirring solution of 2-butyne-1,4-diol (2.00 g, 23.0 mmol) in anhydrous CH_2Cl_2 (20 mL) in an oven-dried round-bottomed under an inert atmosphere. The reaction mixture was stirred at rt for 18 h and then at reflux for 4 h. After cooling to rt, the mixture was washed with an aqueous solution of $NaHCO_3$ (10% w/w, 25 mL) and dried over $MgSO_4$. The solvent was removed under reduced pressure, leaving a ___ residue, which was purified by column chromatography (Teledyne Isco CombiFlash Rf+ system, 12 g SiO_2, hexanes–EtOAc, 0–50%, gradient elution) to yield the title compound as a colourless oil (3.48 g, 20.3 mmol, 88%). **^{1}H NMR** (400 MHz, $CDCl_3$) δ 4.72–4.68 (m, 6H, H_1), 2.11–2.08 (m, 4H, H_2). **^{13}C NMR**

(100 MHz, $CDCl_3$) δ 170.4 (C_2), 80.8 (C_4), 52.2 (C_1), 20.8 (C_3). **HR-ASAP-MS** *m/z*: $[M+H]^+$ = 171.0646 (calculated $C_8H_{11}O_4^+$ = 171.0657). Spectroscopic data are in agreement with literature reports.[56]

Diethyl cycloocta-1,3,5,7-tetraene-1,2-dicarboxylate (18)

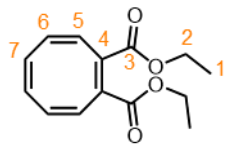

A solution of diethyl but-2-ynedioate (4.47 g, 26.0 mmol) in benzene (100 mL), was stirred under UV irradiation (254 nm, 8 × 9 W light bulbs) for 5 days, removing the reaction and cleaning the vessel with a solution of NaOH in MeOH nce a day to prevent the build-up of a polymer coating. The solvent was removed under reduced pressure and the crude residue purified by column chromatography (Teledyne Isco CombiFlash Rf+ system, 80 g SiO_2, EtOAc–hexanes, 0–30%) to yield the title compound as a yellow oil (2.29 g, 9.2 mmol, 36%). **^{1}H NMR** (599 MHz, $CDCl_3$) *δ* 7.17 (d, *J* = 3.6 Hz, 2H, H_5), 6.06–6.01 (m, 2H, H_6), 5.95–5.91 (m, 2H, H_7), 4.26–4.09 (m, 4H, H_2), 1.25 (t, *J* = 7.1 Hz, 6H, H_1); **^{13}C NMR** (151 MHz, $CDCl_3$) *δ* 165.7 (C_3), 142.8 (C_5), 132.7 (C_7), 132.6 (C_4), 130.3 (C_6), 61.1 (C_2), 14.3 (C_1); **HR-ASAP-MS** *m/z*: $[M+H]^+$ = 249.1109 (calculated $C_{14}H_{17}O_4^+$ = 249.1127).

1,2-Bis(hydroxymethyl)cyclooctatetraene (21)

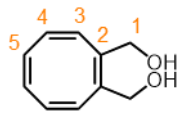

DIBAL-H (1.0 M in toluene, 28.6 mL, 28.6 mmol) was added dropwise over 1 h to a solution of **18** (1.42 g, 5.72 mmol) in anhydrous CH_2Cl_2 (16 mL) at −78 °C in an oven-dried round-bottomed flask under an inert atmosphere. The reaction mixture was allowed to warm to rt and stirred for 2 h. The reaction was cooled to −20 °C and quenched with methanol (5 mL), then H_2O (10 mL). The reaction mixture was then poured into a saturated solution of Rochelle's salt (15 mL), and the suspension was stirred vigorously for 2 h. The organic layer was separated, and the aqueous layer extracted with ethyl acetate (3 × 20 mL). The combined organic fractions were dried over $MgSO_4$, and the solvents removed under reduced pressure. The resulting crude residue was purified by column chromatography (Teledyne Isco CombiFlash Rf+ system, 24 g SiO_2, EtOAc–hexanes, 0–30%) to yield the title compound as a yellow oil (0.66 g, 4.02 mmol, 70%). **^{1}H NMR** (599 MHz, $CDCl_3$) δ 5.98–5.94 (m, 2H, H_3), 5.89–5.81 (m, 4H, $H_{4/5}$), 4.26 (dt, *J* = 12.5, 1.3 Hz, 2H, H_{1a}), 4.14 (d, *J* = 12.6 Hz, 2H, H_{1b}). **^{13}C NMR** (151 MHz, $CDCl_3$) δ 143.6 (C_2),

131.5 ($C_{4/5}$), 131.1 ($C_{4/5}$), 130.6 (C_3), 65.9 (C_1). **HR-ASAP-MS** *m/z*: $[M+H]^+$ = 147.0806 (calculated $C_{10}H_{11}O^+$ = 147.0810).

3,3-Dimethyl-1,5-dihydrocycloocta[e][1,3]dioxepine (22)

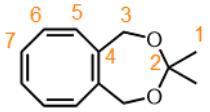

21 (666 mg, 4.02 mmol) and *p*-toluenesulfonic acid monohydrate (77 mg, 0.40 mmol) were dissolved in CH_2Cl_2 (4.0 mL). To this stirred mixture, 2,2,-dimethoxypropane (2.5 mL, 20.0 mmol) was added, and the reaction mixture stirred for 18 h at rt. The reaction was quenched with a saturated aqueous solution of $NaHCO_3$ (10 mL) and extracted with CH_2Cl_2 (2 × 10 mL). The combined organic fractions were washed with brine (10 mL), dried over $MgSO_4$ and the solvent removed under reduced pressure. The resulting crude residue was purified by column chromatography (Teledyne Isco CombiFlash Rf+ system, 12 g SiO_2, hexanes–EtOAc, 0–20%, gradient elution) to yield the title compound as a yellow solid (480 mg, 2.35 mmol, 59%). **^{1}H NMR** (599 MHz, $CDCl_3$) δ 5.86 (dd, *J* = 1.9, 1.0 Hz, 0.5H, $H_{5'/6'/7'}$), 5.83–5.76 (m, 6.5H, $H_{5/6/7/5'/6'/7'}$), 5.67 (d, *J* = 11.1 Hz, 0.5H, $H_{5'/6'/7'}$), 4.21 (d, *J* = 12.7 Hz, 2H, H_3), 4.17–4.12 (m, 0.5H, $H_{3'}$), 4.06 (d, *J* = 15.7 Hz, 0.5H, $H_{3'}$), 3.98 (d, *J* = 12.7 Hz, 2H, H_3), 1.44 (s, 0.75H, $H_{1'}$), 1.41 (s, 1H, $H_{1'}$), 1.35 (s, 6H, H_1). **^{13}C NMR** (151 MHz, $CDCl_3$) δ 142.4 (C_4), 136.8 ($C_{4'}$), 132.5 ($C_{5'/6'/7'}$), 132.1 ($C_{5'/6'/7'}$), 131.6 ($C_{5/6/7}$), 131.6 ($C_{5/6/7}$), 131.1 ($C_{5'/6'/7'}$), 129.8 ($C_{5/6/7}$), 102.0 (C_2), 67.3 (C_3), 64.3 ($C_{3'}$), 24.6 (C_1), 24.3 ($C_{1'}$), 23.5 ($C_{1'}$). **HR-ASAP-MS** *m/z*: $[M+H]^+$ = 205.1213 (calculated $C_{13}H_{17}O_2^+$ = 205.1229)

3,3,10,10-tetramethyl-1,5,8,12-tetrahydrocycloocta[1,2-*e*:5,6-*e'*]bis([1,3]dioxepine) (29)

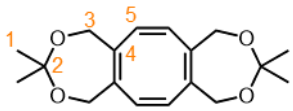

A solution of (DME)$NiBr_2$ (10 mg, 0.03 mmol) in propargyl alcohol (30 g, 534 mmol) was added to an oven-dried round-bottomed flask under an inert atmosphere. $NaBH_4$ (6 mg, 0.15 mmol) was added in several portions over 10 min. Upon cooling to rt, the mixture was stirred for 3 h, and then diluted with methanol (20 mL). 2,2-Dimethoxypropane (30 g, 288 mmol) and *p*-toluenesulfonic acid (0.1 g, 0.6 mmol) were added and the mixture stirred for 18 h. The mixture was cooled to 0 °C and the resulting precipitate was collected by vacuum filtration. The precipitate was suspended in $CHCl_3$ (30 mL) and filtered. The filtrate was collected and the solvent removed under reduced pressure to yield the title compound as a colourless solid (1.8 g, 5.9 mmol, 15%).**^{1}H NMR** (400 MHz, $CDCl_3$) δ 5.80 (s, 4H),

4.21 (d, *J* = 12.6 Hz, 4H), 3.96 (d, *J* = 12.7 Hz, 4H), 1.36 (s, 12H). **HR-ASAP-MS** *m/z*: $[M+H]^+$ = 305.1744 (calculated $C_{18}H_{25}O_4^+$ = 305.1753). Analysis is in agreement with literature reports.[32]

Cycloocta-1,3,5,7-tetraene-1,2,5,6-tetrayl tetramethanol (28)

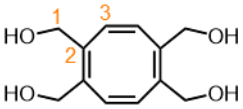

A solution of *p*-toluenesulfonic acid (0.1 g, 0.53 mmol) in methanol–H_2O (1:10, 55 mL) was made. An aliquot of this solution (10 mL) was mixed with **29** (1.0 g, 3.3 mmol), and the suspension was stirred at 50 °C for 3 h. The solution was cooled to rt, filtered, and the solvent was removed under reduced pressure. The resulting crude residue was washed with acetone (20 mL) and recrystallised from methanol to yield the title compound as colourless crystals (680 mg, 3.0 mmol, 92 %). **^{1}H NMR** (400 MHz, CD_3OD) δ 5.97 (s, 4H), 4.16 (d, *J* = 13.3 Hz, 4H), 4.08 (d, *J* = 13.3 Hz, 4H). **HR-ASAP-MS** *m/z*: $[M+Na]^+$ 247.0946 (calculated $C_{12}H_{16}O_4Na^+$ = 247.0946). Analysis is in agreement with literature values.[32]

TCTE Intermediate (38)

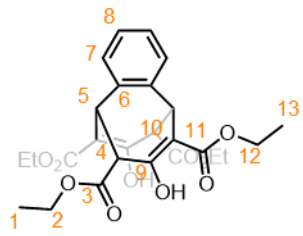

Phthaldialdehyde **37** (1.34 g, 9.9 mmol) and diethyl 1,3-acetonedicarboxylate **34** (4.04 g, 19.8 mmol) were dissolved in ethanol (20 mL). To this mixture, diethylamine (0.05 mL, 0.50 mmol) was added, and the reaction mixture stirred at rt for 18 h. Following this, the reaction mixture was cooled to −20 °C for 72 h. The solvent was decanted, and the colourless solid was washed with cold ethanol, then dried under reduced pressure to yield the title compound as a colourless solid (3.36 g, 6.7 mmol, 68%). **M.P.** 137–139 °C. **^{1}H NMR** (599 MHz, $CDCl_3$) δ 13.28 (s, 2H, OH), 7.16–7.10 (m, 2H, H_8), 7.09–7.03 (m, 2H, H_7), 4.61 (d, *J* = 4.5 Hz, 2H, H_5), 4.43–4.32 (m, 4H, H_{12}), 3.95–3.87 (m, 2H, H_2), 3.87–3.78 (m, 2H, H_2), 1.44 (t, *J* = 7.1 Hz, 6H, H_{13}), 0.95 (t, *J* = 7.1 Hz, 6H, H_1). **^{13}C NMR** (151 MHz, $CDCl_3$) δ 172.8 (C_{11}), 171.0 (C_9), 169.1 (C_3), 138.7 (C_6), 129.3 (C_7), 127.8 (C_8), 101.2 (C_{10}), 61.9 (C_{12}), 61.3 (C_2), 56.1 (C_4), 42.0 (C_5), 14.3 (C_{13}), 14.0 (C_1). **ASAP-HR-MS** *m/z:* $[M+H]^+$ = 503.1924 (Calculated $C_{26}H_{31}O_{10}^+$ = 503.1917).

TCTE-Br$_2$ (39)

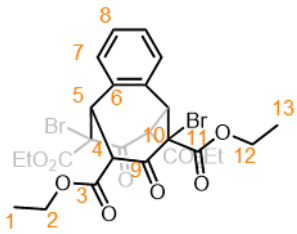

38 (254 mg, 0.50 mmol) and NBS (270 mg, 1.50 mmol) were dissolved in anhydrous $CHCl_3$ (5 mL) in an oven-dried vial under an inert atmosphere, and the reaction mixture stirred at rt for 18 h. The reaction mixture was filtered, the solvent evaporated under reduced pressure, and the crude residue was purified by column chromatography (Teledyne Isco CombiFlash Rf+ system, 24 g SiO_2, hexanes–EtOAc, 0–40%, gradient elution) to yield the title compound as a colourless solid (160 mg, 0.24 mmol , 49%). **M.P.** 170–172 °C. **^{1}H NMR** (700 MHz, $CDCl_3$) δ 7.41–7.38 (m, 2H, H_7), 7.36–7.32 (m, 2H, H_8), 4.81 (d, *J* = 3.6 Hz, 2H, H_5), 4.46–4.34 (m, 6H, $H_{2a,\ 4,\ 12a}$), 4.32–4.23 (m, 4H, $H_{2b,\ 12b}$), 1.36–1.30 (m, 12H, $H_{1,\ 13}$). **^{13}C NMR** (176 MHz, $CDCl_3$) δ 190.1 (C_9), 167.7 (C_3), 166.9 (C_{11}), 134.0 (C_6), 133.3 (C_7), 129.7 (C_8), 74.3 (C_{10}), 64.1 (C_{12}), 62.9 (C_2), 57.3 (C_4), 50.5 (C_5), 14.2 (C_1), 13.7 (C_{13}). **ASAP-HR-MS:** *m/z:* $[M+H]^+$ = 659.0141 (Calculated $C_{26}H_{29}O_{10}Br_2^+$ = 659.0127).

TCTE-Cpr$_2$ (40)

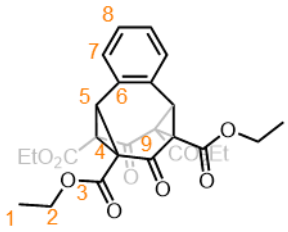

38 (1.0 g, 2.0 mmol) and NBS (1.1 g, 6.0 mmol) were dissolved in anhydrous $CHCl_3$ (10 mL) in an oven-dried vial under an inert atmosphere, and the reaction mixture stirred at rt for 18 h. The reaction mixture was filtered, and the solid washed with $CHCl_3$ (5 mL). To the filtrate, triethylamine (13.9 mL, 10.0 mmol) was added, and the reaction mixture stirred for 6 h. The reaction mixture was then washed with a saturated aqueous solution of NH_4Cl (2 × 10 mL) and dried over $MgSO_4$. The solvent was removed under reduced pressure, and the crude residue was purified by column chromatography (Teledyne Isco CombiFlash Rf+ system, 24 g SiO_2, hexanes–EtOAc, 0–40%, gradient elution) to yield the title compound as a colourless solid (0.75 g, 1.5 mmol 75%). **M.P.** 125–129 °C. **^{1}H NMR** (599 MHz, $CDCl_3$) δ 7.65–7.61 (dd, *J* = 5.7, 3.4 Hz, 2H, H_7), 7.43–7.39 (dd, *J* = 5.7, 3.3 Hz, 2H, H_8), 4.29 (q, *J* = 7.1 Hz, 8H, H_2), 4.05 (s, 2H, H_5), 1.33 (t, *J* = 7.1 Hz, 12H, H_1). **^{13}C NMR** (151 MHz, $CDCl_3$) δ 184.3 (C_9), 164.2 (C_3), 133.3 (C_7), 130.0 (C_6), 129.4 (C_8), 63.3 (C_2), 54.7 (C_4), 40.9 (C_5), 14.1 (C_1). **HR-ASAP-MS** m/z: $[M+H]^+$ = 499.1599 (calculated $C_{26}H_{27}O_{10}^+$ = 499.1604).

TCTE-Diol (47)

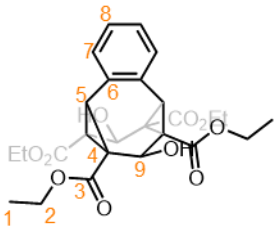

*exo,exo-**47***

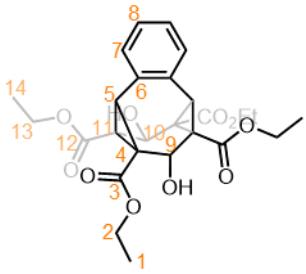

*exo,endo-**47***

$NaBH_4$ (15 mg, 0.40 mmol, 2.0 eq.) was added to a stirred solution of **40** (100 mg, 0.20 mmol, 1.0 eq.) in EtOH (1.33 mL) at 0 °C under Ar. The resulting solution was stirred at rt for 20 h. The reaction was quenched by the addition of 2-propanol and the solvent was removed under reduced pressure. The residue was dissolved in EtOAc (5 mL) and water (5 mL), and the layers were separated. The aqueous layer was extracted with EtOAc (3 × 5 mL) and the combined organics were washed with brine (5 mL), dried ($MgSO_4$) and evaporated under reduced pressure to give the crude product. Purification by column chromatography (Teledyne Isco CombiFlash Rf+ system, 4 g SiO_2, hexane–EtOAc, 0–60%, gradient elution) afforded a 40:60 mixture of *exo,exo*-**47** and *exo-endo*-**47** (45 mg, 0.09 mmol 45%) as a colourless oil. **HR-ASAP-MS** m/z: $[M+H]^+$ = 525.1734 (calculated $C_{26}H_{30}NaO_{10}^+$ = 525.1731). **^{1}H NMR** (400 MHz, $CDCl_3$) δ 7.41–7.31 (m, 2.00H, H_7), 7.25–7.16 (m, 2.00H, H_8), 6.16 (s, 0.60H, *exo,endo*-H_{10}) 5.82 (s, 0.80H, *exo,*exo-H_9), 4.99 (s, 0.60H, *exo,endo*-H_9), 4.30–4.14 (m, 8.00H, H_2, *exo,endo*-H_{13}), 3.26 (s, 0.80H, *exo,exo*-H_5), 3.16 (s, 1.20H, *exo,endo*-H_5), 1.34–1.22 (m, 12.00H, H_1, *exo,endo*-H_{14}). **^{13}C NMR** (101 MHz) δ 170.2 (*exo,endo*-C_{12}), 169.7 (*exo,exo*-C_3), 169.2 (*exo,endo*-C_3), 132.6 (*exo,exo*-C_7), 132.5 (*exo,endo*-C_7), 130.9 (*exo,exo*-C_6), 130.6 (*exo,endo*-C_6), 128.0 (*exo,exo*-C_8), 128.0 (*exo,endo*-C_8), 67.7 (*exo,endo*-C_{10}), 67.4 (*exo,exo*-C_9), 63.6 (*exo,endo*-C_9), 62.4 (*exo,exo*-C_2/ *exo,endo*-$C_{2/13}$), 62.3 (*exo,exo*-C_2/ *exo,endo*-$C_{2/13}$), 62.4 (*exo,exo*-C_2/ *exo,endo*-$C_{2/13}$), 43.4 (*exo,endo*-$C_{4/11}$), 42.5 (*exo,exo*-C_4), 38.3 (*exo,endo*-$C_{4/11}$), 35.0 (*exo,endo*-C_5), 34.8 (*exo,exo*-C_5), 14.2 (*exo,exo*-C_1/ *exo,endo*-$C_{1/14}$), 14.1 (*exo,exo*-C_1/ *exo,endo*-$C_{1/14}$), 14.1 (*exo,exo*-C_1/ *exo,endo*-$C_{1/14}$).

Benzobullvalene (48)

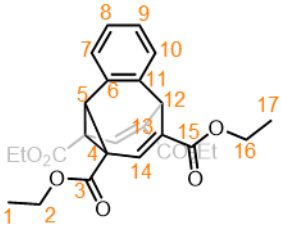

P_2I_4 (365 mg, 0.64 mmol, 2.0 eq.) was added to a stirred solution of a 40:60 mixture of *cis* and *trans*-**47** (161 mg, 0.32 mmol, 1.0 eq.) in anhydrous 2,6-lutidine (3.2 mL) at rt under an inert atmosphere. The resulting solution was stirred at 80 °C for 21 h. The solvent was removed under

reduced pressure and the residue was dissolved in EtOAc (10 mL), and an aqueous solution of 1 M $HCl_{(aq)}$ (5 mL) and saturated $Na_2SO_{3(aq)}$ (5 mL) and the layers separated. The aqueous layer was extracted with EtOAc (3 × 10 mL) and the combined organics were washed sequentially with saturated $NaHCO_{3(aq)}$ (2 × 10 mL) then brine (10 mL), dried ($MgSO_4$) and removed under reduced pressure to give the crude product. Purification by column chromatography (Teledyne Isco CombiFlash Rf+ system, 12 g SiO_2 20–40, hexane–EtOAc, 0–10%, gradient elution) to yield the title compound as a colourless oil (34 mg, 0.07 mmol, 22%). **^{1}H NMR** (400 MHz, $CDCl_3$) δ 7.34–7.22 (m, 6H, $H_{7,8,9,10,14}$), 4.76 (s, 2H, $H_{5,12}$), 4.32–4.16 (m, 8H, $H_{2,16}$), 1.33–1.27 (m, 12H, $H_{1,17}$). **^{13}C NMR** (101 MHz) δ 167.3 ($C_{3,15}$), 133.9 ($C_{6,11}$), 133.1 (C_{14}), 130.7 ($C_{7,10}$), 128.4 ($C_{8,9}$), 62.1 ($C_{2,16}$), 14.3 ($C_{1,17}$). **HR-ASAP-MS** m/z: $[M+H]^+$ = 491.1678 (calculated $C_{26}H_{28}NaO_8^+$ = 491.1676).

(3R,4S)-2,5-Dimethoxytetrahydrofuran-3,4-diol (51)

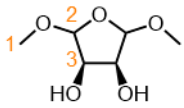

A solution of potassium permanganate (316 mg, 2.0 mmol) and magnesium sulfate heptahydrate (217 mg, 1.8 mmol) in H_2O (6 mL) was added over 30 min to solution of 2,5-dimethoxy-2,5-dihydrofuran, **48** (260 mg, 2.0 mmol) in ethanol (2.5 mL), maintained at 0 °C. Following addition, the reaction was stirred at rt for 4 h, and was left to stand at rt overnight. The mixture was then filtered through a layer of silica gel (5 g), the solvent was removed under reduced pressure, and the residue dissolved in H_2O (20 mL). The aqueous phase was extracted with butanol (5 × 30 mL), the organic fractions were dried over $MgSO_4$, and the solvent removed under reduced pressure to yield the title compound as a yellow oil (165 mg, 1.0 mmol, 50%). **^{1}H NMR** (400 MHz, $CDCl_3$) δ 4.94–4.92 (m, 2H, H_3), 4.17–4.15 (m, 2H, H_2), 3.42 (s, 6H, H_1). **^{13}C NMR** (100 MHz, $CDCl_3$) δ 109.7 (C_3), 75.5 (C_2), 55.8 (C_1) **HR-APCI-MS** *m/z:* $[M+Na]^+$ = 187.0575 (Calculated $C_6H_{12}O_5Na^+$ = 187.0577).[49]

(3R,4S)-3,4-Bis((tert-butyldimethylsilyl)oxy)tetrahydrofuran-2,5-diol (52)

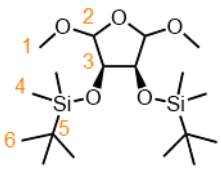

Imidazole (3.73 g, 54.8 mmol) was added to a stirred solution of **51** (1.50 g, 9.1 mmol) in DMF (22.5 mL) at 0°C. Next, *tert*-butyldimethylsilyl chloride (4.13 g, 27.4 mmol) in DMF (22.5 mL) was added, and the reaction mixture stirred at 0 °C for 1 h. The reaction mixture was then poured onto a saturated aqueous solution of NH_4Cl (25 mL), the

aqueous layer extracted with EtOAc (3 × 25 mL), and the organic fractions combined, then washed with a saturated aqueous solution of NH_4Cl (25 mL). The organic fractions were then dried over $MgSO_4$, and the solvent was evaporated under reduced pressure. The resulting residue was suspended in H_2O (10 mL) and filtered, washing the solid with H_2O (10 mL). The solid was collected, dried under reduced pressure and purified by column chromatography (Teledyne Isco CombiFlash Rf+ system, 24 g SiO_2, hexanes–EtOAc, 0–40%, gradient elution) to yield the title compound as a colourless oil (1.10 g, 2.8 mmol, 31%). **^{1}H NMR** (400 MHz, $CDCl_3$) δ 4.80 (dd, *J* = 1.7, 0.6 Hz, 2H, H_2), 4.05 (dd, *J* = 1.7, 0.6 Hz, 2H, H_3), 3.42 (s, 6H, H_1), 0.90 (s, 18H, H_6), 0.08 (s, 6H, H_4), 0.08 (s, 6H, $H_{4'}$). **^{13}C NMR** (100 MHz, $CDCl_3$) δ 109.3 (C_2), 76.8 (C_3), 56.0 (C_1), 26.0 (C_6), 18.4 (C_5), −4.5 (C_4), −4.7 ($C_{4'}$). **HR-APCI-MS** *m/z:* $[M+Na]^+$ = 415.2316 (Calculated $C_{18}H_{40}O_5Si_2Na^+$ = 415.2306).

2,3-O-Isopropylidene-D-ribofuranose (59)

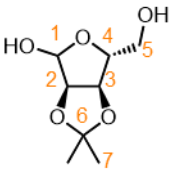

Concentrated sulfuric acid (0.16 mL, 3.0 mmol), was added to a solution of D-ribose (5.0 g, 33.0 mmol) in acetone (67 mL) and the reaction mixture was stirred at rt for 4 h. The solution was neutralised using solid $NaHCO_3$ (1.0 g), filtered, and the solvent removed under reduced pressure. The resulting crude residue was purified by column chromatography (25 g SiO_2, hexanes–EtOAc, 1:2) to yield the title compound as a colourless oil (1.06 g, 26.9 mmol, 81%). **^{1}H NMR** (400 MHz, $CDCl_3$) δ 5.43 (d, *J* = 5.4 Hz, 1H, H_1), 4.85 (d, *J* = 5.9 Hz, 1H, H_3), 4.59 (d, *J* = 5.9 Hz, 1H, H_2), 4.45–4.39 (m, 1H, H_4), 3.82–3.68 (m, 2H, H_5), 1.49 (s, 3H, H_7), 1.33 (s, 3H, $H_{7'}$). **^{13}C NMR** (100 MHz, $CDCl_3$) δ 112.2 (C_6), 102.8 (C_1), 87.7 (C_4), 86.9 (C_2), 81.7 (C_3), 63.6 (C_5), 26.4 (C_7), 24.8 ($C_{7'}$). **HR-APCI-MS** *m/z:* $[M+Na]^+$ = 213.0728 (Calculated $C_8H_{14}O_5Na^+$ = 213.0733).

References

1 H. Dodiuk and S. H. Goodman, in *Handbook of Thermoset Plastics*, Elsevier, 2014, pp. 1–12.

2 M. Zhang and G. De Bo, *J. Am. Chem. Soc.*, 2019, **141**, 15879–15883.

3 A. M. Saitta and M. L. Klein, *J. Phys. Chem. B*, 2000, **104**, 2197–2200.

4 N. Zheng, Y. Xu, Q. Zhao and T. Xie, *Chem. Rev.*, 2021, **121**, 1716–1745.

5 J.-M. Lehn, *Prog Polym Sci*, 2005, **30**, 814–831.

6 L. Li, X. Peng, D. Zhu, J. Zhang and P. Xiao, *Macromol. Chem. Phys.*, 2023, **20**, 2300224

7 J. Zheng, Z. M. Png, S. H. Ng, G. X. Tham, E. Ye, S. S. Goh, X. J. Loh and Z. Li, *Mater. Today*, 2021, **51**, 586–625.

8 M. N. Pomfret, P. B. Sun, Z. Huang, A. C. Freund, T. Miyoshi and M. R. Golder, *Angew. Chem. Int. Ed. Engl.*, 2023, **62**, e202301695

9 B. H. Meier and W. L. Earl, *J. Am. Chem. Soc.*, 1985, **107**, 5553–5555.

10 O. Yahiaoui, L. F. Pašteka, B. Judeel and T. Fallon, *Angew. Chem. Int. Ed. Engl.*, 2018, **57**, 2570–2574.

11 M. Achard, M. Mosrin, A. Tenaglia and G. Buono, *J. Org. Chem.*, 2006, **71**, 2907–2910.

12 M. Jones and L. T. Scott, *J. Am. Chem. Soc.*, 1967, **89**, 150–151.

13 H. E. Zimmerman, R. W. Binkley, R. S. Givens and M. A. Sherwin, *J. Am. Chem. Soc.*, 1967, **89**, 3932–3933.

14 H. E. Zimmerman and P. S. Mariano, *J. Am. Chem. Soc.*, 1969, **91**, 1718–1727.

15 H. D. Patel, T.-H. Tran, C. J. Sumby, L. F. Pašteka and T. Fallon, *J. Am. Chem. Soc.*, 2020, **142**, 3680–3685.

16 O. Yahiaoui, L. F. Pašteka, C. J. Blake, C. G. Newton and T. Fallon, *Org. Lett.*, 2019, **21**, 9574–9578.

17 In *Comprehensive Organic Name Reactions and Reagents*, Wiley, 2010, pp. 1116–1119.

18 D. Seyferth, *Organometallics*, 2001, **20**, 2940–2955.

19 W. E. Konz, W. Hechtl and R. Huisgen, *J. Am. Chem. Soc.*, 1970, **92**, 4104–4105.

20 D. A. Hrovat and W. T. Borden, *J. Am. Chem. Soc.*, 1992, **114**, 5879–5881.

21 M. R. Gottesfeld, F. A. Masoudi and D. E. Hansen, *Tetrahedron Lett.*, 1992, **33**, 447–450.

22 L. A. Paquette, U. Jacobsson and S. V. Ley, *J. Am. Chem. Soc.*, 1976, **98**, 152–158.

23 N. C. Burton, F. G. N. Cloke, S. C. P. Joseph, H. Karamallakis and A. A. Sameh, *J. Organomet. Chem.*, 1993, **462**, 39–43.

24 H. F. König, L. Rummel, H. Hausmann, J. Becker, J. M. Schümann and P. R. Schreiner, *J. Org. Chem.*, 2022, **87**, 4670–4679.

25 E. Grovenstein and D. V. Rao, *Tetrahedron Lett.*, 1961, **2**, 148–150.

26 L. A. Paquette and K. A. Henzel, *J. Am. Chem. Soc.*, 1975, **97**, 4649–4658.

27 G. Muchow, J. M. Brunel, M. Maffei and G. Buono, *J. Org. Chem.*, 1995, **60**, 852–855.

28 D. Bryce-Smith, A. Gilbert and J. Grzonka, *J. Chem. Soc., Chem. Commun.*, 1970, 498.

29 M. Achard, A. Tenaglia and G. Buono, *Org. Lett.*, 2005, **7**, 2353–2356.

30 A. Anand, P. Singh, V. Kumar and G. Bhargava, *RSC Adv.*, 2019, **9**, 25554–25568.

31 G. Schröder, *Angew. Chem. Int. Ed. Engl.*, 1963, **2**, 481–482.

32 T. R. Boussie and A. Streitwieser, *J. Org. Chem.*, 1993, **58**, 2377–2380.

33 M. Jones, S. D. Reich and L. T. Scott, *J. Am. Chem. Soc.*, 1970, **92**, 3118–3126.

34 Yu. V. Tomilov, D. N. Platonov and O. M. Nefedov, *Russ. Chem. Bull.*, 1999, **48**, 2178–2180.

35 D. Yang and J. M. Cook, *J. Org. Chem.*, 1976, **41**, 1903–1907.

36 U. Weiss and J. M. Edwards, *Tetrahedron Lett.*, 1968, **9**, 4885–4887.

37 B. Föhlisch, E. Widmann and E. Schupp, *Tetrahedron Lett.*, 1969, **10**, 2355–2358.

38 R. Gompper and M. Schwarzensteiner, *Angew. Chem. Int. Ed. Engl.*, 1982, **21**, 438–439.

39 W. W. Win, K. G. Grohmann and L. Todaro, *J. Org. Chem.*, 1994, **59**, 2803–2808.

40 W. D. Closson, P. Wriede and S. Bank, *J. Am. Chem. Soc.*, 1966, **88**, 1581–1583.

41 P. Girard, J. L. Namy and H. B. Kagan, *J. Am. Chem. Soc.*, 1980, **102**, 2693–2698.

42 R. A. Batey and W. B. Motherwell, *Tetrahedron Lett.*, 1991, **32**, 6211–6214.

43 H. Suzuki and H. Tani, *J. Syn. Org. Chem. Jpn.*, 1985, **43**, 76–83.

44 A. Krief and V. N. Telvekar, in *Encyclopedia of Reagents for Organic Synthesis*, John Wiley & Sons, Ltd, Chichester, UK, 2009.

45 K. Rebsamen and G. Schröder, *Chem. Ber.*, 1993, **126**, 1425–1427.

46 K. Rebsamen, H. Röttele and G. Schröder, *Chem. Ber.*, 1993, **126**, 1429–1433.

47 D. L. Hufford, D. S. Tarbell and T. R. Koszalka, *J. Am. Chem. Soc.*, 1952, **74**, 3014–3018.

48 G. Jones, in *Organic Reactions*, Wiley, 2011, pp. 204–599.

49 M. Villacampa, M. Martínez, G. González-Trigo and M. N. M. Söllhuber, *J. Heterocycl. Chem.*, 1992, **29**, 1541–1544.

50 M. N. Deshpande, M. Jawdosiuk, G. Kubiak, M. Venkatachalam, U. Weiss and J. M. Cook, *J. Am. Chem. Soc.*, 1985, **107**, 4786–4788.

51 S. H. Bertz and G. Dabbagh, *Angew. Chem. Int. Ed. Engl.*, 1982, **21**, 306–307.

52 Z. Lv, C. Song, Y. Niu, Q. Li and X. Ye, *Chem. Med .Chem*, 2018, **13**, 338–351.

53 A. García Martínez and M. Oliver Ruiz, *Synthesis*, 1983, **1983**, 663–665.

54 Cl. Schöpf and A. Schmetterling, *Angew. Chem.*, 1952, **64**, 591–592.

55 F. Plasser and F. Glöcklhofer, *Eur. J. Org. Chem.*, 2021, **2021**, 2529–2539.

56 C. Yang, Z.-L. Xu, H. Shao, X.-Q. Mou, J. Wang and S.-H. Wang, *Org. Lett.*, 2015, **17**, 5288–5291.

Chapter 4 | Supramolecular Control of Bullvalene

Abstract

In solution, bullvalene is free to rearrange between an equilibrium distribution of up to 1.2 million degenerate isomers, depending on the substituents present. In the last 20 years, several examples have exhibited an alteration of bullvalene's rearrangements and isomer distribution as part of supramolecular systems such as organometallic complexes or in chemical sensing moieties. There have thus far been very limited studies regarding bullvalene as a molecular guest, as opposed to as a fragment of a molecular host. Herein we present our ongoing work to use bullvalene as molecular guests, instead of as part of the host, in the hope of controlling and exploiting its fluxional properties. A range of supramolecular hosts based on hemicarcerands have been synthesised and investigated as methods of controlling the fluxional behaviour. To date, our attempts to employ hemicarcerands to bind bullvalene guests have proved unsuccessful. This may be due to insufficient cavity volume, although experiments on larger hosts are still ongoing. The octa acid host, a water soluble cavitand capable of capsule formation, has encapsulated several bullvalene guests and preliminary experiments suggest that limits are imposed on their rearrangements. Although, it is necessary to gather much more data in order to draw conclusions from these experiments. Modified cyclodextrins are also used as potential hosts for bullvalene. While there is no evidence for the formation of a supramolecular polymer from tethered bullvalene complexes, permethylated cyclodextrin has exhibited potential for binding bullvalene. Investigations regarding the effect this binding has on the bullvalene core are underway.

Acknowledgments

The following people are gratefully acknowledged for their contribution to this chapter: Luke Nicholls for contributions to the synthesis of **7** and **H1**. Synthesis and encapsulation experiments using **H4** were performed in collaboration with Professor Bruce C. Gibb, Yahya A. Ismaiel, and Jenny Kim at Tulane University. Dr. Yulong Son synthesised and obtained a crystal structure for **50**. Dr. Aisha Bismillah synthesised **72** and performed titrations with **1**, she also performed low temperature ^{1}H NMR spectroscopy for all BV structures herein. We also thank the Royal Society of Chemistry for a Researcher Development and Travel Grant.

4.1 Introduction

The Fischer key-lock model (Figure 1a) of enzyme binding was presented in 1894, and stated that in binding to an enzyme, a substrates structure and shape must be complementary to that of the enzyme for binding to take place.[1] In 1958, this theory was superseded by Koshland's induced fit model (Figure 1b) which stated that the introduction of the substrate to the binding site of the enzyme prompts an alteration in the enzyme's shape, resulting in the best binding possible.[2] Both of these theories regard the vital role that preorganisation and complementarity play in natural biological systems, such as enzymes or DNA.[3,4] Furthermore it is not just the binding of the substrate but also that of the transition state and products that are vital for the catalytic activity of enzymes. Another alternative binding model is conformational selection. In this model, a conformational change occurs in the host before the substrate is bound.[5] Often, whether or not a process occurs *via* conformational selection or induced fit depends on the concentration of the ligand present. Conformational selection dominates at low concentrations, and induced fit at higher concentrations.[6]

In order to develop a greater understanding of these systems, supramolecular chemists have experimented thoroughly with concepts such as molecular templation[7] and self-organisation.[8] This work has led to the development of entirely new fields of chemistry, such as dynamic combinatorial chemistry, that are concerned with the ability of molecules to adapt and interact with one another in a variety of conditions.[9,10] Bullvalene (**BV**) is a fluxional molecule, which may occupy a plethora of different shapes through Cope rearrangements. Work has been performed regarding BVs behaviour as part of supramolecular systems, however, almost entirely regarding its ability to adapt as an part of the host.[11–15] Much work is still yet to be performed in order to understand the use of BV as a supramolecular guest (Figure 1c), and the potential ramifications for its fluxional behaviour. In contrast to intermolecular systems such as dynamic covalent libraries, the alteration of binding behaviour in BV is independent of concentration, and their rearrangements do not require stimuli.

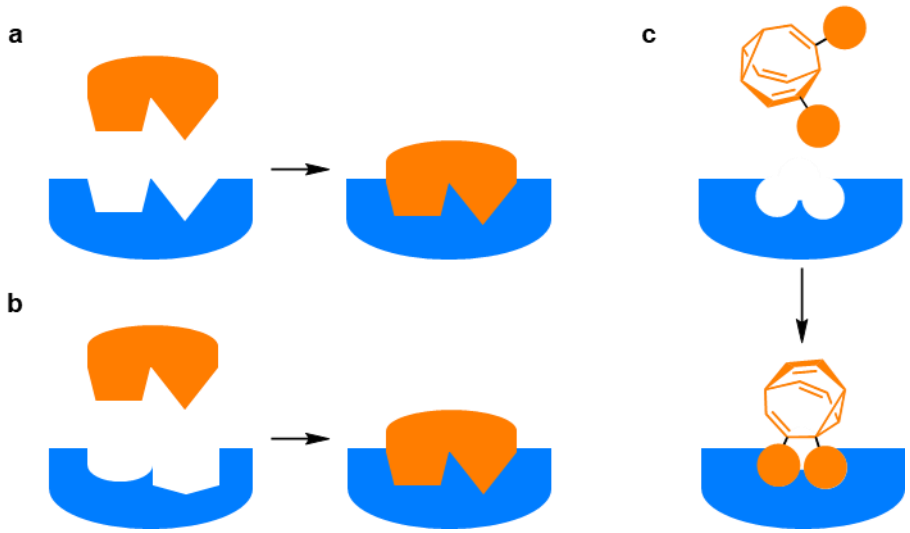

Figure 1: Illustrations of (a) the lock and key model. (b) The induced fit model. (c) Bullvalene's adaptive binding to a host.

4.2 Supramolecular Hosts for Bullvalene

The aim of this project was to use steric constraints imposed by a closed shell cavity in order to exert control over the rearrangement of a BV framework.[16–19] Each possible BV isomer has different shapes, polarities and molecular volumes (Figure 2). As a result, steric constraints may affect the stability of each isomer, exhibiting thermodynamic control.

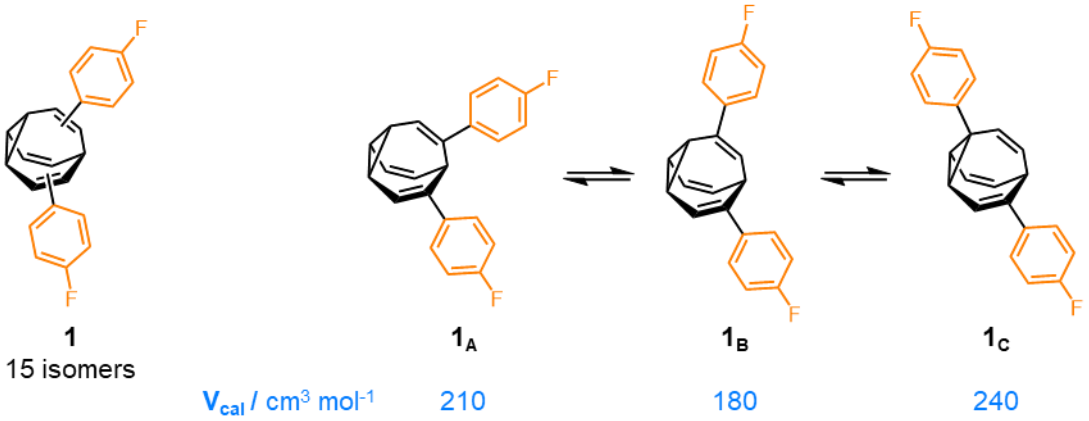

*Figure 2: Three isomers of di-p-fluorophenyl BV **1** and their relative molecular volumes.*

Furthermore, the relative transition energies of each Cope rearrangement may also differ, resulting in kinetic control of BV rearrangement. This would manifest itself in increased or decreased rates of rearrangements. The greater the steric constraints imposed upon the BV molecule, the more likely it is that control will be observed. For this reason, in our attempts to encapsulate BVs and use them as molecular guests, the smaller and more closed a cavity is, the more likely it is to result in a controlling the rates of rearrangements. However, one consideration that must be made is the size of

the cavities in which BV may feasibly bind. Rebek *et al.* stated in 1998 that most favourable binding occurs for molecular capsules when the volume of the guest is around 55% that of the cavity.[20] This is used as a general rule for cavitands by supramolecular chemists. This, alongside comparisons to guests in the literature, is what guided us in our selection of hosts.

Furthermore, loss of conformational freedom in BV systems when bound to a host molecule may make binding unfavourable. As such, closed shell cavities, which make decomplexation significantly more difficult are the most desirable molecular hosts. Moreover, many hemicarcerands are soluble in organic solvents so variable temperature NMR spectroscopy for the investigation of BV systems is made more facile. These complexes are usually formed at higher temperatures over long periods and do experience some decomplexation over time in solution. How favourable the binding of the guest is to the host is related to host-guest interactions, which contribute to the intrinsic binding energy (Figure 3).

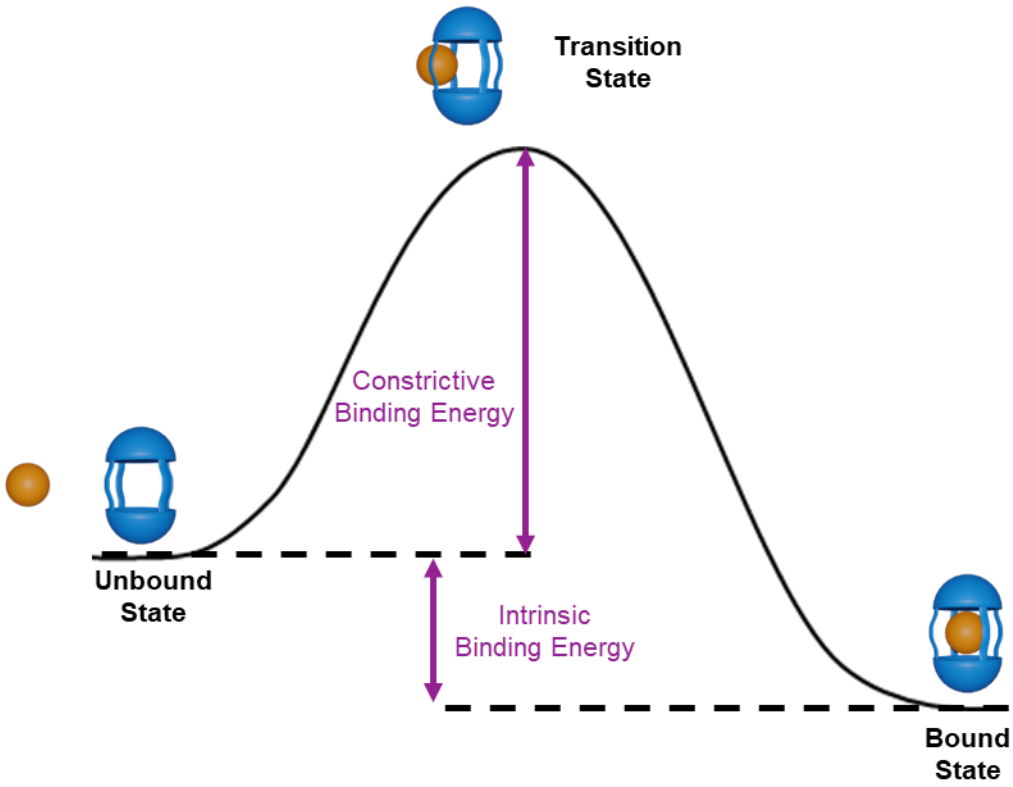

Figure 3: Illustration of constrictive and intrinsic binding energy for a guest encapsulated in a hemicarcerand.

Nonetheless, another possibility is to use water-soluble hosts to employ the hydrophobic effect for complexation. BV systems in bulk solution demonstrate resonance deconvolution in ^{1}H NMR spectra between −40 and −60 °C, enabling

isomer assignment. However, if rearrangement is significantly slowed due to the aforementioned steric constraints, this deconvolution may occur at a higher temperature.

4.3 Hemicarcerands

The first hosts investigated were related closely to Cram *et al.*'s hemicarcerand work from the late 1980s and 1990s.[21–26] As mentioned in Chapter 1, these compounds start as calixarene scaffolds, which are then developed further to modify and rigidify their cavity's shape and size.

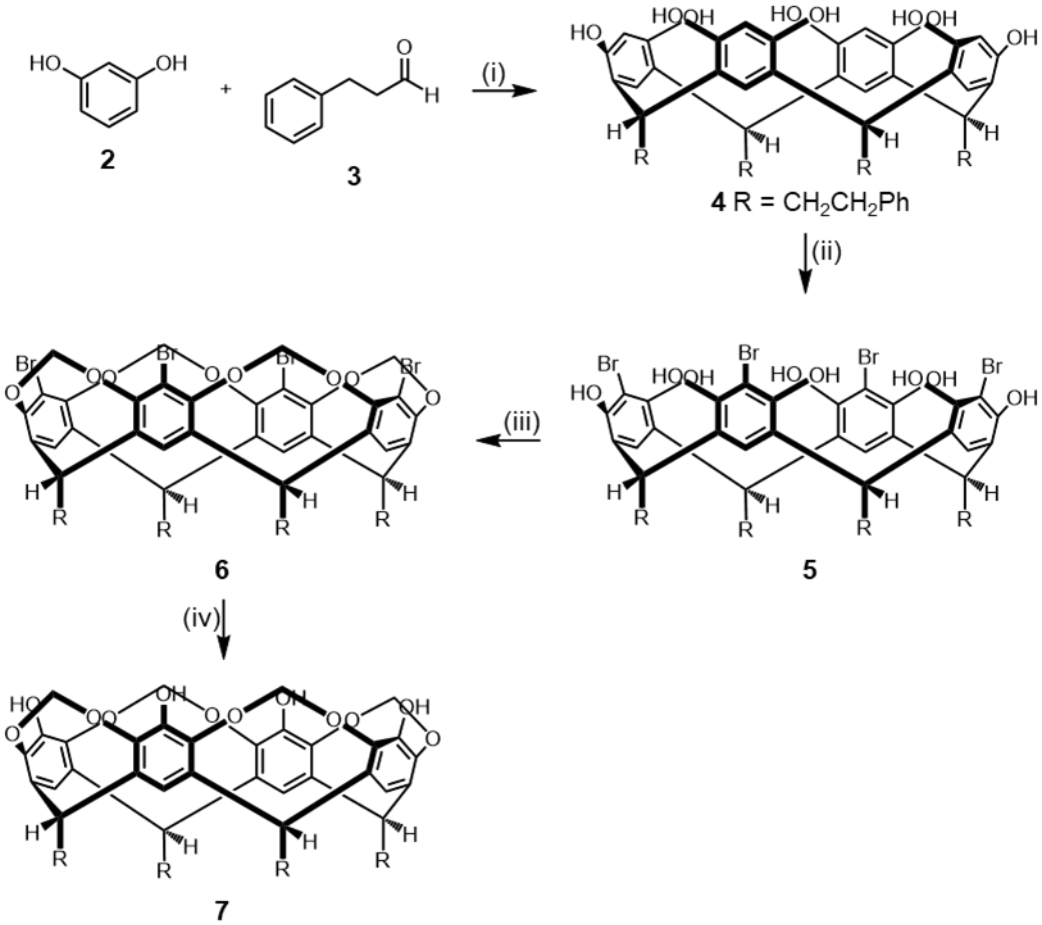

Scheme 1: Synthesis of tetrol cavitand **7**. *(i) HCl/ EtOH, reflux, 5 d, 81%. (ii) NBS, 2-butanone, rt, 18 h, 53%. (iii) CH_2BrCl, $CsCO_3$, DMF, 63 °C, 3 d, 71%. (iv) (a) ^{n}BuLi, −78 °C, 20 min. (b) $B(OMe)_3$, rt, 1 h. (c) H_2O_2/ NaOH, −78 °C to rt, 18 h, 28%.*

Firstly, the combination of resorcinol **2** and dihydrocinnamaldehyde **3** in ethanol with an acid catalyst resulted in the synthesis of calix[4]arene **4**. Compound **4** is then brominated in the presence of *N*-bromosuccinimide to yield **5**, which then undergoes a Williamson ether synthesis with bromochloromethane to yield the rigidified cavitand **6**.[27–29] Compound **6** is then lithiated using ^{n}BuLi, followed by boronation with

trimethyl borate and finally treatment with a sodium hydroxide/ hydrogen peroxide solution to yield tetrol **7** (Scheme 1).[27,30]

This synthesis is a replication of previous synthetic routes to yield similar compounds. The yield achieved in the literature for the formation of **7** were significantly higher (45%) than what we were able to achieve in our initial attempts (19% and 28%). The side products of this reaction (step iv) appeared by ^{1}H NMR spectroscopy to be protodeborylated during the final step resulting in mono-, di- and triol analogues of **7**. A similar synthesis by Schalley *et al.* in 2008 reported the functionalisation of unsubstituted calixarene **8** to form tetramethoxy calixarene **9** in a single step (Scheme 2), closely resembling that of the conversion of **6** to **7** in Scheme 1. The main difference between the two preparations is the use of ^{s}BuLi instead of ^{n}BuLi, which is a stronger base and is thus capable of deprotonating weak carbon acids, such as **8**.[31]

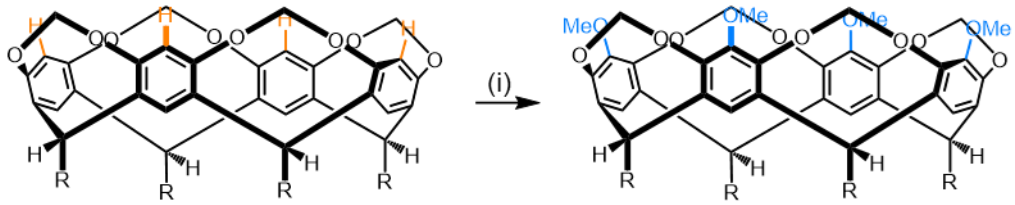

8 R = $(CH_2)_4CH_3$ **9**

*Scheme 2: Synthesis of tetrol **9** from unsubstituted calixarene **8**. (i) (a) ^{s}BuLi, −78 °C, 30 min. (b) $B(OMe)_3$, rt, 1 h. (c) H_2O_2/ NaOH, −78 °C to rt, 18 h. (d) MeI, K_2CO_3, acetone, reflux, 52%.*[31]

This reaction proceeds *via* the same lithiation, borylation, hydroxylation pathway as the step in Scheme 1, however it also negates the need for the low-yielding bromination step. As a result, this step was incorporated into our synthesis of tetrol **7**. Instead, **4** is rigidified by the formation of an "upper rim" calixarene **10**, which undergoes subsequent bromine-lithium exchange, borylation and hydroxylation in one step to form **7** (Scheme 3).

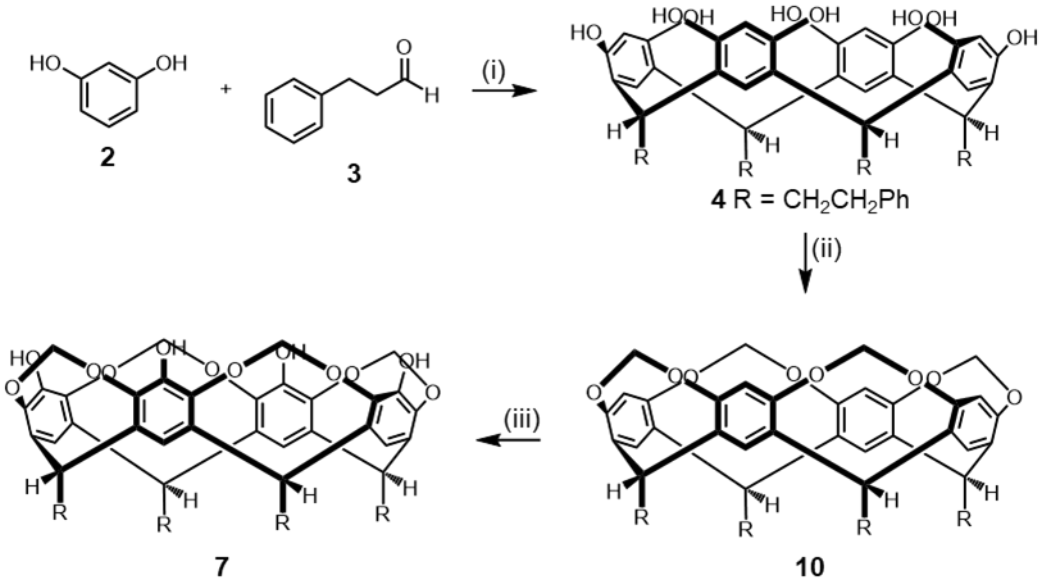

*Scheme 3: Alternative synthesis for tetrol **7**. (i) HCl/ EtOH, reflux, 5 d, 81%. (ii) CH_2BrCl, DMF, 63 °C, 3 d, 81%. (iii) (a) ^sBuLi, −78 °C, 30 min. (b) $B(OMe)_3$, rt, 1 h. (c) H_2O_2/ NaOH, −78 °C to rt, 18 h, 66%.*

This new route results in a three-step synthesis to tetrol **7**, with an overall yield of 43%, as opposed to previous methods, which in our attempts yielded just 9% over four steps. Compound **7** is a precursor for much of the work performed in this chapter, so the ability to synthesise it over fewer step with a higher yield is crucial.

4.3.1 Butyl-bridged Hemicarcerands

The preliminary binding studies in this project are based on smaller hemicarcerands, and as the project progressed, hemicarcerands with larger cavities and different binding methods were explored. This was an intentional decision as a smaller cavity size would exert more steric constraints upon the encapsulated BV, resulting in more thermodynamic and/or kinetic control. For this reason, the first hemicarcerand **H1**, was synthesised with butyl linkers. A cavity of this size was shown to encapsulate bicyclic diazirine **11** in a previous publication by Warmuth *et al.*.[16]

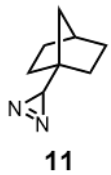

*Figure 4: Chemical structure of bicyclic aziridine **11**.*

The guest selected in this case was synthesised over two steps from TMS–acetylene **12** and **COTT**. Firstly, a Co(I) catalysed cycloaddition resulted in TMS–BDT **13**, which was then subjected to a photorearrangement in the presence of a photosensitiser, yielding BV **14** in a reasonable yield over two steps (Scheme 4).[32,33]

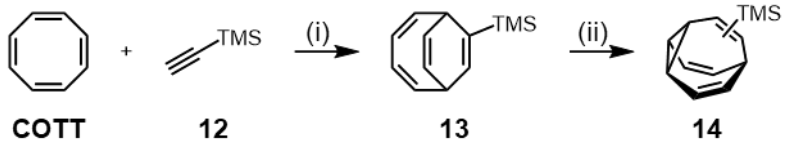

*Scheme 4: Synthesis of TMS-BV **14**. (i) $CoBr_2$(dppe), ZnI_2, Zn Dust, DCE, rt, 18 h, 96%. (ii) Thioxanthone, THF, 365 nm, rt, 6 h, 33%.*

Initial attempts to perform this Co(I) cycloaddition yielded no product, as not enough time was left for the formation of the active Co(I) catalyst from the Co(II) precatalyst.[34,35] This occurs over roughly 30 minutes, however, time is rarely the best method to determine when the catalyst has formed. The Co(II) precatalyst is a deep green colour, and the Co(I) catalyst is a dark brown colour. Screening of conditions determined that it is important to observe this colour change before adding the last reactants otherwise very little product is obtained.

To make the host we first require the synthesis of the desired linker group with appended leaving groups. For butyl-linked hemicarcerand **H1**, this required butane-1,4-diol **15** to be converted to busulfan **16** (Scheme 5).

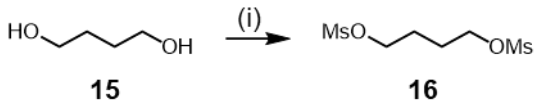

*Scheme 5: Synthesis of busulfan **16**. (i) MsCl, NEt_3, CH_2Cl_2, rt, 18 h, 58%.*

Once the linker was synthesised, combination of **16** with tetrol cavitand **7** resulted in a mixture of tribridged hemicarcerand **17** and hemicarcerand **H1** (Scheme 6).

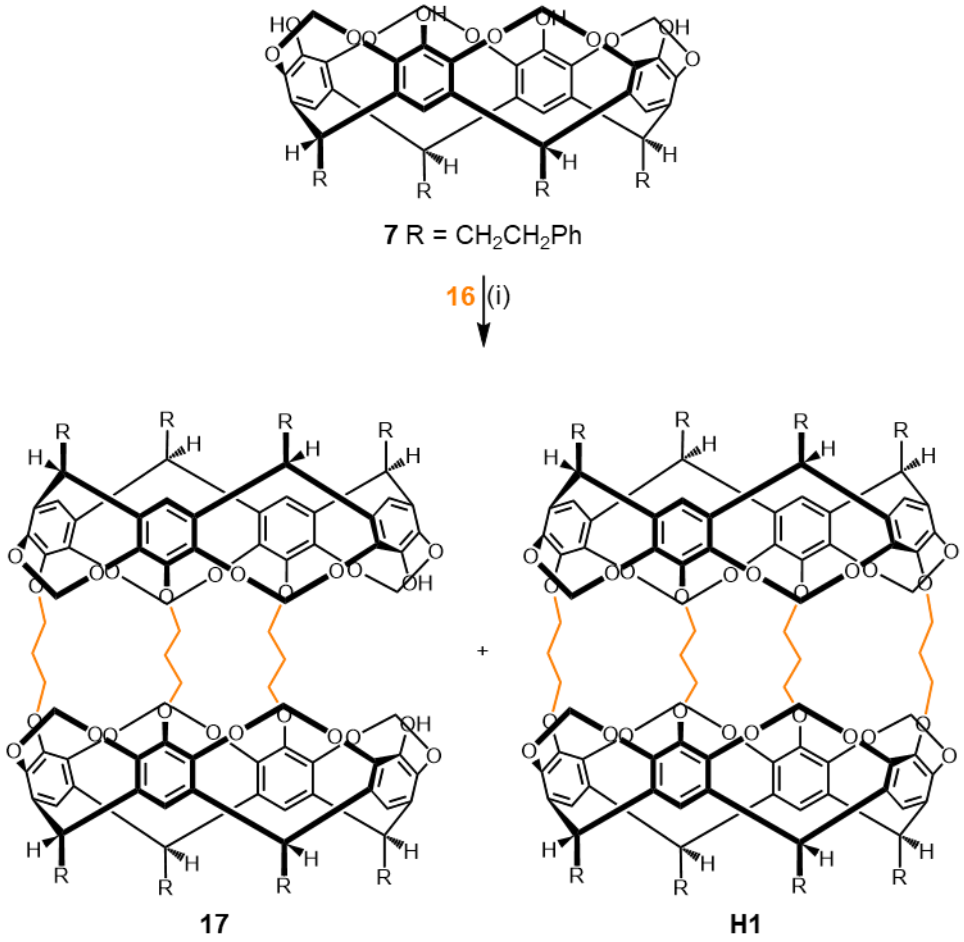

*Scheme 6: Synthesis of **17** and **H1** from **7**. (i) Busulfan **16**, Cs_2CO_3, DMA, rt, 18 h, **17** = 41%, **H1** = 12%.*

Compounds **17** and **H1** were then used in attempts to encapsulate TMS–BV **14**. The first attempt involved the strategy used by Warmuth *et al.* in their 2003 paper (Scheme 7).[16]

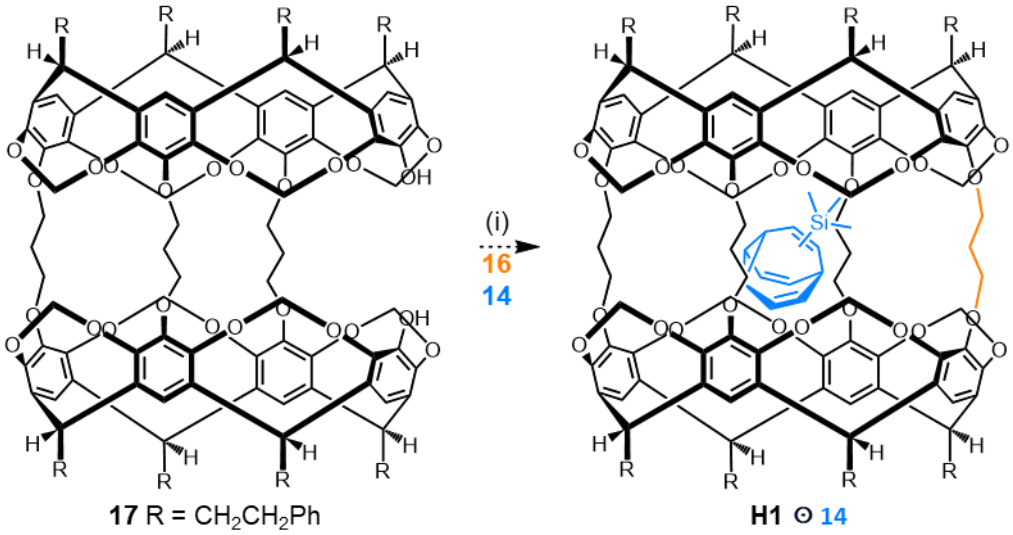

*Scheme 7: Attempted encapsulation of **14** in **H1**. (i) **14**, **16**, Cs_2CO_3, Ph_2O, rt, 4 d. No encapsulation observed.*

In this method, **17** was combined with **16** in order to form **H1**, however this time the reaction was performed in the presence of an excess of molecular guest, **14**. This reaction must be performed in a bulky solvent, such as diphenyl ether or HMPA[16], in order to ensure no competitive binding from the solvent.

The alternative method of binding **14** in **H1** was performed in a more direct manner—that is, the heating of a mixture of **14** and **H1** in diphenyl ether to 160 °C over a period of three days in an attempt to "force in" the molecular guest (Scheme 8).

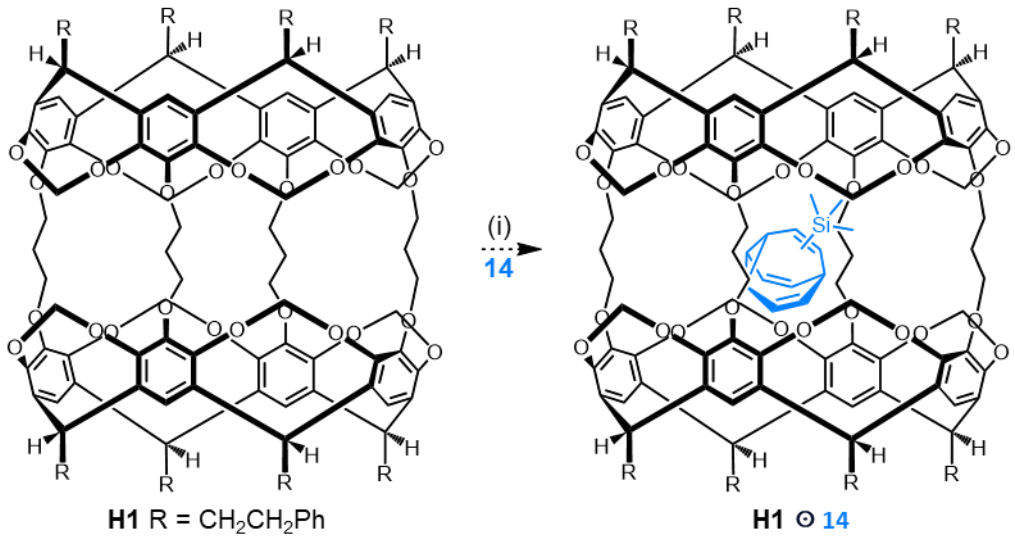

*Scheme 8: Second attempted encapsulation of **14** in **H1**. (i) **14**, Ph_2O, 160 °C, 3 d. No encapsulation observed.*

Since neither of these attempted encapsulations showed any signs of success in ^{1}H NMR spectroscopy, it was postulated that this cavity may be too small to encapsulate BVs. As such, we continued on in the search for hemicarcerands with slightly larger cavities.

4.3.2 Phenylene Hemicarcerands

The next host must therefore be slightly larger in order to accommodate larger guests, such as our substituted BVs. It should be noted that substituted BVs are preferred over **BV** itself for binding in these limited-volume cavities. This is because the presence of substituents may increase the effects of the steric constraints as the different isomers vary in size and shape considerably, whereas in **BV** all isomers are identical.

The next host that was synthesised was based upon a 2021 publication by Dyker *et al.* on an adaptive hemicarcerand, consisting of four *m*-xylyl linkers.[36] In this work, a crystal structure was reported of the hemicarcerand encapsulating two benzonitrile molecules, along with other substituted aromatic compounds. Although substituted

phenyl rings are more planar than BV molecules, it was our hypothesis that the inclusion of two benzonitrile molecules suggests inclusion of BV compounds may occur.

The linker for this hemicarcerand was synthesised over two steps from isophthalic acid **18** by reduction to 1,3-dimethanol benzene **19** and chlorination to **20** (Scheme 9).[37,38]

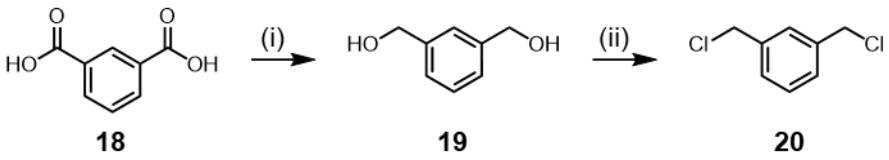

18 **19** **20**

Scheme 9: Synthesis of linker for phenylene hemicarcerand. (i) $LiAlH_4$, THF, 60 °C, 18 h, 76%. (ii) $SOCl_2$, NEt_3, CH_2Cl_2, rt, 3 h, 60%.

With **20** in hand, hemicarcerand **H2** can be synthesised in a similar method to that in Scheme 6, by heating in the presence of cesium carbonate (Scheme 10).

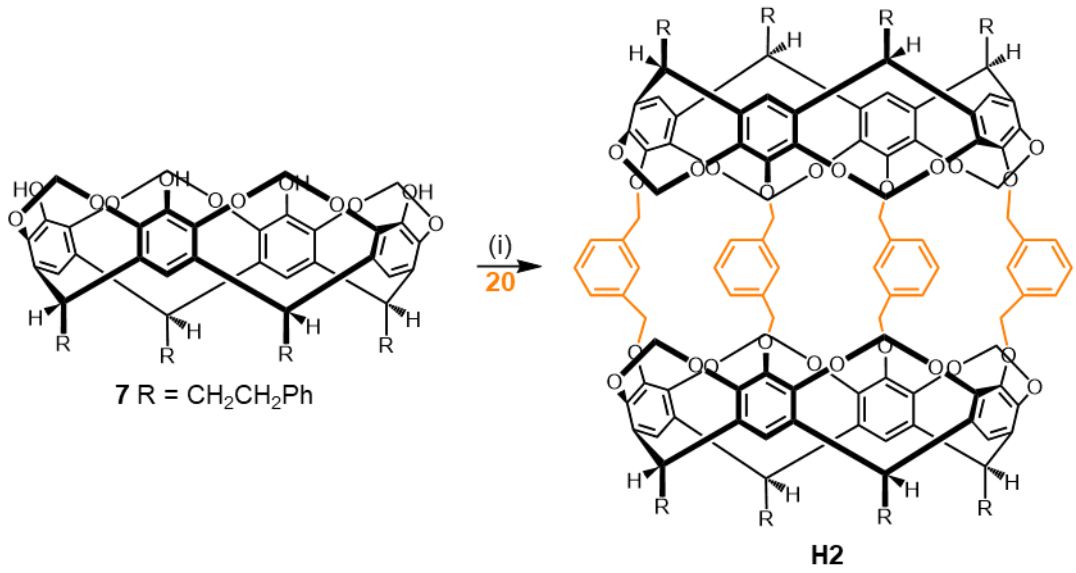

7 R = CH_2CH_2Ph

H2

*Scheme 10: Synthesis of hemicarcerand **H2**. (i) **20**, Cs_2CO_3, NMP, 60 °C, 2 d, 12%*

Two BVs were synthesised for encapsulation in hemicarcerand **H2**, the first of which uses propargyl alcohol **21** to synthesise methanol BDT **22**, which is converted to **23** *via* a photorearrangement. A similar process converts 3-hexyne **24** to diethyl BDT **25**, and again a photorearrangement forms diethyl BV **26**. The main difference between the two processes is the use of trifluoroethanol (TFE) as the solvent in the synthesis of **22**, as opposed to 1,2-dichloroethane (DCE) for **25**. Furthermore, the reaction in TFE is performed at 55 °C, as opposed to at room temperature in DCE (Scheme 11).

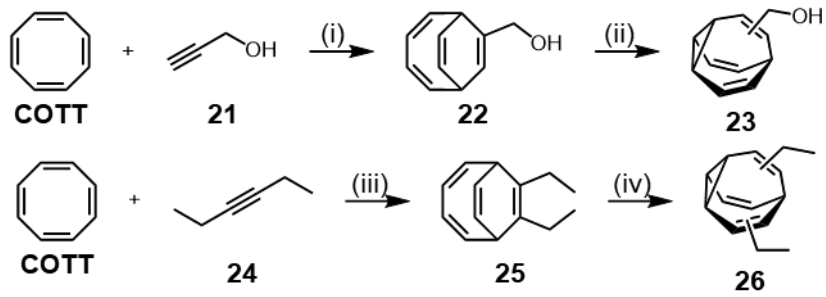

*Scheme 11: Synthesis of BVs **23** and **26**. (i) $CoBr_2$(dppe), ZnI_2, Zn Dust, TFE, 55 °C, 18 h, 76%. (ii) Thioxanthone, THF, 365 nm, rt, 6 h, 76%. (iii) $CoBr_2$(dppe), ZnI_2, Zn Dust, DCE, rt, 18 h, 69%. (ii) Thioxanthone, THF, 365 nm, rt, 6 h, 29%.*

As a monosubstituted BV, **23** only has four unique isomers, characterised by substitution at each of BV's four unique positions. In contrast, **26**, a homodisubstituted BV, consists of 15 unique isomers with three enantiomer pairs. While any degree of BV encapsulation would be considered successful and allow for investigation of the effect of steric constraints on kinetics and thermodynamics, monosubstituted BVs may only show very little if any alteration. This is because rearrangements may still occur simultaneously with rotation and/or translation of the BV core, resulting in similar properties to those observed free in solution. Disubstituted BVs on the other hand are limited in their rotation and the isomers present may be determined by the relative positions of the substituents inside the molecular cavity.

Attempts were made to encapsulate both **23** and **26** in **H2** by heating the intended host and 150 equivalents of guest in diphenylether at 120 °C over three days (Scheme 12). As no encapsulation was observed, the temperature was increased to 160 °C and further to 180 °C, but still no encapsulation occurred. Thus, it was determined this host is unsuitable for BVs.[39,40]

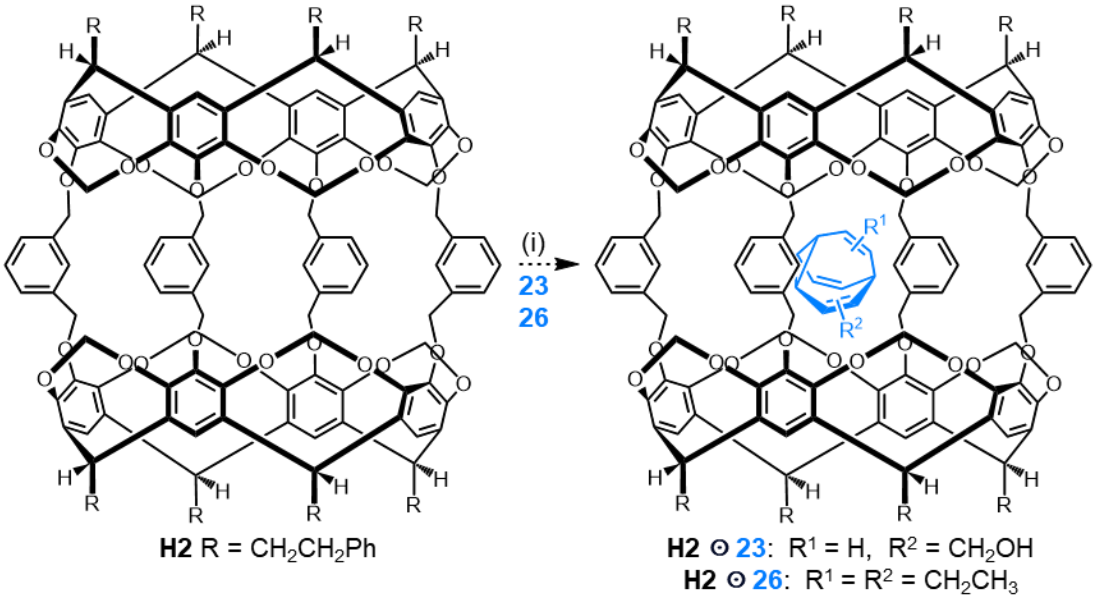

*Scheme 12: Attempted encapsulation of BVs **23** and **26** in hemicarcerand **H2**. (i) **23** or **26**, Ph_2O, 180 °C, 3 d.*

4.3.3 Imine Hemicarcerands

The third hemicarcerand synthesised is from a 1991 report by Cram *et al.* and involves a larger cavity and apertures. This imine-based hemicarcerand is known to encapsulate much larger single molecules such as ferrocene **27**, [2.2] cycloparaphenylene **28**, and adamantadine **29** (Figure 5).[22,41]

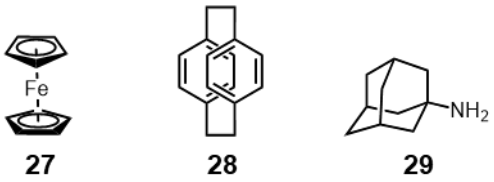

*Figure 5: Chemical structure of ferrocene **27**, [2.2] cycloparaphenylene **28** and adamantadine **29**.*

The synthesis of this host can utilise tetrabromocavitand **6** (Scheme 1), which undergoes bromine-lithium exchange and is formylated with DMF to yield **30** (Scheme 13).

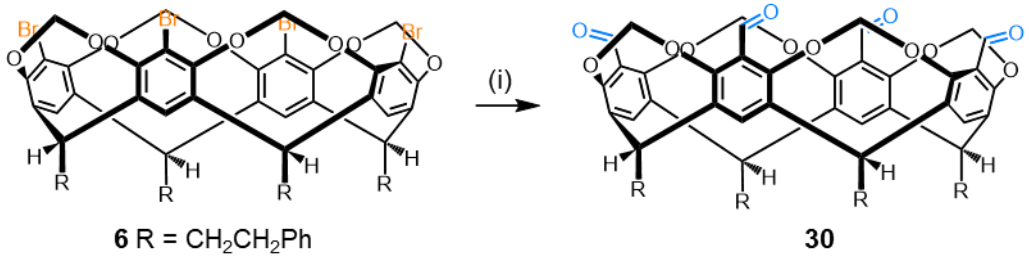

*Scheme 13: Synthesis of tetral **30**. (i)(a) ^{n}BuLi, THF, −78 °C to 0 °C, 30 min. (b) DMF, −78 °C to rt, 1 h, 18%.*

The following step is an imine formation with *m*-phenylenediamine **31** to give imine hemicarcerand **H3**. This step was initially performed by Cram *et al.* in anhydrous pyridine at 65 °C over four days resulting in a yield of 45%.[22]

Another work from 1998 published by Kaifer *et al.* used magnesium sulfate in chloroform as a method to remove water from the solution to push the equilibrium towards the imine. This method yielded just 39% over six days.[41]

Two years after Kaifer *et al.*'s synthesis, Stoddart *et al.* published a new route, using catalytic amounts of TFA in the reaction. This gives a significantly higher yield (55%) while only stirring for one day, thus, this method was used (Scheme 14).[42] When this efficient reaction was performed, the yield obtained was 79%, giving 45 mg of the hemicarcerand **H3**.

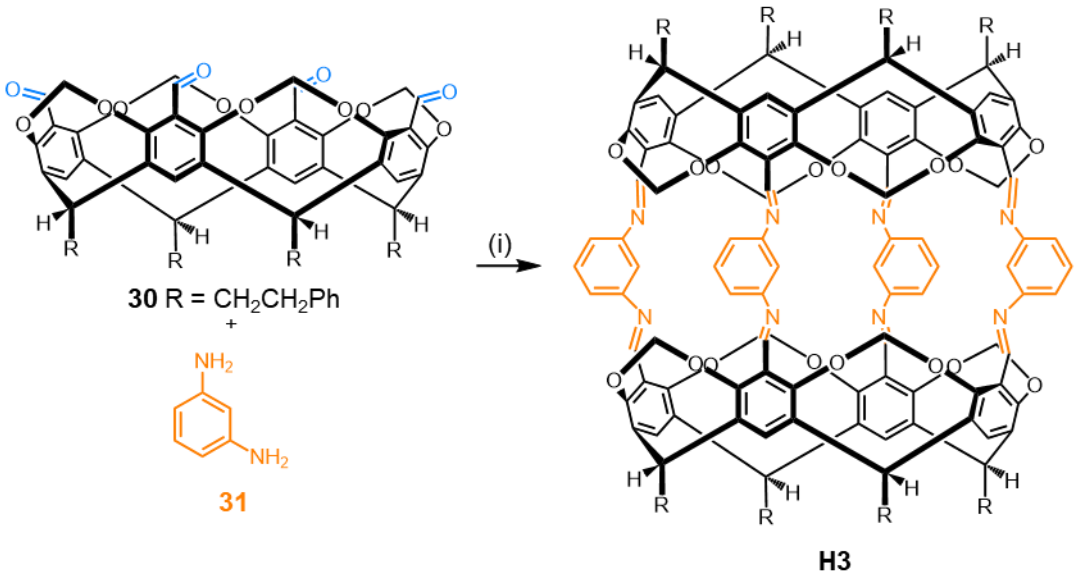

*Scheme 14: Synthesis of imine hemicarcerand **H3**. (i) **31**, TFA, $CHCl_3$, rt, 18 h, 79%.*

Similarly to the hemicarcerands mentioned previously, encapsulation must be carried out using a solvent that is too large for encapsulation, or in a bulk liquid phase of the guest molecule. The encapsulation in bulk guest is difficult, because BVs generally form a viscous oil or waxy solid and so is not as capable at dissolving H**3** as other guests. The solvent of choice for Cram *et al.* in their initial 1991 paper was tripiperidyl phosphine oxide **33**, synthesised from the combination of phosphoryl chloride **32** and six equivalents of piperidine (Scheme 15).[43]

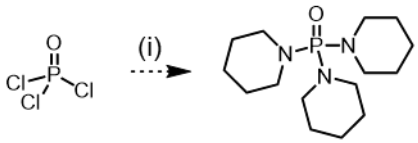

32 **33**

*Scheme 15: Synthesis of tripiperidyl phosphine oxide **36**. (i) Piperidine, MeCN, rt, 6 h, crude mixture obtained.*

As of yet, it has been challenging to drive this reaction to completion, and as such, some residual **34** and **35** remain present (Figure 6). Vacuum distillation at very high temperature and low pressures is usually required to separate **33** from these side products, as such, a method that would push this reaction to completion would be preferred.

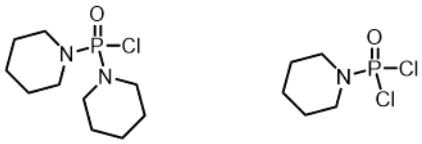

34 **35**

*Figure 6: Residual side products from formation of **36.***

This work is still ongoing and once the solvent has been synthesised, attempts at encapsulating different BV species will be undertaken. However, other work was carried out simultaneously which yielded more promising results.

4.4 Octa-Acid Host

The octa-acid host is a cavitand with a deep, hydrophobic cavity capable of binding hydrocarbon guests readily in aqueous solutions.[44–46] This part of the project was performed in collaboration with the Gibb group at Tulane University, who first synthesised this particular cavitand host.[44]

The synthesis of this compound (Scheme 16) begins with the acid catalysed, thermodynamically controlled reaction of resorcinol **2**, with an aldehyde substitute **36** in methanol to form **37**. Calixarene **37** is then rigidified by reaction with **38** (which is synthesised in one step from dibromobenzaldehyde) to form tetrabromide **39**. Reaction with 3,5-dihydroxybenzyl alcohol **40** results in the formation of octa-ol **41**, which undergoes a Parikh–Doering oxidation to form octaaldehyde **42**. This is the only step

which is purified chromatographically. Further oxidation of **42** results in the formation of the desired octa-acid cavitand host **H4** which may then be used in binding studies.

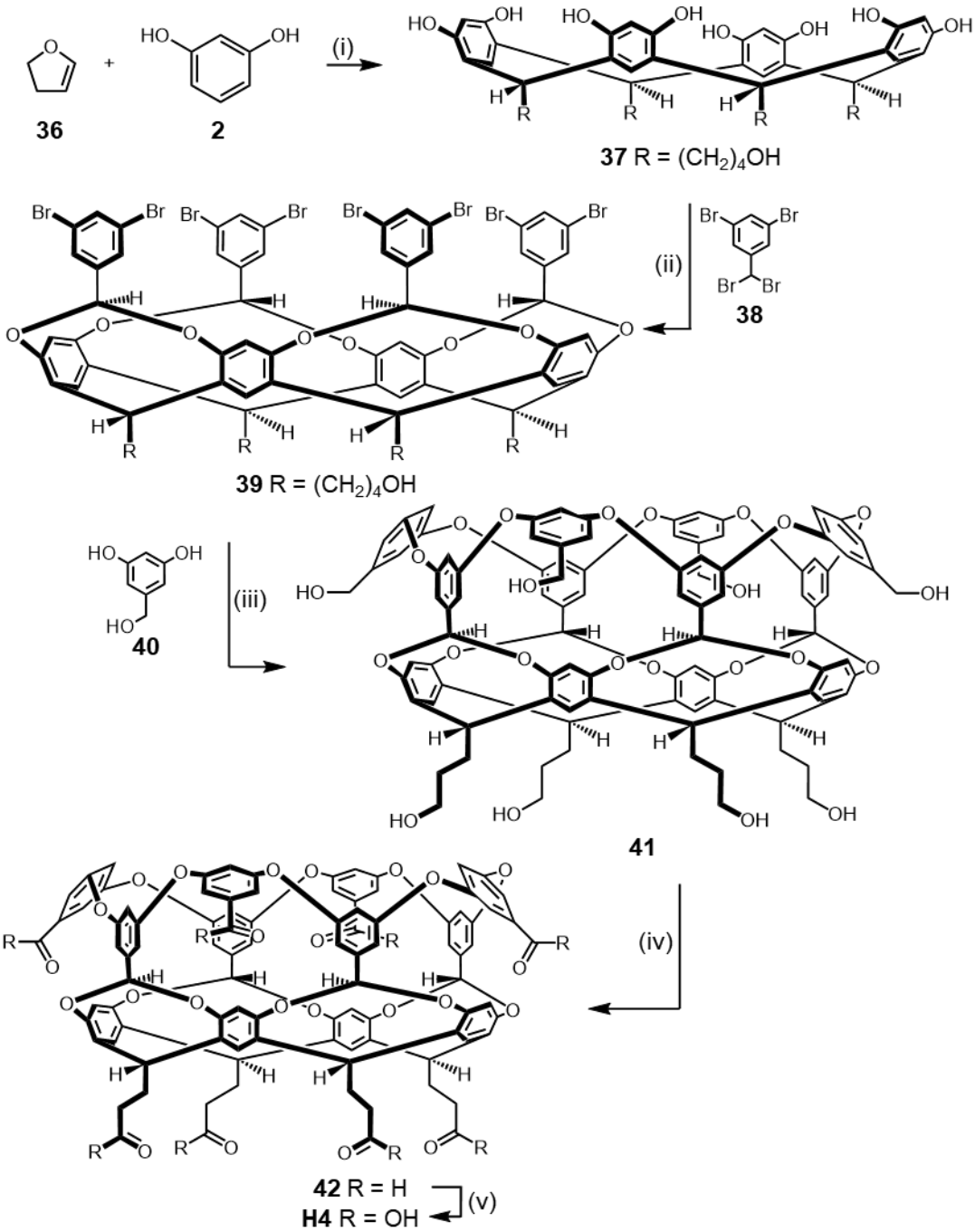

*Scheme 16: Synthesis of octa-acid cavitand **H4**. (i) HCl / MeOH, 50 °C, 5 d, 82%. (ii) **38**, DBU, DMA, 50 °C, 2 d, 45%. (iii) **40**, K_2CO_3, CuBr, pyridine, reflux. (iv) SO_3.pyridine complex, NEt_3, DMSO. 45% (v) NaH_2PO_4, $NaClO_2$, DMSO, 60 °C, 74%*

The guests selected for these binding studies were **BV**, diethyl BV **28**, and pentyl BV **47** (Figure 7). All three of these guests were synthesised using the same methods discussed in Scheme 11, from relevant BDTs as intermediate compounds.

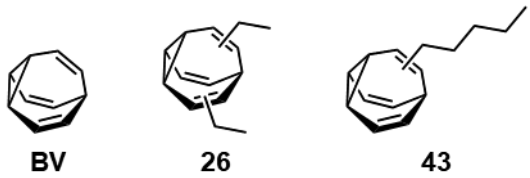

*Figure 7: The BVs selected as appropriate guests for Octa-acid host **H4**.*

The first guest to be bound was **BV** (Figure 8). On account of the broadening of **BV**'s ^{1}H NMR signals (a result of its rapid rearrangements) and the low analyte concentration, none of the proton signals are observed in the spectrum of the complex. However, it may be observed easily that the peaks corresponding to the host protons are shifted, suggesting encapsulation.

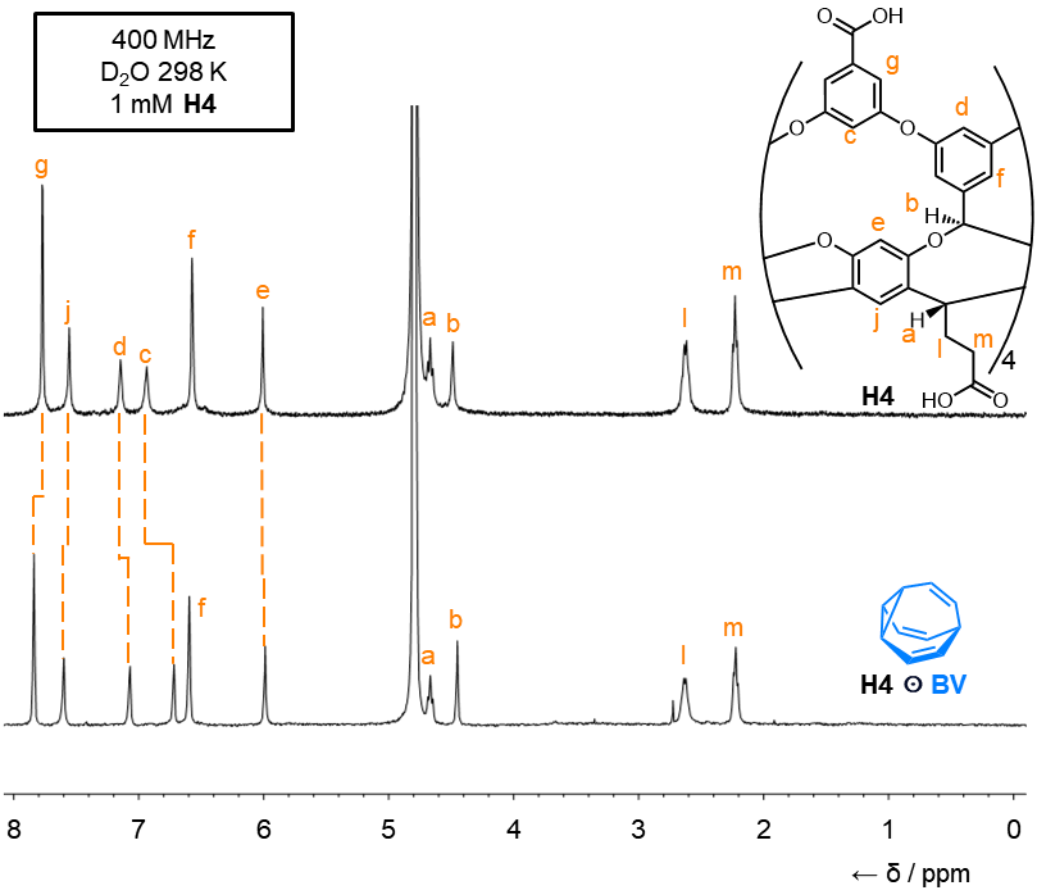

*Figure 8: ^{1}H NMR spectra of the unbound host **H4** and the complex of **H4** and **BV**.*

In order to better observe the encapsulation of BVs in **H4**, substituted BVs should be used. Hence, alkyl-substituted BVs **26** and **43** were selected (Figure 9), due to **H4**'s previously reported ability to bind to long alkyl chains.[45,46]

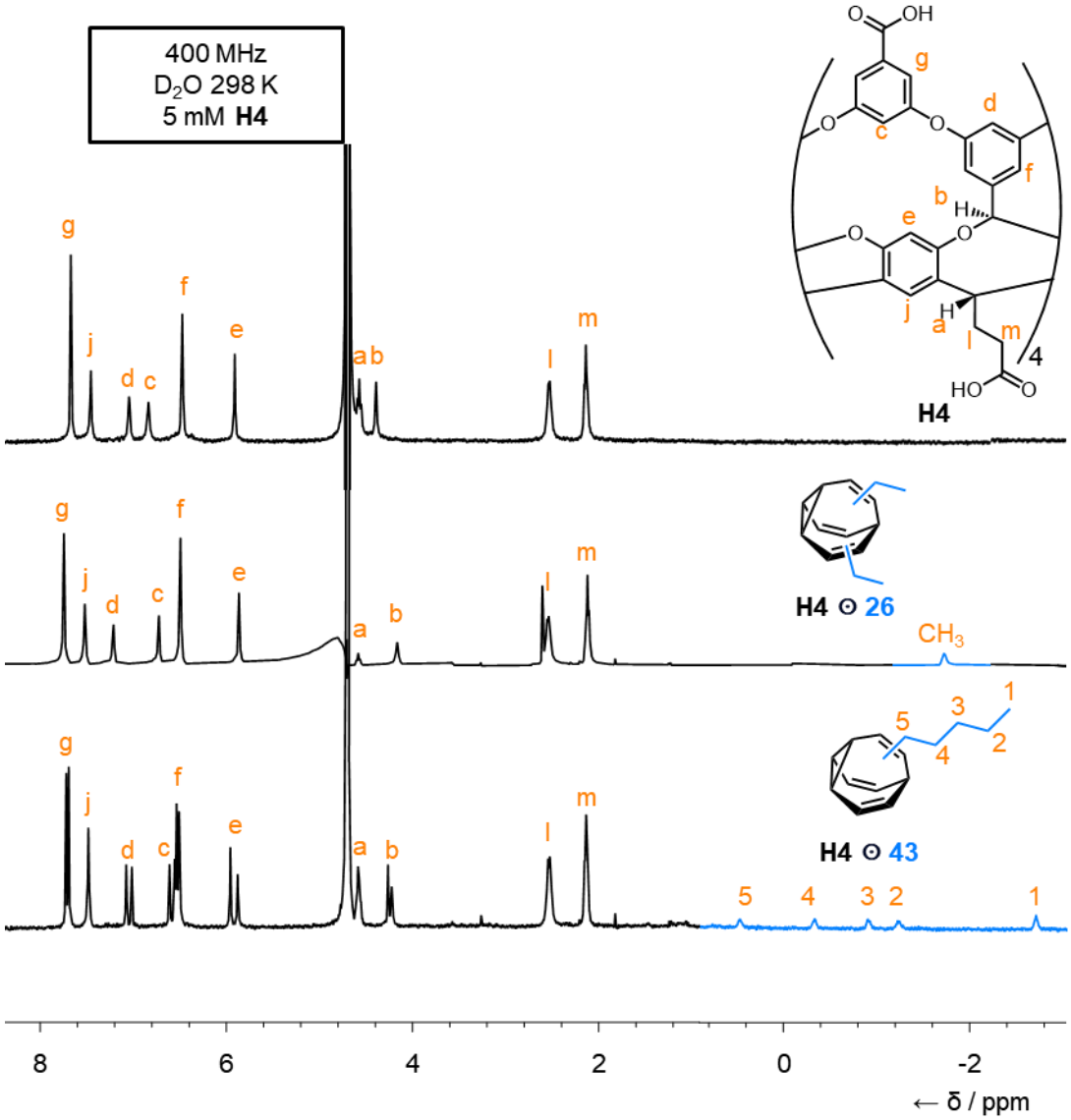

*Figure 9: ^{1}H NMR spectra of the unbound host **46** and the complexes of **28** and **47** with **46**.*

Peaks corresponding to the alkyl substituents are clearly visible in these spectra, all of which are shifted upfield as a result of their encapsulation in **H4**. A particularly interesting result is the desymmetrization of the host signals in the spectrum for **H4 ⊙ 43**, which are doubled in close proximity to one another. This is most likely due to the asymmetry of the complex **H4 ⊙ 43**. Similarly, Δδ increases as alkyl peaks are encapsulated further into the hydrophobic cavity, so the separation of peaks 1 to 5 would imply a structure where the BV core is encapsulated in one side of the capsule dimer, with the alkyl chain present in the other side (Figure 10). All three complexes

were analysed by DOSY NMR spectroscopy, in order to evaluate their binding mode. As was established in Chapter 1, the octa-acid host **H4** is capable of forming 1:1, 2:1, and 2:2 complexes with different molecular guests. For **BV**, **26** and **43** the diffusion coefficient values connote the presence of only 2:1 complexes.

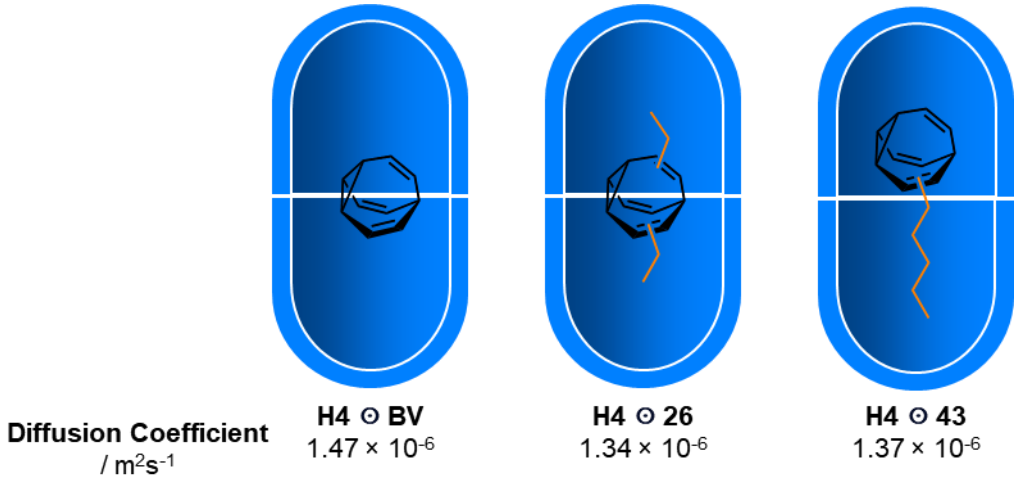

*Figure 10: Illustration of complexes of **BV**, **25**, and **43** with **H4**.*

With encapsulation established, in order to further analyse the complexes that have formed, variable temperature ^{1}H NMR spectroscopy is required. However, due to the encapsulation taking place in aqueous solution, low temperature NMR spectroscopy is limited to 0 °C. For this reason, methods of freezing point depression must be investigated. Two routes were initially considered. Firstly, the addition of salts to aqueous solutions is known to cause freezing point depression. For example, a saturated solution of sodium chloride (23.3% w/w) freezes at −21 °C, and a 29% w/w solution of calcium chloride freezes as low as −50 °C. This is a highly efficient method of freezing point depression, however, addition of high concentrations of salts is known to result in poor shimming, and lower quality data. The second method is through the addition of methanol (Table 1).

Table 1: Freezing point depression of methanol water mixtures.

% vol MeOH	**13**	**24**	**35**	**46**	**56**
F.P. / °C	−7	−18	−26	−40	−54

One difficulty experienced in achieving freezing point depression of our system using this method is that the encapsulation is occurring *via* the hydrophobic effect. Thus, as the proportion of methanol in bulk solution is increased, the guest will become more soluble in the bulk solution, and encapsulation will become less efficient. When higher

proportions of methanol are used, the capsule may shuttle between an open state, where the guest is not present in the cavity, and a closed state, where the guest is encapsulated. Shuttling introduces an additional dynamic feature is which must be resolve, further to the resolution of BV's Cope rearrangements. Addition of methanol to a **H4 ⊙ 43** complex results in the alteration of different host resonances (Figure 11). Some resonances broaden and coalesce, whilst others split into two peaks. Most notably, the peaks representing bound **43** at 0.54 ppm and −2.66 ppm are no longer observed. This may suggest that shuttling of the host capsule is occurring, or that a molecule of deuterated methanol has become encapsulated. In either case, the substituent on **43** may be present in two different environments, resulting in the peak broadening into the baseline. A further experiment with non-deuterated methanol may confirm this hypothesis but is yet to be undertaken.

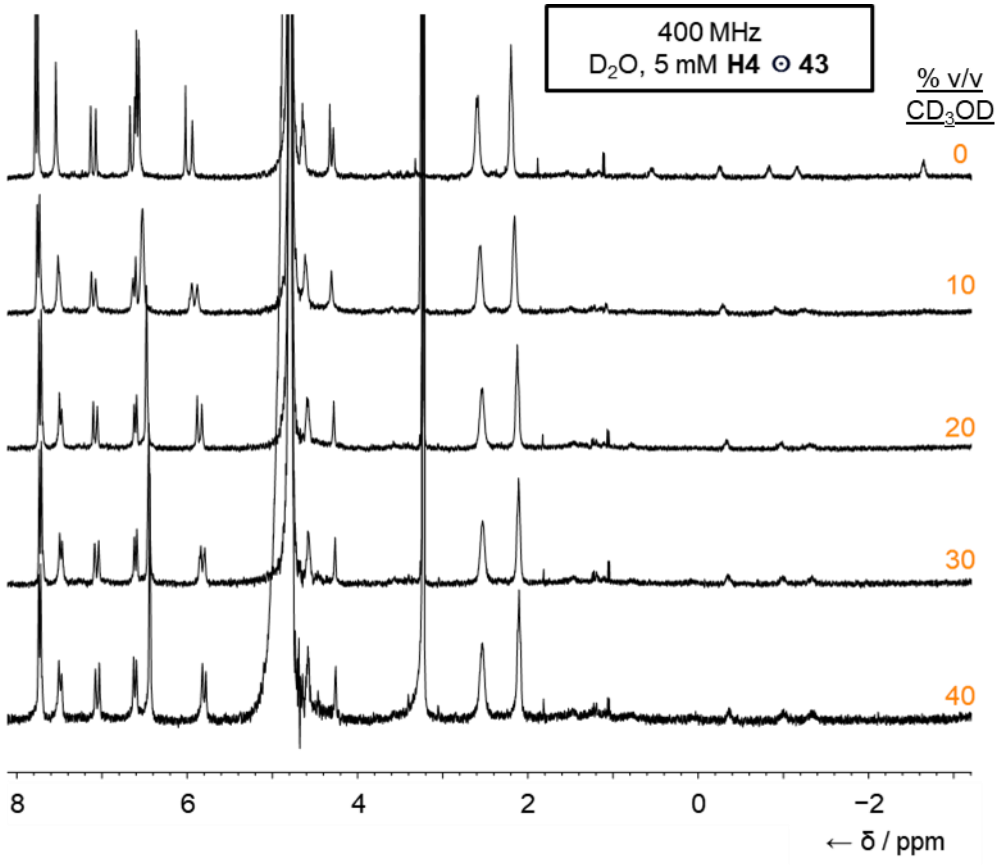

*Figure 11: Addition of CD_3OD to a **H4 ⊙ 43** complex to investigate complexation change.*

For these experiments, diethyl BV **26** was investigated due to its disubstituted nature. This means that the rearrangement will more likely be limited, compared to monosubstituted BVs where rearrangement may be accompanied by rotation/ translation of the cage, resulting in less control imposed by steric constraints.

Preliminary experiments have included performing low temperature ^{1}H NMR spectroscopy on 5 mM solutions of a **H4 ⊙ 26** complex in 9:1 water: methanol (Figure 12). This ratio of water to methanol lowers the freezing point of the solution to around −6 °C.

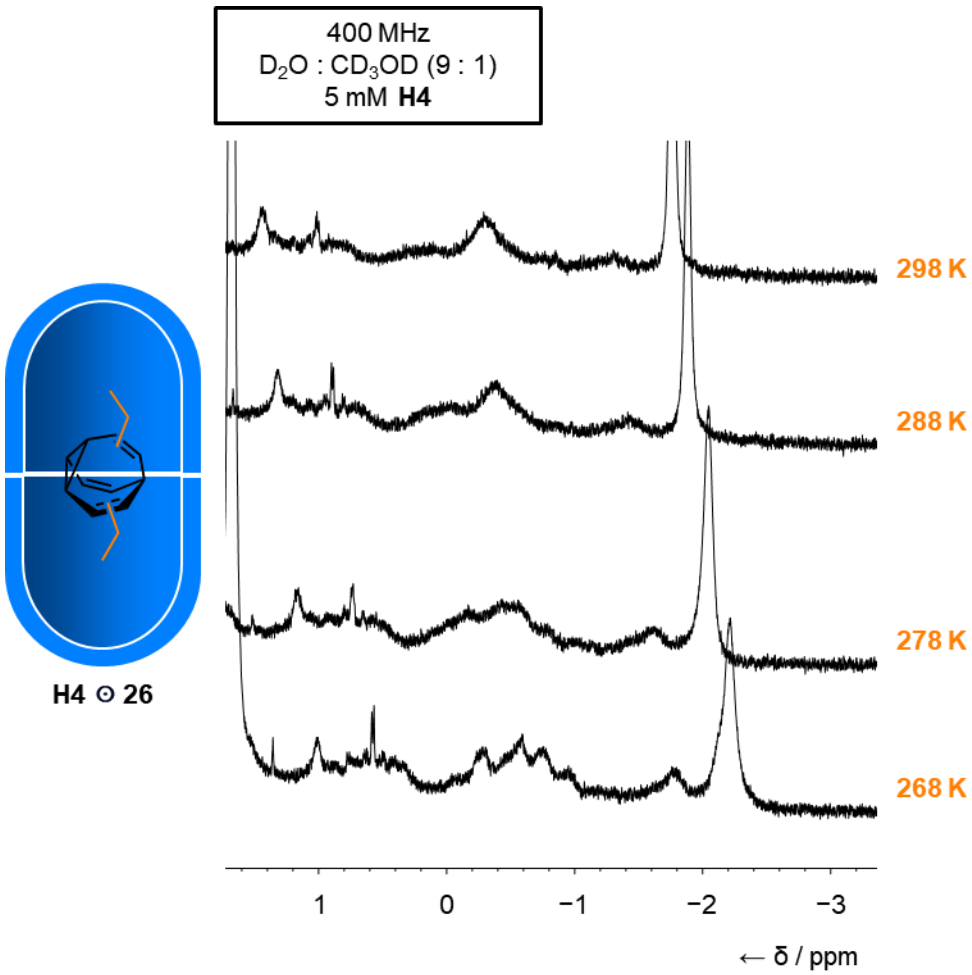

*Figure 12: Low temperature partial ^{1}H NMR spectra of the **H4 ⊙ 26** complex in water/ methanol mixture.*

Whilst this work is only exploratory in nature, it is clear to see that the broad peaks observed at room temperature appear to deconvolute near 268 K. Furthermore, some peaks in the spectrum begin to sharpen from an initially broad state in the baseline. This is indicative of the rearrangements of **26** occurring more slowly at these temperatures. When performing low temperature ^{1}H NMR spectroscopic analysis of BVs free in solution, this level of definition is usually only observed at low temperatures (≤ 243 K). Thus, although no concrete conclusions are to be drawn from these initial results, they do suggest that encapsulation may be a plausible method of exerting control over BV's fluxional behaviour. This result may be seen as an indication to keep investigating, as opposed to a conclusion in and of itself.

As a result of these initial findings, more BVs with longer alkyl chains (**44**–**46**, Figure 13) are currently being synthesised to monitor the extent to which their rearrangement may be affected by their encapsulation in the octa-acid host **H4**. Increasing the length of the chain will hopefully increase the strength of host–guest interactions, further slowing rearrangements.

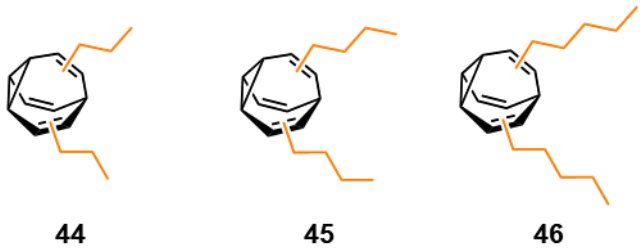

*Figure 13: New potential BV guests for use in octa-acid host **H4**.*

4.5 Cyclodextrin Hosts

The final potential molecular host for BV explored in this thesis is β-cyclodextrin (**β-CD)**. According to Fallon *et al.*'s computational publication, substituted BVs are well-suited to bind to **β-CD**.[47] Initially, a solution of **β-CD** and BV **26** in water was crystallised by slow evaporation of the solvent over a period of weeks. The result was a crystal structure with two diethyl BVs **26** present in two **β-CD** cavities. However, the structure of the two BVs was disordered inside the cavity, showing an undefined cage in both cavities, which had their 1° faces directed towards one another. (Figure 14).

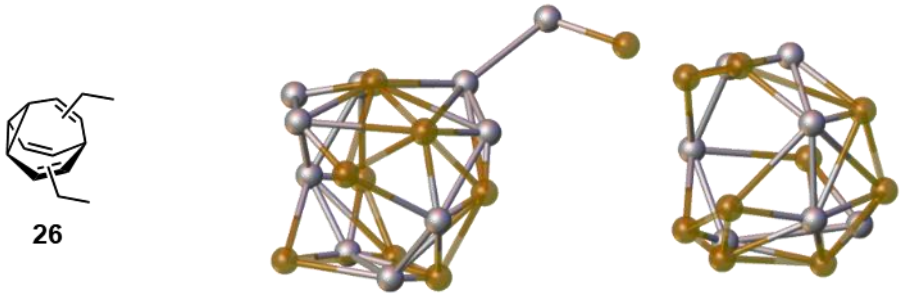

*Figure 14: Structure of BV **26** and unresolved crystal structure inside β-CD cavity. The β-CD is not shown.*

This result, while disappointing, did prove experimentally that **β-CD** may act as a molecular host for substituted BVs. Our aim in this project therefore was to exhibit how this interaction may exert control over the rearrangement of the fluxional BV species.

As mentioned in Chapter 1, there are many examples in literature for supramolecular polymers involving CDs with small hydrophobic tethers, as well as intramolecular complexes with tethered CDs (Figure 15).[48,49]

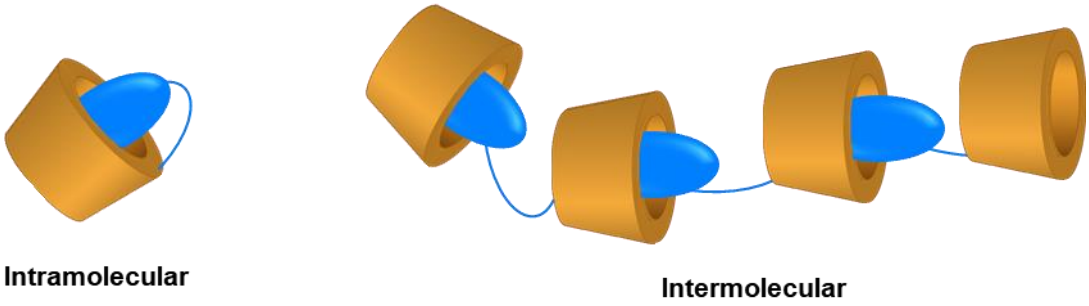

Figure 15: Illustration of possible complex formations of tethered CDs.

Our first step towards the formation of these complexes is the functionalisation of **β-CD**, which may be achieved through a path of tosylation, forming **47**, followed by azidation in the presence of sodium azide and potassium iodide to form **48**. Finally, a Staudinger reduction is performed on the azido-CD **48** to yield monoamino-CD **49** in reasonable yield (Scheme 17).

This synthesis achieves in three steps a large quantity of amino-CD **49**, without requiring chromatography. Instead, each functionalised β-CD may be isolated from the reaction mixture through differences in solubility alone.

There are several literature procedures which differ in both purification as well as reagents for step (iii) in Scheme 17. In particular, multiple literature procedures use "concentrated aqueous ammonia"[50] (ammonium hydroxide solution[51]) in the final step converting **48** to **49**. This is not necessary, as a Staudinger reduction only requires triphenylphosphine and water in order to convert an azide to an amine.[52] There is one synthesis which converts **47** directly to **49** by stirring for seven days in the presence of ammonium hydroxide, however, our synthesis is overnight for each step and so **49** is obtained much more quickly.[53] In general, the procedure performed was closest to that published by Carmona *et al.* in 2021.[54]

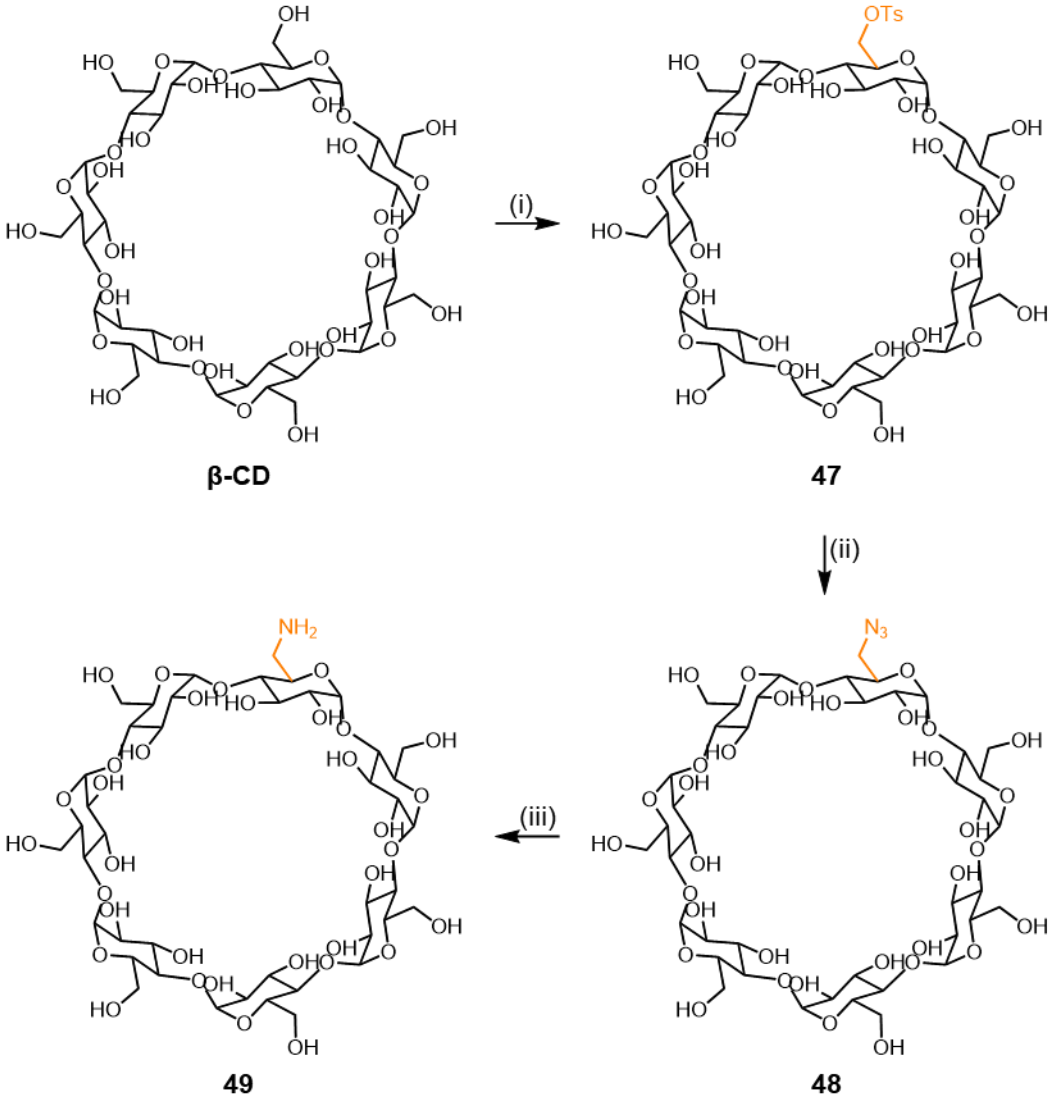

*Scheme 17: Synthesis of **49** from β-CD. (i) p-TsCl, NaOH, H_2O, rt, 1 h, 29%. (ii) NaN_3, KI, DMF, 65 °C, 18 h, 74%. (iii) PPh_3, H_2O, DMF, rt, 18 h, 84%.*

Previous work in the group involved a reductive amination of **BBO** with **49** in order to form tethered β-CD **50** (Scheme 18).

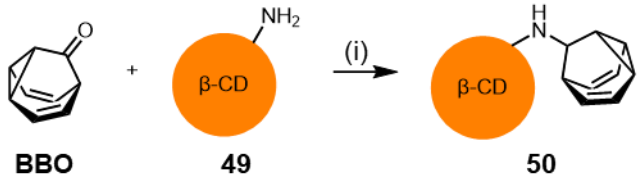

*Scheme 18: Synthesis of **BBO**- β-CD complex **50**. (i) $NaCNBH_3$, MeOH, AcOH, 60 °C, 18 h.*

Single-crystal X-ray analysis of the resulting complex **50** confirmed the formation of a supramolecular polymer structure (Figure 16). This demonstrates that this kind of complex is possible with fluxional molecules. Unfortunately, inside the β-CD cavity, the barbaralane (BB) structure was not resolved, as it may still rearrange between its

two isomeric forms *via* a Cope rearrangement. The absence of any further substitution on the BB cage results in no selectivity for either isomer in the intermolecular structure.

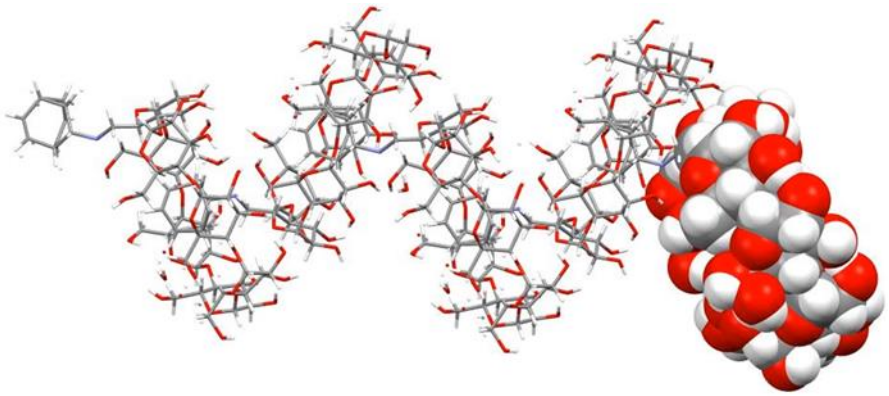

*Figure 16: Crystal structure of **50**, exhibiting supramolecular polymer structure.*

It may be observed from this crystal structure that the adjacent units of **50** alternate in a repeating pattern of two units. The helicity and orientation of this structure may be altered and tailored by changing the nature and length of the tether as exemplified by Inoue *et al.* in 2003.[55]

4.5.1 Tosyl Bullvalenes for Complex Formation

The first method attempted for the formation of a BV analogue of complex **50** was based on first forming a tosylate bullvalene, which could then undergo a nucleophilic substitution, using amino-β-CD **49** as the nucleophile. It is important that the BV-β-CD formed has another substituent present on the BV core so that the different isomers may be distinguished inside the β-CD cavity. For this reason, an ethyl substituent is introduced to the BV, which can both act as an anchor into the β-CD cavity and potentially allow for a biasing of the isomer distribution. To begin, 2-pentyn-1-ol **51** is used to form BDT **52**, and subsequently BV **53** (Scheme 19). Heterodisubstituted BV **53** has 30 unique isomers, nine pairs of enantiomers and 12 achiral isomers.

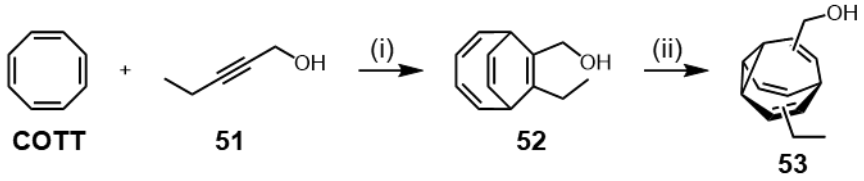

*Scheme 19: Synthesis of BV **53**. (i) $CoBr_2$(dppe), ZnI_2, Zn Dust, TFE, 55 °C, 18 h, 76%. (ii) Thioxanthone, THF, 365 nm, rt, 6 h, 76%.*

Attempts to tosylate **52** and **53** resulted in very little conversion to product, and our attempt at purification by chromatography resulted in the formation of a bright blue impurity. Due to conjugation present in both **52** and **53**, it is proposed that some type of elimination in either cage may be occurring. Furthermore, tosylating **51** was successful, giving tosylated alkyne **54**, however, no evidence of **55** was ever found by ^{1}H NMR spectroscopy or mass spectrometry following attempted cycloadditions (Scheme 20).

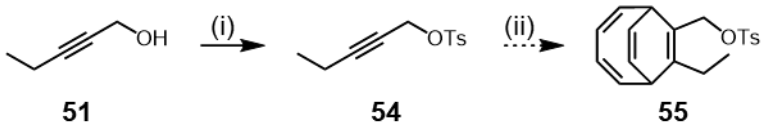

*Scheme 20: Attempted synthesis of tosyl BDT **55**. (i) TsCl, KOH, Et_2O, 0 °C, 4 h. (ii) $CoBr_2(dppe)$, ZnI_2, Zn Dust, TFE, 55 °C, 18 h. No product obtained.*

As a result of the failure to yield tosylated BDTs or BVs by this route, it was determined that an alternative route to form BV-β-CD was required.

4.5.2 Reductive Amination Pathway

The pathway that was chosen next was based upon the Swern oxidation of BV **56** to form dialdehyde BV **57** (Scheme 21) reported by Fallon *et al.*, who then subjected **57** to a nucleophilic attack to form two point chiral centres appended to the BV core.[56,57] This is not, however, the first synthesised BV aldehyde, which was by Schroder *et al.* in 1983.[15]

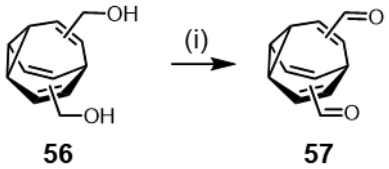

*Scheme 21: Swern oxidation of **56** to form **57**. (i) $(COCl)_2$, DMSO, NEt_3, −78 °C, 4 h, 78%.*

Swern oxidation of **53** was performed to yield BV **58**, which occurred readily (Scheme 22). However, this aldehyde is unstable and degrades back into **53**, as well as a number of potential different aldehydes.

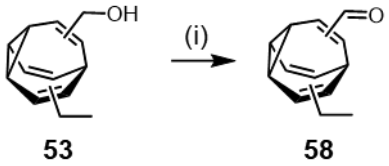

*Scheme 22: Synthesis of aldehyde BV **58**. (i) $(COCl)_2$, DMSO, NEt_3, −78 °C, 4 h.*

The instability was observed after a crude reaction mixture was left over a period of three days. The formation of **58** can be confirmed by the broad aldehyde peak around 9 ppm (Figure 17). It is clear that some BV has degraded in the reaction by the sharp peaks around 4 and 6 ppm, but **58** still constitutes the majority of the mixture. After three days, the broad aldehyde peak was no longer observed, and other sharp peaks between 9–10 ppm have appeared, connoting the degradation of the BV core in **58** to other aldehydes. Supporting this theory is the presence of much larger sharp peaks, exhibiting non-fluxional compounds. Moreover, broad peaks are observed around 2, 4 and 6 ppm, distinctive of BV, which would signify degradation of the aldehyde motif to other BV structures. On account of these two potential degradation pathways, the aldehyde should be used *in situ*.

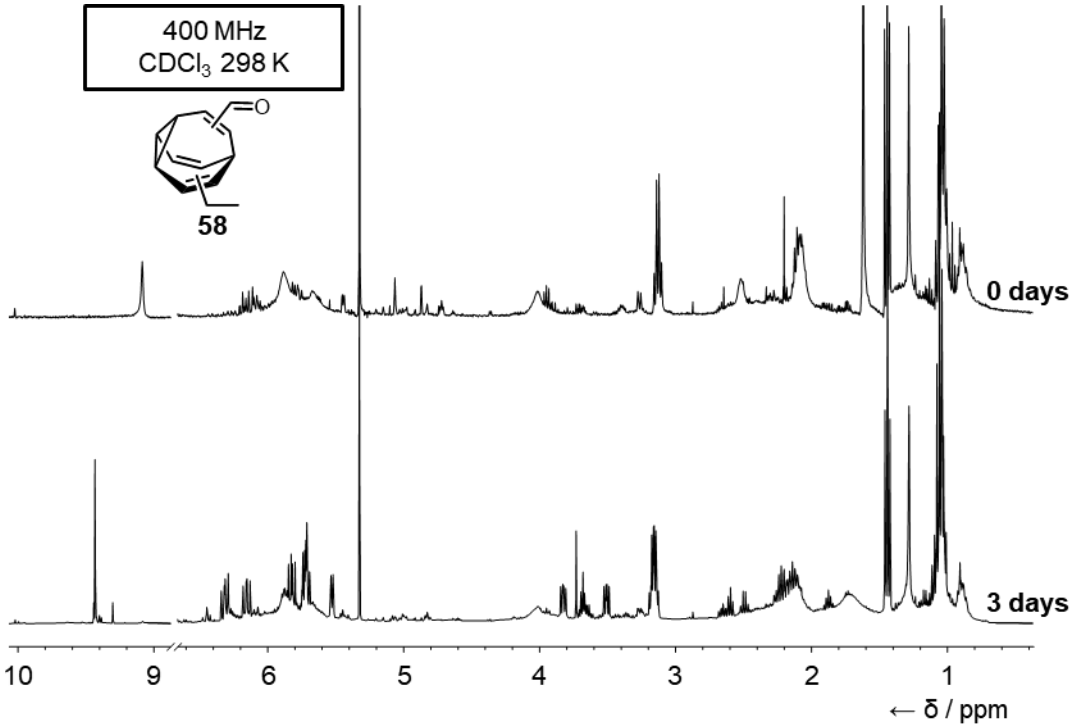

*Figure 17: ^{1}H NMR spectra of the crude mixture for the formation of **58** immediately after reaction, and 3 days later.*

Crude mixtures of **58** are therefore used in lieu of possible purification, in attempts to add amino β-CD **49** by a reductive amination pathway (Scheme 23).

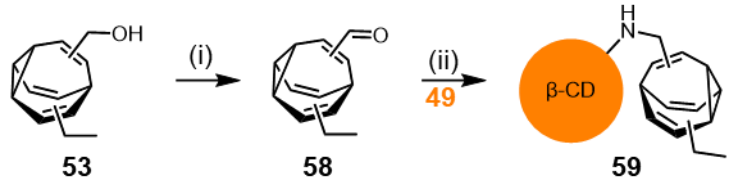

*Scheme 23: Synthesis of BV-β-CD complex **59**. (i) $(COCl)_2$, DMSO, NEt_3, −78 °C, 4 h. (ii) **53**, AcOH, $NaCNBH_3$, DMF, 100 °C, 18 h.*

DMF was chosen as the solvent for this reaction, due to the poor solubility of the reactants and products. At the end of the reaction, the mixture was poured onto acetone, which precipitates both **49** and **59**. This precipitate is then isolated and washed with methanol, which **49** is scarcely soluble in, but **49** is insoluble in, thus isolating a potential product. Mass spectrometry identified a peak that may correspond to **59**, however, it should be noted that potential side products from the degradation of the BV core in **59** may have the same molecular mass. Therefore, while this does suggest the complex may have formed, it does not negate the possibility of degradation to side products. ^{1}H NMR spectroscopic analysis was also undertaken in DMSO-d_6, however, due to the already broad peaks of both BV, as well as mono-substituted β-CDs, no conclusions may be confidently drawn from the data gathered.

The aim of this project is to form a single crystal of **59**, with the hope that one single BV isomer would be present due to its energetic preference inside the β-CD cavity. This is another reason why β-CDs were chosen specifically—due to their chiral cavity. If one isomer does preferentially bind over others in a potential supramolecular polymer structure, it will also selectively bind one enantiomer over another, meaning that each of BV **59**'s 30 isomers will have a unique binding mode in the β-CD's binding pocket.

No crystals were observed in any experiment (Table 2), potentially due to the presence of impurities, or presence of both intramolecular and intermolecular complexes (Figure 15). The formation of amorphous solid was instead the result of most experiments.

*Table 2: Crystallisation attempts for **59**.*

Technique	Solvent	Antisolvent
Slow Cooling	H_2O	–
Slow Cooling	DMF	–
Slow Evaporation	H_2O	–
Slow Evaporation	DMF	–
Slow Evaporation	MeOH	–
Vapour Diffusion	H_2O	EtOH
Vapour Diffusion	H_2O	Acetone
Vapour Diffusion	DMF	Toluene

Layer Diffusion	H_2O	MeOH
Layer Diffusion	H_2O	EtOH
Layer Diffusion	H_2O	THF
Layer Diffusion	DMF	MeOH
Layer Diffusion	DMF	EtOH
Layer Diffusion	DMF	THF
Layer Diffusion	DMF	H_2O
Layer Diffusion	MeOH	CH_2Cl_2
Layer Diffusion	MeOH	$CHCl_3$
Layer Diffusion	MeOH	THF
Layer Diffusion	MeOH	DCE
Layer Diffusion	MeOH	Toluene
Layer Diffusion	MeOH	EtOAc

As discussed previously, the length and type of linker in tethered β-CD compounds such as **59** determine their binding mode, and the orientation of the neighbouring complexes. As such, an analogue of **59** was synthesised with a slightly longer tether (Scheme 24). The longer tether was installed by using 3-hexyn-1-ol **60** in the cycloaddition with **COTT** to form BDT **61**. This is rearranged to form BV **62**, which undergoes a Swern oxidation to form **63** and reductive amination to yield **64**.

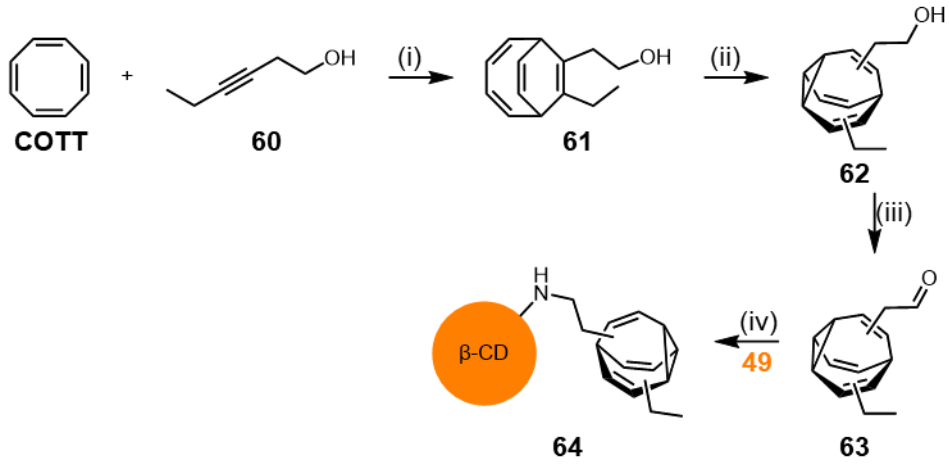

Scheme 24: Synthesis of BV-β-CD complex ***64****. (i) $CoBr_2$(dppe), ZnI_2, Zn Dust, TFE, 55 °C, 18 h, 61%. (ii) Thioxanthone, THF, 365 nm, rt, 6 h, 38%. (iii) $(COCl)_2$, DMSO, NEt_3, −78 °C, 4 h.. (ii)* ***53****, AcOH, $NaCNBH_3$, DMF, 100 °C, 18 h.*

Under all of the same crystallisation conditions, again, no crystals were obtained. Attempts at using prep HPLC, to purify samples of **59** and **64** are currently underway

however, we are still awaiting the data. Crystallisation may be made more facile with a pure sample of the BV-β-CD complexes

4.5.3 Alternative Tethered Structure

We are currently working toward the synthesis of an alternative structure, which replaces the ethyl group on the BV cores of **59** and **64** with an aromatic ring. The hypothesis is that the more rigid binding anchor will remove the ability for the intramolecular complex to form, resulting in the crystallisation of only a supramolecular polymer.

The difficulty in synthesising this molecule is caused by the installation of the aromatic ring. As discussed in Fallon *et al*.'s work regarding BV synthesis, aromatic rings present during the photorearrangement step result in majority lumibullvalene products, and no desired BV will form. As a result, to introduce aromatic groups, boronate esters are installed on alkynes and Suzuki couplings performed on the resulting boronate ester BV.[33,58]

Therefore, the BV needs both an alcohol for eventual Swern oxidation and reductive amination with amino-β-CD **49**, as well as a boronate ester for coupling of the aromatic group (Scheme 25). Starting with propargyl alcohol **21**, silyl protection results in alkyne **65** which may be lithiated and subsequently borylated, resulting in alkyne **66**. Alkynic boronate esters are more prone to protodeborylation than alkenic boronate esters. As such, the cycloaddition was undertaken before deprotecting the alcohol. BDT **67** is thus formed, which is as far as this synthesis has currently progressed. The future of this synthesis will be deprotection to BDT **68**, followed by photorearrangement to **69**, and subsequent Suzuki–Miyaura coupling to **70**. Finally, a Swern oxidation and reductive amination will form BV-β-CD complex **71**. Work on this route is still ongoing.

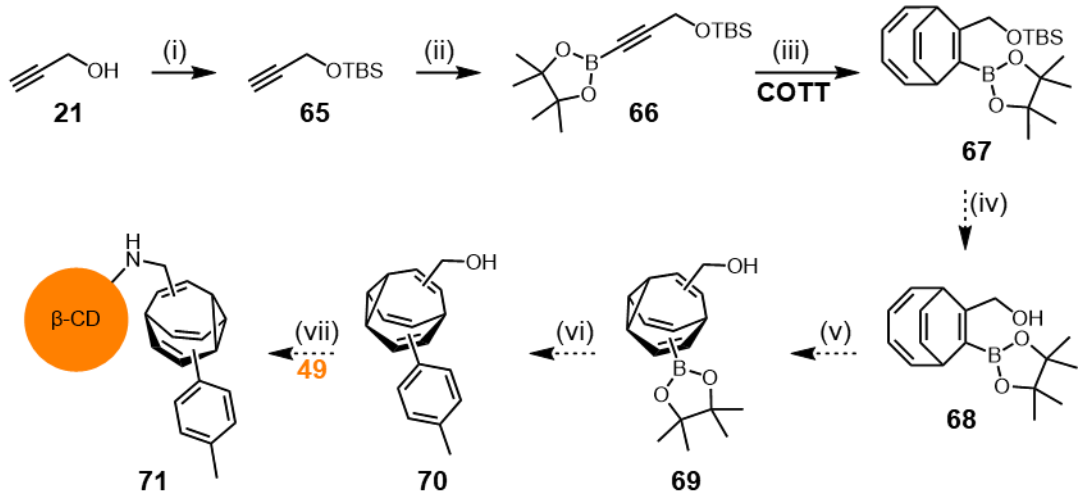

*Scheme 25: Proposed synthesis of BV-β-CD complex **71**. (i) TBS-Cl, imidazole, 0 °C, 2 h, 71%. (ii)(a) ^{n}BuLi, THF, −78 °C, 1 h. (b) ^{i}PrOBpin, THF, −78 °C, 2 h, 90%. (iii) $CoBr_2(dppe)$, ZnI_2, Zn Dust, DCE, rt, 18 h, 40%. (iv) Deprotection of alcohol. (v) Photorearrangement. (vi) Suzuki Coupling. (v)(a) Swern (b) Reductive Amination.*

4.5.4 Methylated Cyclodextrins

The final attempted example of supramolecular complexes of BV is the use of permethylated β-CD **72**. Compound **72** may be synthesised in a single step from **β-CD** using sodium hydride and methyl iodide (Scheme 26).[59]

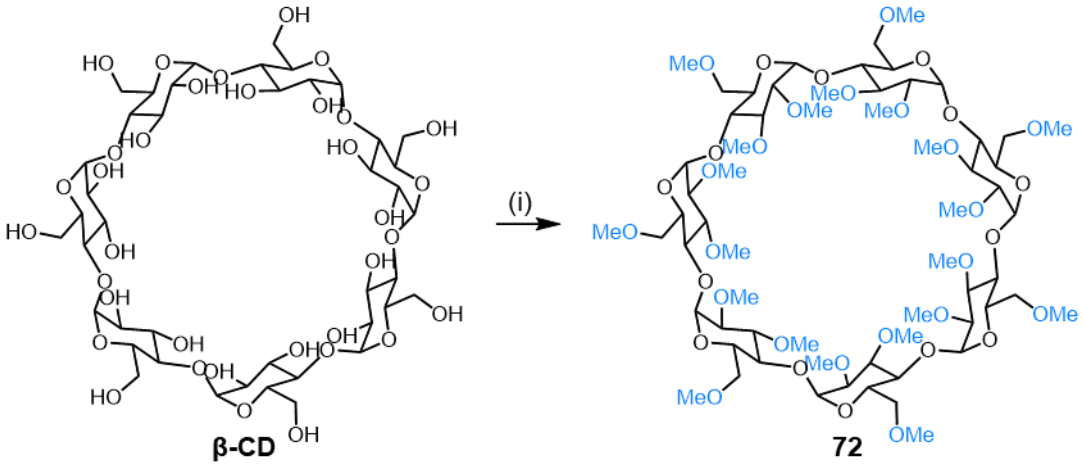

*Scheme 26: Synthesis of **72** from **β-CD**. (i)(a) NaH, DMSO, rt, 1 h. (b) MeI, 0 °C to rt, 24 h, 52%.*

Compound **72** as a modified β-CD is soluble in organic solvents, and as such is an appropriate host for BV binding studies. Firstly, however, a suitable BV should be synthesised. Trichloroethylene **73** may be converted to bis-Bpin alkyne **74** *via* lithium carbide. **74** may then undergo a cycloaddition with **COTT** to form bis-Bpin BDT **75**. Photorearrangement gives bis-Bpin BV **76**. Following the formation of **76**, *p*-

bromofluorobenzene was used in a Suzuki coupling, resulting in the formation of **1**, a homodisubstituted BV (Scheme 27).[33,60]

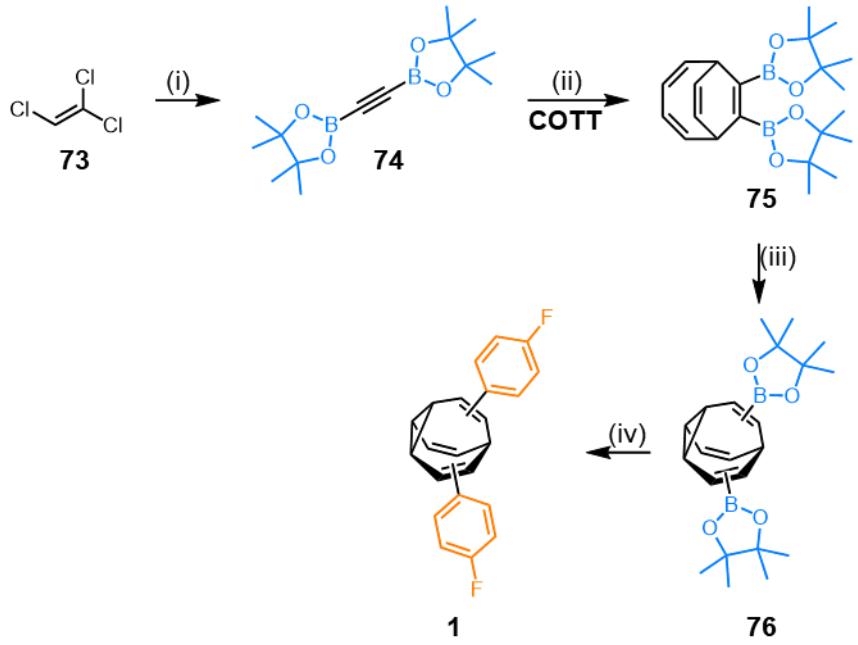

*Scheme 27: Synthesis of BV **1**. (i)(a) ^{n}BuLi, THF, Et_2O, −78 °C to rt, 12 h. (b) ^{i}PrOBpin, −78 °C to rt, 6 h, 69%. (ii) **COTT**, $CoBr_2(dppe)$, ZnI_2, Zn Dust, DCE, rt, 18 h, 66%. (iii) Thioxanthone, THF, 365 nm, rt, 6 h, 63%. (iv) p-BrFPh, $Pd(PPh_3)_4$, THF, 10% $NaOH_{(aq)}$, 60 °C, 18 h, 43%.*

BV **1** was selected for binding to **72** due to the presence of rigid linkers to the BV core, such as to emphasise the binding modes of unique isomers. Furthermore, the presence of fluorine atoms makes analysis *via* ^{19}F-CPD (carbon proton decoupled) NMR spectroscopy possible.

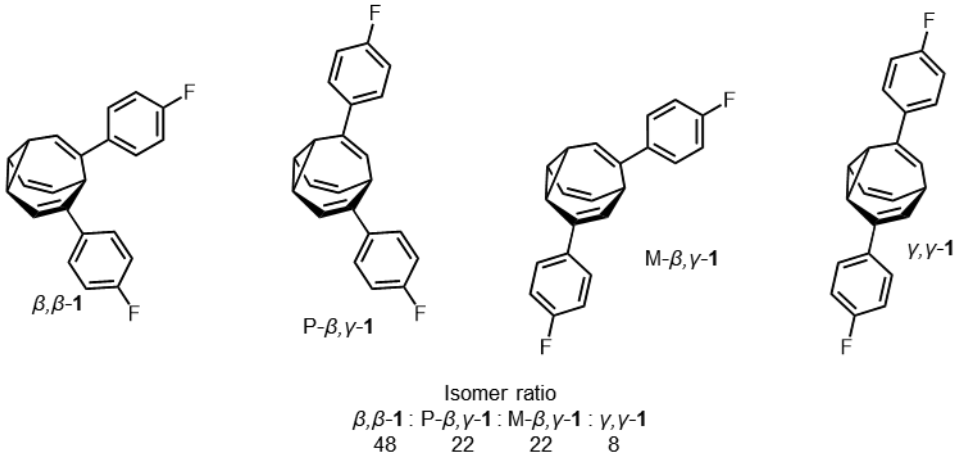

*Figure 18: Isomers of **1** present in solution according to NMR spectroscopy.*

As a homodisubstituted BV, **1** is capable of occupying any one of 15 unique isomers, including three enantiomer pairs. Low temperature NMR spectroscopic analysis has determined that of these 15 isomers, only four are present in significant amounts, these

are the *β,β*-, P-*β,γ*-, M-*β,γ*- and *γ,γ*- isomers (present in a 48:22:22:8 ratio respectively, Figure 18).

In the binding studies, a hexafluorobenzene capillary is used for referencing in the ^{19}F CPD NMR spectra. The reference is added in a capillary to ensure that there is no competitive binding with other species in solution. Preliminary experimental data exhibit **1** binding in the cavity of **72**, which may be observed in the splitting of each peak in the ^{19}F CPD NMR spectrum. The chiral nature of **72**'s cavity breaks the symmetry of the different isomers of **1**, resulting in peak splitting (Figure 19).

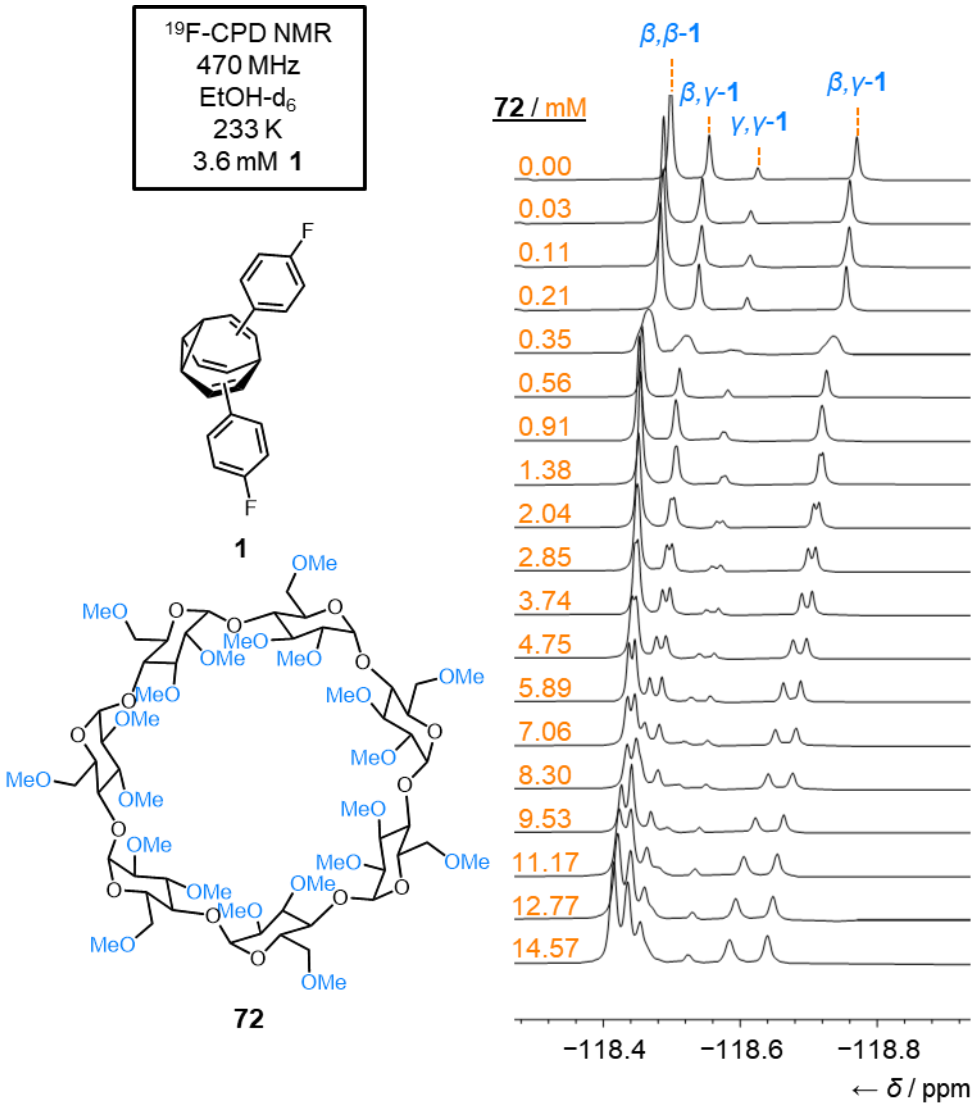

*Figure 19: ^{19}F NMR titration of host **72** into **1**.*

The next step for this project is to determined binding constants for each isomer individually, and to analyse whether the isomer distribution changes due to preferential binding with one isomer over another. However, one difficulty in examining the individual binding constants is that it may not be assumed that

rearrangements only occur when **1** is free in solution. In reality, Cope rearrangements may occur when **1** is in the bound state, resulting in potentially different transition state energies between similar isomers. Work is ongoing to deconvolute the two processes and further to probe how the rearrangements of **1** are altered in binding events with **72**.

4.6 Conclusions and Future Work

Throughout this project, multiple novel BVs have been successfully synthesised and analysed. Furthermore, several novel manipulations of the BV cores have been attempted, both successful, such as reductive aminations on **58** and **63** as well as unsuccessful manipulations such as tosylation of **52** and **53**, exploring new synthetic territory. Encapsulation of BVs in hemicarcerand hosts has proved difficult, with no encapsulation observed as of yet. However, two hemicarcerand guests, **H1** and **H2**, have been successfully synthesised and encapsulations attempted. An additional guest with larger aperture and cavities, **H3**, is still yet to be fully investigated. Two more hosts, **H4** and **72** have been synthesised and exhibited binding to certain BVs, these experiments include the first reports of BVs binding to non-CD hosts.

The formation of a host guest complex in organic solvents would allow for easier low temperature ^{1}H NMR analysis of BVs behaviour than those in aqueous solutions. On the other hand, the aqueous soluble **H4** has exhibited encapsulation of several BV guests. Furthermore, preliminary experiments suggest that steric constraints imposed by **H4** may have an effect on the rate at which substituted BVs can rearrange. Further analysis of these complexes as well as synthesis of alternative, more suitable guests are ongoing.

Thus far, synthesis of tethered BV-β-CD complexes **59** and **64** have proven difficult, and subsequent crystallisation attempts have failed. Another potential complex **71** has been proposed and work towards this target molecule is underway. Moreover, the use of permethylated β-CD **72** as a molecular host for BV **1** has potential to affect the fluxional behaviour of **1**. In order to construct a formal and accurate conclusion, further and more data must be gathered and analysed.

Experimental

C-phenethylcalix[4]resorcinarene (4)

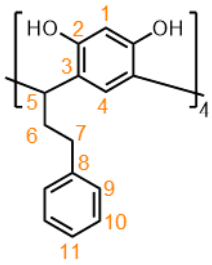

3-phenylpropanal (33.9 g, 250 mmol) was added dropwise to a solution of resorcinol (27.8 g, 250 mmol) in a mixture of ethanol (200 mL), and concentrated hydrochloric acid (50 mL) at 0 °C. The reaction mixture was stirred at rt for 24 h, and then heated to reflux for a further 5 d. The solution was cooled, filtered, and the precipitate washed with a 1:1 mixture of ethanol and H_2O (50 mL), then dried under reduced pressure to yield the title compound as a light orange powder (45.8 g, 50.6 mmol, 81%). **M.P.** = 320–325 °C (decomposition). **^{1}H NMR** ($(CD_3)_2CO$, 600 MHz) δ 8.52 (s, 7H, OH), 7.75 (s, 4H, H_1), 7.23–7.15 (m, 20 H, $H_{9,10,11}$), 6.29 (s, 4H, H_4), 4.42–4.37 (m, 4H, H_5), 2.62–2.59 (m, 16H, $H_{6,7}$). **^{13}C NMR** ($(CD_3)_2CO$, 150 Hz) δ 152.0 (C_2), 142.6 (C_8), 128.6 ($C_{9/10}$), 128.3 ($C_{9/10}$), 125.6 (C_{11}), 124.8 (C_1), 124.4 (C_3), 102.9 (C_4), 36.1 (C_7), 34.7 (C_6), 33.8 (C_5). **HR-ESI-MS** m/z: $[M+H]^+$ = 905.4093 (calculated $C_{60}H_{57}O_8^+$ = 905.4054). Analysis is in agreement with literature values.[28]

Tetrabromo resorcinarene (5)

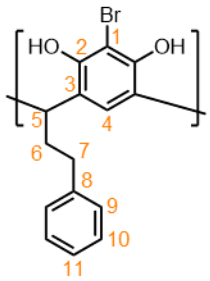

NBS (22.6 g, 127 mmol) was added slowly over 5 min to a stirring solution of **4** (28.8 g, 32 mmol) in 2-butanone (180 mL). The reaction was stirred at rt for 18 h. The solid was filtered, washed with cold 2-butanone (100 mL) and dried under reduced pressure to yield the title compound as a light orange powder (20.5 g, 17 mmol, 53%). **M.P.** = 280–285 °C (decomposition). **^{1}H NMR** ($(CD_3)_2CO$, 600 MHz) δ 7.76 (s, 4H, H_4), 7.24–7.12 (m, 20H, $H_{9,10,11}$), 4.55–4.51 (m, 4H, H_5), 2.62–2.57 (m, 16H, $H_{6,7}$).**^{13}C NMR** ($(CD_3)_2CO$, 150 Hz) δ 149.0 (C_2), 142.1 (C_8), 128.5 ($C_{9/10}$), 128.4 ($C_{9/10}$), 125.7 (C_{11}), 125.2 (C_1), 123.6 (C_3), 100.1 (C_4), 36.2 (C_7), 35.8 (C_6), 33.8 (C_5). **HR-ESI-MS** m/z: $[M+H]^+$ = 1217.0414 (calculated $C_{60}H_{53}Br_4O_8^+$ = 1217.0474). Analysis is in agreement with literature values.[28,29]

Tetrabromo cavitand (6)

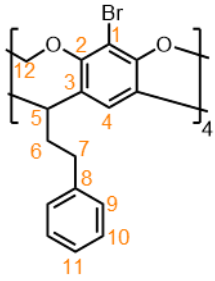

A solution of **5** (4.5 g, 3.7 mmol) in DMF (20 mL) was added slowly to a stirring solution of K_2CO_3 (15.3 g, 111 mmol) and bromochloromethane (5.0 mL, 73.7 mmol) in DMF (100 mL) and the reaction mixture stirred at rt for 24 h. Another portion of bromochloromethane (5.0 mL, 73.7 mmol) was added, and the reaction stirred at 45 °C for 24 h. Another portion of bromochloromethane (5.0 mL, 73.7 mmol) was added, and the reaction was heated to 63 °C for 3 d. The reaction mixture was allowed to cool to rt and neutralised with hydrochloric acid (1 M, 100 mL). The precipitate was obtained by filtration, stirred in methanol (50 mL) for 3 h, the solid filtered again, and dried under reduced pressure to yield the title compound as a light brown solid (3.5 g, 2.8 mmol, 76%). **M.P.** = 275–278 °C (decomp.). ^{1}**H NMR** ($CDCl_3$, 600 MHz) δ 7.25–7.21 (m, 12H, $H_{10,11}$), 7.15–7.12 (m, 8H, H_9), 7.08 (s, 4H, H_4), 5.98 (d, 4H, *J* = 7.2 Hz, H_{12b}), 4.97 (t, 4H, *J* = 7.8 Hz, H_5), 4.42 (d, 4H, *J* = 7.2 Hz, H_{12a}), 2.69–2.64 (m, 8H, H_7), 2.54–2.47 (m, 8H, H_6). ^{13}**C NMR** ($CDCl_3$, 150 Hz) δ 152.5 (C_2), 141.3 (C_8), 139.3 (C_3), 128.9 ($C_{10/11}$), 128.5 (C_9), 126.4 ($C_{10/11}$), 119.0 (C_4), 114.1 (C_1), 98.6 (C_{12}), 37.9 (C_5), 34.4 (C_7), 32.5 (C_6). **HR-ESI-MS** m/z: $[M+H]^+$ = 1265.0432 (calculated $C_{64}H_{53}Br_4O^+$ = 1265.0474). Analysis is in agreement with literature values.[27]

Cavitand (10)

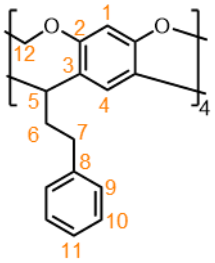

DMA (105 mL) was added to **4** (4.0 g, 4.4 mmol) and K_2CO_3 (18.3 g, 132 mmol) and the mixture was stirred for 20 min. Bromochloromethane (6.6 mL, 102 mmol) was added dropwise, and the reaction mixture stirred at rt for 24 h. Another portion of bromochloromethane (6.6 mL, 102 mmol) was added and the reaction mixture heated to 65 °C for 48 h. Upon cooling to rt, hydrochloric acid (1M, 60 mL) added. The precipitate was obtained by filtration, washed with H_2O (60 mL), methanol (100 mL) and dried under reduced pressure to yield the title compound as a white solid (3.4 g, 3.6 mmol, 81%). ^{1}**H NMR** ($CDCl_3$, 600 MHz) δ 7.26–7.20 (m, 12H, $H_{10,11}$), 7.17–7.14 (m, 12H, $H_{1,9}$), 6.54 (s, 4H, H_4), 5.77 (d, 4H, *J* = 6.0 Hz, H_{12b}), 4.84 (t, 4H, *J* = 6.6 Hz, H_5), 4.47 (d, 4H, *J* = 6.0 Hz, H_{12a}), 2.71–2.66 (m, 8H, H_7), 2.56–2.50 (m, 8H, H_6). ^{13}**C NMR** ($CDCl_3$, 150 MHz) δ

155.2 (C_2), 141.8 (C_1), 138.4 (C_8), 128.8 ($C_{10/11}$), 128.6 (C_9), 126.2 ($C_{10/11}$), 120.6 (C_1), 116.9 (C_4), 99.7 (C_{12}), 36.6 (C_5), 34.6 (C_7), 32.5 (C_6). **HR-APCI-MS** m/z: $[M+H]^+$ = 954.4210 (calculated $C_{64}H_{58}O_8^+$ = 954.4126).

Tetraol Cavitand (7)

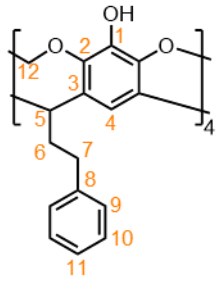

Method A (Scheme 1): **6** (5.34 g, 4.4 mmol) was dissolved in anhydrous THF (800 mL) in an oven-dried round-bottomed flask under an inert atmosphere, and was cooled to −78 °C. ^{n}BuLi (2.5 M in hexane, 30 mL, 75 mmol) was added and the solution stirred at for 20 min. Trimethyl borate (20 mL, 180 mmol) was added, the solution warmed to rt, and stirred for 1 h. The reaction mixture was again cooled to −78 °C and a mixture of hydrogen peroxide (15% w/w, 50 mL) and NaOH (3.0 g, 75 mmol) in H_2O (50 mL) added slowly. After warming to rt, the reaction was stirred for 18 h. Sodium metabisulfite (20 g) was then added, the remaining organic solvent removed under reduced pressure and the precipitate filtered. The crude precipitate was then purified by column chromatography was purified by column chromatography (Teledyne Isco CombiFlash Rf+ system, 40 g SiO_2, hexanes–EtOAc, gradient elution) to yield the title compound as a colourless solid (1.26 g, 1.2 mmol, 28%).

Method B (Scheme 3): **10** (1.05 g, 1.1 mmol) was dissolved in anhydrous THF (15 mL) in an oven-dried round-bottomed flask under an inert atmosphere and was cooled to −78 °C. ^{s}BuLi (1.3 M in cyclohexane, 8.5 mL, 11.0 mmol) was added, and the solution stirred for 30 min. Trimethyl borate (1.23 mL, 11.0 mmol) was added, the solution warmed to rt and stirred for 1 h. The reaction mixture was again cooled to −78 °C and a mixture of hydrogen peroxide (30% in water, 8.0 mL, 78.4 mmol) and NaOH (0.88 g, 22.0 mmol) in H_2O (8 mL) added slowly. The reaction was warmed to rt and stirred for 18 h, then quenched with sodium sulfite (10% w/w in water, 30 mL) and extracted with EtOAc (2 × 20 mL). The combined organic fractions were washed with H_2O (20 mL) and brine (20 mL), dried over $MgSO_4$, and the solvent removed under reduced pressure. The resulting crude residue was purified by column chromatography (Teledyne Isco CombiFlash Rf+ system, 24 g SiO_2, hexanes–EtOAc, gradient elution) to yield the title compound as a white solid (0.74 g, 0.7 mmol, 66%). ^{1}**H NMR** ($(CD_3)_2CO$, 600 MHz) δ 7.90 (s, br, 4H, OH), 7.25–7.17 (m, 20H, $H_{9,10,11}$),

7.15 (s, 4H, H_4), 5.84 (d, 4H, J = 7.2 Hz, H_{12b}), 4.79 (t, 4H, J= 7.8 Hz, H_5), 4.43 (d, 4H, *J* = 7.2 Hz, H_{12a}), 2.69–2.64 (m, 8H, H_7), 2.61–2.55 (m, 8H, H_6). **^{13}C NMR** ($(CD_3)_2CO$, 150 Hz) *δ* 143.7 (C_2), 143.5 (C_1), 143.5 (C_8), 139.6 (C_3), 129.5 ($C_{9/10}$), 129.4 ($C_{9/10}$), 126.7 (C_{11}), 111.4 (C_4), 100.9 (C_{12}), 38.3 (C_5), 35.4 (C_7), 33.2 (C_6). **HR-ESI-MS** m/z: $[M+H]^+$ = 1017.3825 (calculated $C_{64}H_{57}O_{12}^+$ = 1017.3850)

$CoBr_2$(dppe) Catalyst

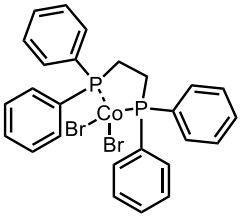

Anhydrous THF (20 mL) was added to $CoBr_2$ (1.08 g, 4.9 mmol) and 1,2-bis(diphenylphosphino)ethane (2.03 g, 5.1 mmol) in an oven-dried round-bottomed flask under an inert atmosphere. The reaction mixture was then stirred at rt for 6 h. The precipitate formed was filtered, washed with pentane (50 mL), and then dried under reduced pressure at 50 °C for 18 h to yield the title compound as a green solid (2.8 g, 4.5 mmol, 93%). The catalyst was used in synthesis without any further purification or analysis.

((2Z,4Z)-Bicyclo[4.2.2]deca-2,4,7,9-tetraen-7-yl)trimethylsilane (13)

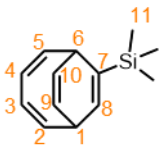

ZnI_2 (640 mg, 2.0 mmol) was added to a microwave vial, which was then flame-dried under reduced pressure, allowed to cool, and flushed with argon. Zn dust (200 mg, 3.0 mmol) and $CoBr_2$(dppe) (630 mg, 1.0 mmol) were added to the vial, and the vial evacuated and flushed with argon three times. 1,2-Dichloroethane (10 mL) was added, and the catalyst mixture stirred at rt until the mixture fully changes color from green to brown. Cyclooctatetraene (1.1 mL, 10.0 mmol) and trimethylsilylacetylene (2.9 mL, 20.0 mmol) were added slowly, and the reaction mixture stirred at rt for 48 h. Diethyl ether (10 mL) was added to the reaction mixture, and the mixture stirred for 15 min. The reaction mixture was passed through a silica plug (10 g), eluting with diethyl ether (100 mL), and the solvent removed under reduced pressure. The resulting crude residue was purified by column chromatography (Teledyne Isco CombiFlash Rf+ system, 40 g SiO_2, hexanes) to yield the title compound as a colourless solid. (1.95 g, 0.96 mmol, 96%). **^{1}H NMR** ($CDCl_3$, 600 MHz) δ 6.21–6.15 (m, 2H, $H_{2,5}$), 5.91 (d, 1H, *J* = 4.8 Hz, H_8), 5.79–5.68 (m, 4H, $H_{5,6,9,10}$), 3.39–3.36 (m, 1H, H_6), 3.28–3.23 (m, 1H, H_1), 0.11 (s, 9H, H_{11}). **^{13}C NMR** ($CDCl_3$, 150 Hz) δ 141.9 ($C_{5/2}$), 140.3 ($C_{5/2}$), 135.2 (C_7), 129.0 (C_8), 124.5 ($C_{5/6/9/10}$), 124.0 ($C_{5/6/9/10}$), 122.4 ($C_{5/6/9/10}$), 121.3 ($C_{5/6/9/10}$), 36.8 (C_6), 35.9 (C_1), −1.1 (C_{11}). Analysis is in agreement with literature values.[58]

Trimethylsilyl bullvalene (14)

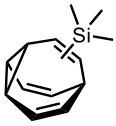

A solution of **13** (607 mg, 2.70 mmol) and thioxanthone (6 mg, 0.03 mmol) in anhydrous THF (10 mL) in an oven-dried vial under an inert atmosphere, was irradiated an 18 W 365 nm LED array for 5 h at 5 °C. The solvent was removed under reduced pressure, and the resulting crude residue was purified by column chromatography (Teledyne Isco CombiFlash Rf+ system, 40 g SiO_2, hexanes) to yield the title compound as a colourless solid (193 mg, 0.95 mmol, 33%). **M.P.** = 64–66 °C **^{1}H NMR** (400 MHz, $CDCl_3$) δ 6.39–5.52 (br m, 5H), 2.96–1.69 (br m, 4H), 0.06 (s, 9H). **HR-APCI-MS** *m/z*: $[M+H]^+$ = 203.125319 (calculated $C_{13}H_{19}Si^+$ = 203.125054). Analysis is in agreement with literature values.[58]

Busulfan (16)

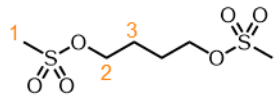

Methanesulfonyl chloride (5.2 ml, 67 mmol) was added at 0 °C to a stirred solution of 1,4-butanediol (2.53 g, 28 mmol) and triethylamine (16 ml, 120 mmol, 4.1 eq.) in CH_2Cl_2 (75 ml) and the solution allowed to warm to rt and stirred overnight. H_2O (50 ml) was added and the mixture was extracted with CH_2Cl_2 (3 × 40 ml). The combined organic fractions were then washed with H_2O (40 ml) and brine (40 ml), dried over $MgSO_4$, and the solvent removed under reduced pressure. The resulting crude residue was then recrystallised from ethanol and dried under reduced pressure to yield the title compound as a colorless solid (3.98 g, 16 mmol, 58%) **M.P.** = 114–118 °C. **^{1}H NMR** ($CDCl_3$, 600 MHz) δ 4.34–4.25 (m, 4H, H_2), 3.03 (s, 6H, H_1), 1.96–1.86 (m, 4H, H_3).**^{13}C-NMR** ($CDCl_3$, 150 Hz) δ 68.8 (C_2), 37.4 (C_1), 25.4 (C_3). **HR-ESI-MS** m/z: $[M+H]^+$ = 247.0305 (calculated $C_6H_{14}O_6S_2^+$ = 247.0310).

Tributyl hemicarcerand (17)

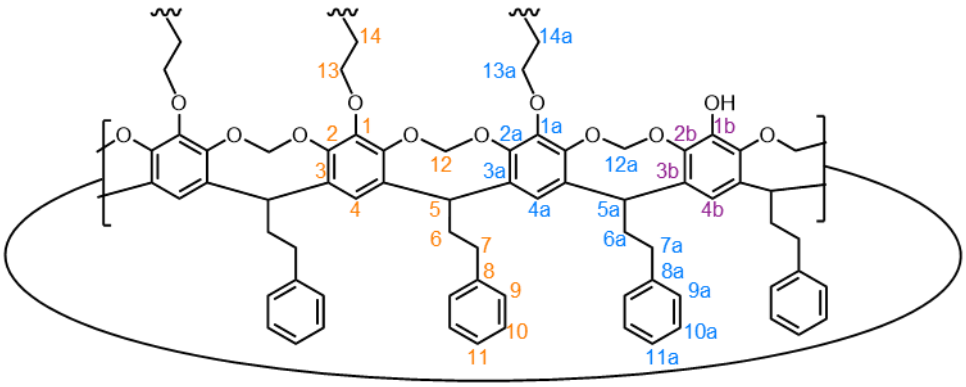

DMA (16 ml) was added to **7** (82 mg, 0.08 mmol) and Cs_2CO_3 (0.574 g, 1.8 mmol), and the mixture was stirred for 10 min at rt. Compound **16** (96.2 mg, 0.39 mmol). was added and the reaction mixture stirred for 18 h. The reaction mixture was poured into an aqueous solution of NaCl (10% w/v in H_2O, 25 mL). The fine precipitate was obtained by centrifuge (10,000 rpm, 10 min), dried under reduced pressure and purified by column chromatography (Teledyne Isco CombiFlash Rf+ system, 24 g SiO_2, CH_2Cl_2), to yield the title compound as a colourless solid (37 mg, 0.02 mmol, 41%). ^{1}**H NMR** ($CDCl_3$, 600 MHz) δ 7.26–7.20 (m, 24H, $H_{9,\ 9a,\ 10,\ 10a}$), 7.19–7.13 (m, 16H, $H_{11,\ 11a}$), 6.91–6.80 (m, 7H, $H_{4,\ 4a,\ 4b}$), 6.65 (s, 1H, $H_{4,\ 4a,\ 4b}$), 5.97–6.05 (m, 3H, $H_{12,\ 12a}$), 5.89–5.80 (m , 5H, $H_{12,\ 12a}$), 4.89–4.76 (m, 8H, $H_{5,\ 5a}$), 4.32–4.26 (m, 8H, $H_{12,\ 12a}$), 4.01–3.82 (m, 16H, $H_{7,\ 7a}$), 2.55–2.43 (m, 16H, $H_{6,\ 6a}$), 2.06–1.97 (m, 12H, $H_{14,\ 14a}$). ^{13}**C NMR** ($CDCl_3$, 150 Hz) δ 149.2 ($C_{2/\ 2a/\ 2a/\ 2b}$), 149.0 ($C_{2/\ 2a/\ 2a/\ 2b}$), 148.9 ($C_{2/\ 2a/\ 2a/\ 2b}$), 148.8 ($C_{2/\ 2a/\ 2a/\ 2b}$), 145.0 ($C_{1/\ 1a/\ 1b}$), 144.7 ($C_{1/\ 1a/\ 1b}$), 144.4 ($C_{1/\ 1a/\ 1b}$), 142.0 ($C_{8/\ 8a}$), 141.9 ($C_{8/\ 8a}$), 139.1 ($C_{3/\ 3a/\ 3a/\ 3b}$), 138.9 ($C_{3/\ 3a/\ 3a/\ 3b}$), 138.8 ($C_{3/\ 3a/\ 3a/\ 3b}$), 138.3 ($C_{3/\ 3a/\ 3a/\ 3b}$), 128.6 ($C_{10/\ 10a}$), 128.6 ($C_{10/\ 10a}$), 128.7 ($C_{9/\ 9a}$), 128.7 ($C_{9/\ 9a}$), 126.1 ($C_{11/\ 11a}$), 114.1 ($C_{4/\ 4a/\ 4b}$), 113.8 ($C_{4/\ 4a/\ 4b}$), 110.1 ($C_{4/\ 4a/\ 4b}$), 100.0 ($C_{12/\ 12a}$), 99.4 ($C_{12/\ 12a}$), 74.1 ($C_{13/\ 13a}$), 73.4 ($C_{13/\ 13a}$), 37.2 ($C_{5/\ 5a}$), 37.1 ($C_{5/\ 5a}$), 34.7 ($C_{7/\ 7a}$), 34.6 ($C_{7/\ 7a}$), 32.4 ($C_{6/\ 6a}$), 32.3 ($C_{6/\ 6a}$), 27.1 ($C_{14/\ 14a}$), 26.8 ($C_{14/\ 14a}$).

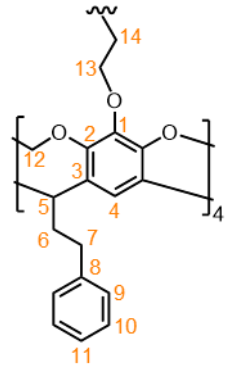

The tetrabridged carcerand **H1** was successfully isolated as a side product (11.1 mg, 4.9 μmol, 12%). ^{1}**H NMR** ($CDCl_3$, 600 MHz) δ 7.24–7.20 (m, 24H, $H_{10,\ 11}$), 7.18–7.14 (m, 16H, H_9), 6.85 (s, 8H, H_4), 5.81 (d, 8H, J = 7.2 Hz, H_{12}), 4.84 (t, 8H, J = 8.1 Hz, H_5), 4.29 (d, 8H, J = 7.2 Hz, H_{12}), 3.92 (s, 16H, H_{13}), 2.72–2.65 (m, 16H, H_7), 2.52–2.44 (m, 16H, H_6), 2.00 (s, 8H, H_{14}). ^{13}**C NMR** ($CDCl_3$, 150 MHz) δ 148.9 ($C_{1/\ 2/\ 3}$), 145.0 ($C_{1/\ 2/\ 3}$), 142.0 ($C_{1/\ 2/\ 3}$), 139.1 (C_8), 128.7 (C_9), 128.6 (C_{10}), 126.2 (C_{11}), 113.8 (C_4), 99.4 (C_{12}), 73.4 (C_{13}), 37.3 (C_5), 34.7 (C_7), 32.5 (C_6), 27.1(C_{14}).

1,3-Dimethanol benzene (19)

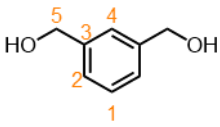

$LiAlH_4$ (2.4 M in THF, 50 mL, 120 mmol) was added dropwise over 1 h at 0 °C to a solution of isophthalic acid (10 g, 60 mmol) in anhydrous THF (250 mL) in an oven-dried round-bottomed flask

under an inert atmosphere. The reaction was stirred at 0 °C for 1 h, then heated and stirred at 60 °C for 18 h. The reaction was quenched by sequential addition of ispropanol (20 mL), methanol (10 mL) and H_2O (10 mL). The reaction was then diluted with H_2O (200 mL), and the suspension filtered through Celite® (5 g). The solid was washed with EtOAc (250 mL) and CH_2Cl_2 (250 mL). The organic solvents were removed under reduced pressure and the aqueous phase was extracted with EtOAc (3 × 200 mL). The organic fractions were dried over $MgSO_4$, and the solvent removed under reduced pressure to yield the title compound as a yellow oil (6.32 g, 46 mmol, 76%). **^{1}H NMR** (599 MHz, $CDCl_3$) δ 7.39–7.34 (m, 2H, $H_{1,4}$), 7.31–7.27 (m, 2H, H_2), 4.70 (s, 4H, H_5). **^{13}C NMR** (151 MHz, $CDCl_3$) δ 141.4 (C_3), 129.0 (C_1), 126.4 (C_2), 125.7 (C_4), 65.4 (C_5). **HR-ESI-MS** m/z: $[M–OH]^+$ = 121.0647 (calculated $C_8H_9O^+$ = 121.0653)

1,3-Di(chloromethyl) benzene (20)

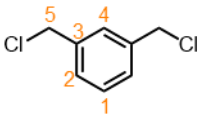

A solution of thionyl chloride (9.6 mL, 132 mmol) in anhydrous CH_2Cl_2 (15 mL) was added dropwise to a stirred solution of **19** (6.1 g, 44 mmol) and triethylamine (18.5 mL, 133 mmol) in anhydrous CH_2Cl_2 (25 mL) in an oven-dried round-bottomed flask under an inert atmosphere. After stirring for 3 h at rt, H_2O (50 mL) was added and the mixture extracted with CH_2Cl_2 (3 × 50 mL). The combined organic fractions were washed with H_2O (100 mL) and a saturated aqueous solution of Na_2CO_3 (100 mL), dried over $MgSO_4$, and the solvent removed under reduced pressure. The resulting crude residue was passed through a silica plug (10 g) eluting with hexanes–CH_2Cl_2 (1:9, 200 mL), and the solvent was removed under reduced pressure. The solid was triturated with cold ethanol (20 mL) and dried under reduced pressure to yield the title compound as a colourless solid (5.1 g, 29 mmol, 66%). **M.P.** = 31–33 °C. **^{1}H NMR** (599 MHz, $CDCl_3$) δ 7.44–7.42 (m, 1H, H_4), 7.38–7.34 (m, 3H, $H_{1,2}$), 4.59 (s, 4H, H_5). **^{13}C NMR** (151 MHz, $CDCl_3$) δ 138.2 (C_3), 129.3 (C_1), 128.8 (C_4), 128.7 (C_2), 45.9 (C_5). **HR-APCI-MS** m/z: $[M−Cl]^+$ = 139.030972 (Calculated $C_8H_8Cl^+$ = 139.030904).

Tetrol-m-xylyl hemicarcerand (H2)

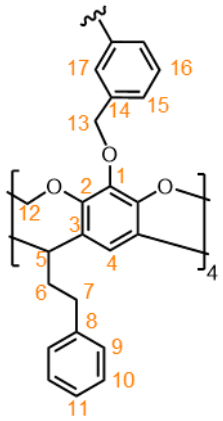

A mixture of **7** (584 mg, 0.58 mmol), **20** (500 mg, 2.85 mmol) and $CsCO_3$ (4.13 g, 125 mmol) in NMP (425 mL) was stirred at rt for 3 d. Another portion of **20** (500 mg, 2.85 mmol) was added, and the reaction stirred at 60 °C for 2 d. The mixture was allowed to cool to rt, and the solvent was removed under reduced pressure. The residue was partitioned between $CHCl_3$ (100 mL) and aqueous NaCl solution (10% w/w in water, 100 mL), the organic fraction dried with $MgSO_4$ and the solvent removed under reduced pressure. The resulting crude residue was purified by column chromatography (Teledyne Isco CombiFlash Rf+ system, 24 g SiO_2, hexanes–CH_2Cl_2, gradient elution) to yield the title compound as a colourless solid (82 mg, 0.03 mmol 12%). **^{1}H NMR** ($CDCl_3$, 600 MHz) δ 7.52 (s, 4H, H_{17}), 7.36–7.32 (m, 4H, H_{16}), 7.27–7.21 (m, 24H, $H_{10, 11}$), 7.19–7.16 (m, 8H, $H_{9, 15}$), 6.88 (s, 8H, H_4), 5.49 (d, 8H, J = 7.0 Hz, H_{12}), 4.95 (s, 16H, H_{13}), 4.86 (t, 8H, J = 7.9Hz, H_5), 4.23 (d, 8H, J = 7.0 Hz, H_{12}), 2.74–2.69 (m, 16H, H_7), 2.55–2.48 (m, 16H, H_6). **^{13}C NMR** ($CDCl_3$, 150 MHz) δ 148.4 (C_2), 145.2(C_1), 142.0 (C_8), 138.9 (C_3), 138.7 (C_{14}), 128.8 (C_9), 128.6 (C_{10}), 128.1 (C_{16}), 126.8 (C_{15}), 126.2 (C_{11}), 125.8 (C_{17}), 114.1 (C_4), 99.7 (C_{12}), 75.8 (C_{13}), 37.3 (C_5), 34.7 (C_7), 32.6 (C_6).

((2Z,4Z)-Bicyclo[4.2.2]deca-2,4,7,9-tetraen-7-yl)methanol (22)

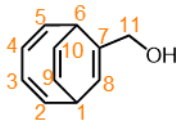

ZnI_2 (320 mg, 1.0 mmol) was added to a microwave vial, which was then heated to 280 °C for 5 mins under reduced pressure, allowed to cool, and flushed with argon. Zn dust (99 mg, 1.5 mmol) and $CoBr_2$(dppe) (360 mg, 0.5 mmol) were added to the vial, and the vial evacuated and flushed with argon three times. Anhydrous 2,2,2-trifluoroethane (5 mL) was added and the catalyst mixture stirred at 55 °C until the mixture fully turns from green to brown. Cyclooctatetraene (526 mg, 5.0 mmol) and then propargyl alcohol (0.6 mL, 10.0 mmol) were added slowly, and the reaction mixture stirred at 55 °C for 18 h. The reaction mixture was allowed to cool to rt and then diethyl ether was added to the reaction mixture, and the mixture stirred for 15 min. The reaction mixture was passed through a silica plug (5 g), eluting with diethyl ether (50 mL), and the solvent removed under reduced pressure. The resulting crude residue was purified by column chromatography (Teledyne Isco CombiFlash Rf+ system, 24 g SiO_2, hexanes–EtOAc,

0–50%, gradient elution) to yield the title compound as a colourless oil (610 mg, 3.8 mmol, 76%). **^{1}H NMR** (400 MHz, $CDCl_3$) δ 6.29–6.17 (m, 2H, $H_{2,5}$), 5.81–5.61 (m, 5H, $H_{3,4,8,9,10}$), 4.18–4.05 (m, 2, H_{11}), 3.47–3.39 (m, 1H, H_6), 3.26–3.16 (m, 1H, H_1). **^{13}C NMR** (101 MHz, $CDCl_3$) δ 141.9 (C_5), 141.4 (C_2), 136.1 (C_7), 124.8 ($C_{3/4/9/10}$), 124.5 ($C_{3/4/9/10}$), 121.2 ($C_{3/4/9/10}$), 121.0 ($C_{3/4/9/10}$), 118.9 (C_8), 64.8 (C_{11}), 36.4 (C_6), 34.9 (C_1). **HR-ESI-MS** *m/z*: $[M+Na]^+$ = 183.0784 (calculated $C_{11}H_{12}NaO^+$ = 183.0780)

Methyl alcohol bullvalene (23)

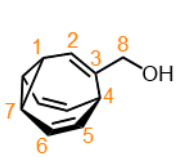

β-**23**

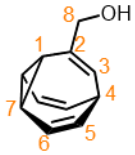

γ-**23**

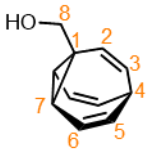

δ-**23**

Isomer ratio		
β-**23**	*γ*-**23**	*δ*-**23**
59	24	17

A solution of **22** (856 mg, 5.3 mmol) and thioxanthone (11 mg, 0.05 mmol) in anhydrous THF (15 mL), in an oven-dried vial under an inert atmosphere, was irradiated an 18 W 365 nm LED array for 5 h, cooled by a water bath at 5 °C. After irradiation was complete, the solvent was removed under reduced pressure, and the resulting crude residue was purified by column chromatography (Teledyne Isco CombiFlash Rf+ system, 40 g SiO_2, hexanes–EtOAc, 0–40%, gradient elution) to yield the title compound as a colourless oil (650 mg, 4.06 mmol, 76%). **^{1}H NMR** (500 MHz, EtOD, 223 K) δ 5.86–5.67 (m, 5.17H, $H_{2,3,5,6}$), 3.93 (s, 0.48H, *γ*-H_8), 3.88 (s, 1.18H, *β*-H_8), 3.48 (s, 0.34H, *δ*-H_8), 2.38–2.06 (m, 3.83H, $H_{1,4,7}$). **^{13}C NMR** (125 MHz, EtOD, 223 K) δ 141.2 (*β*-C_3), 138.8 (*γ*-C_2), 129.7 (*δ*-$C_{3/5/6}$), 129.0 (*δ*-C_2), 128.3 (*δ*-$C_{3/5/6}$), 128.0 (*β*-$C_{5/6}$ / *γ*-$C_{5/6}$), 127.9 (*β*-$C_{5/6}$ / *γ*-$C_{5/6}$), 127.7 (*β*-$C_{5/6}$ / *γ*-$C_{5/6}$), 127.4 (*δ*-$C_{3/5/6}$), 122.0 (*γ*-C_3), 121.8 (*β*-C_2), 71.02 (*δ*-C_8), 68.9 (*γ*-C_8), 67.6 (*β*-C_8), 33.3 (*β*-C_4), 32.1 (*δ*-C_4), 31.8 (*δ*-C_1), 31.2 (*γ*-C_4), 26.0 (*δ*-C_7), 21.8 (*γ*-C_1), 21.3 (*β*-C_1), 20.8 (*γ*-C_7), 19.8 (*β*-C_7). **HR-APCI-MS** *m/z:* $[M+H]^+$ = 161.096685 (Calculated $C_{11}H_{13}O$ = 161.096091)

(2Z,4Z)-7,8-Diethylbicyclo[4.2.2]deca-2,4,7,9-tetraene (25)

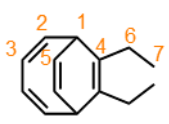

ZnI_2 (160 mg, 0.50 mmol) was added to a microwave vial, which was then heated to 280 °C for 5 mins under reduced pressure, allowed to cool, and flushed with argon. Zn dust (50 mg, 0.75 mmol) and $CoBr_2$(dppe) (150 mg, 0.25 mmol) were added to the vial, and the vial evacuated

and flushed with argon three times. Anhydrous 1,2-dichloroethane (2 mL) was added and the catalyst mixture stirred at rt until the mixture fully turns from green to brown. Cyclooctatetraene (260 mg, 2.5 mmol) and then 1-heptyne (250 mg, 3.0 mmol) were added slowly, and the reaction mixture stirred at rt for 18 h. Diethyl ether (3 mL) was added to the reaction mixture, and the mixture stirred for 15 min. The reaction mixture was passed through a silica plug (5 g), eluting with hexane (100 mL), and the solvent removed under reduced pressure. The resulting crude residue was purified by column chromatography (Teledyne Isco CombiFlash Rf+ system, 24 g SiO_2, hexanes) to yield the title compound as a colourless oil (320 mg, 1.7 mmol, 69%). **^{1}H NMR** (600 MHz, $CDCl_3$) δ 6.25–6.18 (m, 2H, H_2), 5.71–5.67 (m, 2H, H_5), 5.67–5.63 (m, 2H, H_3), 3.17–3.12 (m, 2H, H_1), 2.19–2.02 (m, 4H, H_6), 0.98 (t, *J* = 7.6 Hz, 6H, H_7). **^{13}C NMR** (600 MHz, CDCl3) δ 142.9 (C_2), 131.8 (C_4), 124.4 (C_3), 121.8 (C_5), 39.7 (C_1), 24.5 (C_6), 15.3 (C_7). **HR-ESI-MS** *m/z*: $[M+H]^+$ = 187.1478 (calculated $C_{14}H_{19}^+$ = 187.1487).

Diethyl bullvalene (26)

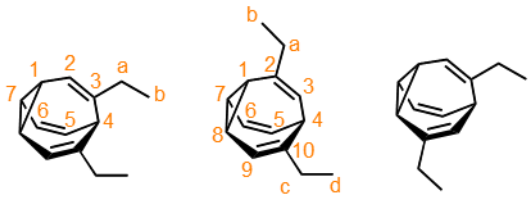

Isomer ratio

β,β-**26**	P-β,γ-**26**	M-β,γ-**26**	3 Other Isomers
54	17	17	2 – 5 each

A solution of **25** (320 mg, 1.7 mmol) and thioxanthone (4 mg, 0.02 mmol) in anhydrous THF (5 mL), in an oven-dried vial under an inert atmosphere, was irradiated an 18 W 365 nm LED array for 5 h, cooled by a water bath at 5 °C. After irradiation was complete, the solvent was removed under reduced pressure, and the resulting crude residue was purified by column chromatography (Teledyne Isco CombiFlash Rf+ system, 12 g SiO_2, hexanes) to yield the title compound as a colourless oil (92 mg, 0.5 mmol, 29%). **^{1}H NMR** (500 MHz, $CDCl_3$, 223 K) δ 5.97–5.83 (m, 2.10H), 5.77 (d, *J* = 11.2 Hz, 0.11H), 5.75–5.63 (m, 1.32H), 5.60–5.51 (m, 0.47H), 2.52–1.93 (m, 0.74H), 1.73–1.34 (m, 0.93H), 1.08–0.93 (m, 6.00H). **^{13}C NMR** (126 MHz, $CDCl_3$, 223 K) δ 144.3 (β,γ-$C_{2/10}$), 144.0, 143.6 (β,β-C_3), 140.6, 140.2 (β,γ-$C_{2/10}$), 140.2, 130.3, 129.9, 128.5, 128.2, 128.1, 127.8 (β,γ-$C_{5/6}$), 127.7, 127.3 (β,β-$C_{5/6}$), 127.2, 127.1, 126.8 (β,β-$C_{5/6}$), 126.5 (β,γ-$C_{5/6}$), 126.2, 121.6, 118.3,

118.2, 118.0 (β,β-C_2), 117.8 (β,γ-$C_{3/9}$), 117.5 (β,γ-$C_{3/9}$), 40.0, 35.0, 34.9, 34.8, 34.8, 34.6, 34.3, 33.7, 33.3, 33.3, 32.9, 32.8, 32.7, 32.6, 32.0, 30.8, 30.7, 29.9, 29.8, 29.6, 29.4, 29.4, 28.2, 27.9, 27.7, 27.3, 23.1, 23.0, 23.0, 22.8, 19.9, 19.8, 19.6, 19.2, 14.7, 14.6, 14.5, 13.3 (β,γ-$C_{b/d}$), 13.2 (C_b), 12.9 (β,β-C_b), 12.5 ($C_{b/d}$), 12.4 ($C_{b/d}$), 12.2 ($C_{b/d}$), 12.1 (β,γ-$C_{b/d}$), 12.0 ($C_{b/d}$). **HR-ESI-MS** *m/z*: $[M+H]^+$ = 187.1477 (calculated $C_{14}H_{19}^+$ = 187.1487). Excess peaks are present due to trace isomers present in solution.

Tetraformyl cavitand (30)

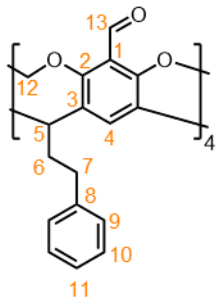

^{n}BuLi (2.5 M in hexanes, 2.3 mL, 5.8 mmol) was added at −78 °C to a stirred solution of **6** (730 mg, 0.6 mmol) in anhydrous THF (20 mL) in an oven-dried round-bottomed flask under an inert atmosphere. The reaction mixture was stirred at −78 °C for 20 min, warmed to 0 °C, and stirred for 30 min. The reaction mixture was cooled again to −78 °C, and anhydrous DMF (2.2 mL, 28.8 mmol) added and the mixture stirred for 10 min at −78 °C. The reaction was then warmed to rt, and stirred for 1 h, before quenching the reaction by the addition of an aqueous solution of NH_4Cl (5% w/v in water, 1 mL). The reaction was stirred for a further 5 min and H_2O (25 mL) added. The mixture was extracted with EtOAc (3 × 30 mL), and the organic fractions combined, dried over $MgSO_4$, and the solvents removed under reduced pressure. The resulting crude residue was purified by column chromatography (Teledyne Isco CombiFlash Rf+ system, 24 g SiO_2, hexanes–CH_2Cl_2, gradient elution) to yield the title compound as a colourless solid (110 mg, 0.1 mmol, 18%). **M.P.** = >300 °C (decomp.). **^{1}H NMR** (400 MHz, $CDCl_3$) δ 10.28 (s, 4H, H_{13}), 7.32 (s, 4 H, H_4) 7.29–7.23 (m, 12H, $H_{10,11}$), 7.18–7.13 (m, 8H, H_9), 5.92 (d, 4H, J = 7.5 Hz, H_{12a}), 5.01 (t, 4H, J = 8.0 Hz, H_5), 4.50 (d, 4H, J = 7.5 Hz, H_{12b}), 2.75–2.65 (m, 8H, H_7), 2.59–2.48 (m, 8H, H_6). **^{13}C NMR** (100 MHz, $CDCl_3$) δ 189.9 (C_{13}), 155.0 (C_2), 141.1 (C_8), 139.2 (C_3), 128.9 ($C_{10/\ 11}$), 128.5 (C_9), 126.6 ($C_{10/\ 11}$), 124.8 (C_1), 124.7 (C_4), 100.3 (C_{12}), 36.2 (C_5), 34.4 (C_7), 32.2 (C_6). **HR-ESI-MS** *m/z*: $[M+H]^+$ = 1065.3863 (calculated $C_{68}H_{57}O_{12}^+$ = 1065.3845).

_M_-phenylenediamine imine hemicarcerand (H3)

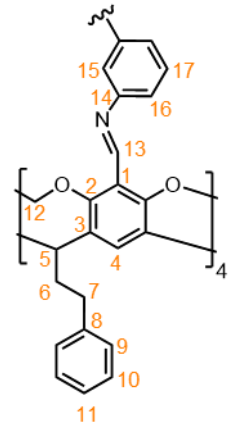

A solution of TFA in $CHCl_3$ (0.01% v/v, 2 mL, 2.4 μmol) was added to a solution of **30** (50 mg, 47 μmol) and 1,3-diaminobenzene **31** (10 mg, 94 μmol) in $CHCl_3$ (8 mL). The reaction mixture was stirred at rt for 18 h. The solvent was removed under reduced pressure and the resulting crude residue was purified by column chromatography (Teledyne Isco CombiFlash Rf+ system, 12 g SiO_2, hexanes–CH_2Cl_2, gradient elution) to yield the title compound as a colourless solid (45 mg, 18.6 μmol, 79%). **M.P.** = >300 °C (decomp.). **^{1}H NMR** (400 MHz, $CDCl_3$) δ 8.49 (s, 8H, H_{13}), 7.40 (t, J = 7.8 Hz, 4H, H_{17}), 7.34–7.16 (m, 48H, $H_{4,\ 9,\ 10,\ 11}$), 6.83 (dd, J = 7.8, 2.1 Hz, 8H, H_{16}), 6.61 (t, J = 2.1 Hz, 4H, H_{15}), 5.73 (d, J = 7.6 Hz, 8H, H_{12a}), 5.08 (t, J = 7.8 Hz, 8H, H_5), 4.69 (d, J = 7.7 Hz, 8H, H_{12b}), 2.79–2.69 (m, 16H, H_7), 2.67–2.54 (m, 16H, H_6). **^{13}C NMR** (101 MHz, $CDCl_3$) δ 32.5 (C_6), 34.6 (C_7), 36.8 (C_5), 100.9 (C_{12}), 115.4 (C_{16}), 118.3 (C_{15}), 122.1 (C_4), 124.5 (C_1), 126.3 ($C_{10/\ 11}$), 128.5 (C_9), 128.8 ($C_{10/\ 11,\ 17}$), 138.7 (C_3), 141.6 (C_8), 153.4 (C_{14}), 154.2 (C_2), 156.6 (C_{13}). **HR-ESI-MS** *m/z*: $[M+H]^+$ = 2417.9361 (calculated $C_{160}H_{129}N_8O_{16}^+$ = 2417.9521).

Dodecol (37)

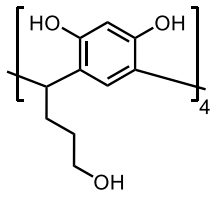

2,3-Dihydrofuran (27.6 mL, 364 mmol) was added over 10 min at 0 °C to a solution of resorcinol (40.0 g, 364 mmol) in methanol (240 mL) and concentrated hydrochloric acid (80 mL). The mixture was stirred at 0 °C for 30 min, and then heated to 50 °C and stirred for 5 d. The reaction mixture was cooled to rt, and the resulting precipitate obtained by filtration was washed with methanol–H_2O (1:1, 50 mL). The solid was then suspended in H_2O (600 mL) and sonicated. The resulting precipitate was collected by filtration and dried under reduced pressure to yield the title compound as a yellow solid (54.0 g, 75.0 mmol, 82%). **^{1}H NMR** (300 MHz, d^6-DMSO) δ 8.89 (s, 8H), 7.20 (s, 4H), 6.13 (s, 4H), 4.31 (t, J = 4.9 Hz, 4H), 4.18 (t, J = 7.8 Hz, 4H), 3.58–3.34 (m, 8H), 2.14–1.99 (m, 8H), 1.39–1.24 (m, 8H). Analysis is in agreement with literature values.[61]

3,5-Dibromobenzal bromide (38)

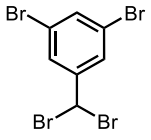

BBr_3 (23.0 mL, 239 mmol) was added to a solution of 3,5-dibromobenzaldehyde (60 g, 227 mmol) in CH_2Cl_2 (500 mL) in an oven-dried round-bottomed flask under an inert atmosphere. The reaction mixture was stirred at rt for 18 h, after which H_2O (250 mL) was added dropwise to quench the reaction. The organic phase was washed with H_2O (2 × 300 mL), dried and decoloured over Na_2SO_4 and active charcoal. The solvent was removed under reduced pressure, and the remaining solid was recrystallised from hexanes to yield the title compound as a white solid (85.4 g, 209 mmol, 92%). **^{1}H NMR** (300 MHz, *d*^{6}-DMSO) δ 7.88 (t, *J* = 1.7 Hz, 1H), 7.81 (d, *J* = 1.7 Hz, 2H), 7.31 (s, 1H). Analysis is in agreement with literature values.[62]

Octabromide (39)

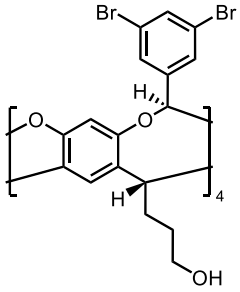

DBU (16.6 mL, 111 mmol) was added to a stirred solution of **37** (10.0 g, 13.9 mmol) and 3,5-dibromobenzal bromide **38** (27.2 g, 66.7 mmol) in degassed DMA (500 mL) and the reaction mixture was heated to 50 °C for 48 h. The DMA was removed under reduced pressure. The residue was dissolved in CH_2Cl_2 (500 mL), washed with H_2O (3 × 300 mL) and dried over Na_2SO_4 for 5 min. The solvent was removed under reduced pressure to around 150 mL, and cooled to −20 °C for 48 h. The precipitate was obtained by filtration, washed with CH_2Cl_2 (150 mL) and dried under reduced pressure to yield the title compound as an off-white solid (10.7 g, 6.3 mmol, 45%). **^{1}H NMR** (400 MHz, *d*^{6}-DMSO) δ 7.95 (s, 8H), 7.73 (s, 4H), 7.15 (s, 4H), 5.51 (s, 4H), 4.72 (t, *J* = 8.1 Hz, 4H), 4.52 (t, *J* = 5.0 Hz, 4H), 3.55 (q, *J* = 5.8 Hz, 8H), 2.49–2.45 (m, 8H), 1.57–1.43 (t, *J* = 7.2 Hz 8H).

Octol (41)

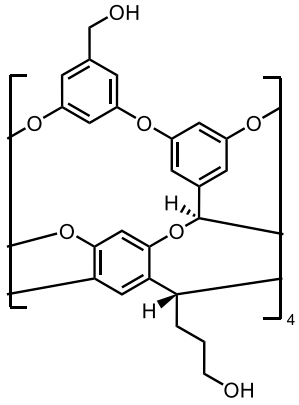

K_2CO_3 (6.64 g, 48.0 mmol) was added to a solution of **39** (6.84 g, 4.0 mmol) and 3,5-dihydroxybenzyl alcohol (3.38 g, 24.0 mmol) in pyridine (300 mL) in an oven-dried round-bottomed flask under an inert atmosphere. The solution was purged with N_2 for 30 min. CuBr (6.90 g, 48.0 mmol) was added to the stirred solution, and the reaction mixture vigorously refluxed for 8 d. The solvent was removed under reduced pressure and the crude residue suspended in THF (250 mL), sonicated for 30 min and filtered through Celite®. The solvent was removed under reduced pressure and the crude residue suspended in hydrochloric acid (1M, 50 mL) and sonicated. The precipitate was obtained by filtration, washed with H_2O (100 mL) and dried under reduced pressure to yield the title compound as a crude, off-white solid (3.6 g, 80–90% purity) which was used in the next step with no further purification.

Octa aldehyde (42)

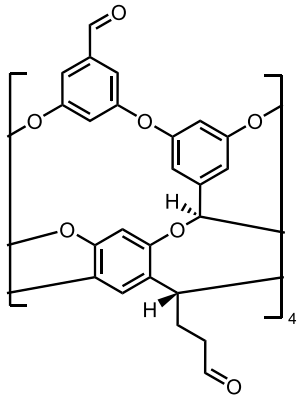

A solution of **41** (1.0 g, 0.61 mmol) in anhydrous DMSO (30 mL) in an oven-dried round-bottomed flask under an inert atmosphere was sonicated for 1 min. Triethylamine (2.73 mL, 19.2 mmol) was added to the stirred reaction mixture. A solution of sulfur trioxide pyridine complex (1.57 g, 9.66 mmol) in anhydrous DMSO (10 mL) was added slowly over 20 mins, and the mixture was stirred at rt for 2 h. An aqueous solution of hydrochloric acid (10% w/w, 20 mL) was added slowly until the solution was acidic, then H_2O (30 mL) was added and the mixture stirred for another 15 min. The precipitate was obtained by filtration, washed with H_2O until the filtrate's pH was neutral, and dried under reduced pressure. The resulting crude residue was purified by column chromatography (Teledyne Isco CombiFlash Rf+ system, 24 g SiO_2, $CHCl_3$–CH_3CN, 0–30%, gradient elution) to yield the title compound as a colourless solid (443 mg, 0.27 mmol, 45%). **^{1}H NMR** (400 MHz, *d*^{6}-DMSO) δ 10.09 (s, 4H), 9.69 (s, 4H), 7.86 (s, 8H), 7.65 (s, 4H), 7.22 (s, 4H) 7.07 (s, 4H), 6.43 (s, 8H), 5.79 (s, 4H), 4.51 (t, *J* = 7.8 Hz, 4H), 4.43 (s, 4H), 2.58 (m, 8H),

2.42 (m, 8H). **^{13}C NMR** (101 MHz, *d*^{6}-DMSO) δ 203.0, 192.0, 160.7, 157.0, 155.9, 140.1, 139.8, 136.5, 121.4, 114.8, 109.4, 106.3, 65.3, 42.0, 36.5, 22.6, 15.4.

Octa acid (H4)

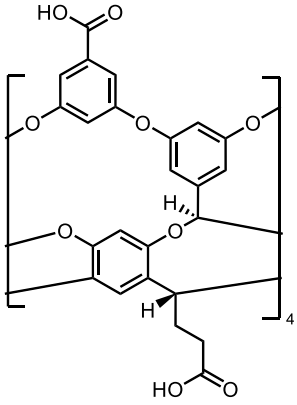

42 (1.5 g, 0.9 mmol) was dissolved in anhydrous DMSO (150 mL), and the solution stirred and heated to 60 °C. Once the solution was heated, a solution of $NaHPO_4$ (6.1 g, 50 mmol) in H_2O (12 mL) was added dropwise, followed by a solution of $NaClO_2$ (2.37 g, 26 mmol) in H_2O (12 mL) and the solution was stirred at 60 °C for 18 h. The solvent was removed under reduced pressure and the solid suspended in hydrochloric acid (20% w/w in H_2O, 100 mL) and sonicated. The precipitate was obtained by filtration, washed with H_2O until the filtrate's pH was neutral, and dried under reduced pressure. The solid was suspended in anhydrous acetone (50 mL), and sonicated for 2 mins, then cooled to 0 °C for 30 min, filtered and washed with anhydrous acetone to yield the title compound as a white solid (1.2 g, 0.7 mmol, 74%). **M.P. =** >250 °C. **^{1}H NMR** (500 MHz, *d*^{6}-DMSO) δ 13.61 (br s, 4H), 12.2 (br s, 4H), 7.78 (s, 8H), 7.70 (s, 4H), 7.17 (s, 4H), 6.98 (s, 4H), 6.41 (s, 8H), 5.78 (s, 4H), 4.57 (t, *J* = 7.8 Hz, 4H), 4.16 (s, 4H), 2.60 (m, 8H), 2.20 (m, 8H).

Encapsulation in Octa Acid Host

H4 (13.1 mg, 7.0 μmol) was added to a stock solution of NaOH (7 mL, 10 mM in D_2O). The stock solution (1 mL, 1 mM **H4**) was added to the guest (1 mg, ~5.0 μmol, ~5-fold excess) and the solution agitated for 3 h. The solution was then filtered through a Durapore® polyvinylidene difluoride (PVDF) membrane to yield the desired complex of **H4 ⊙ G**, which is analysed by ^{1}H NMR spectroscopy.

(2Z,4Z)-Bicyclo[4.2.2]deca-2,4,7,9-tetraene (BDT)

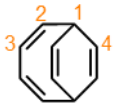

ZnI_2 (640 mg, 2.0 mmol) was added to a microwave vial, which was heated to 280 °C for 5 mins under reduced pressure, allowed to cool to rt, and flushed with argon. Zn dust (200 mg, 3.0 mmol) and $CoBr_2$(dppe) (630 mg, 1.0 mmol) were added to the vial, and the vial evacuated and flushed with argon three times. Anhydrous 1,2-dichloroethane (8 mL) was added and the catalyst mixture

stirred at rt until the mixture fully changed colour from green to brown. Cyclooctatetraene (1.1 mL, 10.0 mmol) was added, and then acetylene (produced by the addition of H_2O to calcium carbide), was bubbled through the reaction mixture for 15 min. A balloon was filled with excess acetylene produced and attached to the reaction vessel, and the reaction mixture stirred at rt for 18 h. Diethyl ether (10 mL) was added to the reaction mixture, and the mixture stirred for 15 min. The reaction mixture was passed through a silica plug (10 g), eluting with hexanes (100 mL), and the solvent removed under reduced pressure. The resulting crude residue was purified by column chromatography (Teledyne Isco CombiFlash Rf+ system, 40 g SiO_2, hexanes) to yield the title compound as a colourless solid. (0.82 g, 6.3 mmol, 63%). **^{1}H NMR** (400 MHz, $CDCl_3$) δ 6.27–6.18 (m, 2H, H_2), 5.87–5.80 (m, 2H, H_3), 5.66–5.60 (m, 4H, H_4), 3.33–3.17 (m, 2H, H_1). **^{13}C NMR** (101 MHz, $CDCl_3$) δ 141.2 (C_2), 124.4 (C_3), 121.3 (C_4), 34.9 (C_1). **HR-GCEI-MS** *m/z*: M^+ = 130.07767 (calculated $C_{10}H_{10}^+$ = 130.07770).

Bullvalene (BV)

A solution of **BDT** (800 mg, 6.14 mmol) and thioxanthone (13 mg, 0.06 mmol) in anhydrous THF (15 mL) in an oven-dried vial under an inert atmosphere, was irradiated by an 18 W 365 nm LED array for 5 h, cooled by a water bath at 5 °C. After irradiation was complete, the solvent was removed under reduced pressure, and the resulting crude residue was purified by column chromatography (Teledyne Isco CombiFlash Rf+ system, 40 g SiO_2, hexanes) to yield the title compound as a colourless solid (200 mg, 1.54 mmol, 25%). **M.P.** = 95–96 °C. **^{1}H NMR** (500 MHz, $CDCl_3$, 223 K) δ 6.05–5.95 (m, 3H, H_2), 5.93–5.86 (m, 3H, H_3), 2.43–2.30 (m, 4H, $H_{1,4}$). **^{13}C NMR** (125 MHz, $CDCl_3$, 223 K) δ 128.2 (C_3), 127.3 (C_2), 30.0 (C_4), 20.5 (C_1). **HR-APCI-MS** *m/z:* $[M+H]^+$ = 131.085586 (Calculated $C_{10}H_{11}^+$ = 131.085527).

(2Z,4Z)-7-Pentylbicyclo[4.2.2]deca-2,4,7,9-tetraene (Pentyl BDT)

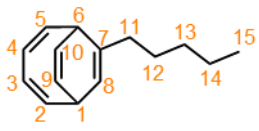

ZnI_2 (640 mg, 2.0 mmol) was added to a microwave vial, which heated to 280 °C for 5 mins under reduced pressure, allowed to cool, and flushed with argon. Zn dust (200 mg, 3.0 mmol) and $CoBr_2$(dppe) (620 mg, 1.0 mmol) were added to the vial, and the vial evacuated and flushed with argon three times. Anhydrous 1,2-dichloroethane (7 mL)

was added and the catalyst mixture stirred at rt until the mixture fully turns from green to brown. Cyclooctatetraene (1.1 mL, 10.0 mmol) and then 1-heptyne (2.6 mL, 20.0 mmol) were added slowly, and the reaction mixture stirred at rt for 18 h. Diethyl ether (5 mL) was added to the reaction mixture, and the mixture stirred for 15 min. The reaction mixture was passed through a silica plug (10 mg), eluting with hexane (100 mL), and the solvent removed under reduced pressure. The resulting crude residue was purified by column chromatography (Teledyne Isco CombiFlash Rf+ system, 40 g SiO_2, hexanes) to yield the title compound as a colourless oil (1.39 g, 6.9 mmol, 69%). **^{1}H NMR** (400 MHz, $CDCl_3$) δ 6.31–6.13 (m, 2H, $H_{2, 5}$), 5.79–5.61 (m, 4H, $H_{3, 4, 9, 10}$), 5.42–5.36 (m, 1H, H_8), 3.26–3.20 (m, 1H, H_6), 3.17–3.10 (m, 1H, H_1), 2.11–2.03 (m, 2H, H_{11}), 1.44–1.17 (m, 6H, $H_{12–14}$), 0.87 (t, *J* = 7.1 Hz, 3H, H_{15}). **^{13}C NMR** (101 MHz, $CDCl_3$) δ 142.1 (C_2), 142.0 (C_5), 136.8 (C_7), 124.5 (C_4), 124.0 (C_3), 121.5 (C_{10}), 121.3 (C_9), 117.0 (C_8), 39.4 (C_6), 35.2 (C_1), 35.1 (C_{11}), 31.7 (C_{13}), 28.8 (C_{12}), 22.7 (C_{14}), 14.2 (C_{15}). **HR-APCI-MS** *m/z*: $[M+H]^+$ = 201.163384 (calculated $C_{15}H_{21}^+$ = 201.163777)

Pentyl bullvalene (43)

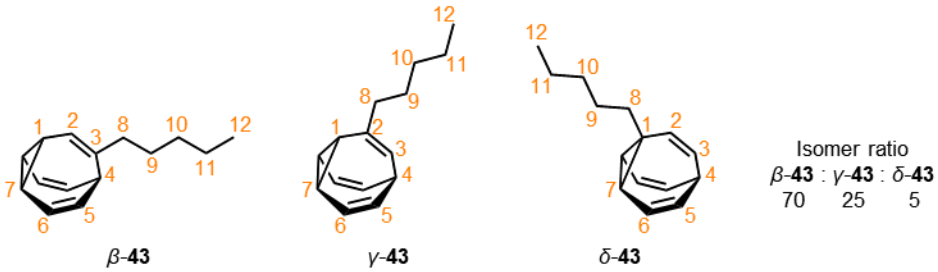

β-**43** *γ*-**43** *δ*-**43**

A solution of **Pentyl BDT** (1.3 g, 6.5 mmol) and thioxanthone (14 mg, 0.06 mmol) in anhydrous THF (15 mL), in an oven-dried vial under an inert atmosphere, was irradiated an 18 W 365 nm LED array for 5 h, cooled by a water bath at 5 °C. After irradiation was complete, the solvent was removed under reduced pressure, and the resulting crude residue was purified by column chromatography (Teledyne Isco CombiFlash Rf+ system, 40 g SiO_2, hexanes) to yield the title compound as a colourless oil (553 mg, 2.8 mmol, 43%). **^{1}H NMR** (500 MHz, $CDCl_3$ 223K) δ 5.98–5.83 (m, 4.05H, H, $H_{2, 3, 5, 6}$), 5.80 (d, *J* = 11.3 Hz, 0.05H, *δ*-H_2), 5.72 (d, *J* = 7.7 Hz, 0.70H, *β*-H_2), 5.58 (d, *J* = 8.8 Hz, 0.25H, *γ*-H_3), 2.44–2.18 (m, 3.95H, $H_{1, 4, 7}$), 2.11–1.98 (m, 2.00H, H_8), 1.47–1.17 (m, 6.00H, $H_{9–11}$), 0.86 (t, *J* = 6.9 Hz, 3.00H, H_{12}). **^{13}C NMR** (126 MHz, $CDCl_3$ 223K) δ 143.1 (*β*-C_3), 139.4 (*γ*-C_2), 130.7 (*δ*-C_2), 128.2 (*δ*-

$C_{5/6}$), 128.0 (γ-C_5), 127.7 (β-C_5), 127.2 (δ-$C_{5/6}$), 127.0 (β-C_6), 126.6 (γ-C_6), 119.3 (β-C_2), 119.3 (γ-C_3), 41.6 (δ-C_8), 41.1 (γ-C_8), 40.2 (β-C_8), 34.5 (β-C_4), 31.5 (β-C_{10}, γ-C_{10}), 30.1, 30.0, 29.8 (γ-C_4), 28.9 (β-C_9), 28.2 (δ-C_9), 28.1 (γ-C_9), 27.5, 23.0 (γ-C_1), 22.9 (δ-C), 22.7 (γ-C_{11}), 22.7 (β-C_{11}), 20.2 (β-C_1), 20.2 (γ-C_7), 19.8 (β-C_7), 14.4 (δ-C_{12}), 14.4 (γ-C_{12}), 14.3 (β-C_{12}). Unassigned carbon environments may represent δ-**43** but no correlations were observed. **HR-APCI-MS** *m/z:* $[M+H]^+$ = 201.164640 (Calculated $C_{15}H_{21}^+$ = 201.163777)

Mono-6-(p-tolylsulphonyl)-6-deoxy-β-cyclodextrin (47)

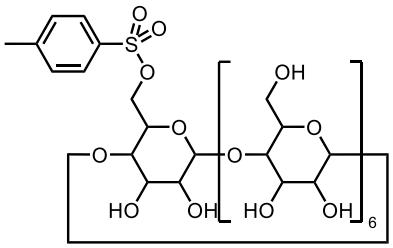

NaOH (3 M in H_2O, 75 mL, 225 mmol) was added over 15 min to a solution of β-cyclodextrin (25.0 g, 22.0 mmol) in H_2O (200 mL), and the reaction mixture was stirred for 30 min. *p*-Toluenesulfonyl chloride (6.3 g, 33.1 mmol) was added portionwise over 30 min, and the reaction mixture was stirred at rt for 1 h after addition. The reaction mixture was then filtered, and NH_4Cl (21.2 g) was added. The mixture stirred at 5 °C for 18 h. The precipitate was obtained by filtration, washed with acetone (200 mL) and dried under reduced pressure to yield the title compound as a colourless solid (8.25 g, 6.4 mmol, 29%). **^{1}H NMR** (400 MHz, DMSO-d_6) δ 7.71 (d, J = 8.2 Hz, 2H, H_{11}), 7.39 (d, J = 8.2 Hz, 2H), 5.82–5.57 (m, 14H), 4.86–4.69 (m, 7H), 4.54–4.39 (m, 5H), 4.36–4.25 (m, 1H), 3.72–3.39 (m, 28H), 3.38–3.11 (m, 14H), 2.39 (s, 3H). **^{13}C NMR** (100 MHz, DMSO-d_6) δ 145.4, 133.2, 130.4, 128.1, 102.7, 102.4, 101.7, 82.0, 81.6, 81.2, 73.6, 73.2, 72.9, 72.5, 60.4, 59.8, 21.8. Analysis is in agreement with literature data.[54]

Mono-6-azido-6-deoxy-β-cyclodextrin (48)

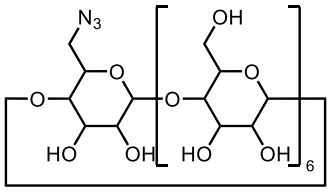

47 (8.25 g, 6.4 mmol) was stirred at 65 °C in anhydrous DMF (80 mL) in an oven-dried round-bottomed flask under an inert atmosphere. To this solution, KI (0.53 g, 3.2 mmol) and NaN_3 (2.08 g, 32.0 mmol) were added, and the reaction mixture stirred at 65 °C for 18 h. The reaction mixture was cooled to rt, and half of the solvent removed under reduced pressure. The solution was then poured into acetone (1 L) and the precipitate obtained by filtration. The solid was washed with

acetone (100 mL) and dried under reduced pressure to yield the title compound as a colourless solid (5.5 g, 4.7 mmol, 74%). **^{1}H NMR** (400 MHz, DMSO-*d*$_6$) δ 5.81–5.57 (m, 14H), 4.86–4.73 (m, 7H), 4.54–4.40 (m, 6H), 3.68–3.47 (m, 28H,), 3.41–3.19 (m, 14H, $H_{2,4}$). **^{13}C NMR** (100 MHz, DMSO-*d*$_6$) δ 102.4, 83.3, 81.9, 73.5, 72.8, 72.4, 70.7, 60.3, 51.5. Analysis is in agreement with literature data.[54]

Mono-6-amino-6-deoxy-β-cyclodextrin (49)

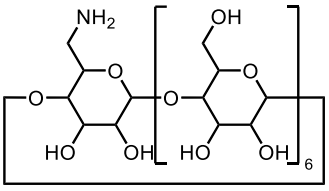

48 (5.5 g, 4.7 mmol) and triphenylphosphine (1.5 g, 5.7 mmol) were stirred in anhydrous DMF (11 mL) in an oven-dried microwave vial under an inert atmosphere for 2 h at rt. H_2O (1.0 mL, 55.5 mmol) was added, and the reaction stirred at rt for 18 h. The reaction mixture was then poured into acetone (100 mL), and the precipitate obtained by filtration. The solid was washed with acetone (3 × 10 mL) and dried under reduced pressure to yield the title compound as a colourless solid (4.5 g, 4.0 mmol, 84%). **^{1}H NMR** (400 MHz, DMSO-*d*$_6$) δ 5.78–5.55 (m, 14H), 4.88–4.73 (m, 7H), 4.61–4.37 (m, 6H), 3.89–3.43 (m, 28H), 3.39–3.17 (m, 14H). **^{13}C NMR** (100 MHz, DMSO-*d*$_6$) δ 102.4, 83.4, 82.0, 73.6, 72.9, 72.5, 72.1, 60.4, 42.1. Analysis is in agreement with literature data.[54]

((2Z,4Z)-8-Ethylbicyclo[4.2.2]deca-2,4,7,9-tetraen-7-yl)methanol (52)

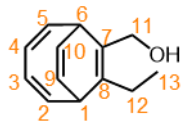

ZnI_2 (32 mg, 0.1 mmol) was added to a microwave vial, which was then heated to 280 °C for 5 mins under reduced pressure, allowed to cool, and flushed with argon. Zn dust (10 mg, 0.2 mmol) and $CoBr_2$(dppe) (32 mg, 0.1 mmol) were added to the vial, and the vial evacuated and flushed with argon three times. Anhydrous 2,2,2-trifluoroethane (1.5 mL) was added and the catalyst mixture stirred at 55 °C until the mixture fully turns from green to brown. Cyclooctatetraene (55 mg, 0.5 mmol) and then 2-pentyn-1-ol (86 mg, 1.0 mmol) were added slowly, and the reaction mixture stirred at 55 °C for 18 h. The reaction mixture was allowed to cool to rt and then diethyl ether was added to the reaction mixture, and the mixture stirred for 15 min. The reaction mixture was passed through a silica plug (1 g), eluting with diethyl ether (10 mL), and the solvent removed under reduced pressure. The resulting crude residue was purified by column chromatography (Teledyne Isco CombiFlash Rf+ system, 12 g SiO_2, hexanes–EtOAc, 0–40%, gradient elution) to yield the title compound as a colourless oil (78 mg, 0.4

mmol, 83%). **^{1}H NMR** (600 MHz, $CDCl_3$) δ 6.31–6.24 (m, 1H, H_5), 6.23–6.16 (m, 1H, H_2), 5.74–5.64 (m, 4H, $H_{3,\,4,\,9,\,10}$), 4.28 (d, *J* = 11.9 Hz, 1H, H_{11a}), 4.08 (d, *J* = 11.9 Hz, 1H, H_{11b}), 3.46–3.40 (m, 1H, H_6), 3.24–3.19 (m, 1H, H_1), 2.27–2.10 (m, 2H, H_{12}), 1.00 (t, *J* = 7.6 Hz, 3H, H_{13}).**^{13}C NMR** (600 MHz, $CDCl_3$) δ 142.5 (C_5), 141.6 (C_2), 135.8 (C_8), 129.3 (C_7), 124.5 ($C_{3/\,4/\,9/\,10}$), 124.3 ($C_{3/\,4/\,9/\,10}$), 121.3 ($C_{3/\,4/\,9/\,10}$), 121.1 ($C_{3/\,4/\,9/\,10}$), 61.0 (C_{11}), 39.5 (C_1), 37.7 (C_6), 24.2 (C_{12}), 15.0 (C_{13}). **HR-ESI-MS** *m/z*: $[M-OH]^+$ = 171.1171 (calculated $C_{13}H_{15}^+$ = 171.1174).

Ethyl methyl alcohol bullvalene (53)

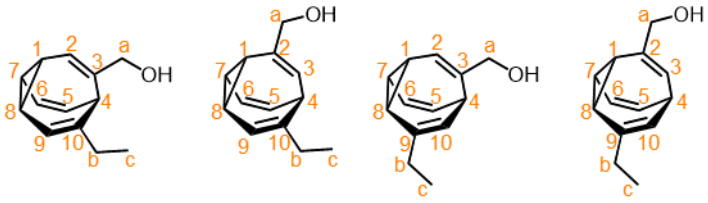

Isomer ratio

β,*β*-**53**	*γ*,*β*-**53**	*β*,*γ*-**53**	*γ*,*γ*-**53**
50	22	20	8

A solution of **52** (448 mg, 2.4 mmol) and thioxanthone (5 mg, 0.02 mmol) in anhydrous THF (8 mL), in an oven-dried vial under an inert atmosphere, was irradiated an 18 W 365 nm LED array for 5 h, cooled by a water bath at 5 °C. After irradiation was complete, the solvent was removed under reduced pressure, and the resulting crude residue was purified by column chromatography (Teledyne Isco CombiFlash Rf+ system, 24 g SiO_2, hexanes–EtOAc, 0–50%, gradient elution) to yield the title compound as a colourless oil (140 mg, 0.7 mmol, 31%). **^{1}H NMR** (500 MHz, $CDCl_3$, 223 K) δ 6.16–5.74 (m, 3.00H, *β*,*β*-$H_{2,\,5,\,6}$, *γ*,*β*-$H_{3,\,5,\,6}$, *β*,*γ*-$H_{2,\,5,\,6}$, *γ*,*γ*-$H_{3,\,5,\,6}$), 5.74–5.63 (m, 0.72H, *β*,*β*-H_9, *γ*,*β*-H_9), 5.62–5.49 (m, 0.28H, *β*,*γ*-H_{10}, *γ*,*γ*-H_{10}), 4.08–3.94 (m, 2.00H, H_a), 2.58–1.95 (m, 6.00H, $H_{1,\,4,\,7,\,b}$), 1.04–0.88 (m, 3.00H, H_c). **^{13}C NMR** (126 MHz, $CDCl_3$, 223 K) δ 144.5, 143.7 (*β*,*β*-C_{10}), 143.7, 140.7, 140.6, 140.5, 140.1 (*β*,*β*-C_3), 137.6, 129.0, 128.2, 128.0, 127.9, 127.6, 127.4 (*β*,*β*-C_6), 127.3, 127.2, 127.0, 127.0 (*β*,*β*-C_5), 126.7, 126.2, 126.2, 122.8, 122.4 (*β*,*β*-C_2), 122.1, 121.7, 118.0 (*β*,*β*-C_9), 117.9 (*β*,*γ*-C_9), 117.6, 117.2, 69.5 (C_a), 68.6 (*β*,*β*-C_a), 68.3 (C_a), 36.60 (*β*,*β*-C_4), 34.8, 34.3, 33.3, 32.6, 32.6 (*β*,*β*-C_b), 31.3, 29.9, 24.2, 23.3 (*β*,*γ*-C_1), 22.9, 22.8, 20.1, 20.0 (*β*,*β*-C_1), 19.7, 19.6, 19.0, 19.0, 18.7, 13.2 (C_c), 13.1 (C_c), 12.9 (*β*,*β*-C_c), 12.2 (C_c). **HR-ESI-MS** *m/z*: $[M-OH]^+$ = 171.1178 (calculated $C_{13}H_{15}^+$ = 171.1174).

Pent-2-yn-1-yl 4-methylbenzenesulfonate (54)

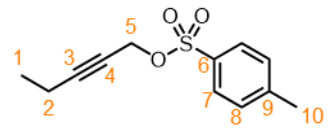

p-Toluenesulfonyl chloride (2.7 g, 14.2 mmol) was added to a solution of 2-pentyn-1-ol (1.0 g, 11.9 mmol) in anhydrous diethyl ether (20 mL) in an oven-dried round-bottomed flask under an inert atmosphere. KOH (800 mg, 14.3 mmol) was added at 0 °C, and the reaction mixture stirred at 0 °C for 4 h. The reaction mixture was then warmed to rt, filtered, and the precipitate extracted with EtOAc (25 mL). The filtrate was then washed with brine (25 mL) and the organic fraction was dried over $MgSO_4$, and the solvent removed under reduced pressure. The resulting crude residue was purified by column chromatography (Teledyne Isco CombiFlash Rf+ system, 24 g SiO_2, hexanes–EtOAc, 0–40%, gradient elution) to yield the title compound as a yellow oil (1.98 g, 8.3 mmol, 70%). **^{1}H NMR** (599 MHz, $CDCl_3$) δ 7.84–7.78 (m, 2H, H_7), 7.35–7.30 (m, 2H, H_8), 4.69 (t, *J* = 2.2 Hz, 2H, H_5), 2.44 (s, 3H, H_{10}), 2.09 (qt, *J* = 7.5, 2.2 Hz, 2H, H_2), 1.01 (t, *J* = 7.5 Hz, 3H, H_1). **^{13}C NMR** (151 MHz, $CDCl_3$) δ 145.0 (C_9), 133.6 (C_6), 129.9 (C_8), 128.3 (C_7), 91.9 (C_3), 71.4 (C_4), 58.9 (C_5), 21.8(C_{10}), 13.3 (C_1), 12.5(C_2). **HR-ASAP-MS** *m/z*: $[M+H]^+$ = 239.0728 (calculated $C_{12}H_{15}O_3S^+$ = 239.0742).

Ethyl (amino-β-Cyclodextrin methyl) bullvalene (59)

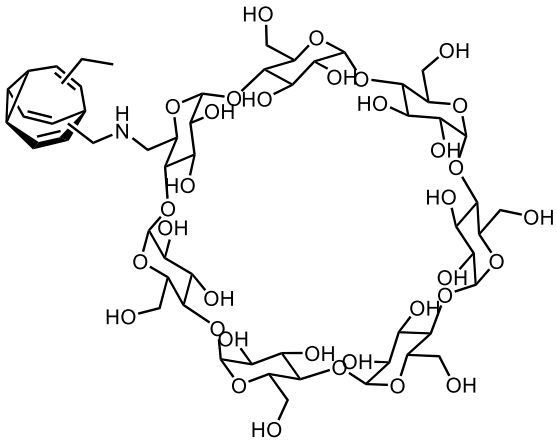

A solution of oxalyl chloride (126 mg, 1.00 mmol) in anhydrous CH_2Cl_2 (5 mL) in an oven-dried microwave vial under an inert atmosphere was cooled to −78 °C. A solution of anhydrous DMSO (156 mg, 1.99 mmol) in anhydrous CH_2Cl_2 (3 mL) was added slowly and the reaction mixture was stirred for 5 mins. A solution of **53** (150 mg, 0.80 mmol) in anhydrous CH_2Cl_2 (4 mL) was added, and the reaction mixture was stirred for another 2 h. Triethylamine (403 mg, 3.98 mmol) was added, and the reaction mixture was stirred for another 2 h. The reaction mixture was quenched with NH_4Cl (213 mg, 3.98 mmol), the reaction mixture warmed to rt, and water (10 mL) was added. The mixture was extracted with CH_2Cl_2 (10 mL), the organic fractions combined, and washed with water (3 × 10 mL) and brine (3 × 10 mL). The organic fraction was dried over $MgSO_4$, and the solvent

removed under reduced pressure to yield (ethylbullvalene)carbaldehyde **58** (130 mg, 0.63 mmol). Compound **58** (130 mg, 0.63 mmol), **49** (784 mg, 0.69 mmol), $NaCNBH_3$ (47 mg, 0.75 mmol) and glacial acetic acid (19 mg, 0.31 mmol) were dissolved in DMF (20 mL) and the reaction mixture stirred at 110 °C for 18 h. The reaction mixture was allowed to cool to rt, and poured onto acetone (100 mL) and the precipitate isolated by filtration. The precipitate was then triturated with methanol (500 mL), and the solvent removed under reduced pressure. The resulting solid may contain the title compound.

((2Z,4Z)-8-Ethylbicyclo[4.2.2]deca-2,4,7,9-tetraen-7-yl)ethan-1-ol (61)

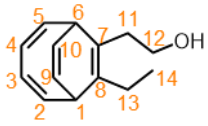

ZnI_2 (640 mg, 2.0 mmol) was added to a microwave vial, which was then heated to 280 °C for 5 mins under reduced pressure, allowed to cool, and flushed with argon. Zn dust (198 mg, 3.0 mmol) and $CoBr_2$(dppe) (630 mg, 1.0 mmol) were added to the vial, and the vial evacuated and flushed with argon three times. Anhydrous 2,2,2-trifluoroethane (10 mL) was added and the catalyst mixture stirred at 55 °C until the mixture fully turns from green to brown. Cyclooctatetraene (1.1 mL, 10.0 mmol) and then 3-hexyn-1-ol (1.7 mL, 15.6 mmol) were added slowly, and the reaction mixture stirred at 55 °C for 18 h. The reaction mixture was allowed to cool to rt and then diethyl ether was added to the reaction mixture, and the mixture stirred for 15 min. The reaction mixture was passed through a silica plug (10 g), eluting with diethyl ether (100 mL), and the solvent removed under reduced pressure. The resulting crude residue was purified by column chromatography (Teledyne Isco CombiFlash Rf+ system, 40 g SiO_2, hexanes–EtOAc, 0–50%, gradient elution) to yield the title compound as a colourless oil (1.24 g, 6.1 mmol, 61%). **^{1}H NMR** (599 MHz, $CDCl_3$) δ 6.29–6.23 (m, 2H, $H_{2,\,5}$), 5.74–5.67 (m, 4H, $H_{3,\,4,\,9,\,10}$), 3.71–3.57 (m, 2H, H_{12}), 3.25–3.22 (m, 1H, H_1), 3.14–3.10 (m, 1H, H_6), 2.63–2.57 (m, 1H, H_{11a}), 2.26–2.11 (m, 3H, $H_{11b,\,13}$), 1.00 (t, J = 7.6 Hz, 3H, H_{14}). **^{13}C NMR** (151 MHz, $CDCl_3$) δ 143.1 (C_2), 142.2 (C_5), 136.7 (C_8), 125.4 (C_7), 124.4 ($C_{3/\,4/\,9/\,10}$), 124.1 ($C_{3/\,4/\,9/\,10}$), 121.3 ($C_{3/\,4/\,9/\,10}$), 121.2 ($C_{3/\,4/\,9/\,10}$), 62.1 (C_{12}), 40.1 (C_6), 39.7 (C_1), 35.1 (C_{11}), 24.5 (C_{13}), 14.8 (C_{14}). **HR-ASAP-MS** *m/z*: $[M+H]^+$ = 203.1436 (calculated $C_{14}H_{19}O^+$ = 203.1436).

Ethyl ethyl alcohol bullvalene (62)

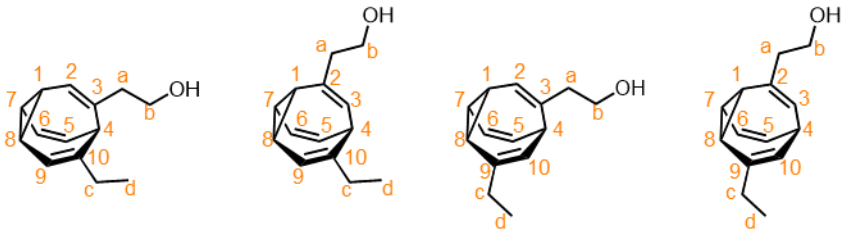

Isomer Ratio

β,β-**62**	γ,β-**62**	β,γ-**62**	γ,γ-**62**
50	23	20	7

A solution of **61** (2.4 g, 11.9 mmol) and thioxanthone (25 mg, 0.12 mmol) in anhydrous THF (40 mL), in an oven-dried vial under an inert atmosphere, was irradiated an 18 W 365 nm LED array for 5 h, cooled by a water bath at 5 °C. After irradiation was complete, the solvent was removed under reduced pressure, and the resulting crude residue was purified by column chromatography (Teledyne Isco CombiFlash Rf+ system, 40 g SiO_2, hexanes–EtOAc, 0–50%, gradient elution) to yield the title compound as a colourless oil (900 mg, 4.4 mmol, 38%). **^{1}H NMR** (500 MHz, $CDCl_3$) δ 5.95–5.79 (m, 2.00H), 5.79–5.72 (m, 1.00H), 5.69 (d, *J* = 6.7 Hz, 0.50H, *β,β*-H_9), 5.64 (d, *J* = 8.1 Hz, 0.20H, *β,γ*-H_{10}), 5.58 (d, *J* = 16.0 Hz, 0.07H, *γ,γ*-H_{10}), 5.53 (d, *J* = 9.0 Hz, 0.23H, *γ,β*-H_9), 3.71–3.55 (m, 2.00H, H_b), 2.52–1.94 (m, 8.00H, $H_{1,4,7,8,a,c}$), 1.04–0.91 (m, 3.00H, H_d). **^{13}C NMR** (126 MHz, $CDCl_3$) δ 144.2 (*γ,β*-C_{10}), 142.9 (*β,β*-C_{10}), 141.0 (*β,γ*-C_9), 140.2 (*γ,γ*-C_9), 137.3 (*γ,β*-C_2), 136.5 (*β,β*-C_3), 134.1 (*β,γ*-C_3), 133.7 (*γ,γ*-C_2), 128.2, 127.8, 127.5 (*β,β*-C), 127.3, 127.1, 126.7 (*β,β*-C), 126.6, 126.6, 126.2, 125.0, 124.5, 124.3 (*β,β*-C), 123.9, 118.6 (*β,β*-C_9), 118.5 (*γ,γ*-C_{10}), 117.7 (*β,γ*-C_{10}), 117.4 (*γ,β*-C_9), 60.1 (*γ,γ*-C_b), 60.1 (*γ,β*-C_b), 60.0 (*β,γ*-C_b), 59.9 (*β,β*-C_b), 44.1 (*β,γ*-C_a), 44.0 (*γ,γ*-C_a), 43.2 (*β,β*-C_a), 43.0 (*γ,β*-C_a), 38.9, 34.7, 34.3, 33.9, 33.6, 33.5, 33.5, 32.8 (*β,β*-C), 32.7, 29.6, 27.9, 23.2, 22.9, 22.2, 20.3, 20.1, 20.1, 19.9, 19.9, 19.6, 19.2, 13.5 (*β,γ*-C_d), 13.1 (*β,β*-C_d), 12.6 (*γ,γ*-C_d), 12.5 (*γ,β*-C_d). **HR-APCI-MS** *m/z*: $[M+H]^+$ = 203.142434 (calculated $C_{14}H_{19}O^+$ = 203.143042).

Ethyl (amino-β-Cyclodextrin methyl) bullvalene (64)

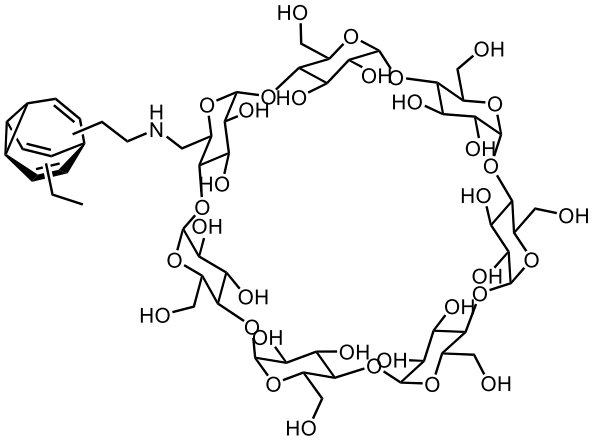

A solution of oxalyl chloride (118 mg, 0.93 mmol) in anhydrous CH_2Cl_2 (4 mL) in an oven-dried microwave vial under an inert atmosphere was cooled to −78 °C. A solution of anhydrous DMSO (145 mg, 1.85 mmol) in anhydrous CH_2Cl_2 (2 mL) was added slowly and the reaction mixture was stirred for 5 mins. A solution of **62** (150 mg, 0.74 mmol) in anhydrous CH_2Cl_2 (3 mL) was added, and the reaction mixture was stirred for another 2 h. Triethylamine (376 mg, 3.71 mmol) was added, and the reaction mixture was stirred for another 2 h. The reaction mixture was quenched with NH_4Cl (198 mg, 3.71 mmol), the reaction mixture warmed to rt, and water (10 mL) was added. The mixture was extracted with CH_2Cl_2 (10 mL), the organic fractions combined, and washed with water (3 × 10 mL) and brine (3 × 10 mL). The organic fraction was dried over $MgSO_4$, and the solvent removed under reduced pressure to yield 2-(ethylbullvalene)acetaldehyde **63** (140 mg, 0.70 mmol). Compound **63** (140 mg, 0.70 mmol), **49** (872 mg, 0.77 mmol), $NaCNBH_3$ (53 mg, 0.84 mmol) and glacial acetic acid (21 mg, 0.35 mmol) were dissolved in DMF (30 mL) and the reaction mixture stirred at 110 °C for 18 h. The reaction mixture was allowed to cool to rt, and poured onto acetone (100 mL) and the precipitate isolated by filtration. The precipitate was then triturated with methanol (500 mL), and the solvent removed under reduced pressure. The resulting solid may contain the title compound, analysis ongoing.

^{t}Butyldimethyl(prop-2-yn-1-yloxy)silane (65)

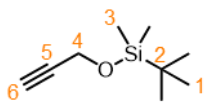

TBS-Cl (8.07 g, 53.5 mmol) was added to a mixture of propargyl alcohol (2.1 mL, 35.7 mmol), and imidazole (3.64 g, 53.5 mmol) in CH_2Cl_2 (100 mL) at 0 °C. The reaction mixture was stirred at 0 °C for 2 h, and quenched with a saturated aqueous solution of NH_4Cl (50 mL), and extracted with EtOAc (3 × 50 mL). The combined organic fractions were then washed with brine (50 mL), dried over $MgSO_4$ and the solvent removed under reduced pressure. The resulting crude residue was purified by column chromatography (Teledyne Isco CombiFlash Rf+ system, 40 g SiO_2, hexanes–EtOAc, 0–50%, gradient

elution) to yield the title compound as a yellow oil (4.30 g, 25.2 mmol, 71%). **^{1}H NMR** (400 MHz, $CDCl_3$) δ 4.31 (d, *J* = 2.4 Hz, 3H, H_4), 2.39 (t, *J* = 2.4 Hz, 1H, H_6), 0.91 (s, 9H, H_1), 0.13 (s, 6H, H_3). **^{13}C NMR** (100 MHz, $CDCl_3$) δ 82.5 (C_6), 72.9 (C_5), 51.6 (C_4), 25.9 (C_1), 18.4 (C_2), −5.1 (C_3). **HR-ESI-MS** *m/z*: $[M+H]^+$ = 170.120272 (calculated $C_9H_{19}OSi^+$ = 170.119968).

^{t}Butyldimethyl((3-(4,4,5,5-tetramethyl-1,3,2-dioxaborolan-2-yl)prop-2-yn-1-yl)oxy)silane (66)

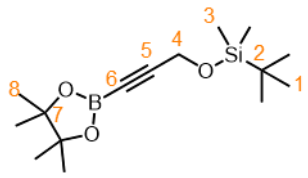

^{n}BuLi (2.5 M in hexane, 11.3 mL, 28.3 mmol) was added to a solution of **65** (4.00 g, 23.5 mmol) in anhydrous THF (40 mL) at −78 °C under an inert atmosphere in an oven-dried round-bottomed flask. The reaction mixture was stirred at −78 °C for 1 h. A solution of 2-isopropoxy-4,4,5,5-tetramethyl-1,3,2-dioxaborolane (5.75 mL, 28.2 mmol) in THF (40 mL) was added to the reaction and the mixture stirred at −78 °C for a further 2 h. The reaction was then quenched with anhydrous HCl (4 M in 1,4-dioxane, 7 mL), and the reaction mixture allowed to warm to rt, and stirred for a further 1 h. The solvent was removed under reduced pressure and the crude solid extracted with diethyl ether (100 mL). The solvent was removed under reduced pressure to yield the title compound as a yellow oil (5.0 g, 16.8 mmol, 71%). **^{1}H NMR** (400 MHz, $CDCl_3$) δ 4.34 (s, 2H, H_4), 1.26 (s, 12H, H_8), 0.89 (s, 9H, H_1), 0.11 (s, 6H, H_3) **^{13}C NMR** (100 MHz, $CDCl_3$) δ 84.4 (C_7), 52.0 (C_4), 25.9 (C_1), 24.7 (C_8), 18.4 (C_2), −5.2 (C_3). **HR-ESI-MS** *m/z*: $[M+H]^+$ = 297.207225 (calculated $C_{15}H_{30}BO_3Si^+$ = 297.205494)

^{t}Butyldimethyl(((2Z,4Z)-8-(4,4,5,5-tetramethyl-1,3,2-dioxaborolan--2-yl)bicyclo[4.2.2]deca-2,4,7,9-tetraen-7-yl)methoxy)silane (67)

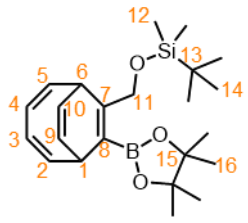

ZnI_2 (43 mg, 0.14 mmol) was added to a microwave vial, which was then heated to 280 °C for 5 mins under reduced pressure, allowed to cool, and flushed with argon. Zn dust (13 mg, 0.20 mmol) and $CoBr_2$(dppe) (42 mg, 0.07 mmol) were added to the vial, and the vial evacuated and flushed with argon three times. Anhydrous 1,2-dichloroethane (1 mL) was added and the catalyst mixture stirred at rt until the mixture fully turns from green to brown. Cyclooctatetraene (0.08 mL, 0.68) and then **66** (250 mg, 0.84 mmol) in dichloroethane (0.5 mL) were added slowly, and

the reaction mixture stirred at rt for 18 h. The reaction mixture was allowed to cool to rt and then diethyl ether was added to the reaction mixture, and the mixture stirred for 15 min. The reaction mixture was passed through a silica plug (0.5 g) , eluting with diethyl ether (10 mL), and the solvent removed under reduced pressure. The resulting crude residue was purified by column chromatography (Teledyne Isco CombiFlash Rf+ system, 12 g SiO_2, hexanes–EtOAc, gradient elution) to yield the title compound as a colourless oil (108 mg, 0.27 mmol, 40%). **^{1}H NMR** (400 MHz, $CDCl_3$) δ 6.29–6.20 (m, 1H, H_2), 6.15–6.06 (m, 1H, H_5), 5.76–5.61 (m, 4H, $H_{3/4/9/10}$), 4.56–4.52 (m, 2H, H_{11}), 3.73 (dd, *J* = 9.0, 5.7, 1H, H_6), 3.43 (dd, *J* = 9.0, 5.7, 1H, H_1), 1.24 (s, 6H, H_{16a}), 1.23 (s, 6H, H_{16b}), 0.89 (s, 9H, H_{14}), 0.32 (s, 3H, H_{12a}), 0.23 (s, 3H, H_{12b}). **^{13}C NMR** (100 MHz, $CDCl_3$) δ 149.6 (C_7), 142.5 (C_2), 141.6 (C_5), 124.8 (C_4), 123.9 (C_3), 122.3 (C_9), 121.5 (C_{10}), 83.1 (C_{15}), 62.4 (C_{11}), 36.9 (C_1), 36.6 (C_6), 26.1 (C_{14}), 25.2 (C_{16a}), 24.7 (C_{16b}), 18.5 (C_{13}), −4.9 (C_{12a}), −5.1 (C_{12b}). **HR-ESI-MS** *m/z*: $[M+Na]^+$ = 423.2498 (calculated $C_{23}H_{37}BNaO_3Si^+$ = 423.2497).

Methoxy Cyclodextrin (72)

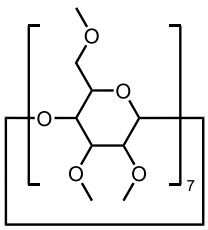

Sodium hydride (60% in mineral oil, 0.88 g, 22.0 mmol) was added to a stirred solution of β-cyclodextrin (0.50 g, 0.44 mmol) in DMSO (15 mL) in an oven-dried round-bottomed flask under an inert atmosphere. The reaction mixture was stirred at rt for 1 h. The reaction mixture was cooled to 0 °C and methyl iodide (1.37 mL, 22.0 mmol) added dropwise. The reaction mixture was warmed to rt and stirred for 24 h. The reaction mixture was cooled to 0 °C and quenched with H_2O (25 mL). The mixture was warmed to rt and extracted with diethyl ether (5 × 20 mL). The combined organic extracts were washed with brine (50 mL), dried with $MgSO_4$ and the solvent removed under reduced pressure. The resulting crude residue was purified by column chromatography (Teledyne Isco CombiFlash Rf+ system, 12 g SiO_2, CH_2Cl_2–MeOH, 0–15%, gradient elution) to yield the title compound as a colourless solid (0.39 g, 0.27 mmol, 62%). **^{1}H NMR** (400 MHz, $CDCl_3$) δ 5.12 (d, *J* = 3.6 Hz, 7H), 3.88–3.76 (m, 14H), 3.64 (s, 21H), 3.61–3.46 (m, 42H), 3.38 (s, 21H), 3.18 (dd, *J* = 9.7, 3.5 Hz, 7H). **^{13}C NMR** (100 MHz, $CDCl_3$) δ 99.1, 82.2, 81.9, 80.4, 71.5, 71.0, 61.6, 59.1, 58.6. **HR-APCI-MS** *m/z*: $[M+H]^+$ = 1429.7094 (calculated $C_{63}H_{113}O_{35}^+$ = 1429.7057). Analysis is in agreement with literature values.

1,2-Bis(4,4,5,5-tetramethyl-1,3,2-dioxaborolan-2-yl)ethyne (74)

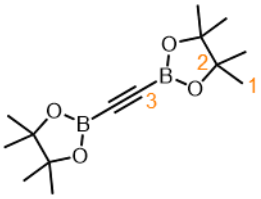

^{n}BuLi (2.5 M in hexanes, 32 mL, 80 mmol) in anhydrous THF/diethyl ether (100 mL, 1:1) was prepared in an oven-dried two-neck round-bottomed flask, under an inert atmosphere, and the solution was stirred at −78 °C. To this, a solution of trichloroethylene (2.4 mL, 26.6 mmol) in anhydrous diethyl ether (25 mL) was added dropwise. The solution was warmed to rt and stirred for 12 h, at which point a white precipitate had formed. This suspension was cooled to −78 °C and transferred *via* cannula, using a 5.0 mm inner diameter Teflon tube to a solution of 2-isopropoxy-4,4,5,5-tetramethyl-1,3,2-dioxaborolane (10.9 mL, 53.3 mmol) in anhydrous diethyl ether (100 mL) in an oven-dried round-bottomed flask, under an inert atmosphere. The mixture was stirred at −78 °C for 4 h, and then warmed to rt and stirred for 2 h. The solution was cooled to −78 °C and anhydrous hydrochloric acid (4 M in dioxane, 13.3 mL) added, and the mixture warmed to rt. The reaction mixture was passed through a silica plug (10 g), washing with diethyl ether (100 mL). The solvent was removed under reduced pressure. The remaining crude solid was washed with cold hexanes (50 mL) to yield the title compound as a colourless solid (5.1 g, 18.3 mmol, 69%). **^{1}H NMR** (400 MHz, $CDCl_3$) δ 1.25 (s, 24H, H_1). **^{13}C NMR** (101 MHz, $CDCl_3$) δ 84.8 (C_2), 24.7 (C_1). **^{11}B NMR** (400 MHz, $CDCl_3$) δ 23.3. **HR-APCI-MS** *m/z*: $[M-+H]^+$ = 279.189167 (calculated $C_{14}H_{25}B_2O_4^+$ = 279.193867).

(2Z,4Z)-7,8-Bis(4,4,5,5-tetramethyl-1,3,2-dioxaborolan-2-yl)bicyclo[4.2.2]deca-2,4,7,9-tetraene (75)

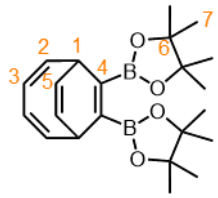

ZnI_2 (336 mg, 1.1 mmol) was added to a microwave vial, which was then heated to 280 °C for 5 mins under reduced pressure, allowed to cool, and flushed with argon. Zn dust (103 mg, 1.6 mmol) and $CoBr_2$(dppe) (325 mg, 0.5 mmol) were added to the vial, and the vial evacuated and flushed with argon. Anhydrous 1,2-dichloroethane (8 mL) was added and the catalyst mixture stirred at rt until the mixture fully turns from green to brown. Cyclooctatetraene (0.6 mL, 5.3 mmol) and then a solution of **74** (1.9 g, 6.8 mmol) in 1,2-dichloroethane (5 mL) were added slowly, and the reaction mixture stirred at rt for 48 h. Diethyl ether (10 mL) was added to the reaction mixture, and the mixture stirred for 15 min. The reaction mixture was passed through a silica plug (10 g), eluting with diethyl ether (100 mL), and the solvent removed under

reduced pressure. The resulting crude residue was purified by column chromatography (Teledyne Isco CombiFlash Rf+ system, 40 g SiO_2, hexanes–EtOAc, gradient elution) to yield the title compound as a colourless solid. (1.32 g, 3.5 mmol, 66%). **^{1}H NMR** (400 MHz, $CDCl_3$) δ 6.19–6.09 (m, 2H, H_2), 5.76–5.67 (m, 4H, $H_{3,5}$), 3.42–3.37 (m, 2H, H_4), 1.27 (s, 24H, H_1). **^{13}C NMR** (101 MHz, $CDCl_3$) δ 140.6 (C_2), 124.8 (C_3), 122.1 (C_5), 83.6 (C_6), 37.4 (C_1), 24.9 (C_7). **HR-ESI-MS** *m/z*: $[M+H]^+$ = 381.2638 (calculated $C_{22}H_{33}{}^{10}B_2O_4^+$ 381.2638)

Bis(4,4,5,5-tetramethyl-1,3,2-dioxaborolan-2-yl) bullvalene (76)

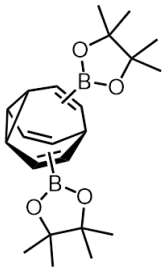

A solution of **75** (1.5 g, 3.9 mmol) and thioxanthone (8 mg, 0.04 mmol) in anhydrous THF (15 mL), in an oven-dried vial under an inert atmosphere, was irradiated an 18 W 365 nm LED array for 5 h, cooled by a water bath at 5 °C. After irradiation was complete, the solvent was removed under reduced pressure, and the resulting crude residue was purified by column chromatography (Teledyne Isco CombiFlash Rf+ system, 24 g SiO_2, hexanes–EtOAc, 0–50%, gradient elution) to yield the title compound as a colourless solid (0.94 g, 2.5 mmol, 63%). **M.P.** = 143–145 °C. **^{1}H NMR** (400 MHz, $CDCl_3$) δ 7.05–6.05 (br m, 2.8H), 4.69–4.22 (br s, 1.2H), 3.68–2.37 (br m, 4H), 1.23 (s, 24H). **HR-ESI-MS** *m/z:* $[M+H]^+$ = 381.2628 (calculated $C_{22}H_{33}{}^{10}B_2O_4^+$ = 381.2638). Analysis is in agreement with literature values.[33]

Bis(*p*-fluorophenyl) bullvalene (1)

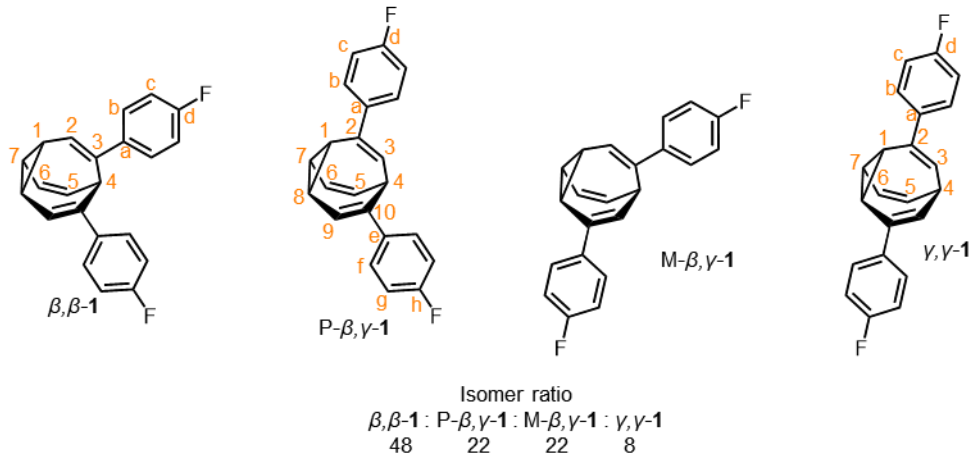

76 (233 mg, 0.6 mmol), *p*-bromofluorobenzene (235 mg, 1.3 mmol) and $Pd(PPh_3)_4$ (25 mg, 0.03 mmol) were added to degassed THF (3.2 mL) and degassed aqueous NaOH solution (10% w/v in H_2O, 1.6 mL) in a microwave vial under an inert

atmosphere. The reaction mixture was stirred at 60 °C for 18 h. The reaction mixture was allowed to cool to rt, and extracted with diethyl ether (10 mL). The organic fraction was dried over $MgSO_4$, and the solvent removed under reduced pressure. The resulting crude residue was purified by column chromatography (Teledyne Isco CombiFlash Rf+ system, 24 g SiO_2, hexanes–EtOAc, 0–50%, gradient elution) to yield the title compound as a yellow gum (84 mg, 0.26 mmol, 43%). **^{1}H NMR** (500 MHz, CD_3CD_2OD, 223 K) δ 7.45–7.29 (m, 2.00H), 7.29–7.14 (m, 2.52H), 7.12–6.97 (m, 3.48H), 6.20–5.74 (m, 4.00H, $H_{2, 3, 5, 6}$, *β,γ*-$H_{9, 10}$), 3.52 (d, *J* = 8.9 Hz, 0.48H, *β,β*-H_4), 3.18 (ap. t, *J* = 9.0 Hz, 0.44H, *β,γ*-H_4), 2.93–2.73 (m, 0.56H, *β,γ*-H_1, *γ,γ*-H_7), 2.63–2.31 (m, 2.52H, H_7, *β,β*-H_1, *γ,γ*-H). **^{13}C NMR** (126 MHz, CD_3CD_2OD, 223 K) δ 163.7 (C-F), 161.9 (C-F), 161.7 (C-F), 161.7 (C-F), 142.7, 141.1, 141.0, 139.9, 139.4, 139.0, 138.4, 129.1, 129.0, 129.0, 128.7, 128.6, 128.6, 128.5, 128.3 (*β,γ*-C), 127.3 (*β,γ*-C), 127.0 (*β,β*-C), 125.8 (*β,β*-C), 124.9 (*β,γ*-C), 123.7 (*β,γ*-C), 116.1, 116.0, 116.0, 116.0, 115.8, 41.6 (*β,β*-C_4), 36.5 (*β,γ*-C_4), 24.3 (*β,γ*-C_1), 23.6 (*γ,γ*-C_7), 22.4 (*β,β*-$C_{1/7}$), 22.4, 21.7, 21.5. **^{19}F NMR** (471 MHz, CD_3CD_2OD) δ −117.88, −117.74, −117.67, −117.61. **HR-ESI-MS** *m/z*: $[M+H]^+$ 319.1289 (calculated $C_{22}H_{17}F_2^+$ = 319.1298).

References

1 D. E. Koshland, *Angew. Chem. Int. Ed. Engl.*, 1995, **33**, 2375–2378.

2 D. E. Koshland, *Proc. Natl. Acad. of Sci. U.S.A.*, 1958, **44**, 98–104.

3 J. B. Wittenberg and L. Isaacs, in *Supramolecular Chemistry*, Wiley, 2012.

4 E. T. Kool, *Chem. Rev.*, 1997, **97**, 1473–1488.

5 F. Paul and T. R. Weikl, *PLoS Comput. Biol.*, 2016, **12**, e1005067.

6 G. G. Hammes, Y.-C. Chang and T. G. Oas, *Proc. Natl. Acad. Sci. U.S.A.*, 2009, **106**, 13737–13741.

7 S. Anderson, H. L. Anderson and J. K. M. Sanders, *Acc. Chem. Res.*, 1993, **26**, 469–475.

8 M. Ruben, J. Rojo, F. J. Romero-Salguero, L. H. Uppadine and J. Lehn, *Angew. Chem. Int. Ed. Engl.*, 2004, **43**, 3644–3662.

9 P. T. Corbett, J. Leclaire, L. Vial, K. R. West, J.-L. Wietor, J. K. M. Sanders and S. Otto, *Chem. Rev.*, 2006, **106**, 3652–3711.

10 J.-M. Lehn, *Chem. Soc. Rev.*, 2007, **36**, 151–160.

11 C. Dohmen, T. Paululat and H. Ihmels, *Chem. Eur. J.*, 2024, **120**, e202304311.

12 A. P. Birvé, H. D. Patel, J. R. Price, W. M. Bloch and T. Fallon, *Angew. Chem. Int. Ed. Engl.*, 2021, **61**, e202115468

13 A. R. Lippert, V. L. Keleshian and J. W. Bode, *Org. Biomol. Chem.*, 2009, **7**, 1529–1532.

14 J. F. Teichert, D. Mazunin and J. W. Bode, *J. Am. Chem. Soc.*, 2013, **135**, 11314–11321.

15 K. Sarma, W. Witt and G. Schröder, *Chem. Ber.*, 1983, **116**, 3800–3812.

16 P. Roach and R. Warmuth, *Angew. Chem. Int. Ed. Engl.*, 2003, **42**, 3039–3042.

17 B. M. O'Leary, R. M. Grotzfeld and J. Rebek, *J. Am. Chem. Soc.*, 1997, **119**, 11701–11702.

18 D. J. Cram, M. E. Tanner and R. Thomas, *Angew. Chem. Int. Ed. Engl.*, 1991, **30**, 1024–1027.

19 R. G. Chapman and J. C. Sherman, *J. Org. Chem.*, 2000, **65**, 513–516.

20 S. Mecozzi and J. Rebek, *Chem. Eur. J.*, 1998, **4**, 1016–1022.

21 D. J. Cram, *J. Incl. Phenom. Macro.*, 1988, **6**, 397–413.

22 M. L. C. Quan and D. J. Cram, *J. Am. Chem. Soc.*, 1991, **113**, 2754–2755.

23 D. J. Cram, R. Jaeger and K. Deshayes, *J. Am. Chem. Soc.*, 1993, **115**, 10111–10116.

24 J. Yoon, C. Sheu, K. N. Houk, C. B. Knobler and D. J. Cram, *J. Org. Chem.*, 1996, **61**, 9323–9339.

25 J. C. Sherman, D. J. Cram, J. A. Bryant, . T Blanda, M. Vincenti and C. B. Knobler, *J. Am. Chem. Soc.*, 1991, **113**, 7717–7727.

26 D. J. Cram, S. Karbach, Y. H. Kim, L. Baczynskyj and G. W. Kallemeyn, *J. Am. Chem. Soc.*, 1985, **107**, 2575–2576.

27 M. G. McKay, T. Cwele, H. B. Friedrich and G. E. M. Maguire, *Org. Biomol. Chem.*, 2009, **7**, 3958.

28 O. Ugono, J. P. Moran and K. T. Holman, *Chem. Commun.*, 2008, 1404.

29 J. A. Bryant, M. T. Blanda, M. Vincenti and D. J. Cram, *J. Am. Chem. Soc.*, 1991, **113**, 2167–2172.

30 J. C. Sherman, C. B. Knobler and D. J. Cram, *J. Am. Chem. Soc.*, 1991, **113**, 2194–2204.

31 S. S. Zhu, H. Staats, K. Brandhorst, J. Grunenberg, F. Gruppi, E. Dalcanale, A. Lützen, K. Rissanen and C. A. Schalley, *Angew. Chem. Int. Ed. Engl.*, 2008, **47**, 788–792.

32 M. Achard, M. Mosrin, A. Tenaglia and G. Buono, *J. Org. Chem.*, 2006, **71**, 2907–2910.

33 H. D. Patel, T.-H. Tran, C. J. Sumby, L. F. Pašteka and T. Fallon, *J. Am. Chem. Soc.*, 2020, **142**, 3680–3685.

34 B. Ma and J. K. Snyder, *Organometallics*, 2002, **21**, 4688–4695.

35 J. Charpentier, F. Voirol, F. Flachsmann, S. Tanner, N. Aeberli, G. Brunner and A. Goeke, *Helv. Chim. Acta*, 2020, **103**, e2000175.

36 D. Danielsiek and G. Dyker, *Eur. J. Org. Chem.*, 2021, **2021**, 1026–1034.

37 M. Dow, F. Marchetti, K. A. Abrahams, L. Vaz, G. S. Besra, S. Warriner and A. Nelson, *Chem. Eur. J.*, 2017, **23**, 7207–7211.

38 J.-J. Ge, C.-Z. Yao, M.-M. Wang, H.-X. Zheng, Y.-B. Kang and Y. Li, *Org. Lett.*, 2016, **18**, 228–231.

39 Y.-S. Byun, O. Vadhat, M. T. Blanda, C. B. Knobler and D. J. Cram, *J. Chem. Soc., Chem. Commun.*, 1995, 1825.

40 C. Sheu and K. N. Houk, *J. Am. Chem. Soc.*, 1996, **118**, 8056–8070.

41 S. Mendoza, P. D. Davidov and A. E. Kaifer, *Chem. Eur. J.*, 1998, **4**, 864–870.

42 S. Ro, S. J. Rowan, A. R. Pease, D. J. Cram and J. F. Stoddart, *Org. Lett.*, 2000, **2**, 2411–2414.

43 M. S. Henriques, D. I. Gorbunov, A. N. Ponomaryov, A. Saneei, M. Pourayoubi, M. Dušek, S. Zvyagin, M. Uhlarz and J. Wosnitza, *Polyhedron*, 2016, **118**, 154–158.

44 C. L. D. Gibb and B. C. Gibb, *J. Am. Chem. Soc.*, 2004, **126**, 11408–11409.

45 K. Wang and B. C. Gibb, *J. Org. Chem.*, 2017, **82**, 4279–4288.

46 C. L. D. Gibb and B. C. Gibb, *J. Am. Chem. Soc.*, 2006, **128**, 16498–16499.

47 Z. Shadfar, O. Yahiaoui, T. A. Collier, T. Fallon and J. R. Allison, *J. Chem. Phys.*, 2021, **154**, 154105.

48 R. A. Dunbar and F. V. Bright, *Supramol. Chem.*, 1994, **3**, 93–99.

49 K. Hirotsu, T. Higuchi, K. Fujita, T. Ueda, A. Shinoda, T. Imoto and I. Tabushi, *J. Org. Chem.*, 1982, **47**, 1143–1144.

50 T. Lee, J. Lim, I. Chung, I. Kim and C.-S. Ha, *Macromol. Res.*, 2010, **18**, 120–128.

51 F. Djedahi-Pilard, J. Dhlos and B. Perly, *Tetrahedron Lett.*, 1993, **34**, 2457–2460.

52 Yu. G. Gololobov, I. N. Zhmurova and L. F. Kasukhin, *Tetrahedron*, 1981, **37**, 437–472.

53 R. J. White, P. G. Plieger and D. R. K. Harding, *Tetrahedron Lett.*, 2010, **51**, 800–803.

54 T. Carmona, J. F. Marco, M. Giménez-Marqués, W. Cañón-Mancisidor, M. Gutiérrez-Cutiño, P. Hermosilla-Ibáñez, E. G. Pérez, G. Mínguez Espallargas and D. Venegas-Yazigi, *Polyhedron*, 2021, **210**, 115509.

55 Y. Liu, Z. Fan, H.-Y. Zhang, Y.-W. Yang, F. Ding, S.-X. Liu, X. Wu, T. Wada and Y. Inoue, *J. Org. Chem.*, 2003, **68**, 8345–8352.

56 O. Yahiaoui, H. D. Patel, K. S. Chinner, L. F. Pašteka and T. Fallon, *Org. Lett.*, 2020, **23**, 1157–1162.

57 O. Yahiaoui, L. F. Pašteka, C. J. Blake, C. G. Newton and T. Fallon, *Org. Lett.*, 2019, **21**, 9574–9578.

58 O. Yahiaoui, L. F. Pašteka, B. Judeel and T. Fallon, *Angew. Chem. Int. Ed. Engl.*, 2018, **57**, 2570–2574.

59 Y. Zhou, E. Lindbäck, L. G. Marinescu, C. M. Pedersen and M. Bols, *Eur. J. Org. Chem.*, 2012, **2012**, 4063–4070.

60 N. Miyaura, K. Yamada and A. Suzuki, *Tetrahedron Lett.*, 1979, **20**, 3437–3440.

61 B. C. Gibb, R. G. Chapman and J. C. Sherman, *J. Org. Chem.*, 1996, **61**, 1505–1509.

62 H. Xi, C. L. D. Gibb and B. C. Gibb, *J. Org. Chem.*, 1999, **64**, 9286–9288.

Chapter 5 | Correlated Shapeshifting and Configurational Isomerisation

Manuscript to be submitted as 'Correlated Shapeshifting and Configurational Isomerization' Burhan A. Hussein, William Maturi, Mary Kate Rylands, Aisha N. Bismillah, Yuzhen Wen, Juan A. Aguilar, Rabia Ayub, Conor D. Rankine, and Paul R. McGonigal.

Abstract

Herein we demonstrate that the rapid 'shapeshifting' constitutional isomerization of a substituted bullvalene is influenced by the *E*-to-*Z* configurational isomerization of a remote carbamate group, giving rise to correlated motion. We find that, while the *E*-configurational isomer of a bulky carbamate favors the *β*-bullvalene constitutional isomer, a noncovalent bonding interaction within the *Z*-carbamate tips the equilibrium toward the *γ*-bullvalene form. Using DFT modelling and NMR spectroscopy, this long-range interaction is identified as being between the bullvalene core and a pendant phenyl group connected to the carbamate. Coupling the constitutional changes of a bullvalene to a reciprocal configurational isomerization through a long-range interaction in this way will allow shapeshifting rearrangements to be exploited as part of collective motion in extended structures.

Acknowledgments

The following people are gratefully acknowledged for their contribution to this chapter: Dr. Burhan A. Hussein for synthesis of **1a** and help in synthesis of **1b**. Mary Kate Rylands grew the crystal of **1a**. Dr. Aisha N. Bismillah performed NMR spectroscopy and contributed to the writing of the experimental. Yuzhen Wen contributed to the writing of the experimental. Dr. Juan A. Aguilar contributed to the NMR spectroscopy performed. Dr. Rabia Ayub and Dr. Conor Rankine performed computational analysis of the compounds. Dr. Paul McGonigal performed computational analysis and wrote the initial draft of the manuscript, which was refined with the author. Preliminary experimental work and supplementary synthesis not written herein was also performed by the author.

5.1 Introduction

The rapid, successive Cope rearrangements of bullvalenes[1] produce a series (Figure 1a) of constitutional isomers. Recent advances in the synthesis of substituted derivatives,[2] alongside the development of related fluxional cages,[3] have led to renewed interest in exploiting these 'shapeshifting' structures as part of functional molecules and materials. Part of the appeal of using bullvalene derivatives is that they juxtapose the rigidity and well-defined bond angles[1e] that are typical of cage-like structures with the rapid structural dynamics that are commonly only found in flexible molecules. They exhibit 'rigid dynamics' at the single-molecule level.[4] Accordingly, investigations have been reported into bullvalene-containing fluorophores,[5] antibiotics,[6] small-molecule receptors,[7] transition metal complexes,[8] rigid-rod polymers[9], and single-molecule junctions.[10]

By contrast, most organic structures, particularly those containing rotatable single bonds, rapidly sample stereoisomeric structures through changes in bond angles and dihedral angles.[11] The resulting isomerization (Figure 1b) is not only influenced by local electronic and steric factors, but also by long-range interactions. Bond rotations of groups that are separated by several covalent bonds but are close together in space can, therefore, become correlated with one another,[12] i.e., the isomerization or motion of one part of the molecule is coupled to a reciprocal conformational or configurational change in another part.

5.2 Correlated Motion

To exploit the shapeshifting rearrangements of bullvalenes in larger collective motions of extended structures,[12d–f] it is necessary to understand how their fluxional Cope rearrangements are influenced (Figure 1c) by isomerization of surrounding groups. Here, we report the isomeric distribution of carbamate-functionalized bullvalenes **1** (Scheme 1) and demonstrate that, even in this structurally simple case, conformational changes can become correlated to shapeshifting isomerization. For one of the compounds (benzhydryl derivative **1b**), we find that while the *E*-carbamate is most stable as its β-substituted bullvalene isomer, bond rotation to the *Z*-carbamate biases the bullvalene unit towards its γ-substituted form instead, i.e., the energetics of bullvalene isomerization and carbamate rotation are coupled to one another. We show that through-space interactions subtly alter the energetics of the dynamic system. As part of this investigation, we have also assessed the extent to which this isomer

distribution can be accurately modelled by comparing the calculated energies of the lowest energy conformers, as opposed to analysing the full conformational landscape.

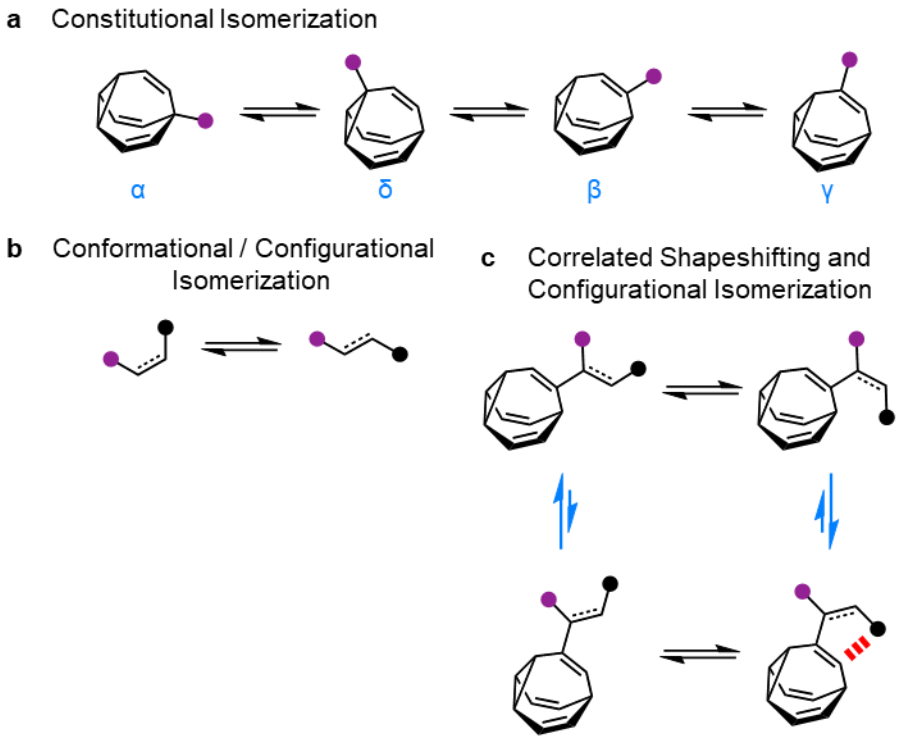

Figure 1. The combination of (a) bullvalene shapeshifting rearrangements between constitutional isomers with (b) conformational and configurational changes by single bond rotations and E-to-Z isomerization are (c) correlated through noncovalent interactions (red) to bias the two bullvalene rearrangement equilibria in opposite directions (blue arrows). Black and purple circles represent appended functional groups.

5.3 Synthesis of Carbamate Bullvalenes

We targeted (Scheme 1) tertiary carbamates **1a** and **1b** derived from benzylamine **2a** and benzhydrylamine **2b**, respectively. The partial double bond character of the carbamate C–N bond (c.f., tertiary amide C–N bonds[13]) gives rise to *E*-to-*Z* configurational isomerization that can be slowed down and observed by dynamic NMR (DNMR) spectroscopy at low temperatures, which we reasoned would allow us to experimentally measure distributions of the configurational and constitutional isomers of **1a** and **1b**. Starting from **2**, we performed (Scheme 1a) a sequence of carbamate formation, alkylation with propargyl bromide, and cobalt(I)-catalysed [6+2] cycloaddition with cyclooctatetraene[2c,14] to produce bicyclo[4.2.2]deca-2,4,7,9-tetraene intermediates **4**. A final photochemical di-π-methane rearrangement step[15] using thioxanthone[2e] as a photosensitizer gave rise to the target bullvalenes **1**.

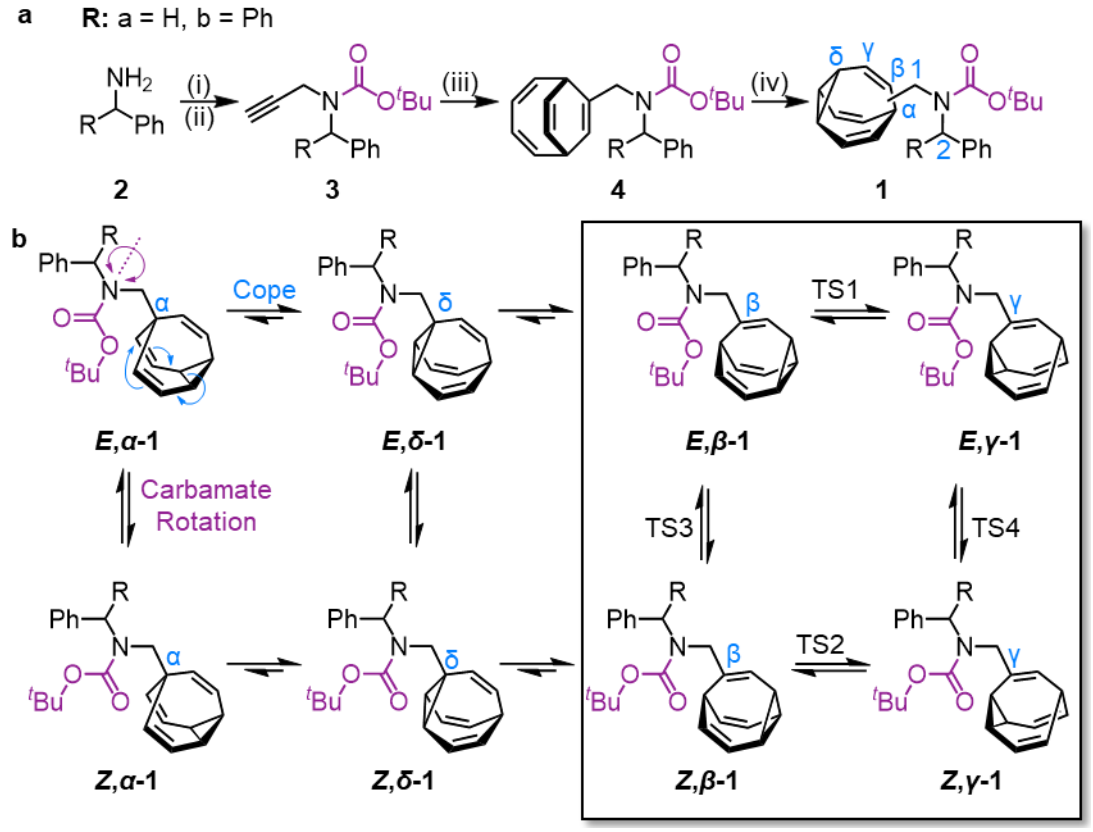

Scheme 1. a) Synthesis of sterically crowded bullvalene carbamates. Reagents and conditions: i) ***2****, Boc_2O, NEt_3, CH_2Cl_2, rt, 24 h; ii) 1. NaH, DMF, 0 °C, 30 min, 2. propargyl bromide, rt, 5 h, 70%* ***3a*** *from* ***2a****, 64%* ***3b*** *from* ***2b****; iii)* ***3****, cyclooctatetraene, $CoBr_2$(dppe), ZnI_2, Zn, TFE, 55 °C, 18 h, 55%* ***4a****, 48%* ***4b****; iv)* ***4****, hv (365 nm), thioxanthone, THF, 25 °C, 3 h, 50%* ***1a****, 54%* ***1b****. b) Eight isomers interchange by Cope rearrangements (horizontal equilibria) and by rotation around the carbamate N–C bond (vertical equilibria).*

There are four possible constitutional isomers of **1** (Scheme 1b), which we label as *α*–*δ* according to the attachment point of the carbamate substituent to the bullvalene cage.[1e] Consecutive Cope rearrangements from the *α*-isomer lead to the *δ*-, *β*-, then *γ*-isomers in a reversible linear sequence. Alternatively, rotation around the carbamate C–N bond interconverts the *E*- and *Z*-configurational isomers. In combination, these two pathways give rise to a set of eight isomers (Scheme 1b).

5.3.1 **1a** ^{1}H NMR Low Temperature Analysis

^{1}H NMR Spectroscopic analysis of the benzyl derivative **1a** in $CDCl_3$ at 313 K (Figure 2a) shows two broad resonances corresponding to the two sets of methylene protons, H1 and H2. Rapid chemical exchange at this temperature averages out the contributions from the different isomers to these two methylene resonances and causes the signals arising from the bullvalene methine groups, Hα–Hδ, to broaden and

partially merge. At 219 K, the reduced rates of Cope rearrangements and carbamate rotation allow signals from the different species to be resolved.

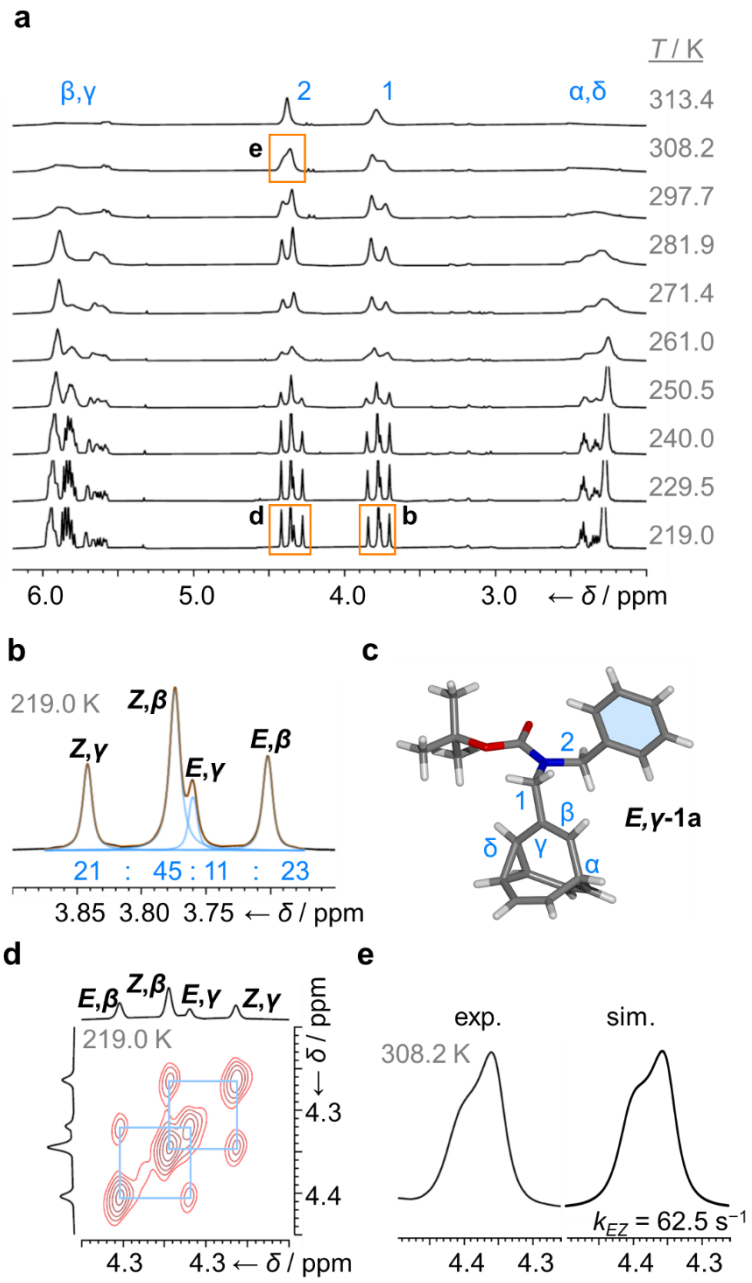

*Figure 2. [1]H DNMR (499 MHz, $CDCl_3$) and crystallographic analyses of **1a**. a) Partial [1]H NMR spectra at temperatures ranging from 219 K to 313 K. Signals are assigned using the labels in Scheme 1. Regions in orange boxes correspond to those shown in panels b, d, and e. b) Line fitting was used to deconvolute the H1 signals at 219 K. An overlay of the experimentally measured (black) and simulated (orange) traces is shown, including the integrals of the four simulated peaks (blue). c) X-ray crystal structure of **E,γ-1a**.[18] d) Partial EXSY NMR spectrum (499 MHz, $CDCl_3$, t_m = 500 ms). Blue boxes indicate cross peaks arising from Cope rearrangements. e) Line-shape analysis for the H2 signal at 308 K, comparing the experimentally measured (exp.) and simulated (sim.) line shapes. See Table S1 for simulation parameters.*

Although there are eight possible isomers, the *α*- and *δ*-forms of mono-substituted bullvalenes are usually several kJ·mol^{-1} higher in energy than the olefin-substituted *β*- and *γ*-forms,[16] so they are not present in sufficient concentrations to be observed. *β*-Substitution is usually preferred over *γ*-substitution by ~1–2 kJ·mol^{-1}.[2c] In keeping with this expectation, line fitting of the H1 peaks indicates (Figure 1b) that four isomers are present in a 45:23:21:11 ratio, which can be assigned to ***Z,β*-1a**, ***E,β*-1a**, ***Z,γ*-1a**, and ***E,γ*-1a**, respectively, using 2D NMR (Figures S1–S4). Shape-selective crystallization[17] from this mixture yields ***E,γ*-1a** (the least populated of the four isomers in solution) as the sole isomer in the solid state (Figure 2c).[18] In energetic terms (Table 1), the solution-phase population corresponds to small Gibbs energy biases ΔG_{exp} of ~1.3 kJ·mol^{-1} toward both *β*-isomers over their *γ*-substituted counterparts, and ΔG_{exp} of ~1 kJ·mol^{-1} for each *Z*-carbamate over its corresponding *E*-carbamate. Therefore, for **1a**, there is no evidence that the *E*/Z-state of the molecule substantially changes the energetics of *β*/*γ*-isomerization, or vice versa. The two isomerization processes do not appear to be correlated.

This system does, however, provide an unusual case of reversible covalent changes occurring in a molecule more rapidly than its bond rotation, i.e., the carbamate isomerization of **1a** proceeds at a slower rate than its Cope rearrangement. Using ^{1}H–^{1}H exchange (EXSY) NMR spectroscopy[19] (Figure 2d) at 219 K, we found that the Cope rearrangements pass through transition states (TS1 and TS2, Scheme 1b) that are ~55–57 kJ·mol^{-1} above the lowest energy isomer, ***Z,β*-1a**, which is typical[20] for bullvalene constitutional isomerization. There are no cross peaks visible between *E*- and *Z*-isomers at this temperature because of the slow carbamate rotation rate. At the higher temperature of 308 K, ^{1}H NMR line-shape analysis (Figure 2e) gives an average rate of carbamate rotation, k_{EZ}, of 62.5 s^{-1}, indicating that TS3 and TS4 lie almost 10 kJ·mol^{-1} higher than TS1 at ΔG_{exp} of ~65 kJ·mol^{-1} relative to ***Z,β*-1a** (Table 1).

5.3.2 **1b** ^{1}H NMR Low Temperature Analysis

Unlike **1a**, the increased steric crowding present in the benzhydryl derivative **1b** leads to correlated isomerization. The additional phenyl ring of **1b** experiences long-range interactions with the bullvalene that influence the solution-phase isomerization equilibria. There are some key clues to this behaviour in the variable-temperature NMR spectra (Figure 3a). Crucially, the distribution of H1 methylene resonances (Figure 3b) has been altered substantially relative to **1a**. The ***Z,β*-1b**, ***E,β*-1b**, ***Z,γ*-1b**,

and ***E,γ*-1b** isomers are present in a 27:16:48:8 ratio, as assigned by 2D NMR (Figures S1–S4). Therefore, the *Z,γ*-isomer is the most favoured form of **1b**, despite being only the third most populated isomer of **1a**. A structural change from a hydrogen substituent to a phenyl group at a remote site has overridden the inherent preference[2c,16] for the bullvalene *β*-isomer in the reaction network, but only when the carbamate is in its *Z*-form (Figure 4a). The benzhydryl carbamate of **1b** also rotates at a faster rate than the benzyl carbamate of **1a**, exhibiting near-identical energy barriers of ~54–58 kJ·mol^{-1} for the four isomerization processes (Table 1).

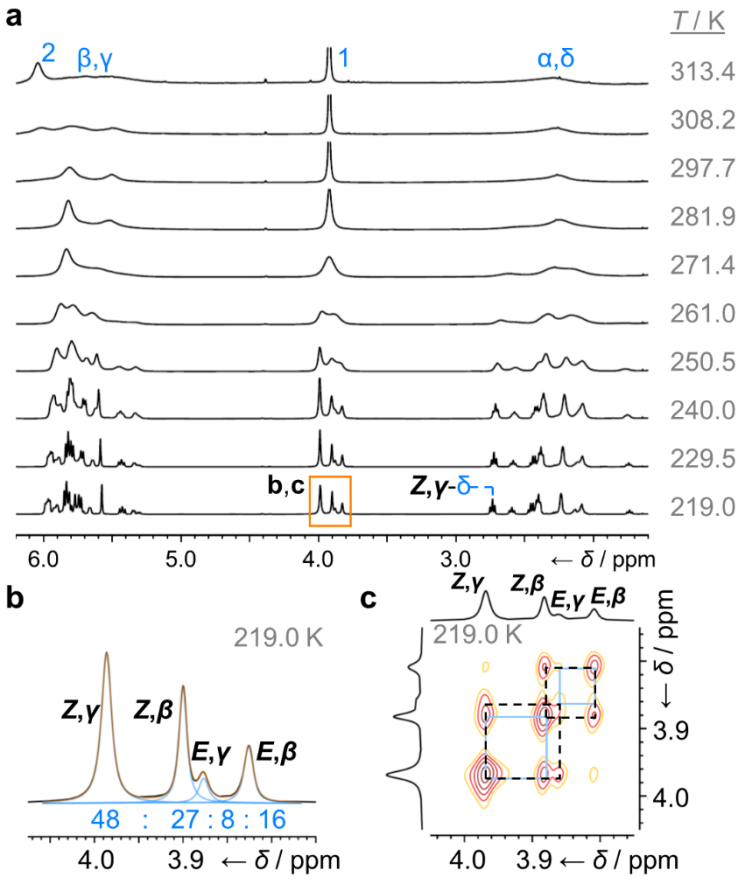

Figure 3. *^{1}H DNMR analysis (499 MHz, $CDCl_3$) of **1b**. a) Partial ^{1}H NMR spectra at temperatures ranging from 219 K to 313 K. Signals are assigned using the labels in Scheme 1. The region in an orange box corresponds to that shown in panels b and c. b) Line fitting was used to deconvolute the H1 signals at 219 K. An overlay of the experimentally measured (black) and simulated (orange) traces is shown, including the integrals of the four simulated peaks (blue). c) Partial EXSY NMR spectrum (499 MHz, $CDCl_3$, t_m = 500 ms). Blue boxes indicate cross peaks arising from Cope rearrangements. Dashed black boxes indicate cross peaks arising from carbamate rotation.*

5.4 Boc-flip Influence on Isomer Distribution

To understand the unusual constitutional isomer distribution of **1b**, we carried out DFT modelling. We generated all the constitutional isomers of **1a** and **1b** and carried out

distance-geometry-based generation of their configurational and conformational isomers before optimizing the geometries at the PBE0-D3/def2-SV(P) level of theory.[21] As there are several rotatable single bonds in the structure of **1**, each of the isomers observed by low-temperature NMR itself represents a rapidly interconverting population of conformers. The relative energies of all the isomers are tabulated in Tables S3 and S4. Cartesian coordinates are available in the Supporting Information. To take one representative example, there are six conformers of ***Z,β*-1a** spanning a range of ~16 kJ·mol^{-1} in energy, of which the two lowest energy structures are within just 2.5 kJ·mol^{-1} of one another.

Table 1. Populations and relative Gibbs energies of the isomers present in the dynamic mixtures and their transition states.

State	**1a**, p / %			**1a**, ΔG / kJ·mol^{-1}		
	p_{exp}[a]	p_{calc1}[c]	p_{calcG}[d]	ΔG_{exp}[a]	ΔG_{calc1}[f]	ΔG_{calcG}[h]
E,α	-[b]	<0.1	<0.1	-[b]	25.5	25.4
Z,α	-[b]	<0.1	<0.1	-[b]	23.1	23.2
E,β	23	18	22	1.2	1.7	1.4
Z,β	45	47	46	0.0	0.0	1.0
E,γ	11	10	13	2.5	2.8	2.3
Z,γ	21	14	18	1.4	2.2	1.7
E,δ	-[b]	<1	<1	-[b]	8.7	8.2
Z,δ	-[b]	<1	1	-[b]	7.2	6.8
TS1	-	-	-	55.6	-[g]	-[g]
TS2	-	-	-	57.2	-[g]	-[g]
TS3	-	-	-	64.9[e]	-[g]	-[g]
TS4	-	-	-		-[g]	-[g]

State	**1b**, p / %			**1b**, ΔG / kJ·mol^{-1}		
	p_{exp}[a]	p_{calc1}[c]	p_{calcG}[d]	ΔG_{exp}[a]	ΔG_{calc1}[f]	ΔG_{calcG}[h]
E,α	-[b]	<0.1	<0.1	-[b]	34.5	34.0
Z,α	-[b]	<0.1	<0.1	-[b]	26.5	26.8
E,β	16	24	23	1.9	1.4	1.2
Z,β	27	18	28	1.0	1.5	0.8
E,γ	8	6	5	3.2	3.8	3.8
Z,γ	48	51	44	0.0	0.0	0.0
E,δ	-[b]	<0.1	<0.1	-[b]	14.8	14.1

Z,δ	-[b]	<1	<1	-[b]	9.5	8.8
TS1	-	-	-	54.5	-[g]	-[g]
TS2	-	-	-	57.4	-[g]	-[g]
TS3	-	-	-	54.8	-[g]	-[g]
TS4	-	-	-	55.3	-[g]	-[g]

[a] Measured at 219 K in $CDCl_3$. [b] The population of α- and δ-isomers is below the detection limit of ^{1}H NMR experiments. [c] Population calculated as a Boltzmann distribution based on the DFT calculated energies of the most stable conformer for each constitutional and configurational isomer (ΔG_{calc1}). [d] Population calculated as a global Boltzmann distribution by summing the populations of all accessible conformers calculated for each constitutional and configurational isomer (ΔG_{calcG}). [e] Apparent Gibbs energy barrier for carbamate rotation (weighted average of TS3 and TS4) at 308 K. [f] Relative Gibbs energies of only the most stable conformer for each isomer calculated at 219 K using PBE0-D3/def2-SV(P).[21i-k,p] [g] Transition states were not modelled. [h] Effective relative Gibbs energies based on the DFT calculated global Boltzmann distribution (p_{calcG}) for the purpose of comparing to ΔG_{exp}.

Despite there being numerous different structures contributing to the overall energetics of *E*-to-*Z* and *β*-to-*γ* isomerization, the experimentally observed populations, p_{exp}, can be approximated reasonably well by analysing just the lowest energy conformers (Table 1). For **1a**, the calculated energies, ΔG_{calc1}, of the lowest energy conformer for each of the four observable isomers gives a Boltzmann distribution, p_{calc1}, that matches closely to p_{exp}. For **1b**, however, this simplified approach incorrectly predicts that more of ***E,β*-1b** is present than ***Z,β*-1b**. Instead, it is necessary to perform a global Boltzmann population analysis (giving p_{calcG}) that takes into account all the accessible conformers in order to reproduce the experimentally observed hierarchy of isomers. This observation indicates that for bullvalene derivatives with several rotatable single bonds, accurate modelling of the

shapeshifting rearrangements requires consideration of the full energetic landscape of accessible conformers.

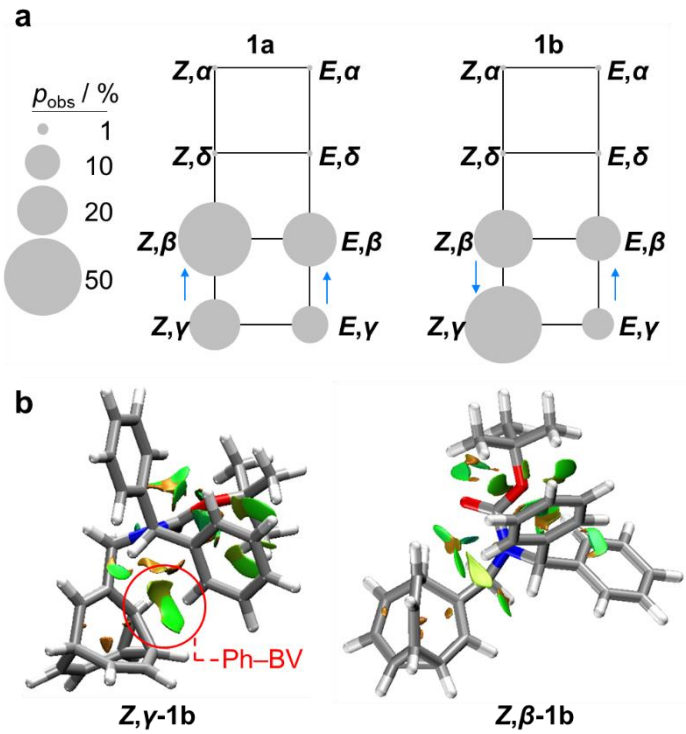

*Figure 4. (a) Network diagrams for the isomerization of **1a** and **1b** showing the experimentally measured populations (p_{exp}) of the β- and γ-isomers at 219 K. According to DFT calculations, the α- and δ-isomers are present in <1%. Blue arrows point to the major species of each Cope rearrangement process, highlighting that the preference for the β- and γ-bullvalene isomers is correlated to the E-to-Z isomerization of **1b**. (b) NCI plots [LC-PBE/def2-TZVP][23] of **Z,γ-1b** and **Z,β-1b** showing the increased Ph–BV interaction in **Z,γ-1b**.*

Noncovalent interaction (NCI) plots[22] generated using the DFT-optimized geometries reveal (Figure 4b and Figures S7–S10) the interactions that are responsible for the correlated isomerization of **1b**. In addition to several close contacts between the crowded *tert*-butyl, carbonyl, and phenyl groups, which are present in all of the isomers, the lowest energy conformer of ***Z,γ*-1b** shows evidence of substantial interaction between an *ortho*-hydrogen of one phenyl ring with the bullvalene cyclopropyl ring (Ph–BV interaction, Figure 4b). This long-range interaction is less significant in the NCI analyses of the other **1b** isomers (Figures S7–S10), such as ***Z,β*-1b** (Figure 4b). Experimental evidence for the interaction in ***Z,γ*-1b** is apparent in its low-temperature ^{1}H NMR spectrum (Figure 3a) as its Hδ resonance is shifted downfield relative to the Hδ signals of the other isomers of **1b**, which is indicative of deshielding caused by the aromatic ring current. The NOESY NMR spectrum (Figure S11) also confirms Hδ undergoes through-space interaction with a phenyl group. Although this Ph–BV interaction appears to be a relatively weak van

der Waals contact, the combination of it together with other subtle differences in the attractive and repulsive noncovalent bonding interactions present in **1b** is evidently sufficient to provide enough of an energetic bias to overcome the ~1–2 kJ·mol^{-1} preference for the *β*-isomer.

5.5 Conclusion

In summary, the shapeshifting constitutional rearrangements of even structurally simple bullvalenes can be influenced by a complementary, remote isomerization process. Given that the energetic differences between bullvalene isomers are often as little as a few kJ·mol^{-1}, relatively subtle noncovalent bonding interactions, including weak van der Waals contacts, are sufficient to reshuffle the proportions of each isomer. In the system presented here, the introduction of an additional phenyl ring to the structure of **1a** causes the *Z*,*γ*-isomer to change from being the third most populous to being the major species of **1b** as a result of a Ph–BV interaction. Programming in switchable long-range interactions may allow for control to be exercised over the large number of constitutional isomers that arise in multi-substituted bullvalene derivatives.

Experimental

tert-Butyl benzyl(prop-2-yn-1-yl)carbamate (4a)

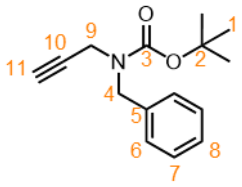

NEt_3 (2.48 g, 24.5 mmol), benzylamine (2.19 g, 20.4 mmol) and Boc_2O (4.90 g, 22.4 mmol) were added sequentially to CH_2Cl_2 (20 mL) at 0 °C. The mixture was allowed to warm to rt and stirred for 24 h. The reaction was quenched with H_2O (50 mL) and the aqueous layer was extracted with CH_2Cl_2 (3 × 20 mL). The combined organic phases were dried over anhydrous $MgSO_4$, and the solvent was removed under reduced pressure to give *tert*-butyl benzylcarbamate as a colourless oil. The crude *tert*-butyl benzylcarbamate (3.79 g, 18.3 mmol) was dissolved in anhydrous DMF (30 mL) in an oven-dried two-necked round-bottomed flask under an inert atmosphere. The mixture was cooled to 0 °C, NaH (658 mg, 27.4 mmol) added and the reaction stirred for 30 min. Propargyl bromide (3.2 mL, 36.6 mmol) was added and the mixture was allowed to warm to rt and stirred for 5 h. The reaction was quenched with $KOH_{(aq)}$ (2.0 M, 30 mL), and the aqueous layer extracted with EtOAc (3 × 30 mL). The combined organic layers were dried over anhydrous $MgSO_4$, and the solvent removed under reduced pressure. The resulting crude residue was purified by column chromatography (Teledyne Isco CombiFlash Rf+ system, 24 g, SiO_2, hexanes−EtOAc, gradient elution) to yield the title compound as a yellow oil (3.15 g, 12.8 mmol, 70%).**^{1}H NMR** (400 MHz, $CDCl_3$, 298 K) δ 7.35–7.27 (m, 5H, $H_{6,7,8}$), 4.55 (s, 2H, H_4), 3.90 (s, 2H, H_9), 2.21 (s, 1H, H_{11}), 1.49 (s, 9H, H_1). **HR-ASAP-MS**: *m/z*: $[M+H]^+$ = 246.1213 (calculated for $C_{15}H_{20}NO_2^+$ = 246.1494). Spectroscopic data were consistent with those published previously.[26]

tert-Butyl benzhydryl(prop-2-yn-1-yl)carbamate (4b)

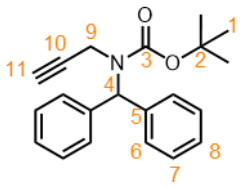

NEt_3 (2.48 g, 24.5 mmol), benzhydrylamine (3.74 g, 20.4 mmol) and Boc_2O (4.90 g, 22.4 mmol) were added sequentially to CH_2Cl_2 (20 mL) at 0 °C. The reaction was allowed to warm to rt and stirred for 24 h. The reaction was quenched with H_2O (50 mL) and the aqueous layer was extracted with CH_2Cl_2 (3 × 20 mL). The combined organic phases were dried over anhydrous $MgSO_4$, and the solvent was removed under reduced pressure to give *tert*-butyl benzhydrylcarbamate as a colourless oil. A portion of the crude *tert*-butyl benzhydrylcarbamate (5.18 g, 18.3

mmol) was dissolved in anhydrous DMF (30 mL) in an oven-dried two-necked round-bottomed flask under an inert atmosphere. The mixture was cooled to 0 °C, NaH (658 mg, 27.4 mmol) was added and the reaction stirred for 30 min. Propargyl bromide (3.2 mL, 36.6 mmol) was added, the mixture was allowed to warm to rt and stirred for 5 h. The reaction was quenched $KOH_{(aq)}$ (2.0 M, 30 mL), then extracted with EtOAc (3 × 30 mL). The combined organic layers were dried over anhydrous $MgSO_4$, and the solvent removed under reduced pressure. The resulting crude residue was purified by column chromatography (Teledyne Isco CombiFlash Rf+ system, 24 g, SiO_2, hexanes−EtOAc, gradient elution) to yield the title compound as a yellow oil (4.15 g, 13.4 mmol, 64%). **^{1}H NMR** (400 MHz, $CDCl_3$, 298 K) δ 7.42–7.23 (m, 10H, $H_{6,7,8}$), 6.48 (s, 1H, H_4), 3.92 (s, 2H, H_9), 2.04 (s, 1H, H_{11}), 1.43 (s, 9H, H_1). **^{13}C NMR** (175 MHz, $CDCl_3$, 298 K) δ 155.1 (C_3), 139.6 (C_5), 128.6 (C_7), 128.4 (C_8), 127.1 (C_6), 80.7 (C_{11}), 80.5 (C_2), 70.4 (C_{10}), 63.7 (C_4), 34.8 (C_9), 28.2 (C_1). **HR-ESI-MS** *m/z*: $[M+Na]^+$ = 344.1615 (calculated $C_{21}H_{23}NNaO_2^+$ = 344.1621).

tert-Butyl-*N*-benzyl-*N*-(((2*Z*,4*Z*)-bicyclo[4.2.2]deca-2,4,7,9-tetraen-7-yl)methyl)carbamate (5a)

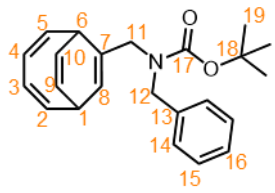

ZnI_2 (61 mg, 0.19 mmol) was added to a microwave vial and heated to 280 °C for 5 mins under reduced pressure, allowed to cool and flushed with argon. $CoBr_2$(dppe) (59 mg, 0.29 mmol) and activated Zn dust (19 mg, 0.10 mmol) were added to the vial which was then sealed and the vial evacuated and flushed with argon three times. Anhydrous 2,2,2-trifluoroethanol (1.5 mL) was added, and the reaction mixture degassed by freeze-pump-thaw. The reaction mixture was stirred for 15 min at rt and then cyclooctatetraene (0.11 mL, 0.96 mmol) was added. Compound **4a** (0.38 mL, 1.44 mmol) was added dropwise over 1.5 h, after which the reaction mixture was stirred for 22 h at 55 °C. The reaction mixture was filtered through a silica plug and eluted with EtOAc. The solvent was then removed under reduced pressure and the crude residue purified by column chromatography (Teledyne Isco CombiFlash Rf+ system, 12 g SiO_2, hexanes–EtOAc, gradient elution) affording the title compound as a colourless oil (185 mg, 0.53 mmol, 55%). An approximately 1:1 mixture of carbamate *E*/*Z* isomers is observed by ^{1}H NMR spectroscopy. **^{1}H NMR** (700 MHz, $CDCl_3$, 298K) δ 7.25–7.27 (m, 2H, H_{15}), 7.21–7.16 (m, 1H, H_{16}), 7.16–7.11 (m, 2H, H_{14}), 6.23–6.20 (m, 1H, H_2), 6.12–6.07 (m,

1H, H_5), 5.79–5.73 (m, 2H, $H_{3,4}$), 5.65–5.63 (m, 1H, H_{10}), 5.60–5.58 (m, 1H, H_9), 5.46–5.42 (m, 1H, H_8), 4.32–4.12 (m, 2H, H_{12}), 3.86–3.67 (m, 2H, H_{11}), 3.37–3.35 (0.5H, m, $H_{6E/6Z}$), 3.26–3.24 (0.5H, m, $H_{6E/6Z}$), 3.14–3.11 (m, 1H, H_1), 1.48–1.44 (m, 9H, H_{19}). **^{13}C NMR** (175 MHz, $CDCl_3$, 298K) δ 155.9 (C_{17}), 141.7 ($C_{5E/5Z}$), 141.6 ($C_{2E/2Z}$), 141.5 ($C_{2E/2Z}$), 141.1 ($C_{5E/5Z}$), 138.4 ($C_{13E/13Z}$), 138.2 ($C_{13E/13Z}$), 132.2 ($C_{7E/7Z}$), 131.6 ($C_{7E/7Z}$), 128.4 (C_{15}), 128.1 ($C_{14E/14Z}$), 127.6 (C_{16}), 127.1 ($C_{14E/14Z}$), 124.8 ($C_{3E/3Z/4E/4Z}$), 124.5 ($C_{3E/3Z/4E/4Z}$), 124.4 ($C_{3E/3Z/4E/4Z}$), 121.1 ($C_{8E/8Z}$), 121.0 ($C_{9E/9Z/10E/10Z}$), 120.8 ($C_{9E/9Z/10E/10Z}$), 120.7 ($C_{9E/9Z/10E/10Z}$), 120.1 ($C_{8E/8Z}$), 79.7 (C_{18}), 48.6 ($C_{12E/12Z}$), 48.4 (C_{11}), 48.2 ($C_{12E/12Z}$), 36.9 ($C_{6E/6Z}$), 36.7 ($C_{6E/6Z}$), 35.0 ($C_{1E/1Z}$), 34.9 ($C_{1E/1Z}$), 28.5 (C_{19}). **HR-ASAP-MS** *m/z*: $[M+H]^+$ = 350.2120 (calculated $C_{23}H_{28}NO_2^+$: 350.2120).

tert-Butyl-*N*-benzhydryl-*N*-(((2*Z*,4*Z*)-bicyclo[4.2.2]deca-2,4,7,9-tetraen-7-yl)methyl) carbamate (5b)

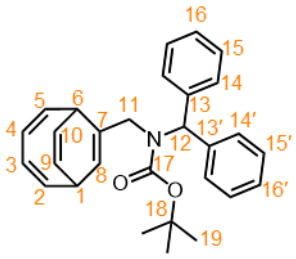

ZnI_2 (61 mg, 0.19 mmol) was added to a microwave vial and heated to 280 °C for 5 min under reduced pressure, allowed to cool and flushed with argon. $CoBr_2$(dppe) (59 mg, 0.29 mmol) and activated Zn dust (19 mg, 0.10 mmol) were added to the vial which was then sealed and the vial evacuated and flushed with argon three times. Anhydrous 2,2,2-trifluoroethanol (1.5 mL) was added, and the reaction mixture degassed by freeze-pump-thaw. The reaction mixture was stirred for 15 min at rt and then cyclooctatetraene (0.11 mL, 0.96 mmol) was added. Compound **4b** (460 mg, 1.44 mmol) was added dropwise over 1.5 h, after which the reaction mixture was stirred for 22 h at 70 °C. The reaction mixture was filtered through a silica plug and eluted with EtOAc. The solvent was then removed under reduced pressure and the crude residue purified by column chromatography (Teledyne Isco CombiFlash Rf+ system, 12 g SiO_2, hexanes/EtOAc, 0–30%, gradient elution) affording the title compound as a colourless oil (194 mg, 0.46 mmol, 48%). **^{1}H NMR** (700 MHz, $CDCl_3$, 298 K) δ 7.31–7.26 (m, 4H, $H_{15/15'}$), 7.26–7.22 (m, 2H, $H_{16/16'}$), 7.18 (d, *J* = 7.6 Hz, 2H, $H_{14/14'}$), 7.13 (d, *J* = 7.5 Hz, 2H, $H_{14/14'}$), 6.24 (s, 1H, H_8), 6.13 (dd, *J* = 11.3, 8.7 Hz, 1H, H_5), 5.98 (m, 1H, H_2), 5.68 (m, 2H, $H_{3,4}$), 5.61–5.56 (m, 1H, H_9), 5.54 (dd, *J* = 8.7, 5.8 Hz, 1H, H_{10}), 5.12–5.09 (s, 1H, H_{12}), 4.25 (s, 1H, H_{11}), 3.63 (s, 1H, $H_{11'}$), 3.16 (d, *J* = 37.2 Hz, 1H, H_1), 3.00 (dd, *J* = 7.0 6.8 Hz, 1H, H_6), 1.32 (s, 9H, H_{19}). **^{13}C NMR** (175 MHz,

$CDCl_3$, 298 K) δ 156.1 (C_{17}), 141.7 (C_2), 141.2 (C_5), 140.8 (C_8), 139.9 ($C_{13,13'}$), 132.0 (C_{12}), 128.9 ($C_{14,14'}$), 128.2 ($C_{15/15'}$), 128.1 ($C_{15/15'}$), 127.1 ($C_{16/16'}$), 126.9 ($C_{16/16'}$), 124.6 (C_4), 124.3 (C_3), 120.9 (C_9), 120.8 (C_{10}), 119.0 (C_7), 80.1 (C_{18}), 63.8 ($C_{11E/11Z}$), 48.5 ($C_{11E/11Z}$), 36.2 (C_1), 34.8 (C_6), 28.3 (C_{19}). **HR-ASAP-MS** *m/z*: $[M+H]^+$ = 426.2429 (calculated $C_{29}H_{32}NO_2^+$: 426.2432). Prime symbols are used in the spectral assignment of **5b** to differentiate between its diastereomers arising from the different environment of two phenyl rings.

Benzyl boc bullvalene (1a)

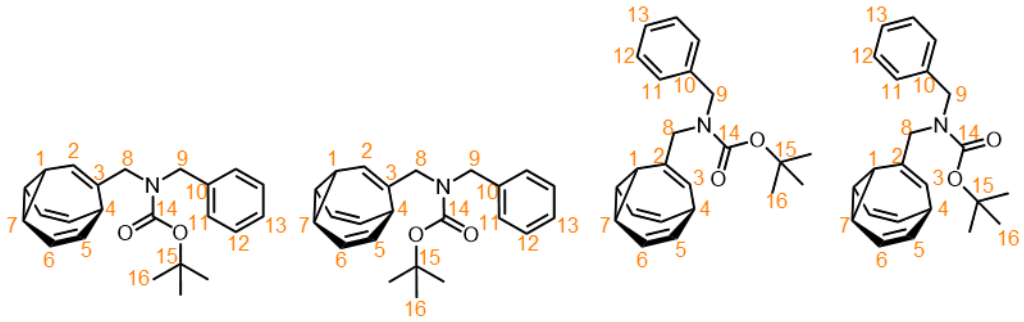

5a (180 mg, 0.51 mmol) and thioxanthene-9-one (1 mg, 0.01 mmol) were dissolved in anhydrous THF (1.2 mL) in an oven-dried microwave vial under an inert atmosphere. The mixture was stirred for 3 h, while being irradiated with 365 nm UV light (3.4 W array of surface mounted 365 nm LEDs) at rt. The solvent was removed under reduced pressure and the crude residue purified by column chromatography (Teledyne Isco CombiFlash Rf+ system, 8 g SiO_2, hexanes/EtOAc, 0–10%, gradient elution; followed by 12 g gold SiO_2, hexanes/CH_2Cl_2, gradient elution) to afford the title compound as a colorless solid (90 mg, 0.26 mmol, 50% yield). **M. P.** = 130–131 °C. **^{1}H NMR** (499 MHz, $CDCl_3$, 219 K) δ 7.39–7.31 (m, 2H, H_{12}), 7.31–7.27 (m, 1H, H_{13}), 7.25–7.15 (m, 2H, H_{11}), 6.00–5.89 (m, 2H, H_6), 5.89–5.77 (m, 2H, H_5), 5.71 (s, 0.45H, *Z,β*-H_2), 5.66 (s, 0.23H, *E,β*-H_2), 5.62 (d, *J* = 8.8 Hz, 0.21H, *Z,γ*-H_3), 5.58 (d, *J* = 8.4 Hz, 0.11H, *E,γ*-H_3), 4.40 (s, 0.46H, *E,β*-H_9), 4.35 (s, 0.9H, *Z,β*-H_9), 4.32 (s, 0.22H, *E,γ*-H_9), 4.26 (s, 0.42H, *Z,γ*-H_9), 3.82 (s, 0.42H, *Z,γ*-H_8), 3.78–3.73 (m, 1.12H, *Z,β*-H_8 and *E,γ*-H_8), 3.69 (s, 0. 0.46H, *E,β*-H_8), 2.48–2.34 (m, 1H, H_4), 2.34–2.24 (m, 3H, H_1 and H_7), 1.48 (s, 3.06H, *E,β*-H_{16} and *E,γ*-H_{16}), 1.46 (s, 5.94H, *Z,β*-H_{16} and *Z,γ*-H_{16}). **^{13}C NMR** (126 MHz, $CDCl_3$, 219 K) δ 156.4 (*E,β*-C_{14} or *Z,γ*-C_{14}), 156.3

(*Z*,*β*-C_{14}), 156.2 (*E*,*γ*-C_{14}), 156.1 (*E*,*β*-C_{14} or *Z*,*γ*-C_{14}), 138.1 (*Z*,*γ*-C_{10}), 138.0 (*Z*,*β*-C_{10}), 137.9 (*E*,*β*-C_{10}), 137.8 (*E*,*γ*-C_{10}), 137.0 (*Z*,*β*-C_2), 136.6 (*E*,*β*-C_2), 134.5 (*Z*,*γ*-C_3), 134.0 (*E*,*γ*-C_3), 128.8 (C_{12}), 128.7 (C_{12}), 128.6 (C_{12}), (128.1–127.2 C_{13}, C_{11}, C_6 and C_5) 128.1, 127.9, 127.9, 127.8, 127.8, 127.7, 127.6, 127.5, 127.5, 127.4, 127.4, 127.3, 127.2, 125.2 (*Z*,*γ*-C_3), 124.9 (*Z*,*β*-C_2), 124.7 (*E*,*γ*-C_3), 123.6 (*E*,*β*-C_2), 80.4 (C_{14}), 80.4 (C_{14}), 80.4 (C_{14}), 53.7 (*E*,*γ*-C_8), 53.3 (*Z*,*γ*-C_8), 52.4 (*E*,*β*-C_8), 52.0 (*Z*,*β*-C_8), 47.4 (*Z*,*γ*-C_9), 47.1 (*Z*,*β*-C_9), 46.9 (*E*,*β*-C_9), 46.8 (*E*,*γ*-C_9), 31.8 (*Z*,*β*-C_1), 31.8 (*Z*,*γ*-C_1), 30.0 (*E*,*β*-C_1), 30.0 (*E*,*γ*-C_1), 28.6 (C_{16}), 28.6 (C_{16}), 28.5 (C_{16}), 21.1 (C_7), 20.9 (C_7), 20.7 (C_7), 20.1 (C_7), 20.1 (C_7), 19.9 (C_7), 19.8 (C_7). **HR-ASAP-MS** *m*/*z* = 350.2137 $[M+H]^+$, calculated for $C_{23}H_{28}NO_2^+$: 350.2120.

Benzhydryl boc bullvalene (1b)

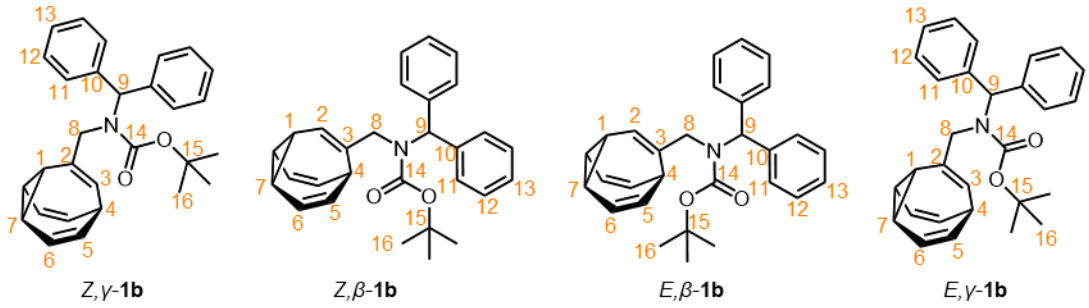

Isomer Ratio
Z,*γ*-**1a** : *Z*,*β*-**1a** : *E*,*β*-**1a** : *E*,*γ*-**1a**
48 : 27 : 16 : 8

5b (140 mg, 0.28 mmol) and thioxanthene-9-one (1 mg, 0.01 mmol) were dissolved in anhydrous THF (1.2 mL) in an oven-dried microwave vial under an inert atmosphere. The mixture was stirred for 3 h, while being irradiated with 365 nm UV light (3.4 W array of surface mounted 365 nm LEDs) at rt. The solvent was then removed in vacuo and the crude residue purified by column chromatography (Teledyne Isco CombiFlash Rf+ system, 8 g SiO_2, hexanes/EtOAc, 0–10%, gradient elution; followed by 12 g gold SiO_2, hexanes/CH_2Cl_2, gradient elution) to afford the title compound as a colourless wax (63 mg, 0.15 mmol, 54% yield). **^{1}H NMR** (499 MHz, $CDCl_3$, 219 K) δ 7.37–7.26 (m, 6H, $H_{12,13}$), 7.22–7.14 (m, 4H, H_{11}), 6.61 (s, 0.16H, *E*,*β*-H_9), 6.19 (s, 0.08H, *E*,*γ*-H_9), 6.02–5.94 (m, 0.96H, *Z*,*γ*-H_6), 5.94–5.79 (m, 2.36H, *E*,*γ*-H_6, *E*,*β*-H_6, *Z*,*γ*-H_5, *Z*,*β*-H_6, *Z*,*β*-H_5), 5.79–5.69 (m, 0.91H, *E*,*γ*-H_5, *Z*,*γ*-H_3, *Z*,*β*-H_9), 5.69–5.65 (m, 0.27H, *Z*,*β*-H_2), 5.55 (s, 0.48H, *Z*,*γ*-H_9), 5.41 (dd, *J* = 11.1, 8.8 Hz, 0.32H, *E*,*β*-H_5), 5.34 (d, *J* = 7.0 Hz, 0.16H, *E*,*β*-H_2), 5.29 (d, *J* = 8.8 Hz, 0.08H, *E*,*γ*-H_3), 3.97 (s, 0.96H, *Z*,*γ*-H_8), 3.88 (s, 0.54H, *Z*,*β*-H_8), 3.86 (s, 0.16H, *E*,*γ*-H_8), 3.81

(s, 0.32H, *E*,*β*-H_8), 2.73 (t, *J* = 8.6 Hz, 0.48H, *Z*,*γ*-H_1), 2.59 (t, *J* = 8.7 Hz, 0.27H, *Z*,*β*-H_4), 2.49–2.43 (m, 0.48H, *Z*,*γ*-H_4), 2.43–2.37 (m, 0.96H, *Z*,*γ*-H_7), 2.32–2.26 (m, 0.08H, *E*,*γ*-H_4), 2.27–2.19 (m, 0.81H, *Z*,*β*-H_1, *Z*,*β*-H_7), 2.18–2.11 (m, 0.24H, *E*,*γ*-H_1, *E*,*γ*-H_7), 2.11–2.02 (m, 0.48H, *E*,*β*-H_1, *E*,*β*-H_7), 1.72 (t, *J* = 8.8 Hz, 0.27H, *Z*,*β*-H_4), 1.42 (s, 1.44H, *E*,*β*-H_{16}), 1.41 (s, 0.72H, *E*,*γ*-H_{16}), 1.10 (s, 2.43H, *Z*,*β*-H_{16}), 1.03 (s, 4.32H, *E*,*β*-H_{16}). **^{13}C NMR** (126 MHz, $CDCl_3$, 219 K) δ 156.3 (*Z*,*γ*-C_{14}), 156.1 (*Z*,*β*-C_{14}), 140.1 (*Z*,*γ*-C_{10}), 140.1 (*Z*,*β*-C_{10}), 139.8 (*Z*,*β*-C_{10}), 139.7 (*E*,*β*-C_{10}), 136.7 (*Z*,*β*-C_3), 136.1 (*E*,*β*-C_3), 135.1 (*Z*,*γ*-C_2), 134.5 (*E*,*γ*-C_2), (128.8–126.0 C_{13}, C_{12}, C_{11}, C_6, C_5 and *Z*,*γ*-C_3) 128.8, 128.7, 128.4, 128.3, 128.2, 128.0, 127.9, 127.5, 127.3, 127.2, 127.1, 127.0, 126.9, 126.8, 126.8, 126.4, 126.1, 126.0, 124.8 (*Z*,*β*-C_2), 122.3 (*E*,*γ*-C_3), 121.2 (*E*,*β*-C_2), 80.3 (C_{15}), 80.1 (C_{15}), 62.8 (*E*,*γ*-C_9), 62.7 (*E*,*β*-C_9), 62.6 (*Z*,*β*-C_9), 62.1 (*Z*,*γ*-C_9), 56.6 (*Z*,*γ*-C_8), 54.3 (*Z*,*β*-C_8), 54.2 (*E*,*γ*-C_8), 51.2 (*E*,*β*-C_8), 31.7 (*Z*,*β*-C_4), 30.4 (*Z*,*β*-C_4), 29.9 (*Z*,*γ*-C_4), 29.6 (*E*,*γ*-C_4), 28.2 (C_{16}), 28.1 (C_{16}), 27.9 (C_{16}), 21.6 (*Z*,*γ*-C_1), 20.4 (*Z*,*β*-C_7 and *E*,*γ*-C_1), 20.2 (*Z*,*γ*-C_7), 20.0 (*E*,*β*-C_7), 19.9 (*E*,*γ*-C_7), 19.7 (*Z*,*β*-C_1), 19.3 (*E*,*β*-C_1). **HR-ASAP-MS** *m*/*z* = 426.2433 $[M+H]^+$, calculated for $C_{29}H_{32}NO_2^+$: 426.2432.

2D NMR Analysis of Isomer Distributions for 1a and 1b

The four most populated isomers of **1b** (Figure S1a) were distinguished through a combination of 1D and 2D NMR experiments (Figure S1 and S2).

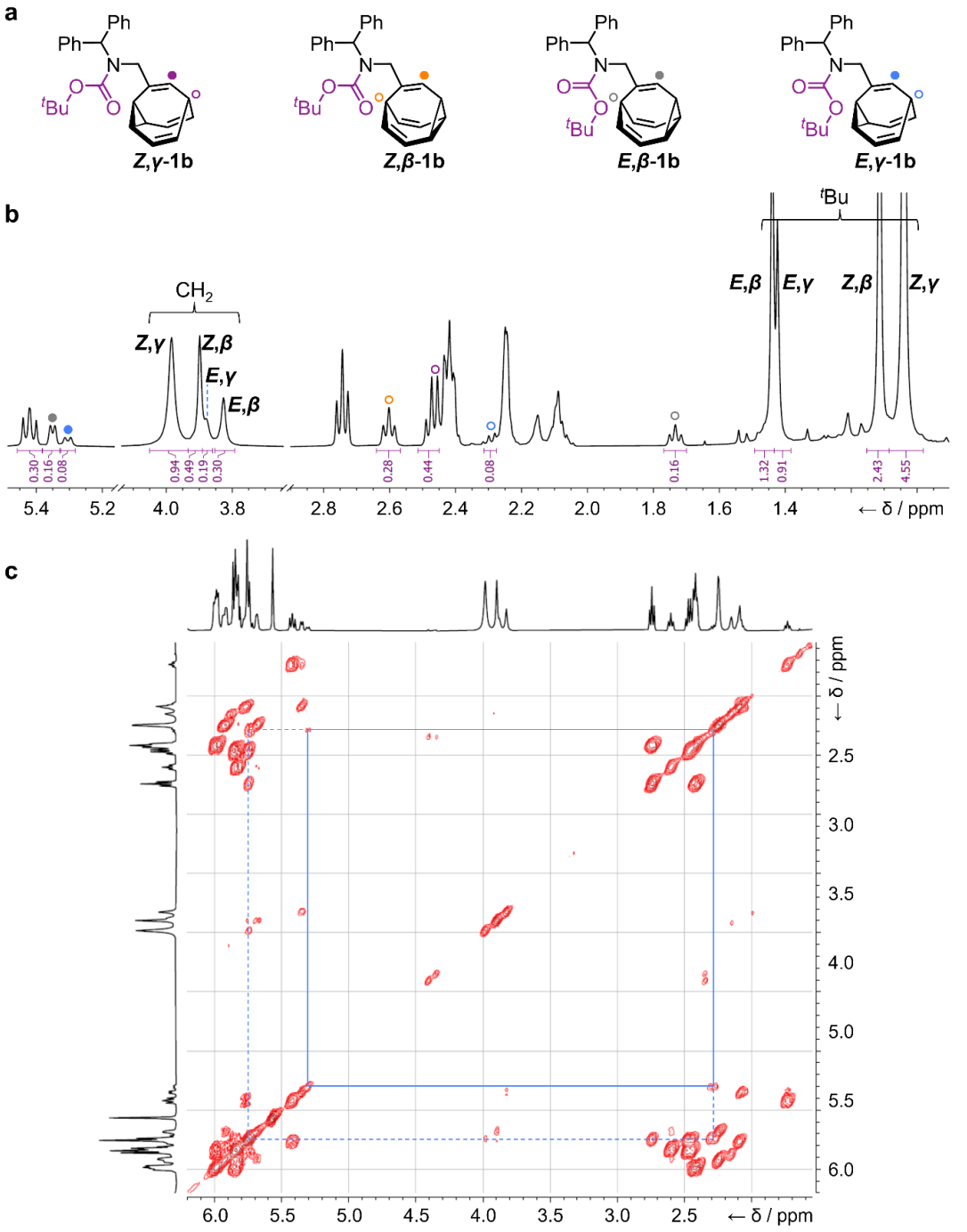

*Figure S1. (a) Structural formulas of the **1b** isomers, which can be assigned in (b) the ^{1}H NMR (499 MHz, 219 K, $CDCl_3$) spectrum with the aid of (c) the ^{1}H–^{1}H COSY spectrum.*

The resonances corresponding to the methylene group (CH_2) on each isomer appear at 3.8–4.0 ppm in a ratio of 48:27:8:16. Based on its integration, which is half that of the smallest methylene peak, the doublet at ~5.3 ppm (filled blue circle, Figure S1b)

must correspond to a single methine group (a unique CH) of the least populated isomer. Considering its chemical shift and the symmetry of the bullvalene, the resonance can be assigned to the alkene methine environment present on the same arm of the bullvalene as the carbamate substituent. This signal shows a COSY correlation (solid blue lines, Figure S1c) to a peak at ~2.3 ppm (hollow blue circle, Figure S1b). This proton resonance at ~2.3 ppm is associated with a ^{13}C signal at ~30 ppm in the HSQC spectrum (solid blue line, Figure S2a). Trivinyl bridgehead ^{13}C resonances of bullvalenes typically appear at ~30 ppm, whereas cyclopropyl signals appear in the 20–25 ppm region. The only other COSY correlation for the ~2.3 ppm proton environment is to another alkene CH position (dashed blue line, Figure S1c). An additional COSY cross peak to another signal in the sp^3 methine region of the spectrum would be expected if the signal were a cyclopropyl methine, but no such cross peak is observed. These two observations are consistent with one another, and thus allow us to assign the ~2.3 ppm signal as an apical bridgehead methine, rather than a cyclopropyl signal. Consequently, the minor isomer is assigned as a *γ*-substituted bullvalene as its alkene methine correlates to the apical bridgehead.

To distinguish whether this minor isomer has *E*- or *Z*-carbamate stereochemistry, we performed a series of 1D NOESY experiments (Figure S1b). The ^{t}Bu resonances in the 1.0–1.5 ppm region were excited to look for through-space close contacts. Exciting the two most intense ^{t}Bu signals at 1.05 ppm (Figure S2biii) and 1.12 ppm (Figure S2bii) and allowing a mixing time of 250 ms causes magnetization to be transferred to aromatic signals above 7.0 ppm. No such interaction is observed (Figure S2bi) when exciting the overlapping ^{t}Bu signals at ~1.43 ppm (the two least intense peaks). Consequently, the two major isomers are assigned as having *Z* stereochemistry, which brings the ^{t}Bu into closer contact with the Ph groups and gives the observed nuclear Overhauser effect. Conversely, the two minor isomers have *E* stereochemistry.

Overall, therefore, the least populated isomer is assigned as being ***E,γ*-1b**. Using the same assignment procedure for the other isomers, with the additional information about which isomers are in direct exchange provided by EXSY NMR (Figure 3c of the main text) allows identification of the other three isomers in the same manner.

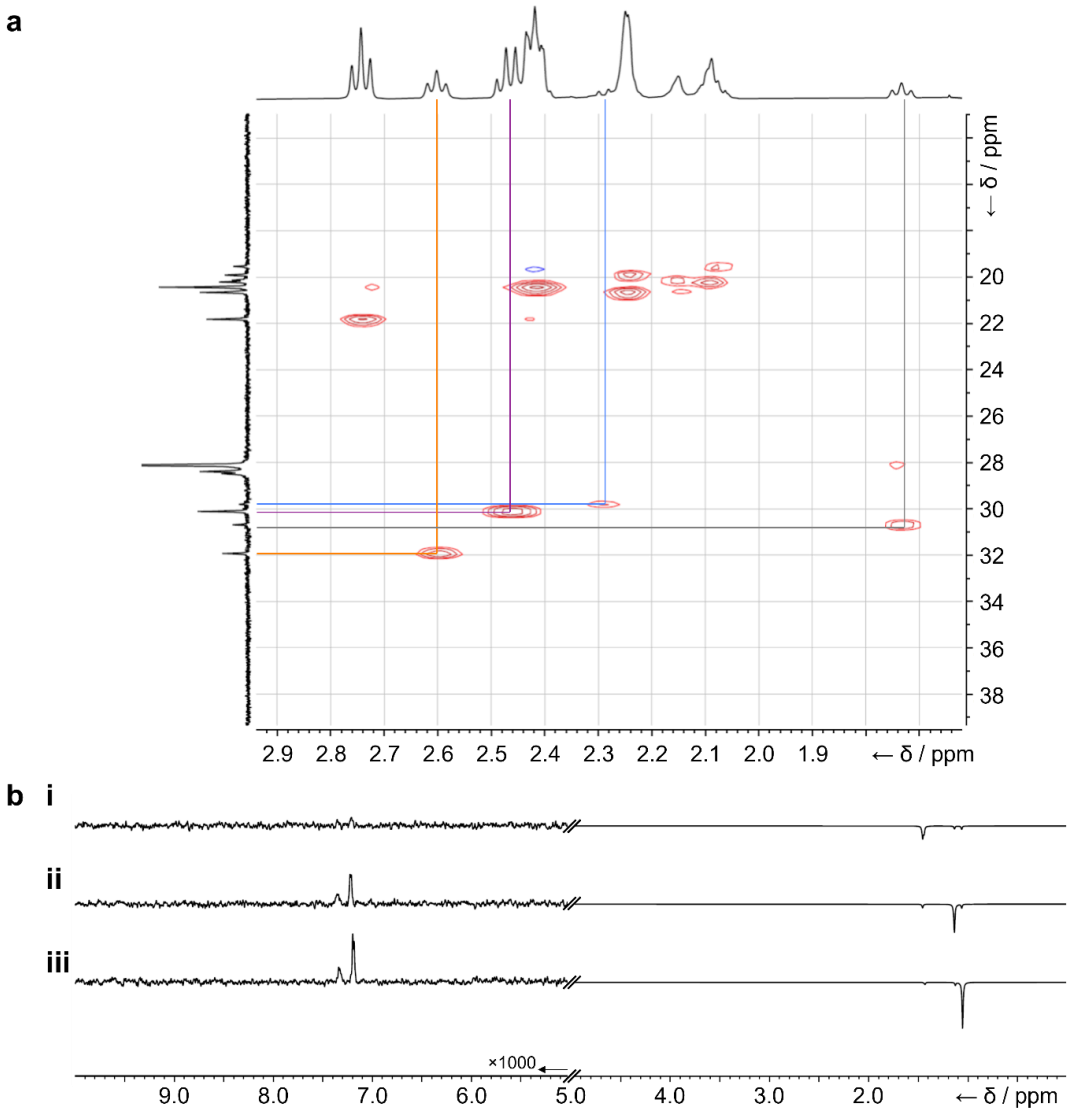

Figure S2. (a) HSQC NMR (499 MHz, 219 K, $CDCl_3$) of ***1b*** *and (b) a series of 1D NOESY spectra acquired using 250 ms mixing times after excitation at frequencies corresponding to (i) 1.43 ppm, (ii) 1.11 ppm and (iii) 1.04 ppm. Note that the intensity of the spectra above 5 ppm has been scaled by a factor of 1000 to show the weak nuclear Overhauser effect between the Ph group and ^{t}Bu signals of the Z-isomers (i.e., spectra ii and iii), which is absent for the E-isomers (spectrum i).*

The isomers of **1a** (Figure S3a) were assigned in a similar manner to **1b** using 2D NMR techniques at ~219 K (Figures S3 and S4).

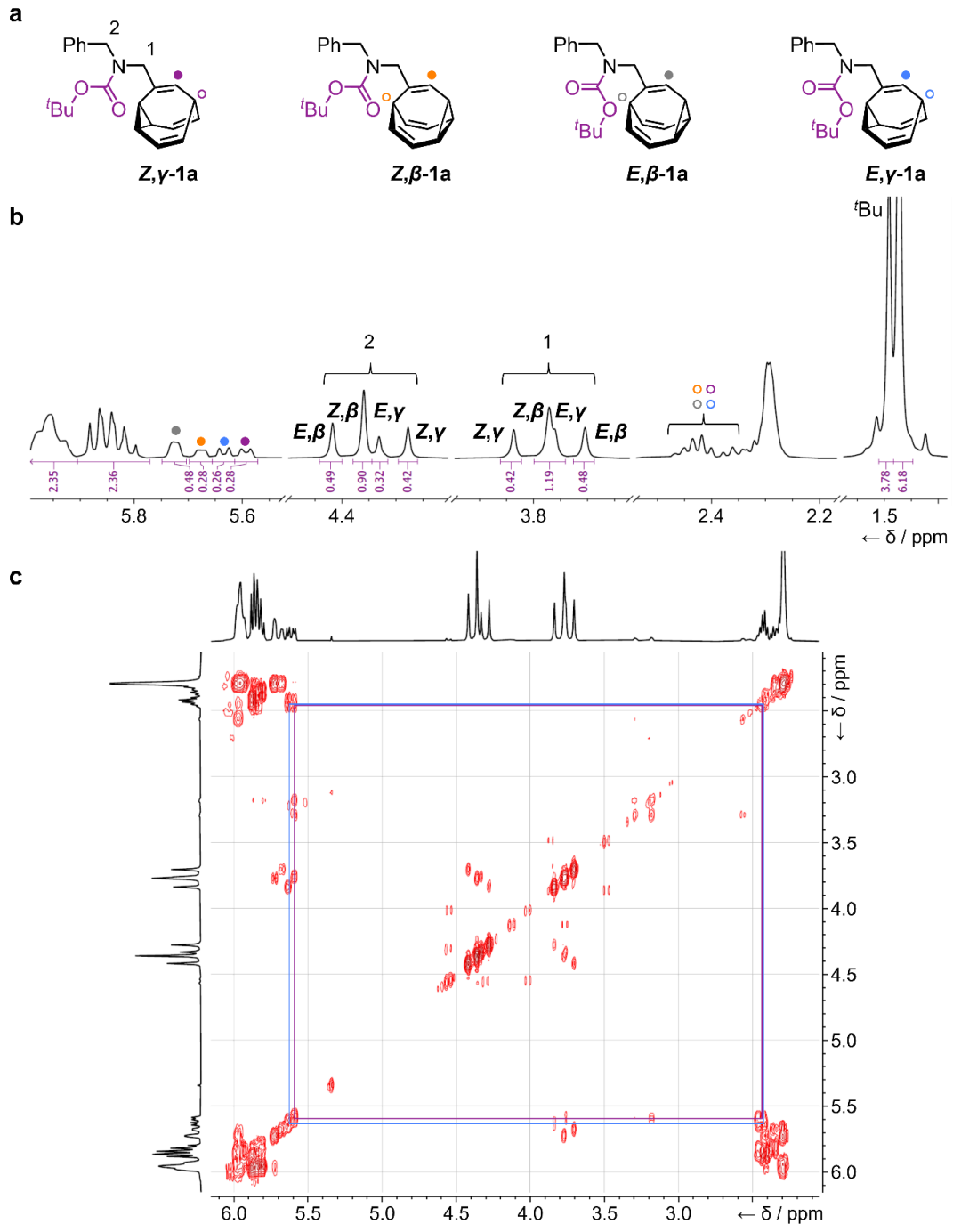

*Figure S3. (a) Structural formulas of the **1a** isomers, which can be assigned in (b) the ^{1}H NMR (499 MHz, 219 K, $CDCl_3$) spectrum with the aid of (c) the ^{1}H–^{1}H COSY spectrum.*

Four signals appear at 5.55–5.75 ppm (Figure S3b) that each correspond to the single alkene methine present on the same arm of the bullvalene as the carbamate substituent. Each of these correlates to a H1 methylene signal by ^{1}H–^{1}H COSY NMR (Figure S3c). The two highest field alkene methines (blue and purple filled circles) appear as

doublets with *J* coupling values of ~8 Hz, whereas the lower field methines (orange and grey filled circles) appear as broad singlets, likely because of them experiencing small *J* coupling (<6 Hz) that is not resolved in the spectrum. The two doublets at high field couple to (blue and purple lines, Figure S3c) a cluster of signals just above 2.4 ppm. These proton resonances can be assigned as apical bridge head positions (hollow circles) by analysis of HSQC (Figure S4a). All four of the apical ^{13}C signals >30 ppm correlate to proton resonances at 2.35 ppm and above, whereas the cyclopropyl ^{13}C signals (at ~20 ppm) correlate the resonances below 2.35 ppm. Therefore, the alkene methine doublets with *J* coupling of 8 Hz (blue and purple filled circles) can both be attributed to γ-substituted bullvalene isomers as they show coupling to neighbouring bridgehead protons, rather than to cyclopropyl signals as would be expected for β-substituted bullvalene isomers. Indeed, the other two alkene methine signals (orange and grey filled circles) show COSY correlations with the cluster of overlapping cyclopropyl methine resonances at 2.3 ppm, which is consistent with them being part of β-substituted bullvalene isomers.

Analysis of a 2D ROESY NMR spectrum (Figure S4b) allows us to distinguish the *E*- and *Z*-carbamate isomers. Of the four peaks in the H2 region (~4.4 ppm), only two show substantial through-space correlation to the ^{t}Bu signals. The H2 position would only be expected to be close in space to the ^{t}Bu group in the *Z*-isomer, i.e., when the benzyl and O^{t}Bu groups are both on the same side of the carbamate C–N bond. Therefore, we can assign the two signals as arising from the *Z*-isomer, as shown in Figure S3a. Consistently with this assignment, we also observe through space correlation in the H1 region (~3.8 ppm) between the highest-field resonance and a ^{t}Bu signal. The H1 position comes into close contact with to the ^{t}Bu when they are both on the same side of the carbamate C–N bond in the *E*-isomer. This resonance can therefore be assigned to the *E* isomer, which matches the assignment made using the H2 region.

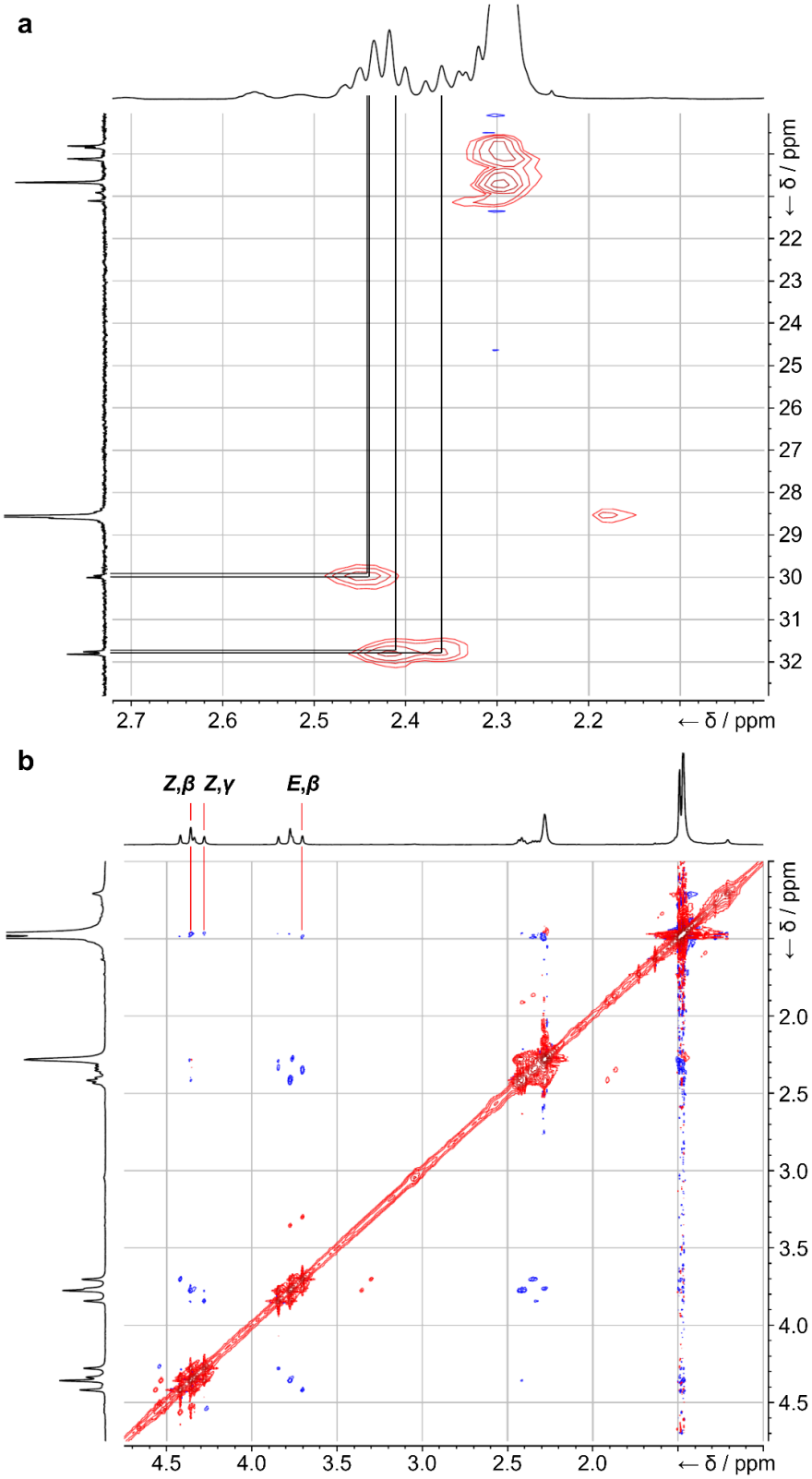

*Figure S4. (a) HSQC NMR (499 MHz, 219 K, $CDCl_3$) of **1a** and (b) ROESY NMR (499 MHz, 222 K, $CDCl_3$) spectra acquired using 250 ms mixing time.*

Line-shape analysis was performed using WinDNMR 7.1. The signal at ~4.35 ppm was simulated as a 2-spin system using the parameters in Table S1. The population of

***E*-1a** was set to 55% based on the experimentally measured *E*-*Z* ratio at 282 K, which was the closest temperature at which the two signals could be resolved. Note that the *E*-*Z* ratio changes with temperature as available thermal energy alters the Boltzmann distribution of isomers, so this 55:45 ratio is slightly different to the 66:33 ratio observed at 219 K (Figure 2b).

Table S1. Parameters for line-shape analysis.

Isomer	δ / ppm	ν / Hz	Population / %	Width at half height / Hz
***Z*-1a**	4.417	2208	45	4
***E*-1a**	4.343	2172	55	4

The line shape best matched the experimental data using combined rates for the forward and backward reaction k_{EZ}+k_{ZE} of 139 Hz. Based on the approximated ratio *E*-*Z* ratio of 55:45 at this temperature, k_{EZ} = 62.5 Hz and k_{ZE} = 76.5 Hz. Using the Eyring equation, the transition state energy relative to ***E*-1a** (Table 1) was then calculated based on this rate, k_{EZ}, at 308 K.

X-Ray Crystallography

E,γ-1a

Crystals of ***E,γ*-1a** suitable for X-ray diffraction were grown by slow cooling of a MeOH solution of **1a** over 48 h from 60 °C to rt.

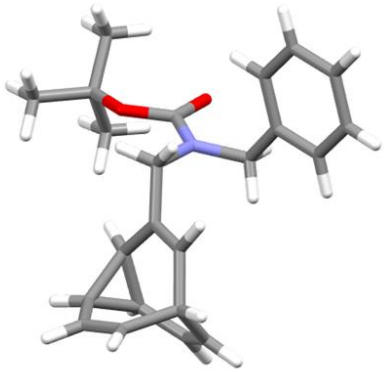

*Figure S5. Solid-state structure of **E,γ-1a***

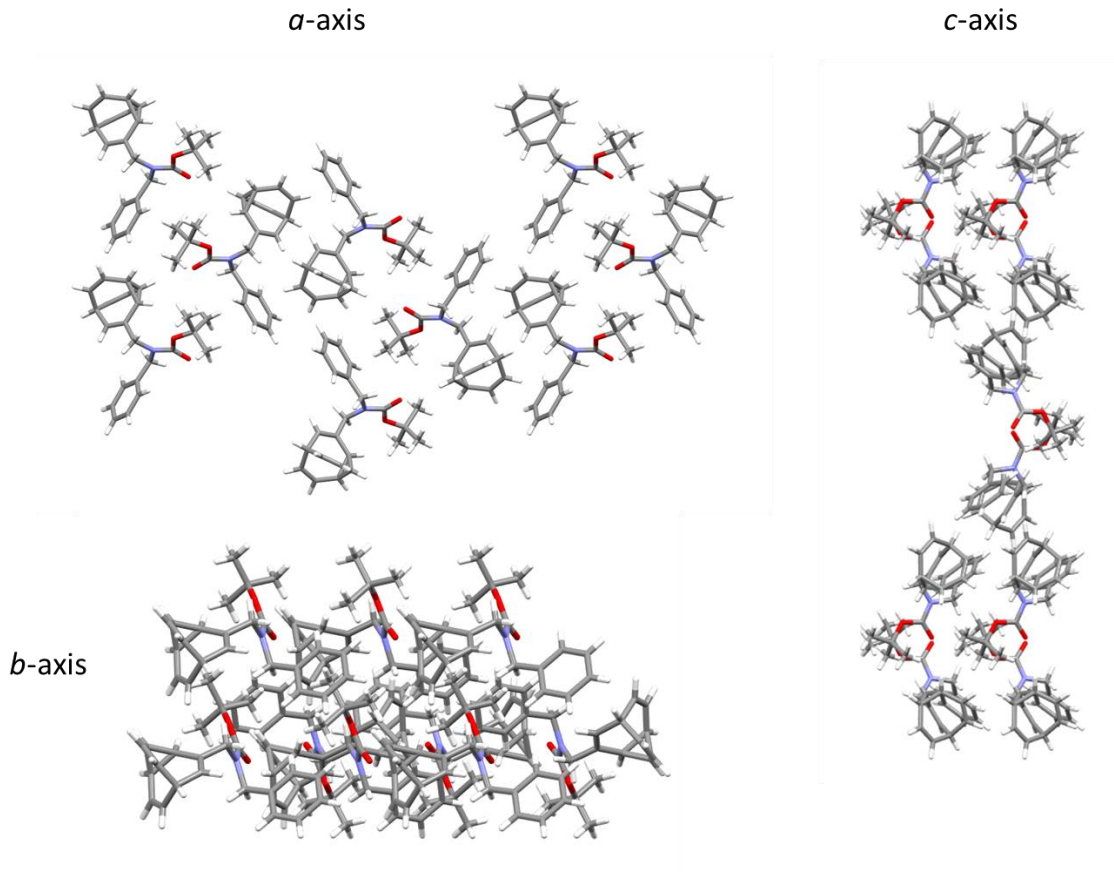

*Figure S6. Solid-state superstructure of **E,γ-1a** viewed along the three unit cell axes.*

*Table S2. Crystal data and structure refinement for **E,y-1a**.*

Empirical formula	$C_{23}H_{27}NO_2$
Formula weight	349.45
Temperature/K	120.00
Crystal system	monoclinic
Space group	$P2_1/c$
a/Å	6.0431(2)
b/Å	26.5905(8)
c/Å	11.6793(3)
α/°	90
β/°	101.7723(10)
γ/°	90
Volume/Å^3	1837.26(9)
Z	4
ρ_{calc}g/cm^3	1.263
μ/mm^{-1}	0.624
F(000)	752.0
2Θ range for data collection/°	6.648 to 144.954
Index ranges	$-7 \leq h \leq 7$, $-32 \leq k \leq 32$, $-14 \leq l \leq 14$
Reflections collected	23653
Independent reflections	3612 [R_{int} = 0.0267, R_{sigma} = 0.0196]
Data/restraints/parameters	3612/0/343
Goodness-of-fit on F^2	1.025
Final R indexes [I>=2σ (I)]	R_1 = 0.0333, wR_2 = 0.0763
Final R indexes [all data]	R_1 = 0.0343, wR_2 = 0.0770
Largest diff. peak/hole / e Å^{-3}	0.25/-0.17

Computational Details

Conformer Generation

All initial sets of Cartesian coordinates sampling the shapeshifting and conformational isomers of **1a** and **1b** were generated *via* the in-house-developed *bullviso*[21a] code. *bullviso* is publicly available under the GNU Public License (GPLv3) on GitLab. The *α*-, *β*-, *γ*-, and *δ*- constitutional isomers of **1a** and **1b** were generated systematically/exhaustively using *bullviso*; the configurational and conformational

isomers were generated according to the experimental-torsion distance geometry (ETDG) with 'basic knowledge' (+K) embedding approach (ETKDGv3)[21b,c] as implemented in RDKit.[21d,e] An RMSD filter with a threshold of 0.5 Å was used to prune the initial set of configurational and conformational isomers. All configurational and conformational isomers passing the RMSD filter were subsequently (pre-)optimized at the GFN2-xTB[21f,g] (extended tight binding; xTB) level of theory using *xtb* (v6.4.1).[21h] An SCF convergence criterion of 1.0×10^{-6} a.u. was used with convergence criteria of 5.0×10^{-6} and 1.0×10^{-3} a.u. for the energy change and gradient, respectively, in all geometry optimizations. All unique configurational and conformational isomers verified at the GFN2-xTB level of theory were progressed to DFT geometry optimization.

DFT Geometry Optimization

All DFT geometry optimizations and energy evaluations of **1a** and **1b** were carried out at the PBE0-D3 level of theory (*i.e.* with the PBE0[21i-k] density functional of Adamo and Barone coupled with the D3[21l] dispersion correction of Grimme *et al.*) using ORCA (v5.0.2).[21m-o] All calculations were carried out under the resolution-of-identity (RI) approximation for the Coulomb integrals (RIJONX). A tightened SCF convergence criterion of 1.0×10^{-9} a.u. was used in all calculations; convergence criteria of 2.0×10^{-7} and 3.0×10^{-5} a.u. were used for the energy change and gradient, respectively, in all geometry optimizations. The def2-SV(P)[21p] basis set of Weigend and Ahlrichs was coupled with the def2/J[21q] auxilliary basis set; the two were used together throughout. The proper convergence of all geometry optimizations to real minima was verified *via* vibrational frequency inspection.

Table S3. Summary of electronic energies, ESCF, Gibbs energies, G219K, and relative Gibbs energies, ΔG219K, for the isomers of 1a. All values of ΔG219K are tabulated relative to the lowest-energy isomer of 1a. All values are given as evaluated at the PBE0-D3/def2-SV(P) level of theory.

Isomer	E_{SCF} / Hartree	G_{219K} / Hartree	ΔG_{219K} / kJ mol^{-1}
***E*,*α*-1a 01**	−1095.732956	−1095.375206	25.52
***E*,*α*-1a 02**	−1095.729318	−1095.374566	27.20
***Z*,*α*-1a 01**	−1095.732570	−1095.375024	25.99
***Z*,*α*-1a 02**	−1095.731403	−1095.376128	23.10
***E*,*β*-1a 01**	−1095.741678	−1095.382975	5.12

***E,β*-1a 02**	−1095.737860	−1095.383558	3.59
***E,β*-1a 03**	−1095.738638	−1095.381663	8.56
***E,β*-1a 04**	−1095.738406	−1095.384270	1.72
***Z,β*-1a 01**	−1095.743360	−1095.384925	0.00
***Z,β*-1a 02**	−1095.740329	−1095.381090	10.07
***Z,β*-1a 03**	−1095.737793	−1095.378954	15.68
***Z,β*-1a 04**	−1095.738625	−1095.384032	2.35
***Z,β*-1a 05**	−1095.735536	−1095.380528	11.54
***Z,β*-1a 06**	−1095.735650	−1095.379767	13.54
***E,γ*-1a 01**	−1095.738216	−1095.380493	11.64
***E,γ*-1a 02**	−1095.741853	−1095.383440	3.90
***E,γ*-1a 03**	−1095.738483	−1095.383864	2.79
***E,γ*-1a 04**	−1095.736951	−1095.379236	14.94
***E,γ*-1a 05**	−1095.737038	−1095.382241	7.05
***Z,γ*-1a 01**	−1095.737413	−1095.379422	14.45
***Z,γ*-1a 02**	−1095.742396	−1095.383770	3.03
***Z,γ*-1a 03**	−1095.735844	−1095.380942	10.46
***Z,γ*-1a 04**	−1095.738633	−1095.384087	2.20
***Z,γ*-1a 05**	−1095.734835	−1095.379146	15.17
***E,δ*-1a 01**	−1095.732828	−1095.379232	14.95
***E,δ*-1a 02**	−1095.735612	−1095.377426	19.69
***E,δ*-1a 03**	−1095.738989	−1095.381294	9.53
***E,δ*-1a 04**	−1095.733276	−1095.379178	15.09
***E,δ*-1a 05**	−1095.735750	−1095.381609	8.71
***E,δ*-1a 06**	−1095.734896	−1095.378204	17.65
***E,δ*-1a 07**	−1095.733556	−1095.376910	21.04
***Z,δ*-1a 01**	−1095.738673	−1095.381377	9.31
***Z,δ*-1a 02**	−1095.737521	−1095.379167	15.12
***Z,δ*-1a 03**	−1095.735425	−1095.380871	10.64
***Z,δ*-1a 04**	−1095.730421	−1095.374776	26.65
***Z,δ*-1a 05**	−1095.736382	−1095.382182	7.20
***Z,δ*-1a 06**	−1095.735370	−1095.380924	10.50
***Z,δ*-1a 07**	−1095.731528	−1095.375207	25.51

Table S4. Summary of electronic energies, ESCF, Gibbs energies, G219K, and relative Gibbs energies, ΔG219K, for the isomers of 1b. All values of ΔG219K are tabulated relative to the lowest-energy isomer of 1b. All values are given as evaluated at the PBE0-D3/def2-SV(P) level of theory.

Isomer	E_{SCF} / Hartree	G_{219K} / Hartree	ΔG_{219K} / kJ mol^{-1}
***E,α*-1b 01**	−1326.329764	−1325.913903	35.13
***E,α*-1b 02**	−1326.329254	−1325.912375	39.14
***E,α*-1b 03**	−1326.330206	−1325.913294	36.73
***E,α*-1b 04**	−1326.328153	−1325.914127	34.54
***Z,α*-1b 01**	−1326.330265	−1325.915297	31.47
***Z,α*-1b 02**	−1326.327412	−1325.912654	38.41
***Z,α*-1b 03**	−1326.330711	−1325.917191	26.50
***Z,α*-1b 04**	−1326.331095	−1325.916351	28.70
***Z,α*-1b 05**	−1326.329499	−1325.912456	38.93
***E,β*-1b 01**	−1326.336193	−1325.920135	18.77
***E,β*-1b 02**	−1326.341631	−1325.926446	2.20
***E,β*-1b 03**	−1326.334901	−1325.918072	24.18
***E,β*-1b 04**	−1326.337349	−1325.921220	15.92
***E,β*-1b 05**	−1326.339789	−1325.922722	11.98
***E,β*-1b 06**	−1326.340586	−1325.921688	14.69
***E,β*-1b 07**	−1326.339529	−1325.925193	5.49
***E,β*-1b 08**	−1326.341663	−1325.926761	1.37
***E,β*-1b 09**	−1326.337066	−1325.921894	14.15
***E,β*-1b 10**	−1326.337717	−1325.917963	24.47
***Z,β*-1b 01**	−1326.339963	−1325.924910	6.23
***Z,β*-1b 02**	−1326.339003	−1325.922341	12.98
***Z,β*-1b 03**	−1326.338920	−1325.926053	3.23
***Z,β*-1b 04**	−1326.341340	−1325.926574	1.86
***Z,β*-1b 05**	−1326.336576	−1325.922267	13.17
***Z,β*-1b 06**	−1326.336428	−1325.921766	14.49
***Z,β*-1b 07**	−1326.333161	−1325.920896	16.77
***Z,β*-1b 08**	−1326.338822	−1325.923744	9.29
***Z,β*-1b 09**	−1326.342696	−1325.926726	1.46
***E,γ*-1b 01**	−1326.334737	−1325.919762	19.75

***E,γ*-1b 02**	−1326.340859	−1325.925817	3.85
***E,γ*-1b 03**	−1326.335467	−1325.919398	20.70
***E,γ*-1b 04**	−1326.340177	−1325.922525	12.49
***E,γ*-1b 05**	−1326.341056	−1325.925377	5.01
***E,γ*-1b 06**	−1326.337167	−1325.921312	15.68
***E,γ*-1b 07**	−1326.339046	−1325.923956	8.74
***Z,γ*-1b 01**	−1326.337802	−1325.923089	11.01
***Z,γ*-1b 02**	−1326.336611	−1325.921922	14.08
***Z,γ*-1b 03**	−1326.339983	−1325.925903	3.62
***Z,γ*-1b 04**	−1326.336923	−1325.921956	13.99
***Z,γ*-1b 05**	−1326.336091	−1325.922845	11.65
***Z,γ*-1b 06**	−1326.342626	−1325.927283	0.00
***Z,γ*-1b 07**	−1326.340554	−1325.925204	5.46
***Z,γ*-1b 08**	−1326.339281	−1325.926646	1.67
***E,δ*-1b 01**	−1326.333932	−1325.920025	19.06
***E,δ*-1b 02**	−1326.331525	−1325.916638	27.95
***E,δ*-1b 03**	−1326.331585	−1325.917496	25.70
***E,δ*-1b 04**	−1326.333950	−1325.919739	19.81
***E,δ*-1b 05**	−1326.336964	−1325.921466	15.27
***E,δ*-1b 06**	−1326.336430	−1325.919396	20.71
***E,δ*-1b 07**	−1326.334695	−1325.918347	23.46
***E,δ*-1b 08**	−1326.336637	−1325.921647	14.80
***E,δ*-1b 09**	−1326.333283	−1325.919776	19.71
***E,δ*-1b 10**	−1326.335553	−1325.920723	17.23
***Z,δ*-1b 01**	−1326.336584	−1325.922131	13.53
***Z,δ*-1b 02**	−1326.335856	−1325.920566	17.64
***Z,δ*-1b 03**	−1326.337115	−1325.923018	11.20
***Z,δ*-1b 04**	−1326.333331	−1325.917587	25.46
***Z,δ*-1b 05**	−1326.336440	−1325.918593	22.82
***Z,δ*-1b 06**	−1326.334286	−1325.922014	13.83
***Z,δ*-1b 07**	−1326.337932	−1325.923306	10.44
***Z,δ*-1b 08**	−1326.335453	−1325.921372	15.52
***Z,δ*-1b 09**	−1326.336085	−1325.921737	14.56

***Z,δ*-1b 10**	−1326.333951	−1325.917563	25.52
***Z,δ*-1b 11**	−1326.335738	−1325.923665	9.50

NCI Plots

Qualitative analysis of noncovalent interactions was carried out by generating NCI plots. Based on the electron density and the derivative of its gradient, NCI plots visualize attractive, repulsive, and weak (van der Waals) interactions within a molecule or between two molecules.[22] At low densities in the reduced density gradient regions, weak interactions appear which are then mapped as isosurfaces over the molecule. The colour of the isosurface as blue, green, orange or red indicates strongly attractive, weakly attractive, weakly repulsive, and strongly repulsive interactions, respectively. A 2D plot of reduced density gradient *vs*. density and second Hessian λ ((λ2)ρ) also provides qualitative information about these interactions.

Single-point energy calculations were carried out at LC-PBE0/def2-TZVP level to generate wavefunction files using ORCA (v5.0.2).[21m-o] Multiwfn 3.8[26] was used thereafter to generate cuboid and text files.

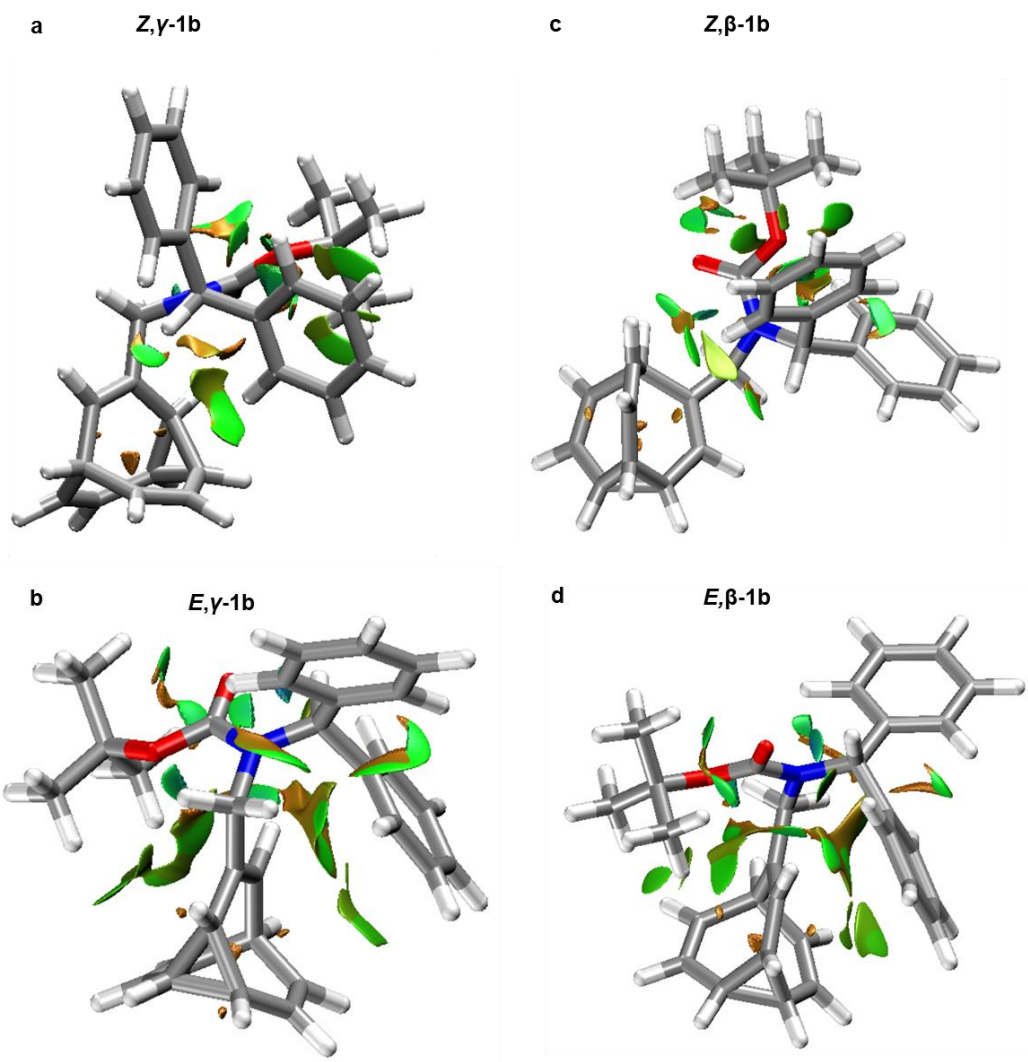

Figure S7: NCI analysis of (a) ***Z,γ-1b*** *(b)* ***Z,β-1b*** *(c)* ***E,γ-1b*** *(d)* ***E,β-1b*** *(grid size: 0.05 a.u; isosurface: 0.5; ρ range: -0.025 – 0.011 a.u) at the LC-PBE0/def2-TZVP//PBE0-D3/def-SV(P) level. The* ***Z,γ-1b*** *shows a strongly attractive interaction between the one Ph group and the bullvalene. The Ph-to-bullvalene interactions are less extensive for* ***Z,β-1b****. For* ***E,γ-1b*** *and* ***E,β-1b*** *the interactions cover a larger area, but include a substantial amount of repulsive character (in orange).*

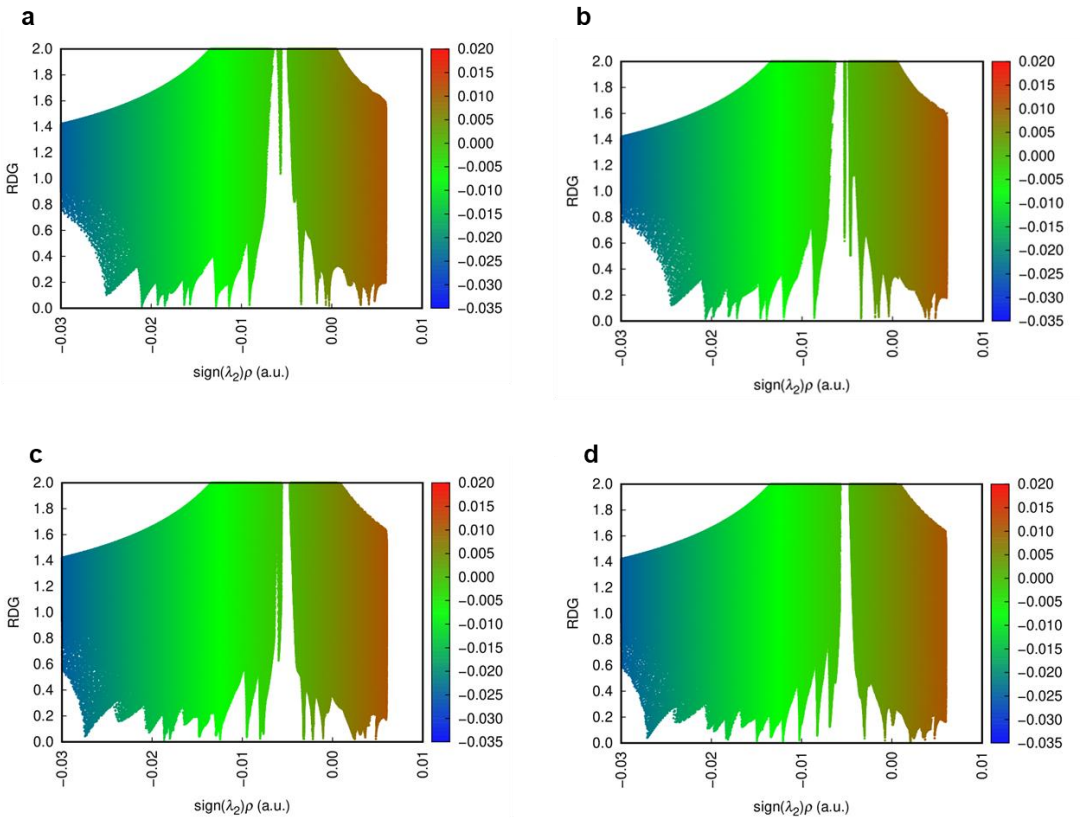

Figure S8: Plots of the reduced density gradient (RDG) versus the electron density multiplied by the sign of the second Hessian eigenvalue at the LC-PBE0/def2-TZVP//PBE0-D3/def-SV(P) level: (a) ***Z,γ-1b*** *(b)* ***Z,β-1b*** *(c)* ***E,γ-1b*** *(d)* ***E,β-1b****.*

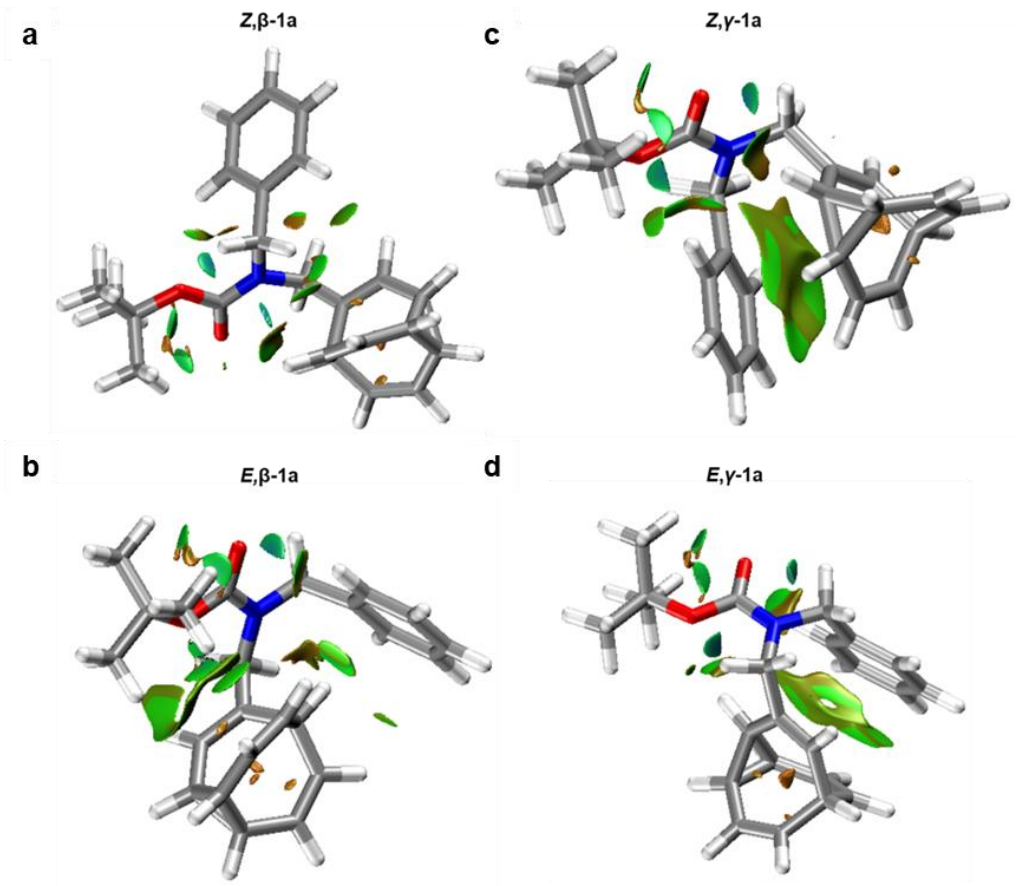

Figure S9: NCI analysis of (a) ***Z,β-1a****, (b)* ***E,β-1a****, (c)* ***Z,γ-1a****, (d)* ***E,γ-1a*** *(grid size: 0.05 a.u; isosurface: 0.5; ρ range: -0.025 – 0.011 a.u) at the LC-PBE0/def2-TZVP//PBE0-D3/def-SV(P) level.*

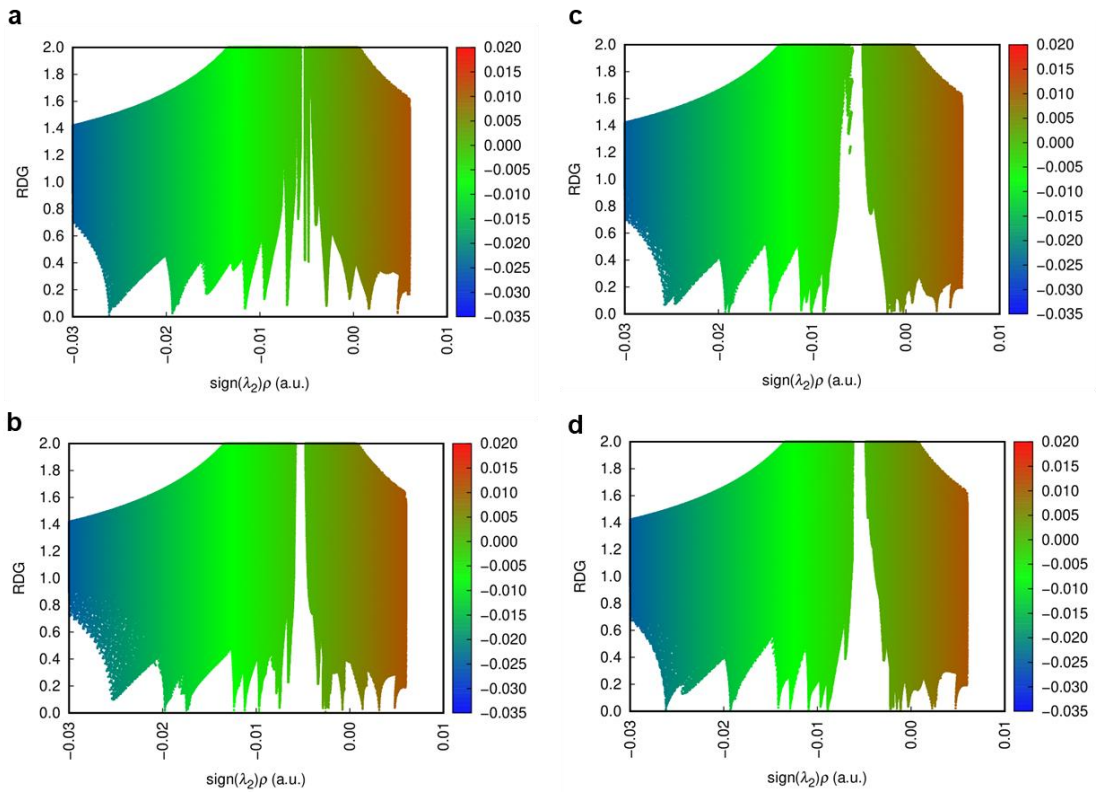

Figure S10: Plots of the reduced density gradient (RDG) versus the electron density multiplied by the sign of the second Hessian eigenvalue at the LC-PBE0/def2-TZVP//PBE0-D3/def-SV(P) level: (a) ***Z,β-1a****, (b)* ***E,β-1a****, (c)* ***Z,γ-1a****, (d)* ***E,γ-1a****.*

NOESY NMR Analysis

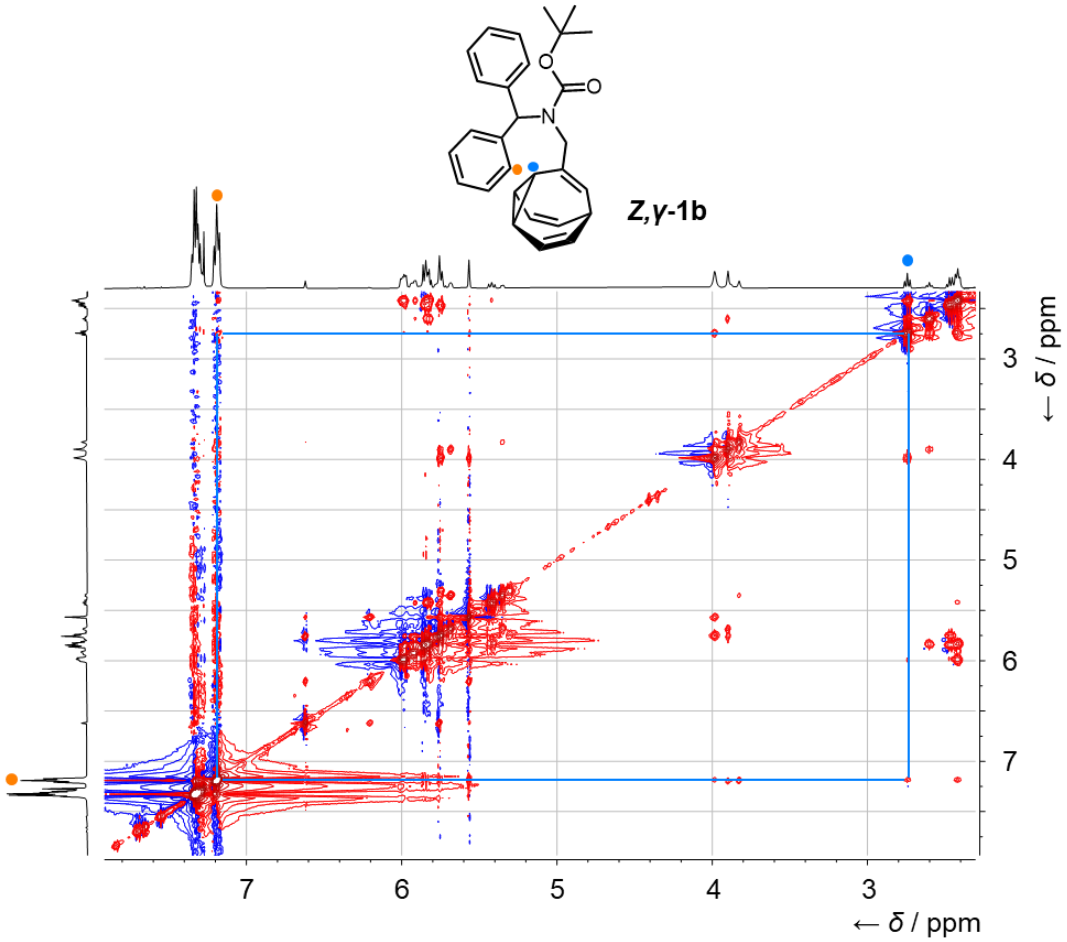

*Figure S11: NOESY NMR (499 MHz, 219 K, $CDCl_3$) of **1b**.*

Analysis of **1b** by NOESY NMR exhibits a through-space correlation between the resonance at 2.73 ppm (filled blue dot, Figure S11) and the resonance at 7.22–7.14 ppm (filled orange dot, Figure S11). These resonances correspond to the δ- position vicinal to the substitution on the bullvalene, and the aromatic proton vicinal to the substitution, both on the *Z,γ*- isomer. This correlation supports the strong attraction occurring between the phenyl ring and bullvalene proton observed in the NCI plot (Figure S7a).

References

1. a) W. von E. Doering, W. R. Roth, *Tetrahedron* 1963, **19**, 715–737; b) G. Schröder, *Angew. Chem., Int. Ed. Engl.* 1963, **2**, 481–482; c) S. Ferrer, A. Echavarren, *Synthesis* 2019, **51**, 1037–1048; d) A. N. Bismillah, B. M. Chapin, B. A. Hussein, P. R. McGonigal, *Chem. Sci.* 2020, **11**, 324–332; e) W. Maturi, R. A. Ives, M. Gill, C. D. Rankine, P. R. McGonigal, *manuscript under review* 2024.
2. a) A. R. Lippert, J. Kaeobamrung, J. W. Bode, *J. Am. Chem. Soc.* 2006, **128**, 14738–14739; b) S. Ferrer, A. M. Echavarren, *Angew. Chem. Int. Ed.* 2016, **55**, 11178–11182; c) O. Yahiaoui, L. F. Pašteka, B. Judeel, T. Fallon, *Angew. Chem. Int. Ed.* 2018, **57**, 2570–2574; d) O. Yahiaoui, L. F. Pašteka, C. J. Blake, C. G. Newton, T. Fallon, *Org. Lett.* 2019, **21**, 9574–9578; e) H. D. Patel, T. H. Tran, C. J. Sumby, L. F. Pašteka, T. Fallon, *J. Am. Chem. Soc.* 2020, **142**, 3680–3685.
3. a) P. R. McGonigal, C. de León, Y. Wang, A. Homs, C. R. Solorio-Alvarado, A. M. Echavarren, *Angew. Chem. Int. Ed.* 2012, **51**, 13093–13096; b) X. Wang, O. Shyshov, M. Hanževački, C. M. Jäger, M. von Delius, *J. Am. Chem. Soc.* 2019, **141**, 8868–8876; c) M. Sanz-Novo, M. Mato, Í. León, A. M. Echavarren, J. L. Alonso, *Angew. Chem. Int. Ed.* 2022, **61**, e202117045; d) A. Sanchez, T. J. Maimone, *J. Am. Chem. Soc.* 2022, **144**, 7594–7599; e) A. Sanchez, A. Gurajapu, W. Guo, W.-Y. Kong, C. J. Laconsay, N. S. Settineri, D. J. Tantillo, T. J. Maimone, *J. Am. Chem. Soc.* 2023, **145**, 13452–13461; f) A. N. Bismillah, T. G. Johnson, B. A. Hussein, A. T. Turley, P. K. Saha, H. C. Wong, J. A. Aguilar, D. S. Yufit, P. R. McGonigal, *Nat. Chem.* 2023, **15**, 615–624.
4. a) H. Deng, M. A. Olson, J. F. Stoddart, O. M. Yaghi, *Nat. Chem.* 2010, **2**, 439–443; b) S. Krause, J. V. Milić, *Commun. Chem.* 2023, **6**, 151; c) P. K. Saha, T. Tran Ngoc, P. R. McGonigal, J. F. Teichert, *manuscript under review* 2024.
5. C. Dohmen, H. Ihmels, T. Paululat, *Eur. J. Org. Chem.* 2022, **2022**, e202201172.
6. A. Ottonello, J. A. Wyllie, O. Yahiaoui, S. Sun, R. A. Koelln, J. A. Homer, R. M. Johnson, E. Murray, P. Williams, J. R. Bolla, C. V. Robinson, T. Fallon, T.

P. Soares da Costa, J. E. Moses, *Proc. Natl. Acad. Sci. U. S. A.* 2023, **120**, e2208737120.

7. a) K. K. Larson, M. He, J. F. Teichert, A. Naganawa, J. W. Bode, *Chem. Sci.* 2012, **3**, 1825; b) J. F. Teichert, D. Mazunin, J. W. Bode, *J. Am. Chem. Soc.* 2013, **135**, 11314–11321.
8. a) A. Birve, H. D. Patel, J. R. Price, W. M. Bloch, T. Fallon, *Angew. Chem. Int. Ed.* 2021, **61**, e202115468; b) C. Dohmen, T. Paululat, H. Ihmels, *Chem. – Eur. J.* 2024, DOI 10.1002/chem.202304311.
9. M. N. Pomfret, P. B. Sun, Z. Huang, A. C. Freund, T. Miyoshi, M. R. Golder, *Angew. Chem. Int. Ed.* 2023, **62**, e202301695.
10. J. R. Reimers, T. Li, A. P. Birvé, L. Yang, A. C. Aragonès, T. Fallon, D. S. Kosov, N. Darwish, *Nat. Commun.* 2023, **14**, 6089.
11. A. Mazzanti, D. Casarini, *Wiley Interdiscip. Rev.: Comput. Mol. Sci.* 2012, **2**, 613–641.
12. a) K. Mislow, *Acc. Chem. Res.* 1976, **9**, 26–33; b) M. Oki, *Angew. Chem., Int. Ed. Engl.* 1976, **15**, 87–93; b) Z. Rappoport, S. E. Biali, *Acc. Chem. Res.* 1997, **30**, 307–314; c) S. Erbas-Cakmak, D. A. Leigh, C. T. McTernan, A. L. Nussbaumer, *Chem. Rev.* 2015, **115**, 10081–10206; d) D. Dattler, G. Fuks, J. Heiser, E. Moulin, A. Perrot, X. Yao, N. Giuseppone, *Chem. Rev.* 2020, **120**, 310–433; e) S. Corra, C. de Vet, M. Baroncini, A. Credi, S. Silvi, *Chem* 2021, **7**, 2137–2150; f) C. L. F. Van Beek, B. L. Feringa, *J. Am. Chem. Soc.* 2024, doi:10.1021/jacs.3c14430.
13. a) E. R. Johnston, R. Fortt, J. C. Barborak, *Magn. Reson. Chem.* 2000, **38**, 932–936; b) J. Clayden, J. H. Pink, *Angew. Chem. Int. Ed.* 1998, **37**, 1937–1939; c) R. A. Bragg, J. Clayden, *Org. Lett.* 2000, **2**, 3351–3354; d) R. A. Bragg, J. Clayden, G. A. Morris, J. H. Pink, *Chem. – Eur. J.* 2002, **8**, 1279–1289.
14. M. Achard, M. Mosrin, A. Tenaglia, G. Buono, *J. Org. Chem.* 2006, **71**, 2907–2910.
15. a) M. Jones, L. T. Scott, *J. Am. Chem. Soc.* 1967, **89**, 150–151; b) M. Jones, S. D. Reich, L. T. Scott, *J. Am. Chem. Soc.* 1970, **92**, 3118–3126.
16. J. F. M. Oth, R. Merényi, J. Nielsen, G. Schröder, *Chem. Ber.* 1965, **98**, 3385–3400.
17. It is known that the energetics of crystal packing can outweigh the small solution-phase energetic bias towards certain isomers within fluxional

mixtures. See a) A. N. Bismillah, J. Sturala, B. M. Chapin, D. S. Yufit, P. Hodgkinson, P. R. McGonigal, *Chem. Sci.* 2018, **9**, 8631–8636; b) J. Nyman, G. M. Day, *CrystEngComm* 2015, **17**, 5154–5165. See also reference 2e.

18. Deposition number 2294194 (for ***E,γ*-1a**) contains the supplementary crystallographic data for this paper. These data are provided free of charge by the joint Cambridge Crystallographic Data Centre and Fachinformationszentrum Karlsruhe Access Structures service.
19. K. Nikitin, R. O'Gara, *Chem. – Eur. J.* 2019, **25**, 4551–4589.
20. R. Merényi, J. F. M. Oth, G. Schröder, *Chem. Ber.* 1964, **97**, 3150–3161.
21. a) bullviso, 2024, https://gitlab.com/conor.rankine/bullviso. b) S. Riniker, G. A. Landrum, *J. Chem. Inf. Model.* 2015, **55**, 2562–2574. c) S. Wang, J. Witek, G. A. Landrum, S. Riniker, *J. Chem. Inf. Model.* 2020, **60**, 2044–2058. d) RDKit: Open-Source Cheminformatics. https://rdkit.org. e) RDKit, 2023, https://github.com/rdkit/rdkit. f) S. Grimme, C. Bannwarth, P. Shushkov, *J. Chem. Theory Comput.* 2017, **13**, 1989–2009. g) C. Bannwarth, S. Ehlert, S. Grimme, *J. Chem. Theory Comput.*, 2019, **15**, 1652–1671. h) C. Bannwarth, E. Caldeweyher, S. Ehlert, A. Hansen, P. Pracht, J. Seibert, S. Spicher, S. Grimme, *WIREs Comput. Mol. Sci.* 2020, **11**, e01493. i) J. P. Perdew, K. Burke, M. Ernzerhof, *Phys. Rev. Lett.* 1996, **77**, 3865–3868. j) J. P. Perdew, K. Burke, M. Ernzerhof, *Phys. Rev. Lett.* 1997, **78**, 1396. k) C. Adamo, V. Barone, *J. Chem. Phys.* 1999, **110**, 6158–6169. l) S. Grimme, J. Antony, S. Ehrlich, H. Krieg, *J. Chem. Phys.* 2010, **132**, 154104. m) F. Neese, *WIREs Comput. Mol. Sci.* 2012, **2**, 73–78. n) F. Neese, *WIREs Comput. Mol. Sci.* 2017, **8**, e1327. o) F. Neese, F. Wennmohs, U. Becker, C. Riplinger, *J. Chem. Phys.* 2020, **152**, 224108. p) F. Weigend, R. Ahlrichs, *Phys. Chem. Chem. Phys.* 2005, **7**, 3297–3305. q) F. Weigend, *Phys. Chem. Chem. Phys.* 2006, **8**, 1057–1065.
22. a) E. R. Johnson, S. Keinan, P. Mori-Sánchez, J. Contreras-García, A. J. Cohen, W. Yang, *J. Am. Chem. Soc.* 2010, **132**, 6498–6506; b) J. Contreras-García, E. R. Johnson, S. Keinan, R. Chaudret, J.-P. Piquemal, D. N. Beratan, W. Yang, *J. Chem. Theory Comput.* 2011, **7**, 625–632.
23. a) H. Iikura, T. Tsuneda, T. Yanai, K. Hirao, *J. Chem. Phys.* 2001, **115**, 3540–3544; b) A. Najibi, M. Casanova-Paez, L. Goerigk, *J. Phys. Chem. A* 2021, **125**, 4026–4035.

24. O. V. Dolomanov, L. J. Bourhis, R. J. Gildea, J. A. K. Howard, H. Puschmann, *J. Appl. Crystallogr.* 2009, **42**, 339–341.
25. G. M. Sheldrick, *Acta Crystallogr. A* 2008, **64**, 112–122.
26. M. Yoshida, Y. Komatsuzaki, M. Ihara, *Org. Lett.* 2008, **10**, 2083–2086.
27. T. Lu, F. Chen, *J. Comput. Chem.* 2012, **33**, 580–592.